UNITED STATES DEPARTMENT OF COMMERCE
HARRY L. HOPKINS, Secretary
NATIONAL BUREAU OF STANDARDS
Lyman J. Briggs, Director

✦

Journal of Research

of the

National Bureau of Standards

✦

Volume 22, No. 6

June 1939

[Published with approval of the Director of the Budget]

UNITED STATES
GOVERNMENT PRINTING OFFICE
WASHINGTON : 1939

For sale by the Superintendent of Documents, Washington, D. C. - - - - - - Price 30 cents
$3.50 per year on subscription

The prices of the separate Research Papers appearing in this JOURNAL are given on the front cover page. If 100 or more copies of any separate are ordered, a discount of 25 percent is allowed. Those who desire copies of separate Research Papers should send their orders and remittances without delay to the Superintendent of Documents, U. S. Government Printing Office, Washington, D. C. This will aid him to determine the number of copies to be printed for sale. Research Papers are not printed from electrotypes, and usually no more reprints can be had when the first and only printing is exhausted.

U. S. DEPARTMENT OF COMMERCE NATIONAL BUREAU OF STANDARDS

RESEARCH PAPER RP1209

Part of Journal of Research of the National Bureau of Standards, Volume 22, June 1939

STANDARDIZATION OF THE LUMINOUS-TRANSMISSION SCALE USED IN THE SPECIFICATION OF RAILROAD SIGNAL GLASSES

By Kasson S. Gibson and Geraldine Walker Haupt

ABSTRACT

This is the first of several papers dealing with the development and description of the signal-glass specifications formulated by the Signal Section of the Association of American Railroads in 1935 and 1938. The present paper gives the spectral transmissions of the basic standards—red, yellow, green, blue, purple, and lunar-white glasses—on which the AAR scale of luminous transmission is based, and defines that scale in fundamental, absolute units. Comparison is made with the scales defined in the 1908 and 1918 signal-glass specifications.

CONTENTS

	Page
I. Introduction	627
II. Association of American Railroads scale of luminous transmission	628
III. Expression of the Association of American Railroads scale of transmission on a fundamental, absolute basis	638
IV. Comparison of the transmission scales as expressed in the 1908, 1918, and 1935 (and 1938) specifications	647

I. INTRODUCTION

This is the first of several papers describing the work of the National Bureau of Standards on the color standardization of railroad signal glasses. This standardization has resulted from the cooperative efforts of the Signal Section of the Association of American Railroads (formerly the American Railway Association), Corning Glass Works, and the National Bureau of Standards. The Bureau's work was actively started in 1930 and has been formally reported to the cooperating organizations at various times since then.[1] These papers will

[1] Standardization of railway signal glasses—Reports on measurements and investigations undertaken by the Colorimetry Section of the National Bureau of Standards at the request of the Signal Section, American Railway Association.

Reports 1 to 5, K. S. Gibson and Geraldine K. Walker, published in Signal Section Proc., Am. Ry. Assoc. 36, 384 (1933):

Report 1. The transmission (ARA scale) of 36 specimens of signal glass relative to transmission of 6 ARA standards marked "J. C. Mock 10-3-30," a report on measurements made at Corning Glass Works December 9-11, 1930 (June 1, 1932).

Report 2. Measurements of spectral and luminous transmissions leading to the derivation of new ARA transmissions for the 36 glasses listed in report 1 (October 24, 1932).

Report 3. Spectral and luminous transmissions and derivation of new values of ARA transmission for the 22 "limit" glasses selected by committee VI, ARA, at Corning, November 5-6, 1931, and engraved "J. C. M. 11-6-31" (December 2, 1932).

Report 4. Chromaticities and luminous transmissions, with illuminants at 1,900° K and 2,848° K, for the 22 "limit" glasses described in report 3 (January 30, 1933).

Report 5. Tentative specifications for railway signal colors (April 27, 1933).

Reports 6 and 7, K. S. Gibson, Geraldine Walker Haupt, and H. J. Keegan, published in Signal Section Proc., Assoc. Am. R. R. 36, 136 (1939):

Report 6. Examination of 65 duplicate limit glasses (July 26, 1934).

Report 7. Colorimetric data leading to specification 59-38 for kerosene hand lantern globes; comparison of specifications 59-38, 69-38, and 69-35; certification of duplicate lantern glasses (September 28, 1938).

present a summary of these reports, to which the reader is referred for additional details, illustrate and discuss the new specifications resulting from this work, namely, AAR Signal Section Specifications 69–35, 69–38,[2] and 59–38,[3] and give supplementary information not elsewhere published. Comparison will also be made with other signal-glass specifications.

The authors acknowledge with pleasure the interest and support of J. C. Mock, signal engineer, Michigan Central Railroad, who has been identified with the railroad signal glass standardization since 1904, and who has served as chairman of subcommittee A (of committee VI, Designs, Signal Section) in charge of the standardization of pressware and disk glasses, and of A. S. Haigh, chairman of subcommittee C in charge of the standardization of lantern glasses and present chairman of committee VI; also the invaluable advice and assistance of H. P. Gage, chief, Optical Division, Corning Glass Works, who has prepared the large number of glasses necessary for the successful carrying out of the signal-glass standardization.

A history of railroad signal-glass standardization prior to 1928 has been given by Dr. Gage in an important paper entitled, Practical Considerations in the Selection of Standards for Signal Glass in the United States.[4] In that paper are noted the signal-glass specifications adopted in 1908 and 1918 by the then Railway Signal Association, the latter specification, No. 6918, being quoted in part. There are also given information on the selection and uses of signal colors and the various types of signal ware and spectrophotometric and colorimetric data on signal glasses in use prior to the adoption of specification 69–35.[5]

II. ASSOCIATION OF AMERICAN RAILROADS SCALE OF LUMINOUS TRANSMISSION

In 1908 the Railway Signal Association, with the cooperation of Corning Glass Works, adopted certain glass roundels, for use with the kerosene flame, to represent the most desirable colors then available for signal purposes. The colors were designated as red, yellow, green, blue, purple, and lunar white. Each of these roundels was designated arbitrarily as having a "photometric value" of 100, regardless of the absolute or true value of its luminous transmission. They were also designated as the "standard" or "medium intensity" roundels. To allow the necessary manufacturing tolerances, certain limits of photometric value above and below the standard were specified, such as "light" and "dark" limits of 120 and 80, 125 and 75, or 130 and 70, within which a glass would be acceptable for signalling purposes. Chromaticity limits were not specified as such, but the light and dark

[2] AAR Signal Section Specification 69–38, Signal Glasses (Exclusive of Kerosene Hand Lantern Globes); approved, 1938. The 1935 issue of this specification appeared in that year under the number 69–35. The differences between 69–35 and 69–38 are very slight, and no change at all was made in the transmission scale. The present transmission scale will be considered to have been established in 1935, although the data on which it is based were obtained and reported in 1930–32.

[3] AAR Signal Section Specification 59–38, Kerosene Hand Lantern Globes; approved, 1938. The present AAR scale of transmission is incorporated in Specification 59–38 (so far as applicable) as well as in 69–38. Specifications 59–38 and 69–38 may be obtained from R. H. C. Balliet, secretary, AAR Signal Section, 30 Vesey Street, New York, N. Y.

[4] Proc. Int. Cong. Illum., Saranac Inn, N. Y., p. 834 (September 1928).

[5] Further information on the early history of railroad signal-glass standardization is given in reports by Mr. Mock and Dr. Gage, Signal Section Proc., Am. Ry. Assoc., **30**, 373, 377 (1933).

limits were apparently tacitly used as chromaticity limits.[6] By specifying the spectral transmissions of the standard roundels, a fundamental record of the colors of the glasses was attempted. The values so specified are given in table 1 and illustrated in figures 1 to 6.

TABLE 1.—*Spectral transmissions of the standard or medium roundels, designated as having a value of* $T_{RRA}=100$; *1908 specification* [1]

Wave length		Red	Yellow	Green	Blue	Purple	Lunar white
Fraunhofer line	(Millimicron equivalent)						
		%	%	%	%	%	%
A	(761)	60	0	0	0	0	0
a	(716)	65	38	0	0	42	62
B	(687)	70	50	0	0	42	49
C	(656)	72	43	0	0	0	17
D	(589)	0	41	4	3	0	15
E	(527)	0	12	27	4	0	25
b	(517)	0	9	40	6	0	38
F	(486)	0	3	45	24	2	65
G	(431)	0	0	25	40	43	74
H	(397)	0	0	0	46	42	0

[1] Values taken from a copy of the original Specifications for Signal Roundels, Lenses, and Glass Slides, Proc. Ry. Signal Assoc. vol. 5 (1908), kindly furnished the authors by R. H. C. Balliet, present secretary, AAR Signal Section.

In 1918, as a result of improvements in glass-making technique, the medium values for red, yellow, and green roundels were increased from 100 to 130, 120, and 150, respectively, with corresponding increases in the light and dark limits. A new specification was formulated, designated both as 1918 and 6918, in which new tables of spectral transmission were given for the medium roundels. These values are given in table 2 and illustrated in figures 1 to 6. They are considered further below.

This extension of the transmission (photometric) limits to higher values was based in considerable part, apparently, on values obtained by direct photometric comparisons of glasses of somewhat differing chromaticity, which introduced undesirable personal uncertainties common to heterochromatic photometry. The situation was eventually made still worse with the introduction of "electric purples," "electric lunar whites" (glasses designed for use solely with incandescent-lamp illuminants), and other types of glass differing notably in both luminous transmission and chromaticity from the original standards having transmission values designated as 100. Furthermore, the original standards had become lost. The first step in the present standardization, therefore, was to select new replicas of the lost standards and measure and define the transmissions of these new standards in fundamental terms.

Although the original standards were missing, the transmission scale itself had undoubtedly been maintained close to its original value by means of duplicate working standards at Corning Glass Works. To reestablish the scale on an official basis, Mr. Mock, in October 1930, endorsed six roundels as the new ARA standards, engraving each "J. C. Mock, 10–3–30." The designated trans-

[6] However, the 1908 specification does state that "The manufacturer must submit samples of glasses showing the extreme limits of colors which it is proposed to furnish. These shall bear labels showing the photometric values • • •." There were also given in the specification certain qualitative restrictions tending to prevent glass of undesirable color from being used. This original specification is considered further in section IV, below.

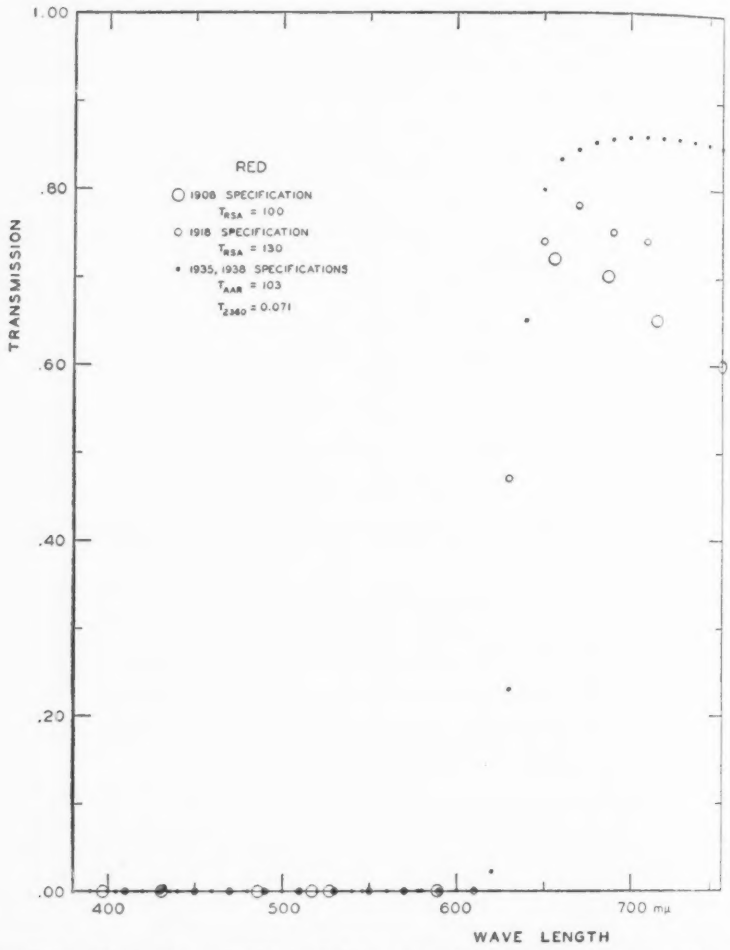

FIGURE 1.—*Spectral transmissions defining the scales of luminous transmission for glasses designated as* red, *as established respectively in the 1908 and 1918 specifications of the Railway Signal Association and in the 1935 and 1938 specifications of the Signal Section of the Association of American Railroads.*

The 1938 specifications, now in effect, are designated as AAR Signal Section Specifications 59–38 and 69–38.

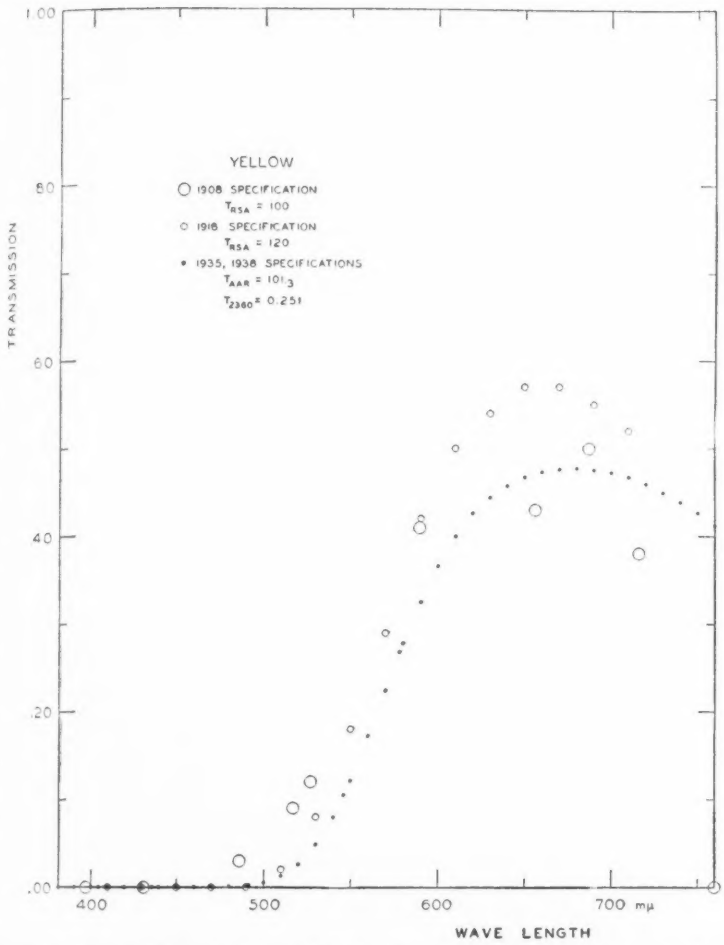

FIGURE 2.—*Spectral transmissions defining the scales of luminous transmission for glasses designated as* yellow, *as established respectively in the 1908 and 1918 specifications of the Railway Signal Association and in the 1935 and 1938 specifications of the Signal Section of the Association of American Railroads.*

The 1938 specifications, now in effect, are designated as AAR Signal Section Specifications 59–38 and 69–38.

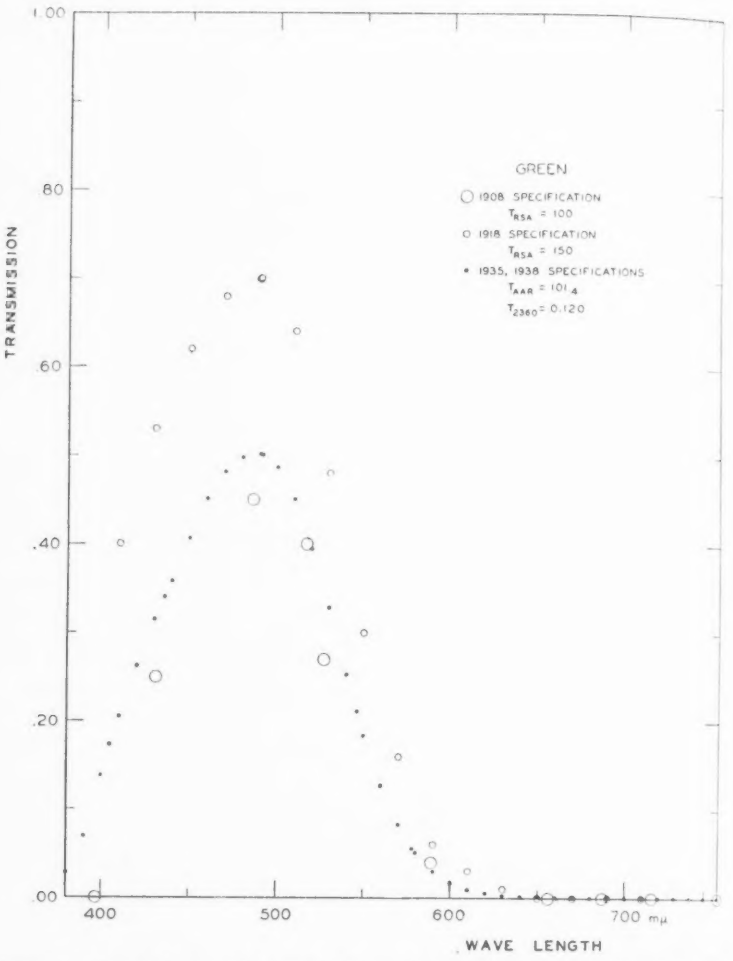

FIGURE 3.—*Spectral transmissions defining the scales of luminous transmission for glasses designated as* green, *as established respectively in the 1908 and 1918 specifications of the Railway Signal Association and in the 1935 and 1938 specifications of the Signal Section of the Association of American Railroads.*

The 1938 specifications, now in effect, are designated as AAR Signal Section Specifications 59-38 and 69-38.

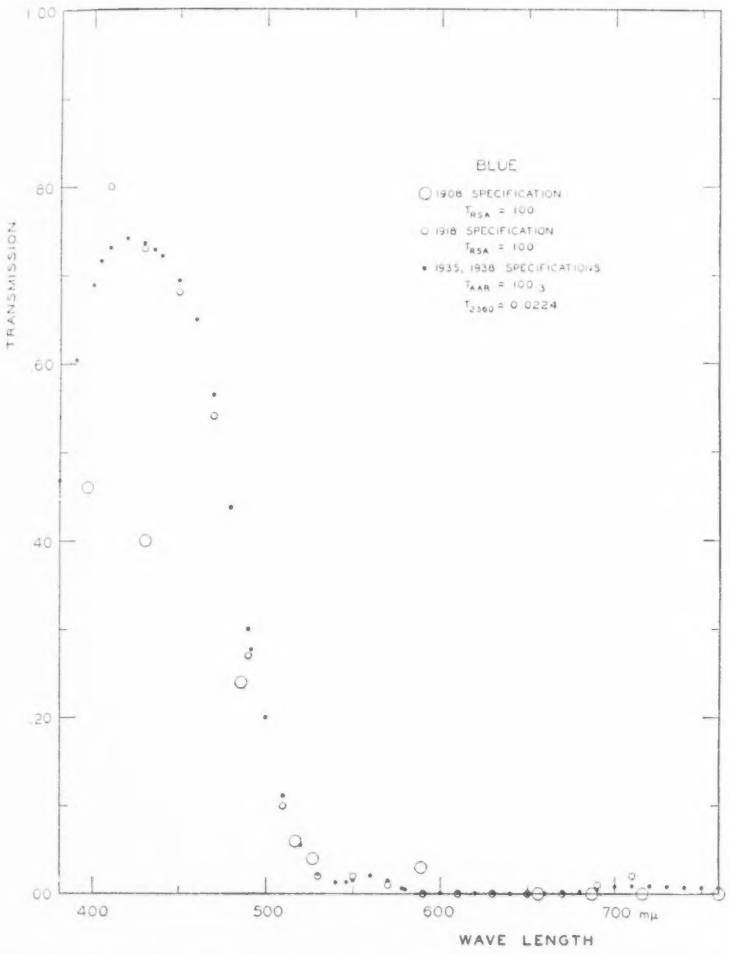

FIGURE 4.—*Spectral transmissions defining the scales of luminous transmission for glasses designated as* blue, *as established respectively in the 1908 and 1918 specifications of the Railway Signal Association and in the 1935 and 1938 specifications of the Signal Section of the Association of American Railroads.*

The 1938 specifications, now in effect, are designated as AAR Signal Section Specifications 59-38 and 69-38.

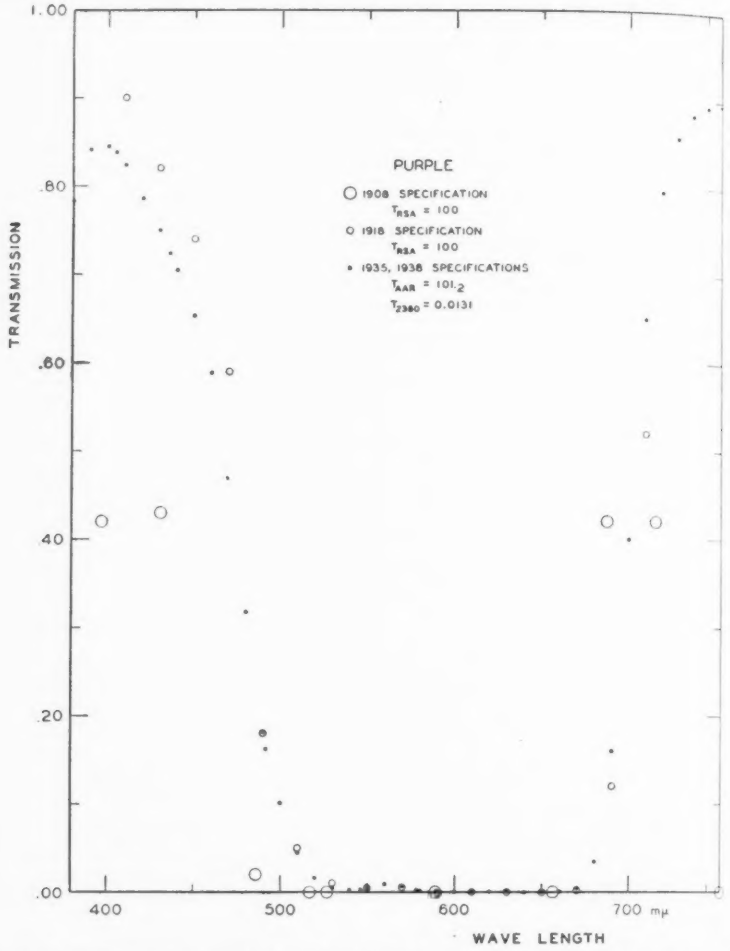

FIGURE 5.—*Spectral transmissions defining the scales of luminous transmission for glasses designated as* purple, *as established respectively in the 1908 and 1918 specifications of the Railway Signal Association and in the 1935 and 1938 specifications of the Signal Section of the Association of American Railroads.*

The 1938 specification, now in effect, is designated as AAR Signal Section Specification 69-38.

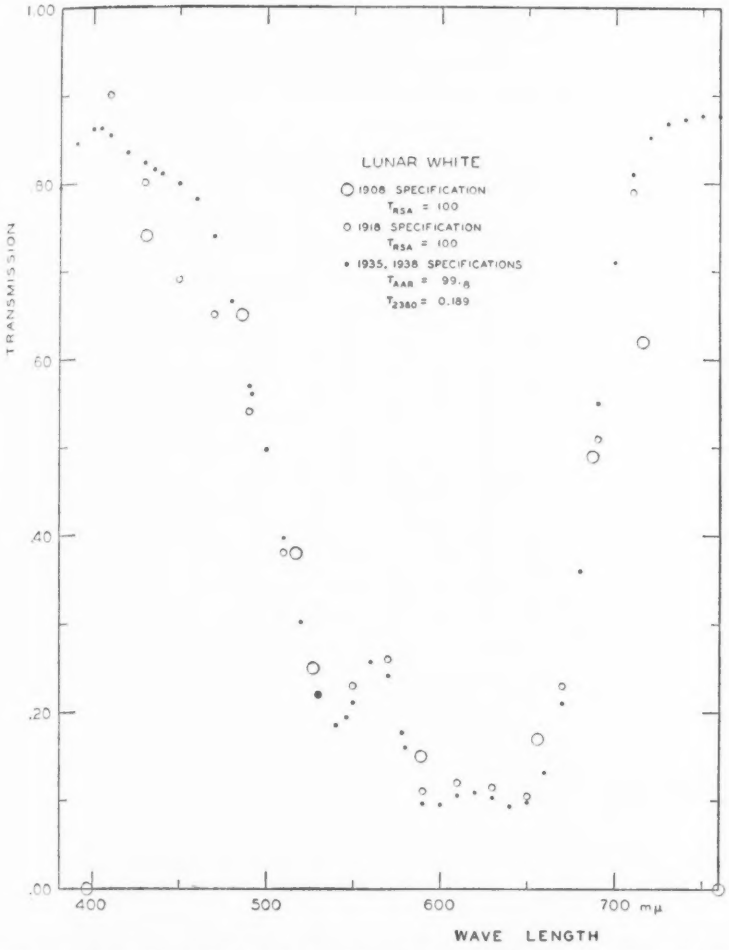

FIGURE 6.—*Spectral transmissions defining the scales of luminous transmission for glasses designated as* lunar white, *as established respectively in the 1908 and 1918 specifications of the Railway Signal Association and in the 1935 and 1938 specifications of the Signal Section of the Association of American Railroads.*

The 1938 specification, now in effect, is designated as AAR Signal Section Specification 69-38.

missions of these standard roundels, which had been previously determined by Corning Glass Works, thereby became transmissions on the ARA scale. They were as indicated in table 3. The designation T_{ARA} is hereinafter used to denote values of luminous transmission on this ARA scale.

TABLE 2.—*Spectral transmissions of the medium roundels, having values of T_{ARA} as indicated; 1918 specification as published*

Wave length / T_{ARA}=	Red 130	Yellow 120	Green 150	Blue 100	Purple 100	Lunar white 100
$m\mu$	%	%	%	%	%	%
410	0	0	40	80	90	90
430	0	0	53	73	82	80
450	0	0	62	68	74	69
470	0	0	68	54	59	65
490	0	0	70	27	18	54
510	0	2	64	10	5	38
530	0	8	48	2	1	22
550	0	18	30	2	0.5	23
570	0	29	16	1	.5	26
590	0	42	6	0	0	11
610	0	50	3	0	0	12
630	47	54	1	0	0	11.5
650	74	57	0	0	0	10.5
670	78	57	0	0	.2	23
690	75	55	0	1	12	51
710	74	52	0	2	52	79

TABLE 3.—*Designations of roundels selected in 1930 as the basis of the ARA scale of luminous transmission*

Identifying number of roundel	Color designation of roundel	Corning values of transmission on ARA scale	Identifying number of roundel	Color designation of roundel	Corning values of transmission on ARA scale
5	Red	97	6	Blue	105
0	Yellow	100	4	Purple	100.3
4	Green	100	3	Lunar white	100

Although the ARA Signal Section and Corning Glass Works desired that fundamental measurements be made on their standard glasses and that such standard glasses be placed in the custody of the National Bureau of Standards, there were objections to using the six standard roundels for these purposes. These roundels were unpolished and relatively large (8 3/8 in. in diameter), and were therefore unsuitable for precise spectrophotometric measurements; furthermore, Corning Glass Works wished to retain them. Accordingly, Dr. Gage prepared six 2-in. polished squares for each of the six signal colors, these 2-in. squares duplicating the respective 8 3/8-in. roundels, both in chromaticity and in transmission, as closely as was feasible. At the request of the ARA subcommittee in charge, one of the authors thereupon went to Corning and measured the values of T_{ARA} for each of these 36 squares in terms of the respective standard roundels, using the same apparatus and method as had been used for several years in

the maintenance of the standards at Corning Glass Works.[7] The values obtained are given in column 4 of table 4.

TABLE 4.—*Data obtained by one of the authors (K.S.G.) at Corning Glass Works on the glasses selected to replace the former ARA standard roundels*

1	2	3	4	5	6	7
Color designation	Number engraved on glass	ARA transmission		Column 4 minus column 3	Color relative to standard	Thickness
		As marked on label	As determined by K.S.G.			
						mm
Red	83	95.2	97.5	+2.3	Red	1.60
	86	101	102.6	+1.6	Match	1.61
	88	105	104.6	−0.4	do	1.61
	91	100	103.1	+3.1	Yellow	5.21
	92	100	106.4	+6.4	do	3.84
	93	97	102.0	+5.0	do	4.15
Mean		(99.7)	102.7	+3.0		
Yellow	114	100	101.3	+1.3	Red	6.60
	115	100	101.7	+1.7	do	6.60
	116	100	102.5	+2.5	do	6.60
	117	100	102.1	+2.1	do	6.60
	118	100	101.1	+1.1	do	6.60
	138	100	101.5	+1.5	do	6.59
Mean		(100)	101.7	+1.7		
Green	110	102	103.1	+1.1	Match	3.68
	111	102	102.7	+0.7	do	3.68
	112	102	102.1	+.1	do	3.70
	113	102	103.3	+1.3	do	3.68
	120	100	100.6	+0.6	do	3.74
	121	100	101.5	+1.5	do	3.74
Mean		(101.3)	102.2	+0.9		
Blue	52	100	101.4	+1.4		4.97
	53	100	100.6	+0.6	More saturated [1]	4.99
	54	100	99.4	−.6		5.00
	79	100	99.7	−.3	More saturated	5.00
	81	100	99.2	−.8		5.00
	82	100	100.7	+.7		4.99
Mean		(100)	100.2	+0.2		
Purple	38	100	101.0	+1.0	Match	4.86
	39	100	101.0	+1.0	do	4.86
	60	100	101.0	+1.0	do	4.83
	66	101	101.2	+0.2	do	4.83
	67	101	101.5	+.5	do	4.83
	68	100	100.3	+.3	do	4.84
Mean		(100.3)	101.0	+0.7		
Lunar white	40	101	101.0	0.0	Blue	6.18
	49	99.5	100.0	+.5	do	6.24
	67	100	98.9	−1.1	do	6.22
	68	100	100.1	+0.1	do	6.21
	69	100	99.5	−.5	do	6.23
	71	100	99.9	−.1	do	6.21
Mean		(100.1)	99.9	−0.2		

[1] The record shows comments on but 2 of the 6 blue glasses. It is uncertain whether the other 4 should be designated "more saturated" or "match."

[7] Details of these measurements are given in report 1, Signal Section Proc., Am. Ry. Assoc. **30,** 384 (1933).

It had been agreed [8] that, of these six 2-in. glass squares of each color, one pair was to be deposited with the National Bureau of Standards, one pair with the secretary or other designated custodian of the ARA, and one pair to remain the property of the Corning Glass Works Optical Laboratory. The Bureau's glasses are identified in table 6 as B and B', the ARA glasses as A and A', and the Corning glasses as C and C'. After the measurements at Corning, noted above, these glasses were taken to the Bureau for further measurement, it having been further agreed that when values had been finally assigned these glasses by the National Bureau of Standards they would then "become the official primary ARA standards and all others, including the present Corning standards, are to be subsidiary to them."

These further measurements at the Bureau are described below. On the basis of these measurements, the individual values of T_{ARA}, given in column 4 of table 4, were to be revised if necessary to secure more precise relative values among the six glasses of a given color; but such revision was not to change the mean values of T_{ARA}, given in column 4 for each color. These mean values were to be retained as correct and final, on the basis of which a fundamental definition of the ARA scale of transmission was to be adopted.

III. EXPRESSION OF THE ASSOCIATION OF AMERICAN RAILROADS SCALE OF TRANSMISSION ON A FUNDAMENTAL, ABSOLUTE BASIS

The measurements on these glasses at the Bureau consisted in:

1. *Measurement of the spectral transmission of the B glass of each color.*—The values obtained are given in table 5 and are illustrated in figures 1 to 6. The instruments and methods, visual and photoelectric, have been adequately described previously.[9] Measurements of transmission (where measurable) were made by one or both methods at every 10 mμ from 380 to 760 mμ, in addition to visual measurements at various wave lengths of the Hg and He spectra from 404.7 to 667.8 mμ. The overlapping of the wave-length ranges of the visual and photoelectric data was extensive in all cases, and the agreement of the data usually good. The values adopted, table 5, are considered uncertain in the last figure given.

2. *Measurement of the ratios of transmission of the A and C glasses to the respective B glasses as a function of wave length.*—The values obtained are illustrated in report 2.[10] From these measured ratios of transmission and the spectral transmissions of the B glasses, the spectral transmissions of the A and C glasses were computed. These are also given in table 5.

---

[8] Memorandum entitled, Plan for Reexamination and Duplication of ARA Color Standards and Limits now Deposited with Corning Glass Works. This memorandum was prepared by H. P. Gage and represented the conclusions of the subcommittee of committee VI, ARA Signal Section, meeting at Corning on October 3, 1930.

[9] K. S. Gibson, *Direct-reading photoelectric measurement of spectral transmission*, J. Opt. Soc. Am. and Rev. Sci. Instr. **7**, 693 (1923).
H. J. McNicholas, *Equipment for routine spectral transmission and reflection measurements*, BS J. Research **1**, 793 (1928) RP30.
K. S. Gibson, *Spectrophotometry at the Bureau of Standards*, J. Opt. Soc. Am. **21**, 564 (1931).

[10] Signal Section Proc., Am. Ry. Assoc. **30**, 390 (1933).

TABLE 5.—*Spectral transmissions of the A, B, and C glasses (comprising 18 of the 36 glasses listed in tables 4 and 6)*

Wave length (millimicrons)	Red			Yellow		Green			Blue			Purple			Lunar white		
	92 *A*	86 *B*	83 *C*	115 *A*	118 *B*	114 *C*	111 *A*	121 *B*	110 *C*	53 *A*	82 *B*	54 *C*	38 *A*	69 *B*	66 *C*	71 *A*	68 *B*	49 *C*
Hg. 404.7	--------	0.0000	-------	--------	0.0000	-------	--------	0.173	-------	--------	0.716	-------	--------	0.838	-------	--------	0.862	-------
Hg. 435.8	--------	.0000	-------	--------	.0000	-------	--------	.340	-------	--------	.728	-------	--------	.724	-------	--------	.815	-------
Hg. 491.6	--------	.0000	-------	--------	.0026	-------	--------	.600	-------	--------	.277	-------	--------	.162	-------	--------	.560	-------
Hg. 546.1	--------	.0000	-------	--------	.1053	-------	--------	.211	-------	--------	.0130	-------	--------	.0031	-------	--------	.194	-------
Hg. 578.0	--------	<.0001	-------	--------	.208	-------	--------	.0554	-------	--------	.0060	-------	--------	.0022	-------	--------	.177	-------
380	0.0000	.0000	0.0000	0.0000	.0000	0.0000	0.028	.028	0.028	0.477	.468	0.472	0.783	.783	0.783	0.795	.795	0.795
90	.0000	.0000	.0000	.0000	.0000	.070	.070	.069	.070	.616	.604	.610	.845	.841	.840	.845	.845	.846
400	.0000	.0000	.0000	.0000	.0000	.0000	.139	.138	.139	.695	.689	.693	.852	.845	.844	.862	.861	.862
10	.0000	.0000	.0000	.0000	.0000	.0000	.207	.205	.206	.738	.731	.737	.830	.824	.824	.854	.854	.855
20	.0000	.0000	.0000	.0000	.0000	.0000	.264	.262	.264	.749	.742	.749	.791	.786	.786	.834	.834	.834
30	.0000	.0000	.0000	.0000	.0000	.0000	.317	.315	.317	.742	.736	.742	.755	.750	.750	.822	.822	.823
40	.0000	.0000	.0000	.0000	.0000	.0000	.360	.358	.359	.726	.721	.726	.709	.705	.705	.810	.810	.812
450	.0000	.0000	.0000	.0000	.0000	.0000	.407	.406	.407	.699	.693	.698	.657	.653	.653	.799	.799	.801
60	.0000	.0000	.0000	.0000	.0001	.0001	.451	.451	.452	.655	.649	.653	.593	.589	.589	.780	.781	.783
70	.0000	.0000	.0000	.0000	.0003	.0003	.481	.481	.481	.569	.564	.567	.473	.471	.473	.738	.739	.741
80	.0000	.0000	.0000	.0000	.0006	.0008	.497	.497	.497	.440	.437	.439	.318	.318	.320	.664	.665	.667
90	.0000	.0000	.0000	.0000	.0021	.0021	.501	.501	.501	.302	.300	.301	.181	.181	.182	.569	.569	.570
500	.0000	.0000	.0000	.0000	.0054	.0055	.486	.486	.485	.201	.200	.200	.1010	.1015	.1023	.497	.497	.497
10	.0000	.0000	.0000	.0000	.0128	.0130	.450	.450	.450	.1120	.1115	.1112	.0443	.0447	.0449	.397	.397	.397
20	.0000	.0000	.0000	.0000	.0261	.0265	.395	.394	.395	.0551	.0550	.0546	.0161	.0163	.0163	.302	.302	.301
30	.0000	.0000	.0000	.0000	.0483	.0489	.330	.328	.329	.0222	.0222	.0220	.0048	.0049	.0049	.220	.220	.219
40	.0000	.0000	.0000	.0000	.0708	.0707	.255	.253	.255	.0131	.0132	.0131	.0027	.0028	.0028	.184	.185	.184
550	.0000	.0000	.0000	.1237	.1218	.1226	.185	.183	.185	.0152	.0152	.0150	.0042	.0043	.0043	.210	.211	.210
60	.0000	.0000	.0000	.174	.172	.173	.1289	.1268	.1289	.0210	.0210	.0208	.0091	.0092	.0092	.257	.257	.257
70	.0000	.0000	.0000	.226	.224	.225	.0644	.0624	.0644	.0146	.0147	.0145	.0067	.0069	.0069	.241	.241	.240
80	.0000	.0001	.0000	.280	.278	.280	.0525	.0509	.0526	.0045	.0046	.0045	.0016	.0017	.0017	.160	.160	.159
90	.0000	.0002	.0002	.327	.325	.326	.0309	.0296	.0309	.0011	.0011	.0011	.0003	.0003	.0003	.0964	.0962	.0954
600	.0001	.0005	.0004	.368	.366	.367	.0174	.0165	.0174	.0008	.0008	.0008	.0002	.0002	.0002	.0951	.0950	.0938
10	.0013	.0019	.0013	.402	.400	.401	.0099	.0093	.0099	.0008	.0008	.0008	.0003	.0003	.0003	.1059	.1058	.1047
20	.065	.022	.015	.428	.426	.428	.0055	.0051	.0055	.0006	.0006	.0006	.0004	.0004	.0004	.1090	.1090	.1082
30	.38	.23	.18	.446	.444	.446	.0030	.0027	.0030	.0004	.0004	.0004	.0003	.0003	.0003	.1036	.1035	.1025
40	.60	.65	.61	.459	.457	.458	.0017	.0015	.0017	.0003	.0003	.0003	.0002	.0002	.0002	.0836	.0835	.0823

TABLE 5.—*Spectral transmissions of the A, B, and C glasses (comprising 18 of the 36 glasses listed in tables 4 and 6)*—Continued

Wave length (millimicrons)	Red			Yellow			Green			Blue			Purple			Lunar white		
	92 *A*	86 *B*	83 *C*	115 *A*	118 *B*	114 *C*	111 *A*	121 *B*	110 *C*	53 *A*	82 *B*	54 *C*	38 *A*	60 *B*	66 *C*	71 *A*	68 *B*	49 *C*
650	.678	.798	.785	.469	.467	.468	.0009	.0008	.0009	.0002	.0002	.0002	.0003	.0003	.0003	.0980	.0980	.0970
60	.717	.833	.823	.475	.473	.474	.0005	.0004	.0005	.0004	.0004	.0004	.0008	.0008	.0008	.132	.132	.131
70	.738	.844	.834	.478	.476	.477	.0002	.0002	.0002	.0009	.0009	.0009	.005	.005	.005	.21	.21	.21
80	.754	.852	.841	.479	.477	.479	.0001	.0001	.0001	.0021	.0021	.0021	.034	.035	.036	.36	.36	.36
90	.764	.856	.846	.477	.475	.477	.0000	.0000	.0000	.0045	.0045	.0044	.16	.16	.16	.55	.55	.55
700	.769	.858	.848	.474	.472	.473	.0000	.0000	.0000	.008	.008	.008	.40	.40	.40	.71	.71	.71
10	.772	.859	.850	.468	.467	.468	.0000	.0000	.0000	.009	.009	.009	.65	.65	.65	.810	.810	.811
20	.770	.858	.850	.460	.459	.460	.0000	.0000	.0000	.0085	.0085	.0085	.798	.795	.795	.851	.852	.853
30	.768	.857	.849	.450	.449	.450	.0000	.0000	.0000	.008	.008	.008	.860	.857	.857	.868	.868	.869
40	.764	.855	.848	.439	.438	.439	.0000	.0000	.0000	.0075	.0075	.0075	.885	.883	.883	.873	.873	.873
750	.758	.852	.845	.427	.426	.427	.0000	.0000	.0000	.007	.007	.007	.896	.893	.893	.876	.877	.877
60	.751	.849	.842	.413	.412	.412	.0000	.0000	.0000	.0065	.0065	.0065	.900	.896	.896	.876	.877	.877
LUMINOUS TRANSMISSION, T_{2360} (C_2=14,350)																		
----------	0.07341	0.07110	0.06628	0.2526	0.2508	0.2520	0.1218	0.1205	0.1217	0.02246	0.02240	0.02233	0.01299	0.01306	0.01312	0.1889	0.1890	0.1882

The uncertainty in these values for the A and C glasses is not much greater than that in the respective values for the B glasses, because the ratios of transmission, T_A/T_B and T_C/T_B could be determined as a function of wave length with high precision. This was possible since for each of the colors, except red, the A, B, and C glasses were of the same melt and approximately of the same thickness and therefore had nearly identical spectral transmissions.

3. *Derivation of the luminous transmissions of the A, B, and C glasses.*—Luminous transmission, T_θ, is herein defined as

$$T_\theta = \frac{\Sigma E_\theta V T}{\Sigma E_\theta V},$$

in which θ is the color temperature of the illuminant, E_θ is the relative spectral energy of the illuminant, V is the relative spectral luminosity (visibility) function, T is the spectral transmission, and in which the summations were made with values taken at every 10 mμ from 400 to 760 mμ. The value of θ was taken at 2,360° K,[11] this being the color temperature, approximately, at which similar determinations had for several years been made at Corning Glass Works. Values of E_{2360} were taken from a published table;[12] values of V were those adopted by the International Commission on Illumination in 1924.[13] The luminous transmissions for illuminant at 2,360° K, T_{2360}, were thus computed and are given in the respective columns at the bottom of table 5.

Figure 7 has been prepared to assist in imparting an understanding of the computation of T_{2360}, as just outlined. In this figure are given the spectral-distribution curves of (1) E_{2360}, arbitrarily unity at 560 mμ, (2) V, arbitrarily unity at the maximum, (3) the light, VE_{2360} (the product of V and E_{2360}, taken at each wave length) for a source at 2,360° K, and (4) the light from this source transmitted through the respective B glasses having spectral transmissions, T, this transmitted light having the distribution TVE_{2360}. The ratio of summations given above in defining T_{2360} is, for each of the six colors, equivalent to the ratio of the area beneath the TVE_{2360} curve to the area beneath the VE_{2360} curve. Furthermore, of course, the areas beneath the TVE_{2360} curves have the same relative values as do the respective values of T_{2360}, the area beneath the curve for the yellow glass being the greatest, that beneath the curve for the purple glass the least, just as the luminous transmission of the yellow glass is the greatest and that of the purple glass the least.

4. *Determination of the relative luminous transmissions of the A, B, and C glasses of each of the six colors from the computed values of* T_{2360}.—These relative transmissions are given in column 5 of table 6, that for the B glass being taken as unity in all cases.

[11] With C_2=14,350 micron-degrees. For continuity with the published reports, all values of color temperature in this paper are expressed on this basis. On the color-temperature scale more recently established at the Bureau (H. T. Wensel, D. B. Judd, and W. F. Roeser, BS J. Research **12**, 527 (1934) RP677), for which C_2=14,320, the same energy distribution is given by 2,355° K. For values of C_2=14,330 (J. F. Skogland, BS Misc. Pub. M86) and 14,360 (H. T. Wensel, *International Temperature Scale and some related physical constants*, J. Research NBS **22**, 375 (1939) RP1189) the respective values of θ are equal to 2,357 and 2,362.

[12] R. Davis and K. S. Gibson, *Filters for the reproduction of sunlight and daylight and the determination of color temperature*, BS Misc. Pub. M114, table 2 (1931). However, the values there given do not extend above 720 mμ. Values from 730 to 760 mμ were used as published in report 2.

[13] Proceedings Sixth Meeting of Intern. Comm. Illum., Geneva, p. 67. These adopted values are those recommended by Gibson and Tyndall (Visibility of radiant energy, Sci. Pap. BS **19**, 131, table 3 (1923) S475) and are incorporated in the so-called 1931 ICI standard observer (Proceedings Eighth Meeting of Intern. Comm. Illum., Cambridge, p. 19 (1931). D. B. Judd, The 1931 ICI standard observer and coordinate system for colorimetry, J. Opt. Soc. Am. **23**, 359 (1933)).

5. *Direct photometric measurement of the relative luminous transmissions of all six glasses of each of the six colors.*—These measurements were made with the Martens photometer by each of three observers [14] and with the illuminant at 2,360° K. The mean values so obtained are given in column 3 of table 6, and in column 4 are shown the average deviations of each observer's values from the mean values of column 3.

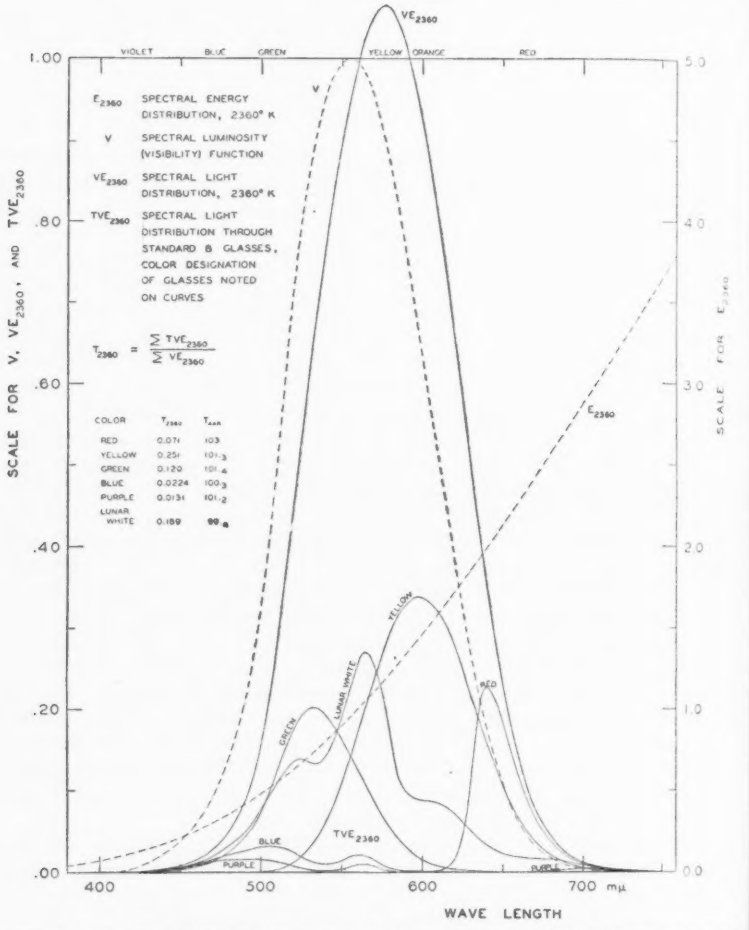

FIGURE 7.—*Spectral-distribution curves of illuminant at 2,360° K and of the light transmitted by the respective B glasses, having values of* T_{AAB} *close to 100.*

These curves illustrate the graphical equivalent of the relation defining T_{2360}.

6. *Adoption of final values of relative luminous transmission for the six glasses of each of the six colors.*—These values are given in column 6 of table 6. For the *A*, *B*, and *C* glasses these relative values are the means of the values obtained by spectrophotometric and photometric methods, columns 5 and 3, respectively. For the other glasses the values of column 3 are carried directly to column 6. Different methods

[14] H. J. Keegan assisted the authors in these observations.

of weighting might perhaps have been used, but the deviations (column 7) of the *A*, *B*, and *C* values in columns 5 and 3 from the mean values of column 6, in no case exceeding 0.3 percent, show that any other reasonable weighting of the values would not give importantly different results.

7. *Conversion of these relative luminous transmissions to the ARA scale.*—It will be recalled that the mean values of column 9 of table 6 (and column 4 of table 4) were to be accepted as correct and final. Therefore, by dividing these mean values of column 9 by the respective mean values of column 6, factors are obtained, one for each color, by which the individual values of column 6 may be converted to revised ARA transmissions. These factors are given in parentheses in place of the means in columns 7 and 8, and the revised transmissions on the ARA scale are given in column 10. These revised transmissions were designated as T'_{ARA} throughout reports 1 to 6. After the American Railway Association changed its name in 1933 to Association of American Railroads, it was deemed desirable to change the symbol T'_{ARA} to T_{AAR}, eliminating the use of the prime mark. The meaning of T_{AAR} is in all cases identical to that of T'_{ARA} wherever the latter is used or published.

8. *Fundamental basis of the T_{AAR} scale.*—The true luminous transmissions, T_{2360}, for the *A*, *B*, and *C* glasses, given in table 5, are also given in column 11 of table 6. From the values of T'_{ARA} in column 10 and these values of T_{2360} in column 11 may be derived the value of T_{2360} equivalent to $T'_{ARA}=T_{AAR}=100.0$. Such values are shown in column 12, together with the mean values thus obtained. These mean values afford a fundamental definition and conversion of values of T_{AAR}, being based upon spectrophotometric measurements, and are the values which should result if direct photometric measurements of the luminous transmissions (T_{2360}) of glasses having values of $T_{AAR}=100.0$ were made by a large number of observers under standard conditions of observation, or if the hypothetical 1931 ICI standard observer could make such measurements. The mean values of column 12 are, however, subject to considerable uncertainty in the last significant figure tabulated. The values of table 7 have therefore been adopted as expressing the fundamental relation between values of T_{AAR} and values of T_{2360}.

TABLE 6.—*Derivation of new ARA transmissions (redefined as AAR transmissions) for the 36 glasses listed in table 4*

1	2		3	4	5	6	7	8	9	10	11	12
Designation			Relative luminous transmission (at 2,360° K), as determined at National Bureau of Standards in 1932					ARA transmission				
Color	Ref.	No.	Mean, by three observers with Martens photometer	Average deviation of each observer from mean	Computed from spectral transmission	Mean, columns 3 and 5	Deviation from mean, col. 3 (or 5) minus col. 6	As labeled at Corning	By K.S.G. at Corning	New ARA transmission T'_{ARA}	Luminous transmission T_{2360}	T_{2360} equivalent to $T'_{ARA}=T_{AAR}=100.0$
Red	C	83	0.9383	0.0051	0.9323	0.9353	±0.0030	95.2	97.5	96.2	0.06628	0.06890
	B	86	1.0000		1.0009	1.0000	.0000	101	102.6	102.9	.07110	.06910
	B'	88	1.0303	.0021		1.0303		105	104.6	106.0		
	C'	91	1.0022	.0213		1.0022		100	103.1	103.1		
	A	92	1.0335	.0120	1.0325	1.0330	.0005	100	106.4	106.3	.07341	.06906
	A'	93	.9886	.0103		.9886		97	102.0	101.7		
Mean				.0102		.9982	(f=102.89)		102.7	102.7		.0690
Yellow	C	114	1.0056	.0015	1.0047	1.0052	.0004	100	101.3	101.8	.2520	.2475
	A	115	1.0098	.0022	1.0073	1.0086	.0012	100	101.7	102.2	.2526	.2472
	A'	116	1.0051	.0018		1.0051		100	102.5	101.8		
	B'	117	1.0038	.0017		1.0038		100	102.1	101.7		
	B	118	1.0000		1.0000	1.0000	.0000	100	101.1	101.3	.2508	.2476
	C'	138	1.0011	.0011		1.0011		100	101.5	101.4		
Mean				.0017		1.0040	(f=101.29)		101.7	101.7		.2474
Green	C	110	1.0134	.0021	1.0098	1.0116	.0018	102	103.1	102.6	.1217	.1186
	A	111	1.0158	.0019	1.0105	1.0132	.0026	102	102.7	102.8	.1218	.1185
	A'	112	1.0087	.0018		1.0087		102	102.1	102.3		
	C'	113	1.0177	.0025		1.0177		102	103.3	103.2		
	B'	120	.9952	.0014		.9952		100	100.6	100.9		
	B	121	1.0000		1.0000	1.0000	.0000	100	101.5	101.4	.1205	.1188
Mean				.0019		1.0077	(f=101.42)		102.2	102.2		.1186

Blue	A'	52	1.0113	.0039		1.0113		100	101.4	101.4		
	A	53	1.0024	.0039	1.0029	1.0026	.0002	100	100.6	100.6	.02233	
	C'	54	.9950	.0040	.9959	.9946	.0010	100	99.4	99.5	.02235	
	C	79	.9924	.0037		.9924		100	99.7	99.5		
	B'	81	.9923	.0015		.9923		100	99.2	99.5		
	B	82	1.0000		1.0000	1.0000	.0000	100	100.7	100.3	.02240	.02233
Mean				.0028		.9991	(f=100.29)		100.2	100.2		.02234
Purple	A'	38	.9942	.0024	.9944	.9943	.0001	100	101.0	100.7	.01299	.01290
	A	39	.9931	.0032		.9931		100	101.0	100.5		
	B'	60	1.0000		1.0000	1.0000	.0000	100	101.0	101.2	.01306	.01291
	B	66	1.0051	.0018	1.5046	1.0048	.0002	101	101.2	101.7	.01312	.01290
	C'	67	1.0004	.0025		1.0004		101	101.5	101.3		
	C	68	.9937	.0023		.9937		100	100.3	100.6		
Mean				.0024		.9977	(f=101.23)		101.0	101.0		.01290
Lunar white	C'	40	1.0214	.0015		1.0214		101	101.0	101.9		
	C	49	.9979	.0024	.9959	.9969	.0010	99.5	100.0	99.4	.1882	.1893
	A'	67	.9977	.0022		.9977		100	98.9	99.5		
	B'	68	1.0000		1.0000	1.0000	.0000	100	100.1	99.8	.1890	.1894
	B	69	.9946	.0006		.9946		100	99.5	99.2		
	A	71	.9972	.0010	.9993	.9982	.0010	100	99.9	99.6	.1889	.1897
Mean				.0015		1.0015	(f=99.75)		99.9	99.9		.1895

TABLE 7.—*Relation between values of T_{AAR} and of T_{2360}, which defines the luminous transmission scale established in the 1935 and 1938 AAR signal-glass specifications*

Color designation of glass	AAR transmission, T_{AAR}	Equivalent luminous transmission, 1931 ICI standard observer, illuminant 2,360° K, T_{2360}	Color designation of glass	AAR transmission, T_{AAR}	Equivalent luminous transmission, 1931 ICI standard observer, illuminant 2,360° K, T_{2360}
Red	100.0	0.069	Blue	100.0	0.022[1]
Yellow	100.0	.247	Purple	100.0	.029
Green	100.0	.119	Lunar white	100.0	1.190

[1] The original derived value was 0.1895 (table 6). This was at first cut back to 0.189 and was so published in report 5 and in J. Opt. Soc. Am. **24**, 57 (1934). Later work has, however, indicated that 0.190 is a more accurate conversion factor than 0.189.

It may be noted that these conversion factors are valid only at 2,360° K; in fact, the T_{AAR} scale, by definition, exists only at this color temperature of illuminant. The variation of absolute luminous transmission, T_θ, with color temperature, θ_f of illuminant will be shown for various signal glasses in a later paper.

The question may perhaps arise as to why, in a fundamental analysis and standardization of signal glasses and colors such as the present, the ARA scale of transmission was not entirely discarded in favor of the absolute scale. It is obviously just as convenient, and from the scientific standpoint preferable, to insert absolute rather than relative values in a specification. Such a change was not made, however, for the following reason:

The ARA scale of transmission (with perhaps some variation, see below) has been in existence for over 30 years and has been universally used by the signal engineers and glass manufacturers to designate the luminous transmission of a glass relative to its respective standard ($T_{ARA}=100$). It would be a matter of considerable inconvenience for the engineers and manufacturers to use a new scale, and continual reference to a conversion table would be necessary for a long time. Such confusion was deemed unnecessary and was avoided by the procedure outlined in this section, whereby the existing scale was kept in effect with relatively minor revisions but was placed on a consistent absolute basis by means of the conversion factors specified.

In accord with the understanding noted earlier in the paper, the A and A' glasses have been deposited with the Signal Section of the Association of American Railroads (letter of 1–5–38, Director NBS to Mr. Balliet, secretary, AAR Signal Section), the C and C' glasses have been deposited with Corning Glass Works (letter of 1–5–38, Director NBS to Corning Glass Works), and the B and B' glasses are in the custody of the Colorimetry and Spectrophotometry Section of the National Bureau of Standards. It should be noted, however, that the present standardization of the AAR scale of luminous transmission, being based upon fundamental measurements and computations, is independent of these standard glasses which were used in its determination, and if these material standards ever become lost or damaged, the accuracy and usefulness of the scale, as defined in table 7, will in no wise be affected.

IV. COMPARISON OF THE TRANSMISSION SCALES AS EXPRESSED IN THE 1908, 1918, AND 1935 (AND 1938) SPECIFICATIONS

It is of interest to compare the present AAR transmission scale, as defined for the six signal colors by the data of table 7, with the RSA scales, defined by the data of tables 1 and 2, taken from the 1908 and 1918 specifications, respectively. From the continuity of the signal-glass standardization since 1908, as outlined above, huge differences between the three scales[15] are not to be expected. On the other hand, it would be very surprising if the personal errors of heterochromatic photometry, which have been involved in the production and the maintenance of the earlier scales and to some extent in the transfer of standards illustrated in table 4, and the lack of precision of some of the earliest spectrophotometric data, did not cause real or apparent changes of many percent in the true luminous transmission of glasses having values of T_{RSA} or T_{AAR} equal to 100, as defined in the various specifications.

Reference to the spectral-transmission data of figures 1 to 6 is of interest in this connection. The spectral quality of the glasses would seem to have improved since 1908, particularly in the case of the yellow, blue, purple, and lunar-white glasses. This is indicated by the increase of transmission at the high transmissions, accompanied in many cases by a decrease of transmission at the low transmissions. On the basis of these data one would judge that glasses of purer, more saturated colors had been developed with no loss of luminous transmission; or, of greater practical importance, that signal glassware of considerably greater transmission had been developed with no loss of distinctness of the signal color. However, it is understood that no intentional changes have ever been made in the composition of the blue, purple, or lunar-white glasses. Probably, therefore, the apparent differences in these graphs are largely due to spectrophotometric error in the earlier data. Changes in either the type of glass or the medium value have been made at various times with the red, yellow, and green glasses, but these will be considered in the later papers.

It had been hoped to make accurate comparison of the three transmission scales from these spectrophotometric data by (1) deriving the luminous transmission, T_{2360}, of the glasses from the 1908 and 1918 data, as had been done from the 1935 data, and (2) reducing these values of T_{2360} by the proper ratio ($T_{RSA}/100$) to get the value of T_{2360} corresponding to $T_{RSA}=100$. However, the 1908 data are so meager that the uncertainties of interpolation would largely defeat the purpose. Furthermore, their reliability is open to some question, not only for the reason noted above but also in view of (1) the erratic values for the yellow glass at the longer wave lengths and (2) the zero values of transmission for certain of the glasses at the *A* line (761 mμ), which, in view of present knowledge of the spectral absorption of glasses, cannot be correct if the data at the *a* and *B* lines are reasonably accurate.

The 1918 data are more extensive and reliable, however. The data are given at every 20 mμ (table 2), and values of T_{2360} computed from these data should afford an interesting comparison. To make this

[15] In the preceding parts of the paper the various transmission scales to which reference is made in the present section have been mostly treated as various versions of the same scale. It is more convenient in this section to consider them as separate scales.

comparison as valid as possible, the values so computed have been compared with similar values computed from the recent spectrophotometric data (table 5) for the same wave lengths (every 20 mμ) instead of using the values of T_{2360} given in tables 5 and 6. The values for the *B* glasses were used for this purpose. Results are given in table 8.

It will be noted that none of the differences is as large as 10 percent. The differences for the blue and purple standards [16] are subject to large uncertainty, because but one significant figure is given in the 1918 spectral-transmission data for these glasses (table 2) in the region of high luminosity (510 to 650 mμ). The differences for the yellow, green, and lunar-white standards are subject to less uncertainty from this cause. Those for the yellow and green are probably explainable by the uncertainties of heterochromatic photometry. Reference to column 4 of table 6 shows average deviations for the red glasses up to 2 percent, and the chromaticity differences involved in those comparisons are probably much less than those present when the changes from 100 to 120 and 150 were made for the respective yellow and green medium glasses. (It follows, of course, that the close agreement shown in table 8 for the red standards is fortuitous.) The reason for the difference in the values for the lunar-white standards is uncertain.

Inspection of figures 1 to 6 would indicate that the original (1908) yellow and lunar-white standards would have a T_{2360} value considerably in excess of both the 1918 and the 1935 standards, but no certain differences are indicated by the data for the standards of the other colors. As already explained, it seemed inadvisable to attempt computations of T_{2360} from the 1908 data.

TABLE 8.—*Comparison of values of T_{2360} computed for values of $T_{RSA}=100.0$ from the 1918 specification, with similar values for $T_{AAR}=100.0$ computed from data on which the 1935 specification is based*

Color designation	T_{2360}		ΔT_{2360} (column 2 minus column 3)	Percentage of change in T_{2360} (column 4 divided by column 3, × 100)
	$T_{RSA}=100.0$ (1918)	$T_{AAR}=100.0$ (1935)		
Red	0.0662	0.0672	−0.0010	−1.5
Yellow	.268	.247	+.021	+8.5
Green	.129	.119	+.010	+8.4
Blue	.0203	.0221	−.0018	−8.1
Purple	.0134	.0124	+.0010	+8.1
Lunar white	.199	.189	+.010	+5.3

Question may also be raised as to the agreement of the ARA scale, as exemplified by the roundels endorsed by Mr. Mock in 1930, table 3, both with the 1918 RSA scale and with the 1935 AAR scale now in effect. This cannot be answered certainly without making spectral-transmission measurements on the roundels selected by Mr. Mock. However, if the values of T_{ARA} were assigned to these roundels by the same Corning observer as assigned the values of T_{ARA} for the six squares of each color, as given in column 3 of table 4, it may be concluded, by comparing the mean values of columns 3 and 4 of table 4, that the ARA and AAR scales are in close agreement. The differences are approximately 3 percent for the red, 2 percent for the yellow, and

[16] That is, hypothetical glasses having values of T_{RSA} or $T_{AAR}=100.0$.

1 percent or less for the glasses of the other colors. For the green, blue, purple, and lunar-white glasses, therefore, the 1930 ARA scale is in very close agreement with the 1935 AAR scale, and hence differs from the 1918 RSA scale by approximately the same values as are given in the last column of table 8. For the yellow glasses the ARA scale is intermediate between the RSA and AAR scales. For the red glasses the AAR scale appears intermediate between the other two, but the various data are too uncertain for any definite statement.

In conclusion, the authors wish to call attention to the pioneering work of the railroad signal engineers in color specification. No search of the literature has been made, but, so far as the authors are aware, the 1908 specification was the first effort, at least in this country, to place the colorimetric part of a purchase specification on a fundamental basis. This specification was the result of cooperation between the Railway Signal Association and Corning Glass Works. It followed logically the very excellent treatment given in a paper [17] entitled, The Roundel Problem, by Wm. Churchill of Corning Glass Works.

This 1908 specification contained the following features essential to all complete and adequate colorimetric specifications:

1. It was based fundamentally on spectrophotometric analysis of the standards.

2. It specified tolerances within which the manufactured product must come.

That the spectrophotometric analyses and the colorimetric specifications were somewhat inadequate, judged by present-day criteria, in no wise detracts from the foresight and judgment leading to the formulation of a specification so far in advance of its time. The lack of spectrophotometric precision was largely remedied in the 1918 specification, but the adequate colorimetric specification of the tolerances had to wait until first the Optical Society of America [18] and then the International Commission on Illumination [19] had set up computational procedures and data suitable for such purpose.[20] It is interesting to note, however, that the "mixture diagram", so essential in specifying the chromatic properties of signal lights, was illustrated in colors and used by Dr. Churchill in his study of the characteristics of signal glassware, to which reference has just been made.

WASHINGTON, March 28, 1939.

[17] Presented at the Ninth Annual Meeting of the Railway Signal Association, Niagara Falls, N. Y., October 10–12, 1905.

[18] Report of Committee on Colorimetry for 1920–21, L. T. Troland, Chairman, J. Opt. Soc. Am. and Rev. Sci. Instr. *6*, 527 (1922).

[19] Proceedings of the Eighth Session, Cambridge, p. 19 (1931).

[20] This will be treated in the next paper.

U. S. Department of Commerce National Bureau of Standards

RESEARCH PAPER RP1210

Part of Journal of Research of the National Bureau of Standards, Volume 22, June 1939

DEVELOPMENT OF A FIBROUS TEXTURE IN COLD-WORKED RODS OF COPPER

By Herbert C. Vacher

ABSTRACT

Mono- and bicrystalline rods of copper were subjected to different degrees of cold-swaging and were examined with X-ray diffraction and metallographic methods. The results indicate that swaging causes the crystals to rotate until either an octahedral or a cubic axis becomes parallel with the rod axis. Whether the crystal assumes the octahedral or the cubic orientation depends upon which axis initially formed the smaller angle with the rod axis. Crystals approaching the octahedral orientation developed secondary crystals, after approximately 60-percent reduction in area. On further swaging, these secondary crystals approached the cubic orientation. Crystals initially approaching the cubic orientation remained one crystal after 95-percent reduction in area.

CONTENTS

	Page
I. Introduction	651
II. Procedures and results	652
1. Material and swaging	652
2. Changes in orientation resulting from swaging	653
3. Appearance of the ends of swaged rods	655
4. Metallographic examination	656
5. Orientations of secondary crystals	657
III. Discussion	662
1. Manner of changing the orientation of a copper crystal by swaging	662
2. Bending of slip planes and a possible origin of secondary crystals	664
3. Fibrous texture of cold-worked rods	665
IV. Summary	667
V. References	667

I. INTRODUCTION

X-ray diffraction patterns indicate that a severely cold-worked metal consists of small crystal fragments called crystallites. The ultimate size of the crystallite is of the order of 10^{-5} cm and is independent of the cold-working process. However, if the metal is a rod whose diameter has been reduced more than about 30 percent by cold-working, the crystallites are found to be in a position where a particular crystallographic axis is more or less parallel to the rod axis. Other axes of the crystallites are randomly oriented in respect to a direction perpendicular to the rod axis. This type of structure is referred to usually as a fibrous texture and is developed from crystals that initially were randomly oriented. The particular axis, however, that is parallel to the rod axis is not always the same for different metals, for example, in rods of iron or aluminum a dodecahedral axis

and an octahedral axis, respectively, are parallel to the rod axis. Some metals, such as copper, gold, and silver, produce a fibrous texture in which some crystallites have an octahedral axis and others have a cubic axis parallel to the rod axis.

The microstructure of a cold-worked rod shows that crystals initially equiaxed are elongated in the direction of the rod axis and resemble thread-like fibers. The structure within the individual fiber is homogeneous as far as can be ascertained from the literature, that is, the banded structure frequently observed in the crystals of metals cold-worked by flat rolling evidently is not common in round rods. Therefore, it appears that a cold-worked rod consists of fibers which are composed of small crystallites having a preferred orientation.

In copper rods where the fibrous texture consists of two orientations, an octahedral axis or a cubic axis parallel to the rod axis, each fiber must represent one of these orientations. There has been no experimental work to verify this conclusion or to indicate how these apparently stable orientations are developed. In order to supply this information, it is necessary to show the history of the changes in structure occurring when crystals with different orientations are elongated into fibers. This has been done by swaging large crystals of copper and determining the structure after different degrees of cold-work with the usual metallographic and X-ray-diffraction methods.

II. PROCEDURES AND RESULTS

1. MATERIAL AND SWAGING

Electrolytic copper of wire-bar purity was melted in a graphite crucible and with an Arsem furnace. The crucible was shaped to form rods ⅜ in. in diameter and 6 in. long. This procedure produced oxygen-free rods of copper which were then converted by the Bridgman [1] [1] method into rods consisting of one or a few large crystals. To do this, several of the rods were placed in close-fitting holes drilled in a cylinder of graphite and then lowered slowly (about 4 in. per hour) through a furnace maintained at approximately 1,100° C. The resulting rods were 0.337 in. in diameter and usually consisted of from one to four crystals running approximately parallel to the rod axis. Four rods were used in this investigation, two rods each consisting of one crystal and two rods each consisting of two crystals. Both crystals of each bicrystalline rod extended the full length of the rod, so that a cross section always showed two crystals.

Each of the rods was cold-swaged progressively through 19 tapered dies to a reduction in area of approximately 95 percent. Specimens, representing reductions in area of approximately 30, 60, 80, and 95 percent, were cut from the rods and used for examination with the microscopic and X-ray-diffraction methods. Table 1 shows the various steps that were employed in reaching each of the above stages in reduction.

[1] Figures 1 to 9 in brackets indicate the literature references at the end of this paper.

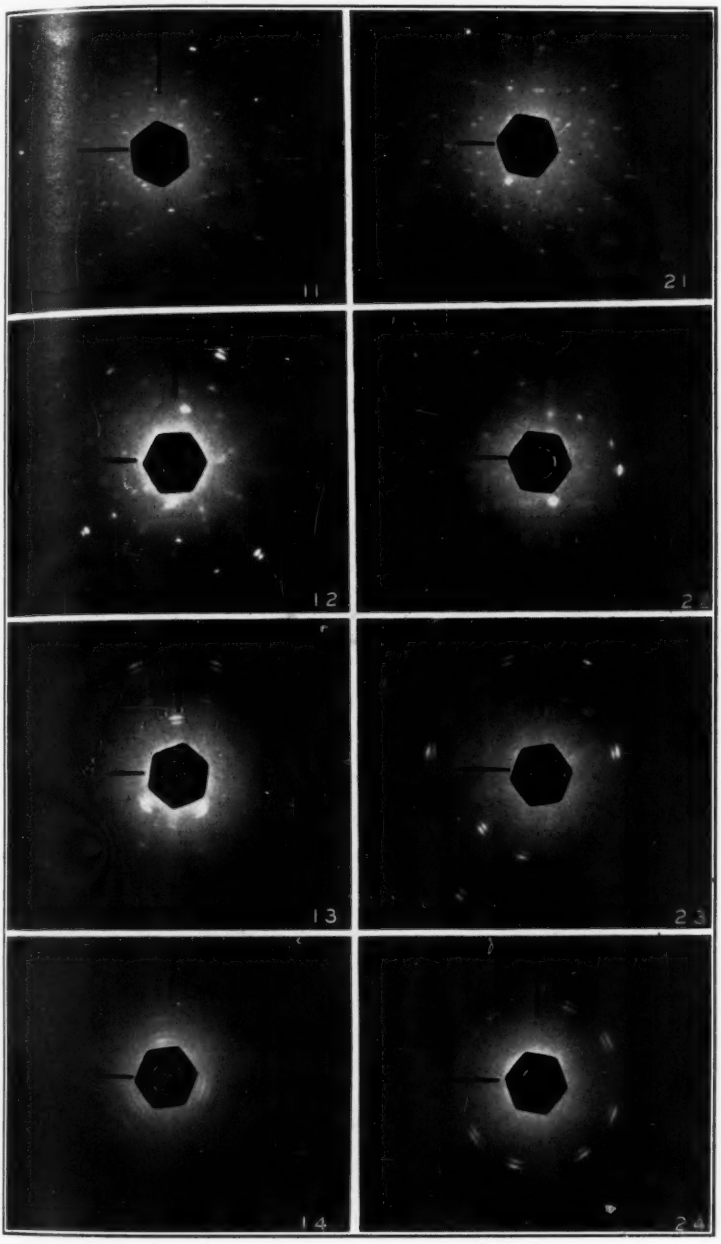

FIGURE 1.—*"Back-reflection" diffraction patterns showing the changes in orientation of monocrystalline rods 1 and 2 after increasing degrees of swaging.*

The first and second digits of the number in the lower right corner of the patterns are the rod number and the identification number shown in table 1, respectively. Unfiltered molybdenum radiation; 28 kvp; 1- by 6-cm pinhole; 3.0-cm film-to-specimen distance.

UNIV. OF MICH.

TABLE 1.—*Dies used in obtaining different degrees of swaging*

Identification number	Diameter of dies	Approximate reduction in area
	in.	%
1		0
2	0.320, 0.305, 0.290, 0.275	30
3	0.265, 0.255, 0.245, 0.235, 0.225, 0.205	60
4	0.195, 0.175, 0.160, 0.145, 0.130	80
5	0.115, 0.100, 0.085, 0.070	95

2. CHANGES IN ORIENTATION RESULTING FROM SWAGING

Patterns indicating diffractions from an area near the center of a crystal, shown in cross sections of the rods, were made by the back-reflection method after deeply etching the rods with diluted nitric acid to remove any effects resulting from their preparation. In making these patterns the collimated X-ray beam was parallel to the rod axis. The source of radiation was a Coolidge tube with a molybdenum target operated at approximately 28 kv. Figure 1 shows the patterns obtained from monocrystalline rods 1 and 2 after different degrees of swaging. Both series of patterns show similar differences in the diffraction spots with increasing degrees of cold-working. However, it is easily seen that the spots in patterns obtained from rod 1 approach an arrangement of threefold symmetry, and those in the patterns obtained from rod 2 approach an arrangement of fourfold symmetry. This indicates that the orientations of the monocrystalline rods 1 and 2 as a whole have changed, so that in the case of rod 1 an octahedral axis is parallel to the rod axis, and in the case of rod 2 a cubic axis is parallel to the rod axis.

The orientation of the crystals after different degrees of swaging was computed from the patterns shown in figure 1 and similar patterns obtained from the crystals in the bicrystalline rods. For patterns of the type shown as 11, 12, 21, and 22, figure 1, Greninger's method [2] was used. In this method a specially constructed graph is used to determine the angles between spots or zonal curves on a back-reflection pattern. Then, by comparing a number of these angles with the angles between crystallographic planes, the spots on the pattern can be identified and the orientation determined. However, for patterns such as 13 and 14, which do not show the characteristic zonal curves of the Laue pattern, a slightly different method was required. The latter patterns show the range of orientations (indicated by the length of the circular arcs) of the crystallites around the rod axis. The average orientation of these crystallites in respect to the rod axis is what is required. This can be obtained accurately by constructing a pole figure. However, when the range of orientations is small, as apparently is the case of the crystallites represented by patterns 13 and 14, the average orientation can be determined approximately by the following procedure:

The pairs of arcs in patterns 13 and 14 are diffractions of the K alpha doublet, and, consequently, the corresponding diffracting planes, can be identified. This is conveniently done by making a drawing showing the diffraction rings corresponding to all of the possible planes that could register diffractions of the K alpha doublet on a 5 by 7 film at the film-to-specimen distance used in obtaining the diffraction patterns. Then, by placing the film over the drawing, the

arcs are identified by their coincidence with the rings of the drawing. The centers of the identified arcs then are plotted stereographically, and the angle of rotation [3] is found which brings corresponding poles of a standard projection in best agreement with the plotted poles. This angle of rotation then is used in locating the cubic, octahedral, and dodecahedral poles. The orientations of the crystals in rods 1, 2, 3, and 4, before and after different degrees of swaging, are shown in table 2.

TABLE 2.—*Orientations of the crystals in rods 1, 2, 3, and 4 after different degrees of swaging*

Specimen number	Reduction in area	Angles between rod axis and crystallographic axis			Specimen number	Reduction in area	Angles between rod axis and crystallographic axis		
		Cubic	Dodecahedral	Octahedral			Cubic	Dodecahedral	Octahedral
	Percent	*Degrees*	*Degrees*	*Degrees*		*Percent*	*Degrees*	*Degrees*	*Degrees*
11	0	40	24	16	31 B[1]	0	40	6	31
12	30	48	30	7	32 B	30	38	14	25
13	60	50	33	4					
14	80	55	35	0	41 A	0	15	32	46
					42 A	30	9	36	47
21	0	17	30	39	43 A	60	8	37	48
22	30	10	36	45					
23	60	5	41	50	41 B	0	49	31	6
24	80	0	45	55	42 B	30	51	33	4
					43 B	60	54	34	1
31 A[1]	0	18	29	38					
32 A	30	10	36	45					
33 A	60	6	39	49					

[1] A and B indicate the two crystals in the bicrystalline rods.

The results show that an 80-percent reduction in area caused an octahedral axis to become parallel to the rod axis in the case of rod 1 and a cubic axis in the case of rod 2. Figure 2 shows the orientations of the rod axis after different degrees of swaging. They lie approximately on a great circle, which indicates that the final orientation resulted from a rotation about one axis. Rod 3 was a bicrystalline rod, crystal A initially having a cubic axis inclined to the rod axis by 18 degrees, and crystal B initially having a dodecahedral axis inclined to the rod axis by 6 degrees. (See specimens 31 A and 31 B, table 2.) The change in orientation of crystal A was similar to that of the single crystal of rod 2. Long diffuse spots made orientation determinations uncertain for crystal B after reductions in area of more than 30 percent. However, the orientations at 30-percent reduction show that the angle between the dodecahedral axis and the rod axis had increased and the angle between the octahedral axis and the rod axis had decreased. Therefore, the change was similar to that which occurred to the crystal of rod 1. Rod 4 was also a bicrystalline rod, in which crystal A (specimen 41 A, table 2) had an initial orientation similar to that of the crystal of rod 2, and crystal B (specimen 41 B, table 2) had an initial orientation similar to that of rod 1. The changes in orientation resulting from 30- and 60-percent reduction in area indicate that swaging produced a tendency for the octahedral axis in crystal B and the cubic axis in crystal A to become parallel to the rod axis. The fact that the changes in orientation of the crystals in the bicrystalline rods were similar to the changes in the monocrystalline rods

strongly suggests that the changes are independent of crystal boundaries and therefore independent of grain size.

The results, as a whole, indicate that when a copper rod consisting of one or more crystals is deformed by swaging, the crystals rotate until either an octahedral or a cubic axis becomes parallel to the rod

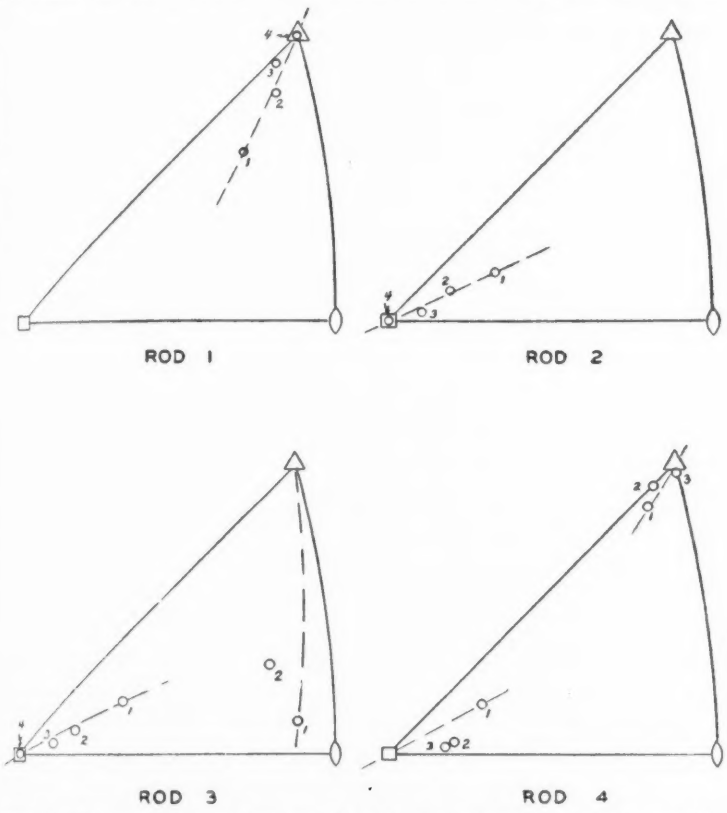

FIGURE 2.—*Stereographic projections showing the orientations of the crystals in rods 1, 2, 3, and 4 after different degrees of swaging.*

The small circles represent the rod axis. The numbers correspond to the identification numbers of table 1.

axis, the choice depending upon which of the two axes initially formed the smallest angle with the rod axis.

3. APPEARANCE OF THE ENDS OF SWAGED RODS

By continued swaging of monocrystalline rods 1 and 2, the ends of the rods developed shapes that are related to their ultimate orientations. These characteristic appearances were developed, in each stage of swaging, at the ends of the rods which, before swaging, had been cut off flat and perpendicular to the rod axis. Figure 3, photographs 1 and 2, show these characteristic surfaces developed at the ends of rods 1 and 2, respectively, in swaging from 60- to 80-percent reduction in area. The depression at the end of rod 1 resembles the inverted corner of a tetrahedron and has a threefold symmetry. It should be

recalled that the diffraction pattern 14, figure 1, which corresponds to this rod and degree of swaging, also has a threefold symmetry. The depression at the end of rod 2 resembles the inverted corner of an octahedron and has a fourfold symmetry. The corresponding diffraction pattern of rod 2 (24, fig. 1) also has a fourfold symmetry. These characteristic surfaces could be recognized at the ends of rods 1 and 2 at stages representing smaller amounts of cold-working, that is, from 0- to 30- or from 30- to 60-percent reduction in area. In swaging from 80- to 95-percent reduction, rod 1 did not develop the characteristic surface observed at lower degrees of swaging, but rod 2 did. The reasons for the difference in the behavior of the two rods become apparent when their macrostructures are examined.

Figure 3, photograph 3, shows the surface developed by a slight reduction in area of bicrystalline rod 4, which had been previously swaged to a reduction of 60 percent. Swaging has caused the larger crystal in the cross section to flow beyond the smaller crystal. Further, the surface of the larger crystal resembles the surface developed at the end of rod 2 (photograph 2) with one quadrant occupied by the smaller crystal. The orientations of the large and small crystals correspond, respectively, to specimens 43*A* and 43*B*, table 2. These orientations are approximately the same as rod 2 and rod 1, respectively, after a 60-percent reduction in area (see specimens 23 and 13, table 2). Therefore, photograph 3 indicates that crystals having orientations similar to rod 1 are more resistant to deformation by swaging than crystals having orientations similar to rod 2. This conclusion was supported by the observation that a single pass through each of the swaging dies of stage 5 reduced the diameter of rod 1 from 0.141 to 0.080 in., whereas similar treatment of rod 2 reduced its diameter from 0.140 to 0.072 in. These results indicate qualitatively that rod 1 was more resistant to deformation by swaging than rod 2.

The correlations between the characteristic surfaces developed by swaging, the relative resistance of crystals to deformation, and their orientations indicate that the manner of the distortion is related to the crystal structure. This will be discussed after presenting the remainder of the results.

4. METALLOGRAPHIC EXAMINATION

The macrostructures of cross sections and longitudinal sections of rods 1, 2, and 3, at various stages of reduction, are shown in figure 4. The light and dark areas shown in the sections of the monocrystalline rod 1 indicate that the rod contains portions differing in orientation. Similar areas, referred to as deformation bands, have been found in the crystals of rolled copper plate [4] and in compressed specimens of iron that were originally monocrystalline [5]. Inasmuch as these areas indicate differences in orientation, they can be considered as representing sections of crystals, some of which were formed as a result of the deformation.

Diffraction patterns from the central portion of rod 1 have shown a progressive change in orientation. This portion of the rod, therefore, is part of the original crystal, and the other crystals near the periphery have formed from it. In order to distinguish between the original crystal and the new crystals, the former is referred to as a primary crystal and the latter as secondary crystals.

FIGURE 3.—*Characteristic surfaces at the ends of the monocrystalline rods 1 and 2 and the bicrystalline rod 4 after swaging.*

In the monocrystalline rods the surface metal flowed more than the central metal, thus forming a depression. In the bicrystalline rod the larger crystal flowed more than the smaller.

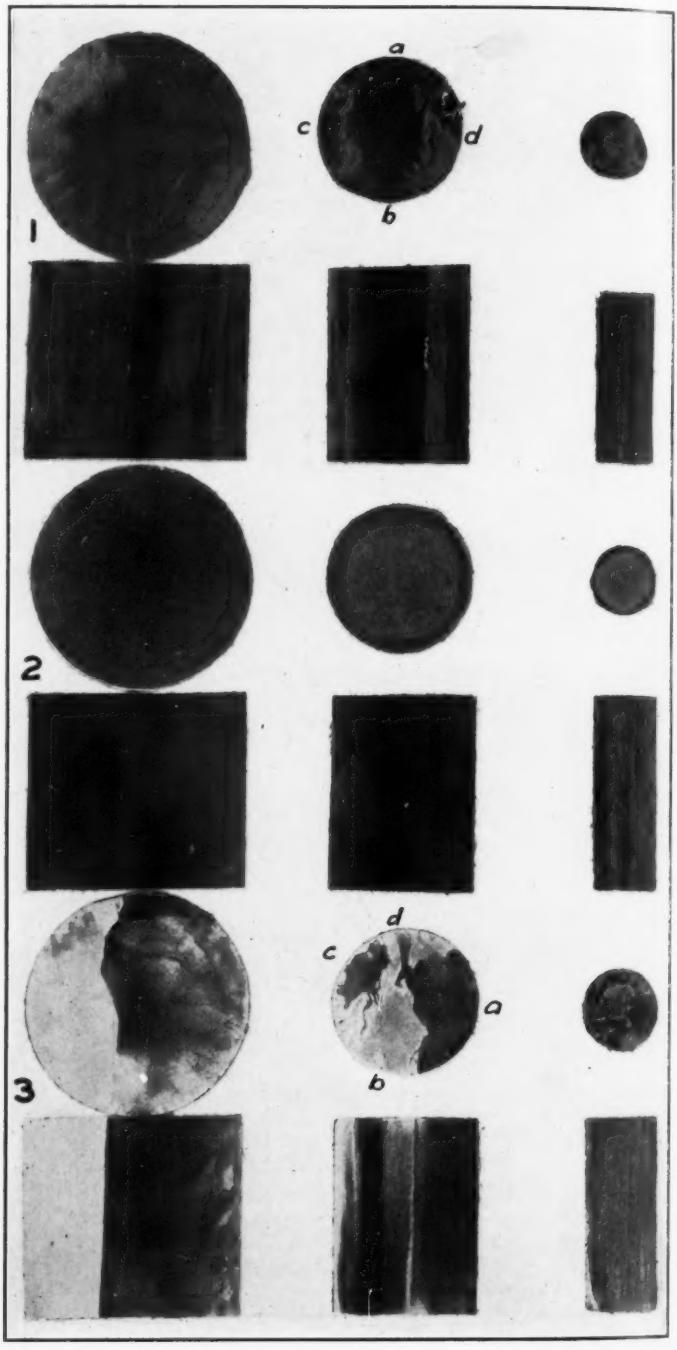

FIGURE 4.—*Macrostructure of monocrystalline rods 1 and 2 and bicrystalline rod 3 at different stages in swaging.*

Secondary crystals, light and dark areas in No. 1, with different orientations from that of the original crystal, developed during swaging. Rod 2, with different initial orientation from that of rod 1, did not develop secondary crystals during swaging. The crystal at the left of the bicrystalline rod 3 followed the behavior of monocrystalline rod 1, the other crystal resembled monocrystalline rod 2. Specimens etched deeply with 10-percent aqueous ammonium persulfate, ×5, with a ring illuminator.

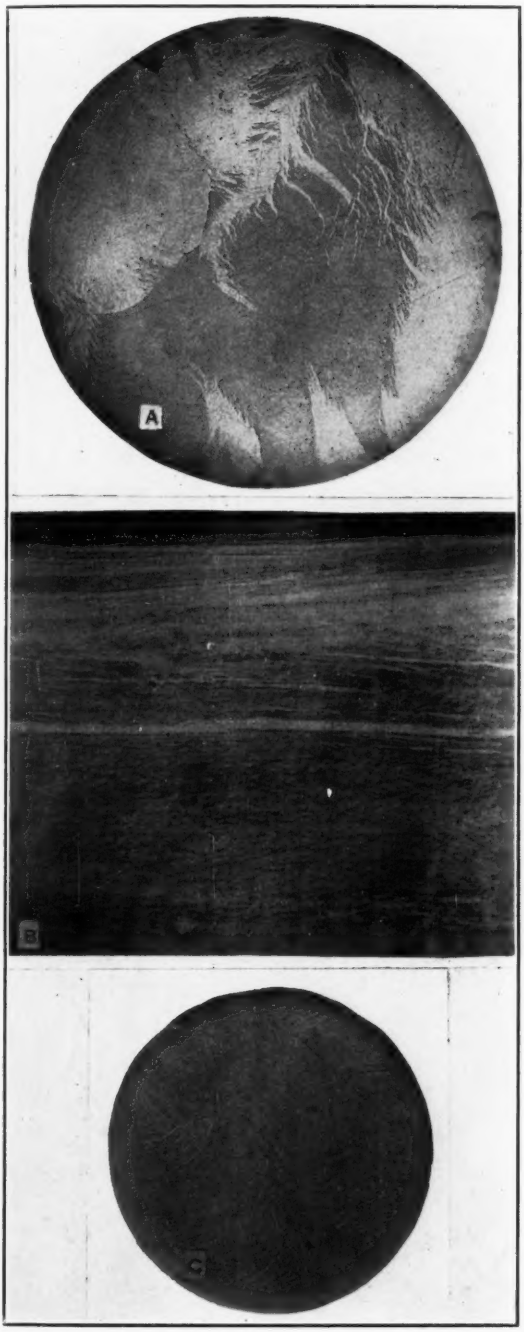

FIGURE 5.—*Typical microstructure of copper crystals after swaging to a 95-percent reduction in area.*

Etched with 10-percent ammonium persulfate. *A*, cross section of rod 3, ×40; *B*, longitudinal section of rod 3, ×40; *C*, cross section of rod 2, ×30.

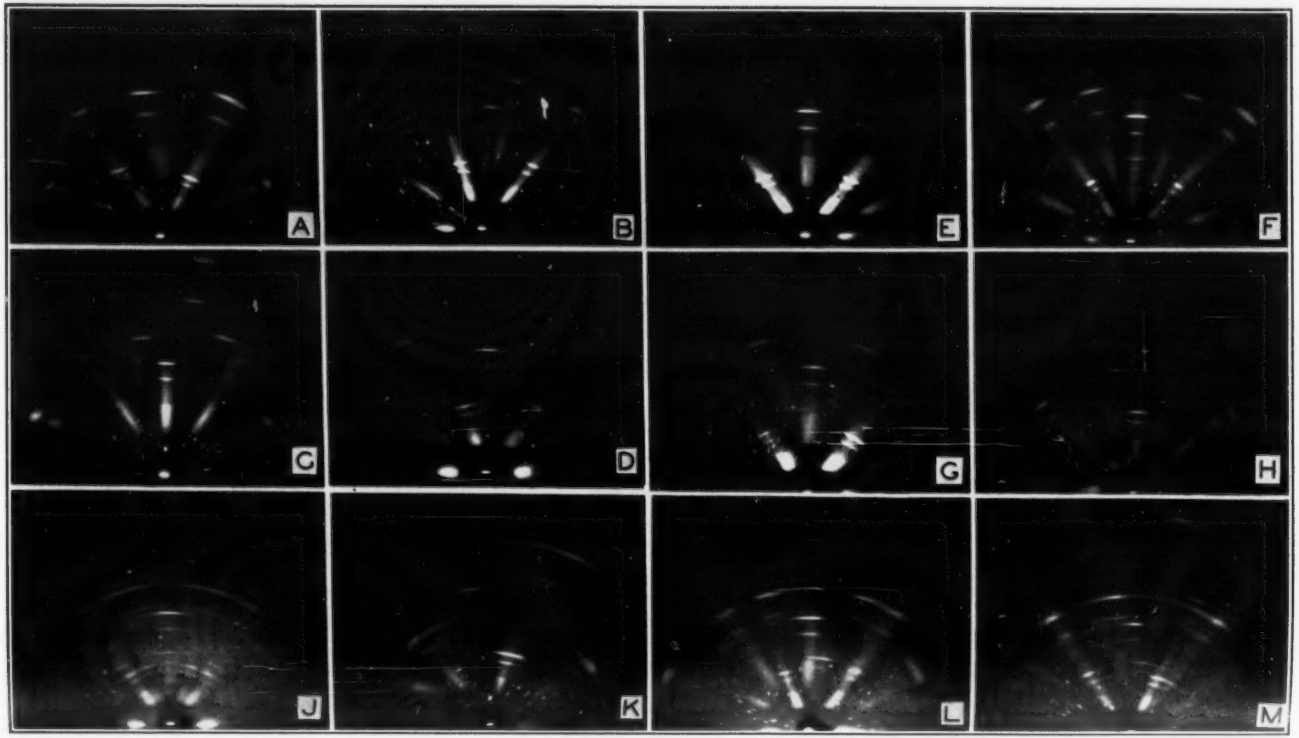

FIGURE 7.—*Typical patterns obtained by means of the "reflection" method from monocrystalline and bicrystalline rods of copper swaged to 80- and to 95-percent reduction in area.*

Unfiltered molybdenum radiation, 28 kvp, 1 mm by 6 cm pinhole, 4.5 cm film-to-specimen distance.

The macrostructure of cross sections of the monocrystalline rod 2 after 60- and 80-percent reductions indicates that it has remained one crystal, and the diffraction patterns 23 and 24, figure 1, indicate that a cubic axis is parallel or nearly so to the rod axis. The orientation of the crystal on the right side of the cross sections of rod 3, figure 4, is approximately the same as the monocrystalline rod 2 after both rods were reduced 60 percent, and like the monocrystalline rod 2, the cross sections of this crystal after 80- and 95-percent reductions show only one crystal. The macrostructure of the crystal on the left side of the cross section, whose orientation after a 30-percent reduction was similar to the initial orientation of the monocrystalline rod 1, shows primary and secondary crystals after 80- and 95-percent reductions, as did the macrostructure of rod 1.

Figure 5 (*A* and *B*) shows the microstructure of cross and longitudinal sections, respectively, of the bicrystalline rod 3 after 95-percent reduction. The light area in the upper left side of the cross section corresponds to one of the two original crystals, and the remainder of the cross section, containing the jagged crystals, corresponds to the other original crystal. Whenever a microscopic examination of a cross section showed that the original crystal had been converted into several crystals, their boundaries were jagged and irregular, as shown in micrograph *A*, figure 5. It appears that crystals formed during the deformation start at the periphery of the rod and grow in an irregular manner toward the center of the rod. This suggests that the newly formed crystals originate in portions of the rod where the distortion is greatest.

Microscopic examination did not show more than one crystal in the cross sections of the monocrystalline rod 2. However, it did show a heterogeneous structure after 95-percent reduction. This structure is shown in micrograph *C*, figure 5, and consists of curved narrow bands having two principal directions forming an angle of approximately 90 degrees. Inasmuch as a cubic axis is parallel to the rod axis, this suggests that the curved bands are related to certain planes in the original crystal that have been bent as a result of the deformation.

The presence of a fiber-like structure in the longitudinal section of rod 2 after 95-percent reduction (fig. 4), the absence of evidence of more than one crystal in the cross section, and the indication of curved planes are important and show that swaging has caused some of the crystallographic planes to bend about axes that are parallel to the rod axis.

The results of the metallographic examination have shown that crystals which rotate so that an octahedral axis tends to become parallel to the rod axis are converted into primary and secondary crystals at a reduction in area of approximately 60 percent. In addition, it has shown that crystals which rotate so that a cubic axis becomes parallel to the rod axis remain one crystal after 95-percent reduction, although the crystallographic planes probably are bent.

5. ORIENTATIONS OF SECONDARY CRYSTALS

In order to obtain more definite information on the orientations of the secondary crystals, diffraction patterns were made by the "reflection method" in which the specimen is mounted so that the surface is grazed by the collimated beam of X-rays. The film is usually flat

and is placed perpendicularly to the collimated beam on the side of the specimen opposite the X-ray tube at a convenient distance (4.5 cm for this work).

The rotational diagram, figure 6, shows the pattern of diffraction spots obtained by the "reflection method," using monochromatic radiation, when a face-centered cubic crystal is rotated with its axis of rotation perpendicular to the X-ray beam and coinciding with either an octahedral or a cubic axis. In figure 6 the axis of rotation is parallel to the line *AB*. The center represents the undiffracted beam, and the solid and dashed rings (Debye rings) represent the loci of diffractions of the *K* alpha radiation and the peak of the white

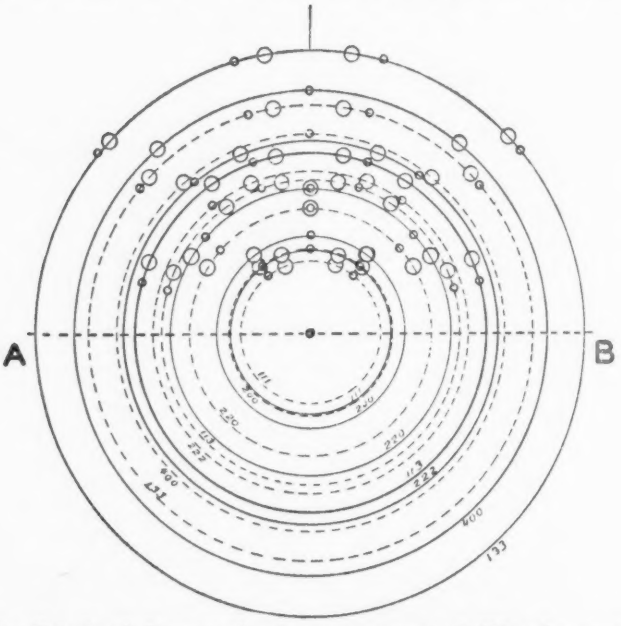

FIGURE 6.—*Rotational diagram showing arrangement of diffraction spots from a face-centered cubic crystal.*

Large and small circles on the concentric rings represent rotations about an octahedral and a cubic axis, respectively.

radiation, respectively. The large and small circles on the rings show the locations of the diffracted beams from the octahedral and cubic rotations, respectively. The correspondence of the spots on this diagram with the spots on a diffraction pattern obtained from a polycrystalline copper rod, when the rod axis was perpendicular to the X-ray beam, indicates that some of the crystals are oriented with an octahedral axis and others with a cubic axis parallel to the rod axis. The pattern *J*, figure 7, is a pattern of this type and was obtained from a cold swaged rod of polycrystalline copper. Previous to swaging, this rod was cut from a cold-drawn rod, annealed at 400° C. for 15 minutes, then swaged to 95-percent reduction in area. Before making the pattern the specimen was deeply etched with diluted nitric acid. This procedure was followed for all subsequent patterns. The method of matching corresponding spots in a diffraction pattern

with spots in a rotational diagram was used by Schmid and Wassermann [6] when studying the textures of wires. It has been used in this investigation to determine the orientations of crystals in rods 1, 2, and 3 after swaging to reductions in area of 80 and 95 percent.

The patterns shown in figure 7, with the exception of *J*, are typical of the patterns obtained from rods 1, 2, and 3 after 80- and 95-percent reductions in area. The patterns *A*, *B*, *C*, and *D* contain spots corresponding only to the large circles of the rotational diagram, figure 6. This indicates that the crystals irradiated by the primary beam are oriented with an octahedral axis parallel to the rod axis. It can be seen also that some of the large circles in the rotational diagram are not represented in the diffraction pattern. This indicates that the crystals, in addition to having an octahedral axis parallel to the rod axis, have other axes that approximately are oriented in respect to a direction perpendicular to the rod axis. The orientations of these crystals would be equivalent to a rotation, of less than 120 degrees, of a single crystal about an octahedral axis which is parallel to the rod axis. Rotation of 120 degrees about an octahedral axis would reproduce the orientation of the crystal. The orientations represented by patterns *A*, *B*, *C*, and *D* are referred to as type *A*. The patterns *E*, *F*, *G*, and *H* contain spots corresponding only to the small circles of the rotational diagram and, like the patterns *A*, *B*, *C*, and *D*, some of the small circles are not represented by spots in the diffraction patterns. The orientations of the crystals represented by the patterns *E*, *F*, *G*, and *H* therefore are equivalent to a rotation, of less than 90 degrees, of a single crystal about a cubic axis which is parallel to the rod axis. A rotation of 90 degrees about a cubic axis would reproduce the orientation of the crystal. The orientations represented by patterns *E*, *F*, *G*, and *H* are referred to as type *B*. The pattern *K* represents orientations intermediate to types *A* and *B* and is referred to as type *C*. This particular pattern indicates orientations such that a cubic axis of the crystals is inclined to the rod axis by about 15 degrees. The patterns *L* and *M* indicate that the beam of X-rays irradiated crystals having orientations corresponding to types *A* and *C*.

The orientations of crystals that would produce patterns of the types *A* and *B* are shown in the projections of figure 8. Projection *A* corresponds to type *A* with an angle of rotation of about 40 degrees [2] about the rod axis. This value is obtained from the arc length of the spots in pattern 14, figure 1. The angle of rotation about axes perpendicular to the rod axis is 15 degrees and is the average value of the arc length of the spots shown in the patterns of figure 7. Projection *B* corresponds to type *B* and shows the angle of rotation about the rod axis to be 30 degrees. This value represents the arc length of the spots in pattern 24, figure 1. The angle of rotation about axes perpendicular to the rod is 15 degrees, the same as projection *A*. It is not to be implied that orientations of types *A* and *B* have definite angles of rotation such as are indicated by projections *A* and *B*. The projections represent in a general way the range of orientations that could produce patterns of the type shown in patterns *A* to *H*, figure 7. Actually, the range of orientations probably would show a larger angle of rotation around the rod axis as the distance between the

[2] The angle of rotation around the rod axis is equivalent to the arc length of the areas containing the poles, and the rotation about an axis perpendicular to the rod axis is equivalent to the arc width of the areas containing the poles.

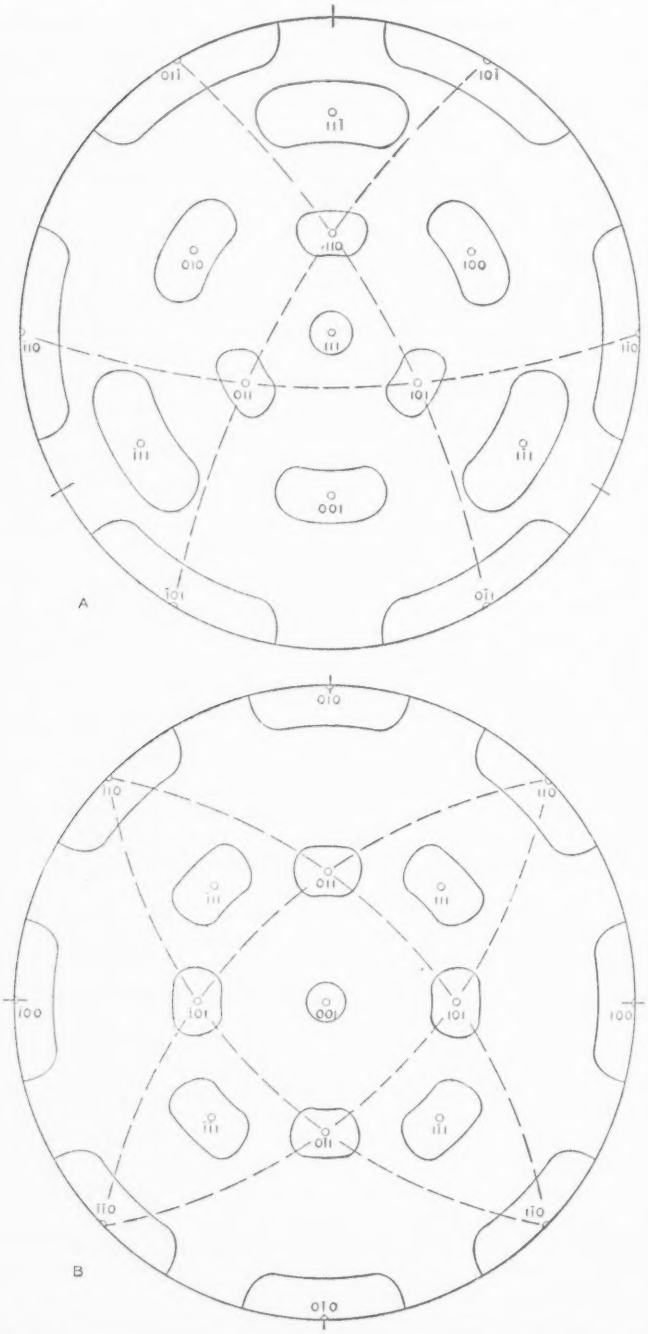

FIGURE 8.—*Stereographic projections showing the octahedral orientation, A, and the cubic orientation, B.*

The rod axis is normal to the projection planes.

center of the rod and the area examined increases. The angle of rotation around the rod axis would increase also as the percentage reduction in area increases.

The macrostructure of a cross section of rod 1 after an 80-percent reduction, figure 4, shows that the primary crystal extends to the periphery at *a* and *b*. Diffraction patterns obtained from areas on the surface of the rod corresponding to *a* and *b* indicated orientations of type *A*. It may be confusing to imply that a crystal seen in the macrostructure has more than one orientation, but this means simply that a macroscopic crystal consists of crystallites with a definite range of orientations, as revealed by diffraction patterns. In order to avoid confusion, the apparent crystal seen in the macrostructure is referred to as a crystal, and its orientation is the average orientation of the crystallites of which it consists. In the case of crystals having orientation ranges of the types *A* and *B*, the average orientation is respectively an octahedral axis and a cubic axis parallel to the rod axis; see projections *A* and *B*, figure 8. Diffraction patterns representing areas corresponding to the secondary crystals of rod 1, shown as *c* and *d* in figure 4, indicated orientations of the type *C*. The experimental set-up and the smallness of areas corresponding to *a*, *b*, *c*, and *d* did not permit a similar correlation of diffraction patterns with macrostructure after 95-percent reduction. However, numerous patterns made with the specimens rotated slightly about the rod axis after each exposure indicated orientations of types *A* and *B*, although some patterns were still a mixture of types *A* and *C*. These results indicate that swaging secondary crystals having orientations of the type *C* changes the orientation into type *B*.

Patterns obtained from rod 2 after 80- and 95-percent reductions indicated orientations only of type *B*. This might be expected as the macro-structure of the cross sections at these reductions, figure 3, did not show any secondary crystals. Patterns obtained from areas on the periphery of the rod corresponding to mark *a*, figure 4, of the bicrystalline rod 3 after an 80-percent reduction indicated orientations of the type *B*. It has been pointed out that this crystal has an orientation similar to the monocrystalline rod 2, and also that it did not show any secondary crystals. Patterns obtained from areas corresponding to *b* indicated a mixture of types *A* and *C*. Areas corresponding to *c* and *d* indicated types *A* and *C*, respectively. Numerous patterns of this rod after a 95-percent reduction, with the specimens rotated slightly after each exposure, indicated orientations of types *A* and *B*. These results indicate that the crystal of the bicrystalline rod which developed secondary crystals was similar to the crystal of rod 1.

The results as a whole indicate that crystals initially having a cubic axis approximately parallel to the rod axis are "stable" during deformation by swaging, whereas crystals whose orientation is changing, so that an octahedral axis tends to become parallel to the rod axis, are unstable. These "unstable" crystals develop secondary crystals with orientations of type *C*, that is, intermediate between having an octahedral axis or a cubic axis parallel to the rod axis. Further distortion by swaging changes the initial orientation of the secondary crystal to an orientation consisting of a cubic axis parallel to the rod axis. The ultimate state, therefore, of a crystal having an initial orientation such that an octahedral axis tends to align itself with the rod axis is a mixture of crystals, each having an octahedral axis or a cubic axis parallel to the rod axis.

III. DISCUSSION

1. MANNER OF CHANGING THE ORIENTATION OF A COPPER CRYSTAL BY SWAGING

It is generally conceded that metallic crystals can be distorted plastically only by slipping on certain crystallographic planes and in certain crystallographic directions. Investigations [7, 8] have shown that when a distortion by tensile or compressive stress occurs in this manner, the crystal changes its initial orientation to an orientation which is stable to a further distortion. In the case of face-centered cubic crystals, such as copper, the distortion takes place on octahedral planes and in dodecahedral directions. There are four octahedral planes in a cubic crystal and three dodecahedral directions in each octahedral plane, and, therefore, there are 12 possible slip systems.

The first stage in the distortion of a copper crystal by a tensile stress involves slip in the system having the greatest resolved shear stress. As the distortion proceeds, the orientation of the crystal changes in a way that is equivalent to rotating the direction of slip so that it tends to become parallel to the tensile stress. This rotation will in time bring the crystal to a position where another slip system has the same resolved shear stress as the active system. The second stage of the distortion then proceeds by an equal amount of slip on each of the active slip planes, until the two active slip directions and the tensile stress direction lie in the same plane, that is, until the icositetrahedral direction [112] coincides with the tensile-stress direction. The change in orientation accompanying the second stage is equivalent to a rotation about a dodecahedral axis. Further distortion does not change this orientation. It is evident, then, that a copper crystal distorted by a tensile stress changes its initial orientation to a stable orientation in a manner equivalent to rotation about two axes.

The distortion of a copper crystal under compressive stress also involves two stages. The first stage is accomplished by slip in the system having the greatest resolved shear stress, and by a change in orientation that is equivalent to a rotation causing a normal to the active slip plane to become more parallel to the compressive stress. The rotation continues until another slip system has the same resolved shear stress as the active system. The distortion then commences the second stage, which is accomplished by two slip systems. The change in orientation during the second stage is equivalent to a rotation about a cubic axis, until the normals of the two active slip planes and the compressive stress direction are in the same plane. In this position a dodecahedral axis coincides with the compressive stress direction. A further distortion does not change this orientation, and, like the distortion by a tensile stress, it was attained in a manner equivalent to rotation about two axes.

The changes in orientation of a copper crystal resulting from a distortion by swaging are accomplished in a somewhat different manner from those resulting from simple tensile or compressive stress. It has been pointed out that the orientations of a copper crystal after different degrees of swaging lie on a great circle when plotted stereographically, as in figure 2. This means that the two stable orientations were attained in a manner equivalent to a rotation about one axis and indicates that the number of active slip systems operating

at the beginning of the distortion was the same as the number operating at the stable orientation, although the degree of activity of the different systems varied until the stable orientation was attained. The two stable orientations attained by swaging are shown in figure 8. The locations of the octahedral planes are shown as great circles (dashed); the dodecahedral directions are at the intersections of the octahedral planes.[3] It is evident that the octahedral planes and dodecahedral directions are symmetrically placed around the rod axis in both of these orientations. It is possible then that these stable orientations were attained by six slip systems symmetrically placed around an octahedral axis in the case of the octahedral orientation, figure 8*A*, and eight slip systems symmetrically placed around a cubic axis in the case of the cubic orientation, figure 8 (*B*).

The attainment of the two stable orientations by six and eight slip systems becomes more probable when they are correlated with the characteristic surfaces developed at the ends of the swaged monocrystalline rods 1 and 2. The short lines shown on the photographs 1 and 2 of figure 3 correspond to the short lines crossing the circumferences of the projections *A* and *B*, figure 8, respectively. It can be seen that the surfaces shown in figure 3 could be formed by slip in six slip systems in the case of the octahedral orientation and eight in the case of the cubic orientation. The fact that surfaces similar to these could be produced before the stable orientation was attained supports the contention that these slip systems were operating from the beginning of the distortion.

It is noteworthy that the arrangements of slip systems in the octahedral and cubic orientations have, respectively, a threefold and a fourfold symmetry to the direction of flow. This suggests that the direction of flow that is required by the deformation might be the factor determining the selection of active slip systems. If this be true, then the stable orientations of copper attained by swaging should be attained regardless of the kind of slip plane or slip direction, because any family of planes or directions has a threefold and fourfold arrangement about an octahedral axis and a cubic axis, respectively. Recent experiments by Barrett [5] appear to support this contention. In his experiments, monocrystalline disks of iron were compressed in such a way that the disc retained its circular shape throughout the compression. This manner of deforming a disk is similar to the deformation of a rod by swaging. In the case of the compressed disc the diameter is increased, and in the case of the swaged rod the diameter is decreased. The body-centered cubic crystals of alpha iron are known to distort by slipping on the dodecahedral (110), icositetrahedral (112), and the hexakis octahedral (123) planes and in an octahedral direction [111]. Barrett's results showed the same stable orientations for body-centered iron as are attained for face-centered crystals of copper, that is, an octahedral axis or a cubic axis parallel to the cylindrical axis of the specimen.

From this discussion the conclusion is drawn that, if the distortion of a crystal produces a cylindrical shape, it would be accomplished by slip systems symmetrical to an octahedral or a cubic axis, and this axis, on continued distortion, would become parallel to the rod axis. In the case of copper there are six slip systems symmetrical to an

[3] In the cubic system crystallographic directions are normal to their corresponding planes, that is, the cubic direction [100] is normal to the cubic plane (100), the dodecahedral direction [110] is normal to the dodecahedral plane (110), the octahedral direction [111] is normal to the octahedral plane (111), etc.

octahedral axis and eight slip systems symmetrical to a cubic axis. The results indicate that the crystals rotate until either an octahedral or a cubic axis becomes parallel to the rod axis, the choice depending upon which of the two axes initially formed the smallest angle with the rod axis. It is pointed out in a subsequent section of this paper that this conclusion does not hold when monocrystalline rods of iron are distorted by swaging.

2. BENDING OF SLIP PLANES AND A POSSIBLE ORIGIN OF SECONDARY CRYSTALS

Deformation by swaging produces a rod which is uniform in diameter, that is, the rod is a perfect circular cylinder. Therefore, in cold-working a monocrystalline rod by swaging, the distorted crystal is a perfect cylinder at all degrees of swaging. Obviously this shape cannot be produced perfectly, and the slip planes remain flat when there are a limited number of slip systems, as discussed in the preceding section. It is reasonable then to conclude that the slip planes which are initially flat become curved during swaging, and that the later stages are accomplished by curved surfaces slipping over one another. This kind of distortion has been called "bend gliding" (Biegegleitung) [8] and has been used to explain the asterism shown in Laue patterns of distorted crystals. Briefly the explanation is that during a distortion the metal between the slip planes is bent over a curvature sufficient to strain some of the interatomic bonds beyond their elastic limit, thereby causing the metal to break into blocks, called crystallites, having approximately the same orientation and each being a perfect crystal. Diffractions from the crystallites produce the asterism of the Laue patterns. If the distortion has been severe, the range of orientations of the crystallites is too large to produce the characteristic radial asterism but does produce a pattern consisting of spots elongated peripherally and arranged on concentric circles, as is shown in figure 7. From this explanation it is seen that the range of orientations of the crystallites is a measure of the amount of bending which the slip planes have undergone. The ranges of orientations of the crystallites in crystals distorted by an amount of swaging equivalent to a reduction in area of 80 to 95 percent have been shown in figure 8. The dimensions of the ranges indicate that the slip planes are curved more around an axis parallel to the rod axis than around an axis perpendicular to the rod axis. The results of the experiments with swaged crystals of copper therefore appear to be consistent with the conclusion that a distortion can be accomplished by the slipping of curved sheets of crystallites over one another.

Heretofore, the shape of the crystallites has not been considered. The shape becomes important when it is remembered that the sheets themselves as well as the directions of their movement must be related to certain crystallographic planes and directions. It seems that this condition can be satisfied, at least for the distortion of copper crystals by swaging, if the assumption is made that certain octahedral planes, spaced equally at a distance of the order of 10^{-5} cm are potential slip planes. Then a distortion sufficiently severe to produce slip on all of the potential slip planes parallel to the three octahedral planes that are symmetrical to an octahedral axis would divide the crystal into crystallites having a rhombohedral shape. The faces of a rhombohedron in this case would be octahedral planes and the

edges would be dodecahedral directions. It is more difficult to shear these unit rhombohedra than it is for them to slide over one another. Consequently, it follows that the more out-of-line they become the more necessary it would be for them to move in directions parallel to their edges.

However, it is interesting to note that each unit rhombohedron would contain two potential slip planes, and that, if slip should occur on these planes, the unit rhombohedron would be divided into two tetrahedra and one octahedron. These potential slip planes represent the only means of destroying the unit rhombohedron. Therefore, these planes must be considered a source of weakness for the unit rhombohedron. This gives a possible explanation for the origin of secondary crystals such as developed during the swaging of monocrystalline rod 1. It is quite possible that during swaging a unit rhombohedron would be rotated to a position where the stresses would be sufficient to cause a shear along the two potential slip planes. The results indicate that this would occur when the angle between a cubic axis of the rhombohedron and the rod axis was approximately 15 degrees. After a number of adjacent rhombohedra had been sheared this portion would begin to slip over the surfaces of the newly formed tetrahedra and octahedra. This kind of a distortion would be equivalent to a distortion by eight slip systems symmetrical to a cubic axis.

It is concluded, therefore, that crystals can be distorted by slipping over curved surfaces composed of crystallites whose surfaces and edges are the slip planes and slip directions in the undistorted crystal. This property gives the crystal a limited amount of plasticity in all directions, similar to the plasticity of amorphous substances, and at the same time permits the distorted crystal to retain the characteristics of a single crystal.

3. FIBROUS TEXTURE OF COLD-WORKED RODS

The structural changes taking place in the crystals of the bicrystalline rods are good examples of crystals behaving according to the conclusions stated in the preceding paragraphs. The flow of metal in each crystal was similar to the flow of metal in the rod as a whole, that is, the cross section was uniformly decreased as the length was increased, and the results showed that the orientation of each crystal was changed progressively to a stable orientation after diffraction patterns had indicated the crystals to be composed of crystallites. From this it is concluded that each crystal in a polycrystalline rod of copper behaves as one of the crystals in the bicrystalline rods. There is, however, a difference in respect to secondary crystals. So far as can be ascertained, secondary crystals are not found in the fiber-like crystals of cold-worked rods of polycrystalline copper.

The crystals of a polycrystalline rod of copper, cold-worked 60 percent or more, would be rotated to either an octahedral or a cubic orientation. If the crystals had been oriented randomly and had not developed secondary crystals, the ratio of the fiber-like crystals having the octahedral orientation to those having the cubic orientation would be equal to 1. Results of Schmid and Wassermann [6] show that this ratio is 1.5. The discrepancy in the two values might be explained on the basis that the material used by Schmid and Wassermann, in their wire-drawing experiments, had a slight degree of

preferred orientation, favoring the stable octahedral orientation, as a result of its previous treatment. It is known that the preferred orientation developed in cold-rolled plates of copper is not completely removed by annealing.

There are apparent exceptions to the conclusion that an octahedral or a cubic orientation is attained when the shape of the crystal produced during the distortion is a cylinder. It has been reported that cold-worked rods of aluminum have only the octahedral orientation[6]. Aluminum is a face-centered crystal; therefore, the slip planes and slip directions are the same as copper. These reported results indicate that a monocrystalline rod of aluminum having a cubic axis parallel to the rod axis would rotate to the octahedral orientation during swaging or would develop secondary crystals that would do likewise. This is not consistent with the results obtained from swaged crystals of copper.

Another exception is found in the work of Barrett [9], who showed that iron crystals of different orientations when swaged or drawn immediately developed numerous secondary crystals. The secondary crystals rotated away from their initial orientation, eventually reaching a stable orientation when a dodecahedral axis became parallel to the rod axis. The resulting state of the original crystal after a 90-percent reduction in area consisted of numerous secondary crystals having a dodecahedral axis parallel to the rod axis, and other axes randomly oriented in respect to a direction perpendicular to the rod axis. From these results, it was concluded that all of the crystals in polycrystalline rods behave in a similar manner, thus accounting for the fibrous texture found in iron rods. The present investigation indicates that the fibrous texture of iron rods differs from that of copper rods in respect to secondary crystals and to stable orientations. In iron rods the original crystals are converted into numerous secondary crystals that rotate to a dodecahedral orientation, whereas in copper rods the original crystals are rotated either to an octahedral or a cubic orientation.

The conclusion, that if the distorted shape was cylindrical, the active slip systems would be symmetrical to an octahedral axis or a cubic axis, which eventually becomes parallel to the cylinder axis, obviously is not correct for iron crystals that are swaged or drawn, although it appears to be correct for iron crystals that are deformed plastically by compression and for copper crystals that are swaged. There is a possible explanation for this apparent inconsistency. In swaging or drawing, the flow of metal is parallel to the rod axis, whereas in compressing a disk the flow of metal is perpendicular to the axis of the disk. If a monocrystalline disk of iron having either an octahedral or a cubic orientation (octahedral or cubic axis parallel to axis of the disk) is compressed, the angles between the direction of flow and the directions of slip are 19.5 and 35 degrees, respectively, whereas if a monocrystalline iron rod having either of these orientations is swaged or drawn, the angles between the direction of flow and the slip directions are 70.5 and 55 degrees, respectively. It seems reasonable then that if the angles between the direction of flow and directions of slip were such as to permit easy flow in compression that in swaging or drawing these angles would be too large for easy flow. The iron crystal, therefore, begins to develop secondary crystals having an easier flow. Crystals of this type are apparently those having a dodec-

ahedral axis parallel to the rod axis. The angle between the directions of slip and flow in this case is 35 degrees. In swaging a copper crystal the angle between the directions of slip and of flow is 35 degrees when the crystal has the octahedral orientation and 45 degrees when the orientation is cubic. In either case an easy flow of material occurs without change in orientation. However, when the orientation is dodecahedral, the angle between the directions of slip and of flow is 60 degrees, which is too large for easy flow without change in orientation. The crystal tends to change its orientation from dodecahedral to octahedral with certain portions forming secondary crystals which rotate toward the cubic orientation.

IV. SUMMARY

Two monocrystalline and two bicrystalline rods of copper were swaged through the same dies to a reduction in area of approximately 95 percent. Small pieces were cut from the swaged rods after 30-, 60-, 80-, and 95-percent reduction in area. The structures of these pieces, as well as the initial structures, were examined by X-ray diffraction and metallographic methods.

In one monocrystalline rod the octahedral axis that was initially inclined to the rod axis by 16 degrees became parallel to the rod axis as a result of swaging, whereas in the other monocrystalline rod, the cubic axis that was initially inclined to the rod axis by 17 degrees became parallel to the rod axis. These apparently stable orientations were also obtained for crystals in the bicrystalline rods when their initial orientations were similar to the initial orientations of the monocrystalline rods. The changes in orientation with different degrees of swaging were equivalent to a rotation of the crystal about one axis. The crystals that rotated to the octahedral orientation developed secondary crystals that rotated to the cubic orientation. The crystals that rotated to the cubic orientation did not develop secondary crystals. Diffraction patterns and the appearance of the ends of the swaged rods indicated that the crystals had been distorted by slipping over curved surfaces and in directions related to the octahedral planes and dodecahedral directions of the undistorted crystal.

The results indicated that the rotation of the crystal to the octahedral orientation was accomplished by the operation of six slip systems symmetrical to the octahedral axis that became parallel to the rod axis, and in a similar manner, the cubic orientation was attained by the operation of eight slip systems symmetrical to the cubic axis that became parallel to the rod axis. Whether the crystal assumes the octahedral or the cubic orientation depends upon which axis initially formed the smaller angle with the rod axis.

V. REFERENCES

[1] P. W. Bridgman, *Certain physical properties of single crystals of tungsten, antimony, bismuth, tellurium, cadmium, zinc, and tin*, Proc. Am. Acad. Arts Sci. **60,** 307–314 (1925).

[2] Alden B. Greninger, *A back-reflection Laue method for determining crystal orientation*, Z. Krist. [A] **90,** 424–432 (1935); Trans. Am. Inst. Mining Met. Engrs. **117,** 61–74 (1935).

[3] Charles S. Barrett, *The stereographic projection*, Trans. Am. Inst. Mining Met. Engrs. **124,** 29–59 (1937).

[4] F. Johnson, *Influence of cold-rolling upon mechanical properties of oxygen-free copper*, J. Inst. Metals **21,** 335–346 (1919).
[5] Charles S. Barrett, *The structure of iron after compression*, Metals Tech. 5, (1938); Am. Inst. Mining Met. Engrs. Tech. Pap. 977.
[6] E. Schmid and G. Wassermann, *The texture of cold-drawn wire*, Z. Physik 42, 779–794 (1927).
[7] E. Schmid and W. Boas, *Crystal Plasticity* (J. Springer, Berlin, 1935).
[8] C. F. Elam, *Distortion of Metal Crystals* (Oxford Press, Cambridge, London, 1935).
[9] Charles S. Barrett and L. H. Levenson, *Structure of iron after drawing, swaging, and elongating in tension*, Metals Tech. **6,** (1939); Am. Inst. Mining Met. Engrs. Tech. Pap. 1038.

WASHINGTON, February 28, 1939.

U. S. Department of Commerce National Bureau of Standards

RESEARCH PAPER RP1211

Part of Journal of Research of the National Bureau of Standards, Volume 22, June 1939

EFFECTS OF METHIONINE, DJENKOLIC ACID, AND BENZYLCYSTEINE ON THE ESTIMATION OF CYSTINE BY THE DROPPING MERCURY CATHODE

By Edgar Reynolds Smith and Clement James Rodden

ABSTRACT

The reduction maximum of cysteine at the dropping mercury cathode, in a buffered solution containing bivalent cobalt, is not affected by methionine or benzylcysteine at concentrations up to somewhat more than twice that of the cysteine. Djenkolic acid reduces the height of this maximum without changing its form or position. By themselves, methionine, benzylcysteine, and djenkolic acid show no reduction wave between 0.8 and 2.1 v.

CONTENTS

	Page
I. Introduction	669
II. Apparatus and materials	670
III. Experimental results	670

I. INTRODUCTION

The determination of cystine or cysteine by means of the polarograph is made in a buffered solution containing a bivalent cobalt salt and is considered to depend upon a catalytic reduction of hydrogen from the sulfhydryl group of the organic complex compound, formed with the cobalt, which produces a characteristic maximum on the current-voltage curve.[1] This method has been used for the estimation of cystine in hydrolysates from protein materials, such as wool [2] and insulin,[3] at concentrations as low as 10^{-6} g/ml of cystine. Under the environmental conditions of the determination, the curve obtained is apparently characteristic of the sulfhydryl group, or of the disulfide group if the latter is first reduced to the sulfhydryl group, at the dropping mercury cathode. Thus, Brdicka found that thioglycolic acid, glutathione, cysteyl-glycine, and an uncertain decomposition product of β β'-dichloroethyl sulfide (mustard gas) [4] exhibit a similar behavior, whereas no such effect is shown by the amino acids glycocoll, asparagine, creatine, creatinine, arginine, leucine, and tyrosine, which do not contain sulfhydryl. Sladek and Lipschutz [5] extended Brdicka's work and found that arginine, β-phenyl-α-alanine, β-phenyl-β-alanine, tryptophane, and histidine exert a suppressive influence on the cysteine wave, and that β-phenyl-β-alanine alone in the buffer solution with

[1] R. Brdicka, Collection Czechoslov. Chem. Commun. **5**, 112 and 148 (1933); Biochem. Z. **272**, 104 (1933).
[2] R. Brdicka, Collection Czechoslov. Chem. Commun. **5**, 238 (1933); Mikrochemie **15**, 167 (1934).
[3] C. Tropp, Klin. Wochschr. **17**, 465 and 1141 (1938).
[4] R. Brdicka, Collection Czechoslov. Chem. Commun. **9**, 76 (1937).
[5] J. Sladek and M. Lipschutz, Collection Czechoslov. Chem. Commun. **6**, 487 (1934).

bivalent cobalt evokes a less pronounced catalytic maximum somewhat resembling that of cysteine, although occurring at a different potential. These results are of parti[illegible] portance in showing what substances may interfere in the [illegible]hic determination of cystine in hydrolysates which conta[illegible] acids.

Some protein molecules conta[illegible], CH_3-S-CH_2-CH_2-$CH(NH_2)$-COOH, which like cystei[illegible]-S-CH_2-$CH(NH_2)$COOH, is a naturally occurring sulfur-containing amino acid. For the proper interpretation of polarographic determinations of cysteine in certain hydrolysates, it is thus necessary to know whether methionine exhibits a current-voltage wave and/or exerts an effect on the cysteine wave. To obtain this information, polarograms were taken of cystine alone, methionine alone, and cystine together with methionine, in buffered solutions containing bivalent cobalt. Polarograms of djenkolic acid, CH_2(S-CH_2-$CH(NH_2)$-COOH)$_2$, and benzylcysteine, C_6H_5-CH_2-S-CH_2-$CH(NH_2)$-COOH, both of which are related to cysteine, were also taken in the same way, because the former has been isolated from the naturally-occurring djenkol bean [6] and the latter, in contrast to methionine, can be readily split to form cysteine.

II. APPARATUS AND MATERIALS

The polarograph used was the type VIII instrument made by the firm of V. & J. Nejedly, Prague, Czechoslovakia, for the automatic photographing of current-voltage curves. The galvanometer had a sensitivity of about 3×10^{-9} amp/mm at a meter distance, which could be varied suitably by means of a calibrated shunt. A sensitivity of 1/200 of full galvanometer sensitivity was used for all the curves shown in this paper.

The cystine was a commercial product (Eastman Kodak Co.) and was not submitted to further purification.

dl-Methionine was prepared by the reduction of homocystine with sodium in liquid ammonia, followed by treatment with methyl iodide in the liquid ammonia solution.[7] It was found by treatment with sodium cyanide and sodium nitroprusside to be free from disulfide. Benzyl-*l*-cysteine was made from cystine by a similar procedure, using benzyl chloride in place of methyl iodide.[8] It was likewise shown to be free from disulfide. Both the methionine and benzylcysteine were prepared by W. I. Patterson, Research Associate of the Textile Foundation at this Bureau.

Djenkolic acid, which also had been prepared from cystine by a similar method, using methylene chloride instead of benzyl chloride,[9] was kindly supplied for this work by Vincent du Vigneaud of the Cornell University Medical School, New York, N. Y.

III. EXPERIMENTAL RESULTS

The solutions for measurement were prepared by mixing solutions of the constituents in 25-ml Erlenmeyer flasks, in the order and amount shown in table 1. As soon as each solution was prepared, it was poured into a cell and its polarogram taken, starting at a potential difference of 0.8 v between the dropping mercury cathode and the

[6] A. J. Hijman and A. G. van Veen, Geneeskund. Tijdschr. Nederland.-Indië **76**, 840 (1936).
[7] V. du Vigneaud, H. M. Dyer, and J. Harmon, J. Biol. Chem. **101**, 719 (1933).
[8] V. du Vigneaud, L. F. Audrieth, and H. S. Loring, J. Am. Chem. Soc. **52**, 4500 (1930).
[9] V. du Vigneaud and W. I. Patterson, J. Biol. Chem. **114**, 533 (1936).

anode pool of mercury and ending at a little more than 2.0 v. The results with solutions 1, 2, and 3 are shown in figure 1, in which the curve for cystine is labelled *C*, for djenkolic acid, *D*, and for methionine, *M*. Aside from their different effects on the cobalt maximum, which appears between 1 and 1.2 v, neither djenkolic acid nor

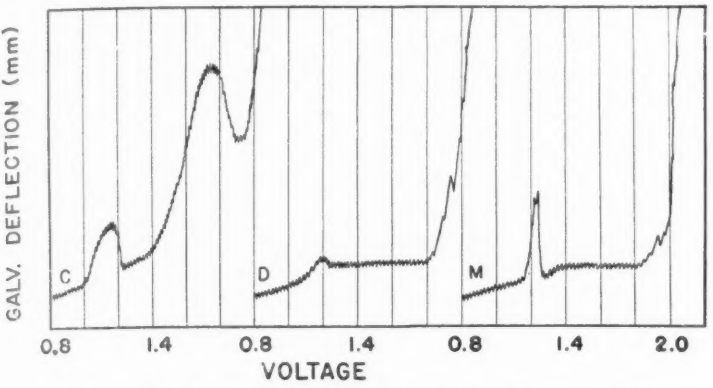

FIGURE 1.—*Cysteine* (*C*), *djenkolic acid* (*D*), *methionine* (*M*).

methionine produces a wave in the range of the cysteine wave. In figure 2, curve *C* is for cystine alone (solution 4), *CD* is for cystine together with djenkolic acid (solution 5), and *CM* for cystine together with methionine (solution 6). The cystine was at the same concentration (2×10^{-5} *M*) in each solution. It is seen that djenkolic acid not only depresses the cobalt maximum but also depresses the cysteine

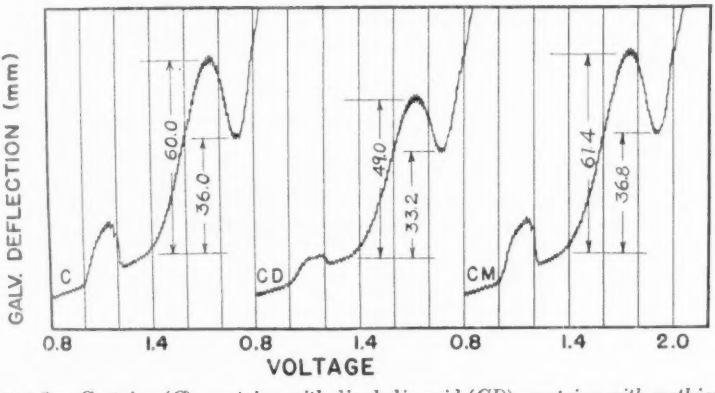

FIGURE 2.—*Cysteine* (*C*), *cysteine with djenkolic acid* (*CD*), *cysteine with methionine* (*CM*).

wave without affecting its shape or position. This behavior was confirmed by repeating the measurements with new solutions. Methionine, however, has no effect on the cysteine wave at these concentrations even though its concentration (5×10^{-5} *M*) exceeds that of the cystine (2×10^{-5} *M*).[10] Thus, it seems justifiable to conclude that

[10] After this work had been completed, similar results with methionine and cystine were reported by Adolf Stern, Eliot F. Beach, and Icie G. Macy at the Ninety-Seventh Meeting of The American Chemical Society at Baltimore, Md. (April 1939).

the polarographic estimation of cystine at large dilutions is unaffected by the presence of methionine at concentrations up to somewhat more than twice that of cystine.

TABLE 1.—*Preparation of solutions*

Solution	1	2	3	4	5	6	7	8	9	10
	ml	*ml*	*ml*	*ml*	*ml*	*ml*	*ml*	*ml*	*ml*	*ml*
Cobaltous chloride (0.8×10^{-3} *M*)	4.0	4.0	4.0	4.0	4.0	4.0	4.0	4.0	4.0	4.0
Water	2.6	2.0	2.5	2.6	1.6	2.1	2.0	2.6	1.6	3.0
Ammonium chloride (0.5 *N*)	2.0	2.0	2.0	2.0	2.0	2.0	2.0	2.0	2.0	2.0
Ammonia (1 *N*)	1.0	1.0	1.0	1.0	1.0	1.0	1.0	1.0	1.0	1.0
Cystine (5×10^{-4} *M*)	0.4	------	------	0.4	0.4	0.4	------	0.4	0.4	------
Djenkolic acid (5×10^{-4} *M*)	------	1.0	------	------	1.0	------	------	------	------	------
Methionine (10^{-3} *M*)	------	------	0.5	------	------	0.5	------	------	------	------
Benzylcysteine (5×10^{-4} *M*)	------	------	------	------	------	------	1.0	------	1.0	------

In figure 3, curve *B* for benzylcysteine (solution 7) shows no interfering wave in the measured range, and a comparison of curve *C* for cystine (solution 8) and curve *BC* for benzylcysteine together with

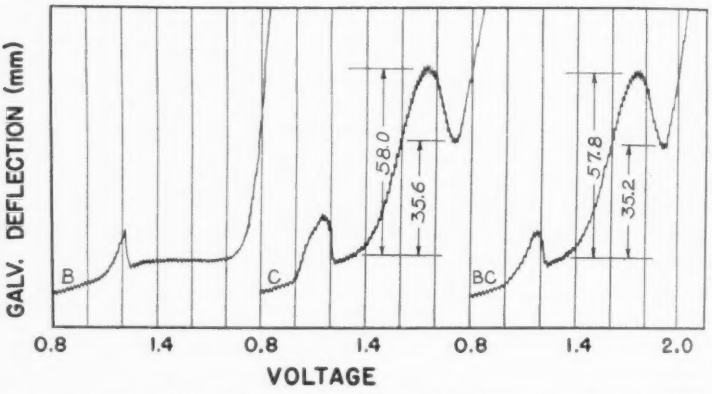

FIGURE 3.—*Benzylcysteine (B), cysteine (C), benzylcysteine with cysteine (BC).*

cystine (solution 9) shows that benzylcysteine, like methionine, is without influence on the cysteine wave. The polarogram for the blank solution, 10, was practically identical with curve *B* of figure 3.

WASHINGTON, April 21, 1939.

U. S. DEPARTMENT OF COMMERCE NATIONAL BUREAU OF STANDARDS

RESEARCH PAPER RP1212

Part of Journal of Research of the National Bureau of Standards, Volume 22, June 1939

NATURE OF ENERGY LOSSES IN AIR CAPACITORS AT LOW FREQUENCIES

By Allen V. Astin

ABSTRACT

The power factors of a number of types of air capacitors have been observed in the frequency range from 60 to 1,000 c/s. The method of measurement permitted evaluation of true, or "absolute," power-factor values as small as 5×10^{-7}. In guard-ring air capacitors the losses occur on the surfaces of the electrodes and give rise to a power factor which is proportional to capacitance (inverse electrode separation). The same type of losses in addition to the losses in the solid insulation, are evident in two-electrode capacitors.

For most two-electrode air capacitors of variable capacitance, C, the loss may be represented by the function $A+B/C$, where A depends upon the electrode material, humidity, and frequency, and B depends upon the insulation material, humidity, and frequency.

Of the 10 metals used as electrode materials in guard-ring capacitors, aluminum gave the greatest power factor and silver plate the smallest. The power factors for the other materials, which included brass, monel metal, stainless steel, nickel, and brass plated with gold, rhodium, and chromium, were only slightly different from that for silver-plated brass, but they were appreciably smaller than the values for aluminum. The power factor of a guard-ring capacitor is a function of humidity and shows a maximum value at relative humidities between 40 and 70 percent at low frequencies. The maximum value is apparently due to a variable conductivity of the moisture layer with thickness.

The loss which occurs in the electrode surface layer is also a function of the homogeneity of the electric field. The nonuniform field in a three-electrode rotating-plate capacitor gives rise to a power factor which decreases as the capacitance is increased.

CONTENTS

		Page
I.	Introduction	673
II.	Calibration of standard for power factor	674
III.	Power factors of two-electrode capacitors	676
IV.	Power factors of three-electrode capacitors	682
V.	Contribution of a surface layer to power factor	687
VI.	Effect of a nonhomogeneous field on power factor	691
VII.	Conclusion	694
VIII.	References	695

I. INTRODUCTION

Previous investigations into the causes of energy losses in air capacitors have in general disclosed four major contributing factors. As summarized by Field and Sinclair [1] [1] these are: (1) a conductance and dielectric absorption loss in the solid insulation; (2) a dielectric absorption loss in dust or lint which sometimes accumulates on the plates of a capacitor; (3) an eddy-current loss in the metallic electrodes; and (4) a loss due to the effective resistance of the leads and electrodes and the contact resistance to the rotating shaft of a variable capacitor. The energy losses from the two latter factors

[1] Figures in brackets indicate the literature references at the end of this paper.

decrease with decreasing frequency and for frequencies below 1,000 c/s are quite negligible. The two remaining factors are, however, inadequate to explain recent observations with high-precision bridges at low frequencies [2, 3, 4]. In the observations reported in these references the effects of losses in both solid insulation and dust were eliminated, but losses were still found in the capacitors. These losses, which have been shown to depend upon the electrode surface, electrode separation, and the frequency, may give rise to power factors of 1×10^{-5} or larger. In order to obtain more information concerning the nature of these losses, a number of guard-ring capacitors have been constructed of various electrode materials and their power factors measured under a wide range of conditions. The power factors were measured by the bridge method described in a previous publication [2], which permitted the determination of the true, or absolute, values in contrast to the relative or difference values which are ordinarily obtained by bridge methods. The precision of the method allowed the evaluation of power factors as small as 5×10^{-7} in the commercial and audio-frequency range.

This method of power-factor evaluation has also been used for observations on the power factors of variable, two-electrode air capacitors. Previously, such measurements have been limited to power-factor-difference methods. From these measurements it has been possible to obtain evidence of the existence of the same type of loss factor that is predominant in a guard-ring capacitor, namely, a loss originating on the surface of the metallic electrodes.

II. CALIBRATION OF STANDARD FOR POWER FACTOR

A three-electrode rotating-plate capacitor has been used as a working standard of power factor and capacitance for all measurements which are included in this paper. This capacitor, which has been described in detail previously [2], has nickel-plated brass electrodes, 3 mm apart when interleaved, and a capacitance range of 1,800 μf. The third electrode permitted the elimination from the measured power factor of the capacitor of any losses in its insulating supports. Although this same result could have been obtained more readily with a guard-ring capacitor, the rotating-plate capacitor proved to be a much more satisfactory working standard for bridge measurements because of the greater ease with which its capacitance could be varied. As indicated above, the power factor of a three-electrode capacitor cannot be assumed equal to zero; hence some other means must be available in order to obtain actual power-factor values. This can be accomplished with the aid of a guard-ring capacitor of adjustable electrode spacing (variable capacitance). As pointed out in the reference previously cited [2], the power factor of such a capacitor is proportional to its capacitance; hence at zero capacitance its power factor would be zero. By determining the rate of change of power factor of a guard-ring capacitor with capacitance and extrapolating to zero capacitance, actual power-factor values may be obtained.

In applying this principle to the power-factor calibration of the three-electrode rotating-plate capacitor it was simpler, because of the greater ease of capacitance adjustment of the rotating-plate capacitor, first to determine its rate of power-factor change with capacitance. Then by using measured differences in the power factors at various

capacitance settings of the rotating-plate capacitor and an adjustable guard-ring capacitor, the rate of power factor change of the latter instrument was determined and extrapolated to zero capacitance. The details of this procedure may be seen by referring to figure 1 (a, b, c), where the curves $C_g - C_s$ represent the power-factor differences at the indicated frequencies of an adjustable guard-ring capacitor, C_g, and the three-electrode rotating-plate capacitor, C_s, at equal capacitance settings. The C_s curves represent the power-factor variations of C_s with capacitance. The ordinates of these curves are fixed arbitrarily by the doubly circled points which represent the power-factor differences, at the indicated frequencies, of C_s and a fixed cylindrical guard-ring capacitor, C_0, having silver-plated electrodes 1 cm apart. The power factor of C_0 thus provides a tentative reference point. The change in power factor with capacitance of C_s with respect to this point was determined by making power-factor-difference measurements with auxiliary capacitors individually and in parallel.[2]

[1] The detail of this procedure is as follows: Let ϕ_{s1} be the phase-defect angle, or power factor, of C_s at a particular scale setting. Let ϕ_{A1} and ϕ_{B1} be the power factors of two other capacitors having the same capacitance as C_s at its setting corresponding to ϕ_{s1}. Then the power-factor differences, $\phi_{s1} - \phi_{B1} = M_1$ and $\phi_{s1} - \phi_{B1} = M_2$, may be measured in the bridge. The two auxiliary capacitors are then connected in parallel, and it is a simple matter to show that the power factor of the combination will be the arithmetical mean of their individual values. The capacitance of C_s is then varied to equal that of the combined auxiliaries and power-factor difference, $\phi_{s2} - (\phi_{A1} + \phi_{B1})/2 = M_3$, measured. Here, ϕ_{s2} is the power factor of C_s at its new scale setting. Combining the values for M_1, M_2, and M_3 it is found that

$$\phi_{s1} - \phi_{s2} = (M_1 + M_2)/2 - M_3,$$

which represents the change in power factor of C_s between two scale settings. Additional points may be obtained by the use of a larger number of auxiliary capacitors.

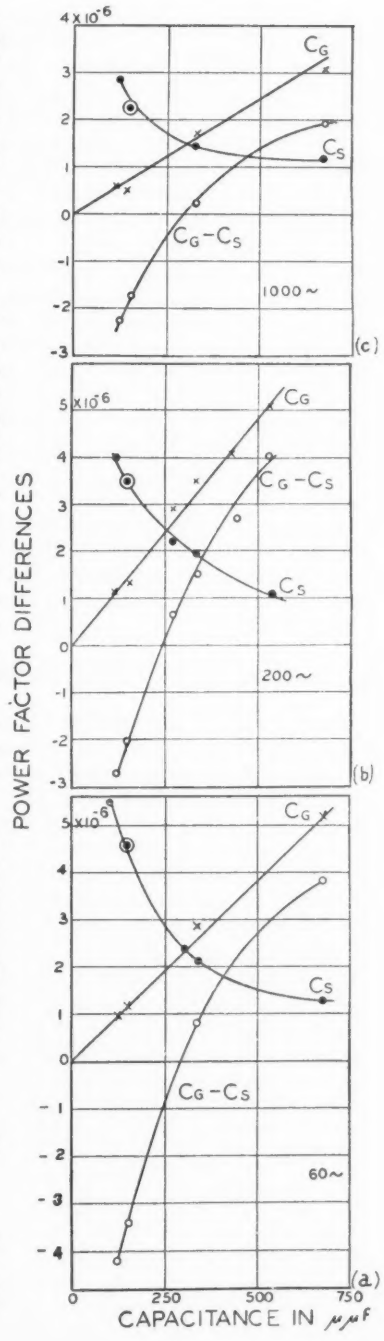

FIGURE 1.—*Power-factor differences and true power-factor values of a variable guard-ring capacitor, C_g, and a three-electrode rotating-plate capacitor, C_s, as functions of capacitance.*

Upon adding the ordinate values of a C_s curve to the corresponding $C_g - C_s$ curve, a C_g curve is obtained which thus represents the power-factor differences of C_g with respect to the fixed power factor of C_0. The slope of the line represents the rate of power-factor change with capacitance and is independent of the power factor of C_0. Since the power factor of a guard-ring capacitor is proportional to its capacitance (a linear relation is obvious from fig. 1 (a, b, c)), the power factor of C_g will be zero at zero capacitance. The line will intercept the arbitrarily chosen zero of the ordinate scale only if the power factor of the reference capacitor, C_0, is zero. It happens in this case that the value of the reference capacitor is zero or at least less than 5×10^{-7} at the indicated frequencies. Accordingly, the curves C_g and C_s represent the true power-factor calibration curves for the two capacitors. However, the method outlined above is applicable even if the reference capacitor has a power factor greater than zero. If such were the case, the intercept of C_g curve would be below the origin, and both the C_g curve and C_s curve would have to be shifted upward by the amount of the intercept to give true power-factor values. It should be pointed out that the proportional relation between the power factor and capacitance of a guard-ring capacitor is assumed from the linear relation, because it has been found that the zero value obtained for C_0 by this process is independent of (1) the frequency, (2) the air pressure (below normal atmospheric pressure) in either C_0 or C_g, and (3) the electrode material and dimensions of the guard-ring capacitor used for the extrapolation.

III. POWER FACTORS OF TWO-ELECTRODE CAPACITORS

In specifying the quality of a two-electrode capacitor of variable capacitance as regards its freedom from power loss under alternating voltage a single expression would be desirable. If the losses in a capacitor were confined entirely to solid insulators in a constant field, its power factor would be inversely proportional to its capacitance giving a power-factor–capacitance product which would be constant for all scale settings. This product, which has been called the "figure of merit" of a capacitor [5] would then be a satisfactory designation of the loss characteristics of a variable air capacitor under the conditions of measurement. Furthermore, if the loss per cycle in the solid insulation were constant with frequency as Chaffe [6] has shown to be the case for a number of insulating materials, the power-factor–capacitance product would be independent of both frequency and scale setting. Unfortunately, the insulators in the best commercial variable air capacitors do not show this property nor are the losses confined only to the solid insulation even at low frequencies when the dust and lint are removed from the electrode surfaces.

In figure 2 are shown the power factors at three frequencies of a precision-type, two-electrode variable air capacitor plotted against the reciprocal of the capacitance. The insulation of the capacitor is Isolantite and the electrodes are of aluminum spaced about 1 mm apart when interleaved. The capacitor is of the common rotating-electrode type. The data in the figure show that neither of the requirements for the constancy of the power-factor–capacitance product is met with this particular capacitor. The power-factor change with

frequency is appreciable and the power factor at each frequency, although linear with the reciprocal of capacitance, is definitely not proportional to it. The finite values of the intercepts on the ordinate axis indicate that a constant must be added to the power factor in order to adequately represent the power-factor variations at a particular frequency.

The results of power-loss observations on a large number of variable air capacitors have indicated that in no case is an equivalent parallel resistance sufficient to represent the losses at one frequency. The

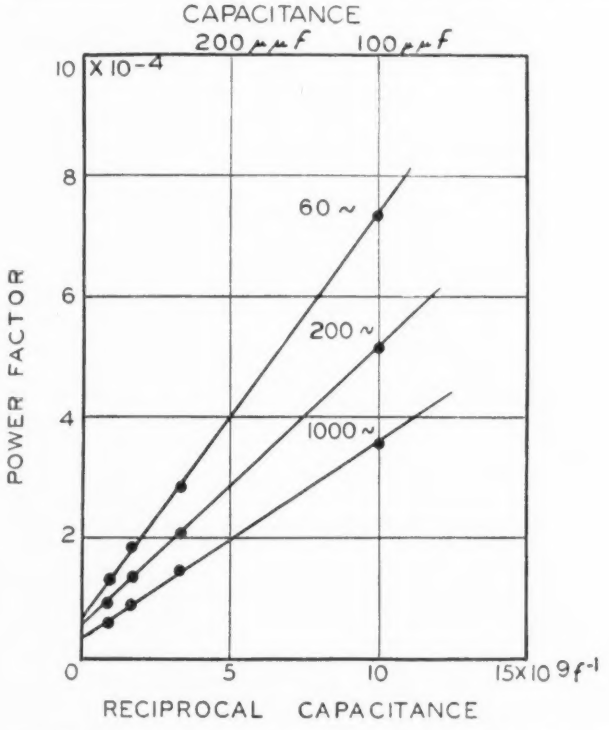

FIGURE 2.—*Power factors at three frequencies of a precision type, two-electrode variable air capacitor with Isolantite insulation.*

Relative humidity about 50 percent.

power factors at 60 cycles of five representative capacitors are shown in figure 3. Curve A represents a National Bureau of Standards type capacitor [7] with fused-silica and amber insulation and brass electrodes about 2.5 mm apart. The power-factor values for 60 c/s shown in figure 2 are shown again by *B*, and *D* represents the values for another capacitor of identical type. The curve *C* represents a capacitor having Isolantite insulation and brass electrodes about 1 mm apart, and *E* is for a capacitor similar to that of *C*, except that the insulation is of clear fused quartz. In each case the power factor is (1) a linear function of the reciprocal of the capacitance and, (2) finite and positive at the extrapolated value for infinite capacitance.

The power factors for each of the capacitors shown in figure 3 can be represented by the function

$$A+B/C,$$

where A is the intercept on the power-factor axis and B is the slope of the curve. The part of the power factor represented by the B/C term may be attributed to the insulation, assuming $B=1/\omega R$, where R is the equivalent parallel resistance of the insulation (in general R is a function of frequency) and ω is 2π times the frequency. The part represented by the A term may be explained by assuming a uniform surface layer on the electrodes, which gives rise to an equivalent resistance, r, in series with the capacitance. The power factor produced by such a resistance would be ωrC, but since r would be inversely proportional to C (electrode area), this power-factor term would be independent of scale setting. It should be noted that values of A are less for the capacitors with brass electrodes than for those with aluminum electrodes.

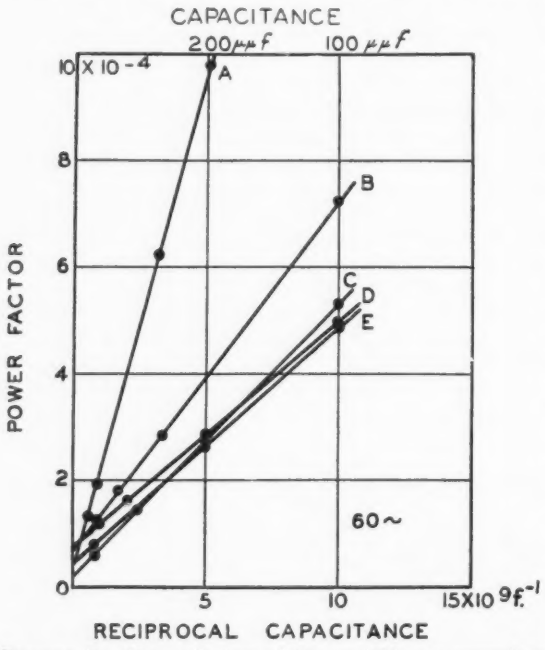

FIGURE 3.—*Power factors of five variable air capacitors with solid insulation observed at 60 c/s and 50 percent relative humidity.*

Insulation and electrode material of the capacitors were as follows: *A*, fused-silica and amber insulation and brass electrodes; *B* and *D*, Isolantite insulation and aluminum electrodes; *C*, Isolantite insulation and brass electrodes; *E*, clear fused-quartz insulation and brass electrodes.

An explanation of the decrease of A with frequency (fig. 2) requires a consideration of the capacitance of the surface layer as well as its resistance. A more complete discussion of this effect, which produces the predominant power factor of a guard-ring capacitor, will be given in a later section of this paper.

The variation of the equivalent parallel resistance, R, with frequency is shown in figure 4 for three of the capacitors represented in figure 3. The values for the B curve were computed from the slopes of the three straight lines of figure 2, using the relation $B=1/\omega R$, where B represents the slope for a particular frequency. The curves A and E were similarly obtained. The values indicated for zero frequency represent actual d-c resistance values obtained from the voltage-current ratio 1 minute after applying the voltage to the capacitor. The dashed curves represent the theoretical resistance values, which are inversely proportional to frequency, that is, the type of variations

to be expected if the power factor represented by the equivalent parallel resistance were independent of frequency. The curves were made to pass through the experimental points for 1,000 c/s. The curve *A* follows this type of variation quite closely, but *B* and *E*, representing capacitors having appreciably lower power factors, depart appreciably from it. The amount of departure is especially indicated by the zero frequency values (d-c resistances) at which point the theoretical curve approaches infinity. Because of the differences in the frequency variation of these resistances, the anomaly is presented of the capacitor having the largest power factor also having the highest d-c resistance and vice versa. This of course is merely coincidental for the particular three capacitors under observation and should not be taken as a generality but rather as a proof that the d-c performance of a capacitor offers little if any information as to its a-c power factor.

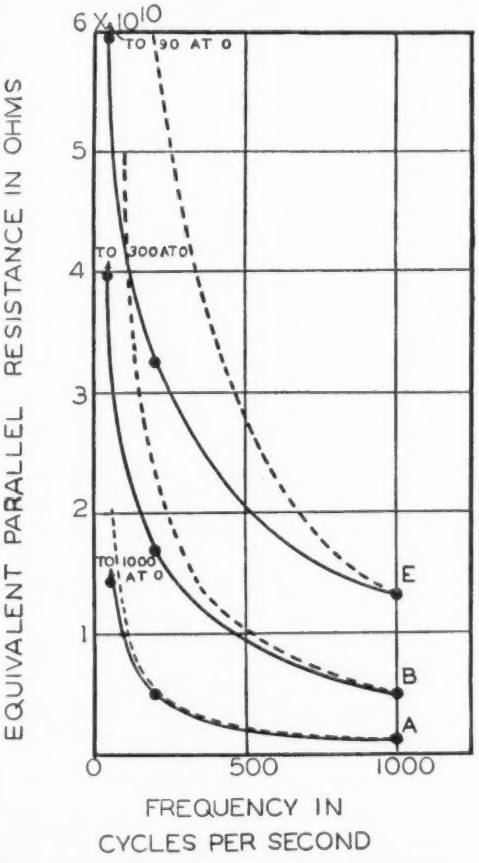

FIGURE 4.—*Equivalent parallel resistances of three air capacitors as a function of frequency.*

Zero values represent 1-minute d-c resistances. Dashed lines represent theoretical resistance values below 1,000 c/s which are inversely proportional to frequency. Curve designations *A*, *B*, and *E* correspond to figure 2.

All of the data represented in figures 2, 3, and 4 were taken at approximately the same temperature and relative humidity, namely, 27° C and 50-percent relative humidity. This was essential for proper comparison of the power factor of the different capacitors. The temperatures normally observed throughout a year in the capacitance laboratory of the National Bureau of Standards vary between 24° and 31° C, which range is sufficiently restricted to produce only slight differences in the power factors of capacitors. However, the seasonal relative humidity, which may range from 15 to 85 percent, causes enormous fluctuations in the power factors of the capacitors. An indication of the spread of values which may be obtained at different humidities is given in figure 5, which shows available data on a capacitor with quartz insulation and brass electrodes (the same capacitor as represented by curves *E*, fig. 3 and 4).

The summer values were taken when the room humidity was at 85 percent, the autumn and spring values at 50 percent, and the winter values at 35 percent. Because of the partial sealing of the insulation in the case of the capacitor, considerable lag was observed in the variations of power factor with humidity changes. This is evident from the values at 60 c/s for autumn and spring, both of which were taken at about 50-percent relative humidity.

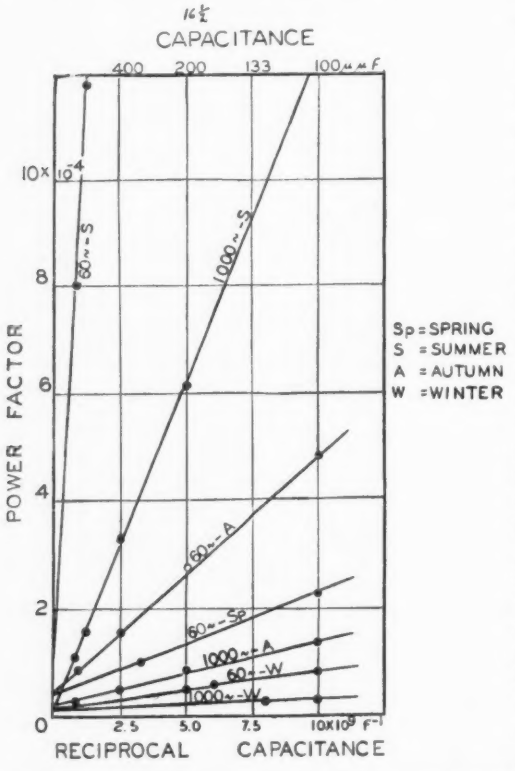

FIGURE 5.—*Curves of power factor vs. reciprocal capacitance of a variable, two-electrode air capacitor at different seasons (different relative humidities).*

It is obvious from the data of figure 5 that any specification concerning the a-c losses in a capacitor of this type would be quite useless unless the insulation of the capacitor were in equilibrium with an atmosphere of clearly defined relative humidity. Likewise, it would be impossible to use such a capacitor as a reference standard for power-factor difference measurements unless proper humidity stability were preserved. It should, however, be pointed out that the range of variations with Isolantite insulation is generally less than that shown in figure 5, the winter values being higher and the summer values lower. The range of values would probably be appreciably lowered by a careful cleaning of the quartz, since the data shown were taken with the capacitor in the same condition as when received from the manufacturer.

From the data so far presented it would appear quite safe to draw the conclusion that the power factor of a two-electrode, variable air capacitor may be represented by the expression $A + B/C$, where A is a function of frequency, humidity, and the properties of the electrode surface material and B is a function of frequency, humidity, and the properties of the insulation material. In general, A and B would appear to decrease with increasing frequency and increase with increasing humidity. Although the expression $A+B/C$ has been found adequate to represent the power factors in most cases, exceptions have been encountered, particularly when the A term is the predominant loss term. Under such circumstances A may not be a constant (at a fixed frequency and humidity) because of variations in

the surface of the electrodes or because stray capacitance increases the effective electrode separation at low capacitance values. Two extreme cases are shown in figure 6. The curve (*a*) is for a capacitor with very good quartz insulation in a low-humidity atmosphere, and somewhat tarnished brass electrodes of 1-mm spacing. The change of slope is very likely due to variations in the electrode surface as the electrodes are rotated for different capacitance settings. The curve (*b*) represents the values for a capacitor with Isolantite insulation and

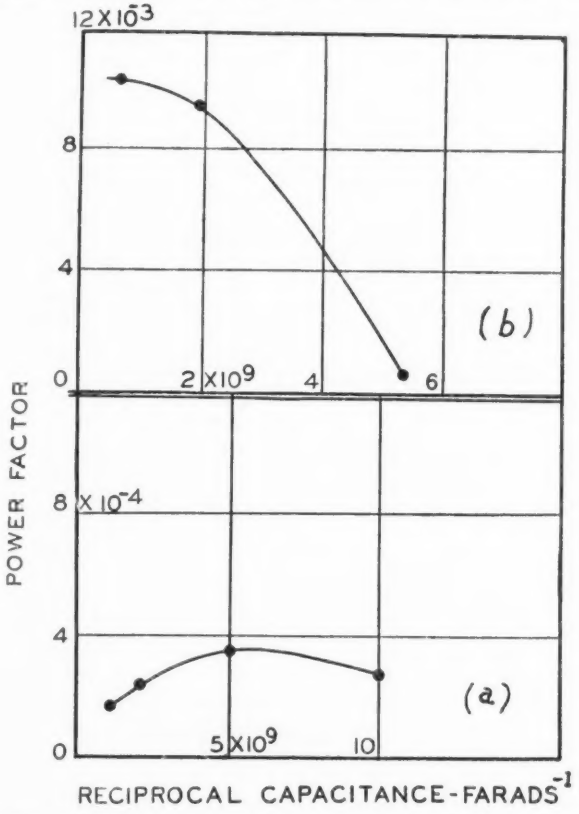

FIGURE 6.—*Power factors of two variable capacitors in which the electrode surface loss is predominant.*

Observations were made at a frequency of 60 c/s.

cadmium-plated electrodes. The plating was extremely heavy and flaky and comparable in thickness to the electrode separation (0.5 mm) and gave rise to the equivalent of a large resistance in series with the capacitance. As the capacitance was decreased the relative effect of stray capacitance, which increases the effective electrode separation of the capacitor, increased, causing a decrease in power factor. Such power-factor behaviors are exceptional, but the possibility of the existence of such is sufficient to require the qualification that the $A+B/C$ type of variation is not followed unless the surface losses are small and uniform.

IV. POWER FACTORS OF THREE-ELECTRODE CAPACITORS

When the power factor of a three-electrode capacitor is measured in an a-c bridge with a Wagner ground, the effect of losses in the solid insulators which support and separate the electrodes may be eliminated. The three-electrode capacitor may be of the guard-ring type or it may have rotor and stator assemblies with a third or guard electrode for carrying the insulating supports. The power-factor-capacitance characteristics of both types of capacitors have been shown previously in figure 1. The guard-ring capacitor, which has a variable electrode spacing, constant electrode area, and an approximately uniform electric field, has a power factor proportional to its capacitance (C_x curves in fig. 1). The rotating plate, guard-electrode capacitor, which has a constant electrode spacing, variable electrode area, and partially nonuniform electric field, has a power factor which decreases with increasing capacitance.

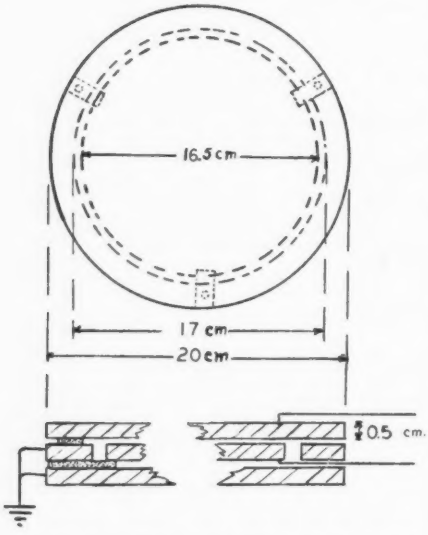

FIGURE 7.—*Plan and section of the guard-ring capacitors used to investigate power factor as a function of electrode material and relative humidity.*

Electrical connections are indicated in the sectional view.

In the guard-ring capacitor the proportional relationship between power factor and capacitance can be most simply represented by an equivalent resistance, r, in series with the capacitance, C. The power factor of such a combination is ωrc. Previous evidence [2] has indicated that the equivalent resistance, r, is due to a surface layer on the electrodes. Accordingly, for a given electrode material and conditions of measurement, r would be inversely proportional to the electrode area, and the power factor would be independent of the electrode area. The manner in which r is related to the properties of a hypotethical surface layer and the frequency will be treated in detail in section V. An explanation of the power-factor characteristics of the rotating-plate capacitor involves a consideration of the nonhomogeneous electric field at the edges of the electrodes and will be given in section VI.

The effect of electrode material and of the measuring conditions on the power factor of a guard-ring capacitor has been studied by preparing capacitors of 10 different materials and by measuring their power factors at various frequencies, temperatures, and relative humidities. The construction of the capacitors is shown in figure 7. These were placed in a sealed air bath in which both the temperature and relative humidity could be controlled. It was found that the losses depended considerably upon the relative humidity, but no definite dependence upon temperature alone in the available range of 20° to 40° C could be determined. Accordingly, all the results at various humidities are given for a single temperature, namely, 30° C.

Electrodes were made of the following materials: brass, aluminum, monel metal, nickel, and stainless steel. In addition, capacitors of brass were plated with the following metals: gold, silver, nickel,

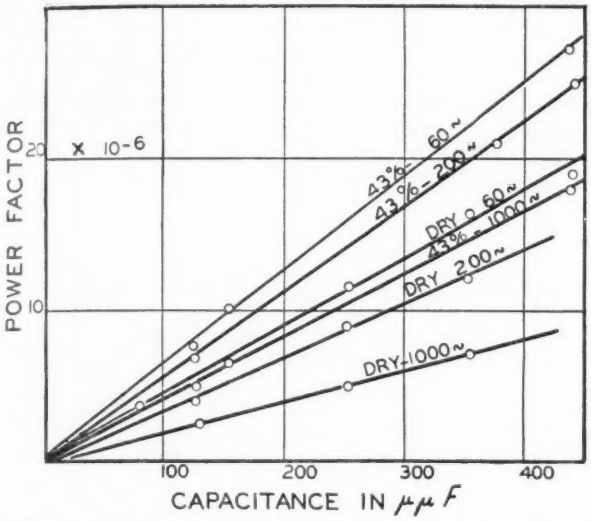

FIGURE 8.—*Power factors of a guard-ring air capacitor with aluminum electrode of variable spacing (variable capacitance).*

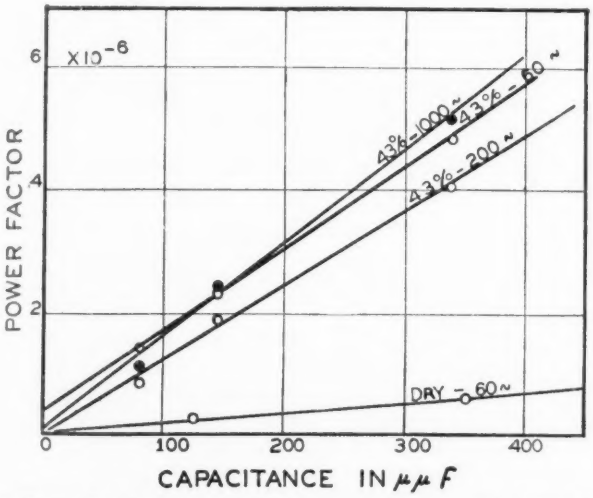

FIGURE 9.—*Power factors of a guard-ring air capacitor with brass electrodes of variable spacing (variable capacitance).*

chromium, and rhodium, and a capacitor of aluminum was anodized. The solid electrodes were ground smooth with fine emery paper and crocus cloth, and all electrodes were cleaned with soap and water and then rinsed thoroughly with water.

The results on aluminum and brass electrodes, the two metals most commonly used for electrodes in capacitors, are shown in figures 8

and 9, for a dry atmosphere and an atmosphere of 43-percent relative humidity. The proportional relationship between power factor and capacitance is again apparent. In figure 10 are shown the results for anodized aluminum electrodes in a dry atmosphere and at 85-percent relative humidity. Here definite departures from the proportional relationship are observed, but these have been traced to changes in the electrode surface between capacitance settings. In taking observations on these electrodes over a range of humidities, it was found that upon returning to the initial humidity a slightly different power

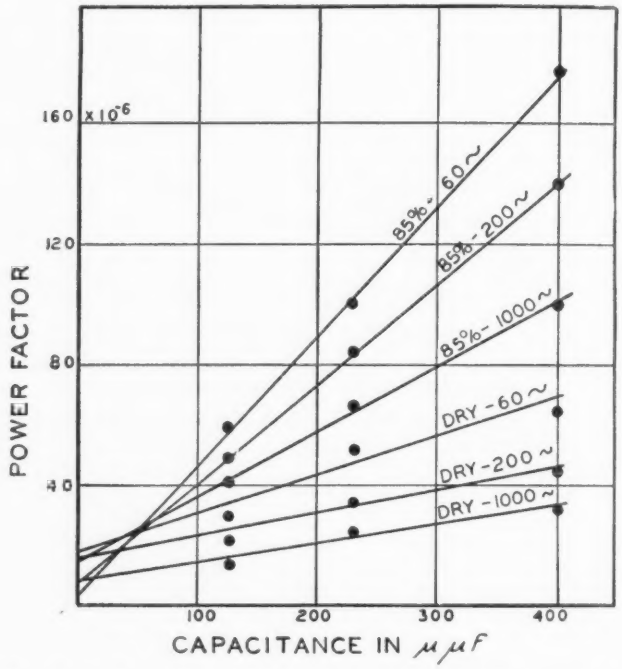

FIGURE 10.—*Power factors of a guard-ring air capacitor with anodized aluminum electrodes of variable spacing (variable capacitance).*

factor was obtained, indicating that the electrode surface was no longer exactly the same as during the first measurement. Since the procedure of observation was to run through a complete humidity cycle at each electrode spacing, it was probable that the same surface conditions no longer existed at the next electrode spacing. When the humidity was kept fixed and values were taken over a range of capacitances, a strictly proportional relationship was always observed. The measured power factors seem to indicate that the effect of the humidity cycle on the surface condition is more of the nature of a permanent change than a hysteresis type effect. Definite indication of a slow change in the nature of an aluminum surface with time is given in figure 11, which shows groups of observations at 60 c/s taken several months apart. The earliest set of data was taken shortly after the grinding of the surfaces, and nothing was done to the surfaces between then and the subsequent measurements except washing

and rinsing. The gradual increase in the slopes of the curves with time probably represents a growth of the oxide layer on the electrodes. The scattering of points from the lines is greater than for a rapid continuous series of observations and is to be expected when the effect being measured is varying.

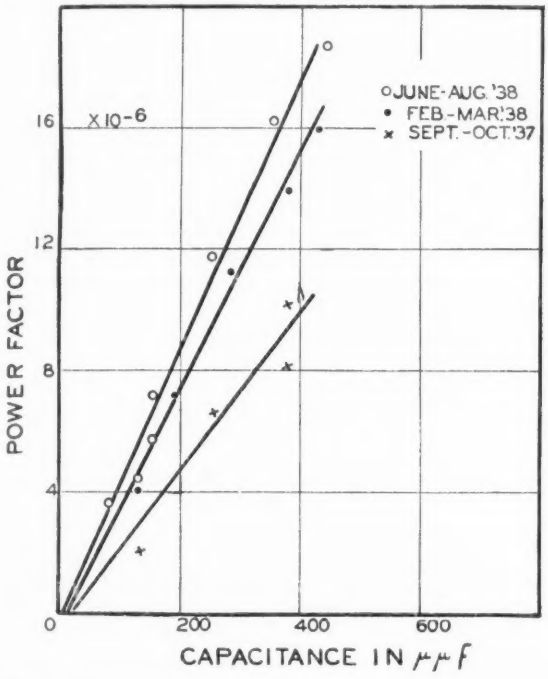

FIGURE 11.—*Power-factor-capacitance curves of a guard-ring air capacitor with aluminum electrodes indicating increase in power factor with time due to aging of electrode surface.*

The slopes of the power-factor–capacitance curves shown so far are functions of the areas of the electrodes. Since the power factors of a guard-ring capacitor are inversely proportional to the electrode separation, the product of power factor and electrode separation should give a term which is a function of the electrode material and the conditions of measurement and is independent of the geometry of the capacitor. Accordingly, this product has been used to express the power-loss measurements on the various electrode materials mentioned above. The results are listed in table 1 as a product of phase-defect angle (which is equivalent to power factor) in microradians and electrode separation in millimeters for eight different relative humidities and three frequencies of measurement. In every case, except for the anodized aluminum, the power factor reaches a maximum between 43 and 75 percent relative humidity, and in general the maximum occurs at a higher humidity at the higher frequencies. In addition, where data at 97 percent are available there appears to be a minimum at about 85 percent relative humidity. The data from the table for aluminum and silver-plated electrodes are shown graphically in figure 12.

TABLE 1.—*Effect of electrode material and relative humidity upon the power factor (phase defect angle) of a guard-ring air capacitor*

Electrode material	Frequency ↓ / Relative humidity (%) →	Phase-defect angle × electrode separation, in microradian-millimeters							
		Dry	32	43	52	63	75	85	97
	c/s								
Rhodium-plated brass	60	0.3	1.6	1.8	1.9	1.4	0.0	0.0	0.0
	200	.3	1.5	1.8	1.9	1.9	1.0	.1	.5
	1,000	.5	1.4	1.8	2.1	2.1	2.0	2.0	2.0
Nickel-plated brass	60	.3	1.2	1.8	1.7	1.6	.7	.5	.....
	200	.5	1.2	1.6	2.1	1.8	1.3	1.0	.....
	1,000	.5	1.2	1.5	2.7	2.2	2.1	1.2	.....
Chromium-plated brass	60	.4	1.4	1.8	1.9	2.0	1.0	.7	.....
	200	.4	1.0	1.6	1.9	2.1	1.2	.8	.....
	1,000	.6	.8	1.5	1.8	1.8	1.8	1.0	.....
Silver-plated brass	60	.0	1.2	1.4	1.6	1.4	.9	.6	.....
	200	.2	1.2	1.0	1.2	1.6	1.5	.9	.....
	1,000	.2	1.3	1.3	1.7	1.8	2.4	1.5	.....
Gold-plated brass	60	.2	1.5	2.0	2.8	2.8	1.1	.8	.....
	200	.2	1.3	1.8	2.5	3.0	1.5	1.2	.....
	1,000	.4	1.2	1.8	2.1	2.6	2.4	1.5	.....
Nickel	60	.4	2.2	3.0	4.0	3.0	1.4	.7	.0
	200	.5	1.9	3.2	2.8	2.6	1.6	1.0	.2
	1,000	.5	1.7	3.7	3.9	2.8	2.5	2.0	1.2
Monel metal	60	.3	1.5	1.5	1.9	1.0	.7	.6	.....
	200	.4	-----	1.4	-----	1.3	.9	.6	.....
	1,000	.5	1.4	1.7	2.0	1.9	1.7	.8	.....
Brass	60	.4	2.0	2.5	3.4	-----	2.2	1.8	2.5
	200	.4	-----	2.4	2.5	3.2	1.3	1.3	.....
	1,000	.9	2.2	2.9	3.6	4.0	2.5	2.5	.....
Stainless steel	60	.3	1.7	2.4	2.1	2.2	1.8	1.6	.....
	200	.4	1.7	1.8	2.2	2.4	1.1	1.4	.....
	1,000	.5	1.1	2.1	3.2	2.8	2.0	1.1	.....
Aluminum	60	7.6	11	12	14	11	5.0	4	5
	200	5.5	8.5	10	11	14	3.8	3.3	9
	1,000	3.7	7.0	7.6	8.6	11.5	6.4	5	6
Anodized aluminum	60	22	66	-----	-----	88	-----	90	110
	200	21	44	-----	-----	61	-----	66	59
	1,000	16	30	-----	-----	48	-----	51	44

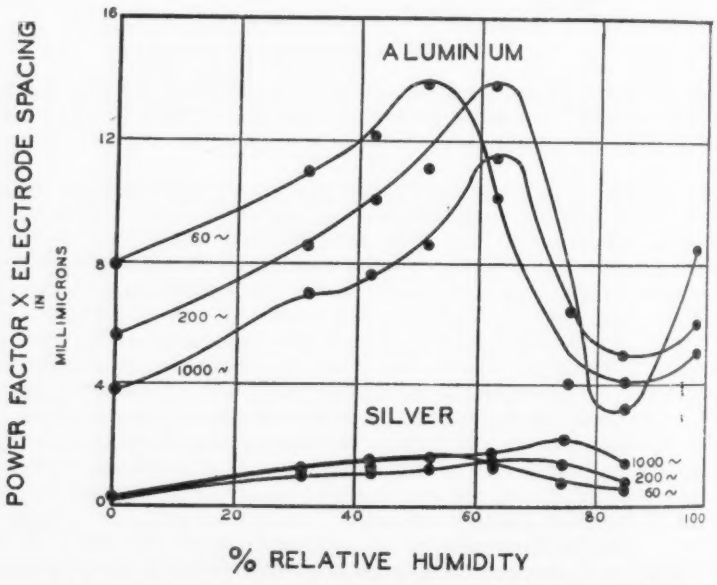

FIGURE 12.—*Losses in guard-ring air capacitors with aluminum and silver electrodes as a function of relative humidity.*

A further examination of table 1 indicates that from the point of view of low power factor, aluminum is definitely the poorest of the materials listed for the electrodes of an air capacitor. This is to be expected because of the relatively thick oxide layer on metallic aluminum. Increasing the thickness of the layer by anodizing produces a marked increase in the observed power factors. Among the remaining materials there is little choice, the silver-plated electrodes showing the lowest power factors by a small margin. With these materials the observed losses appear to be almost entirely due to moisture because only a very slight effect was observed in the dry atmosphere.

In obtaining the above data it was found that cleaning the electrodes and keeping them clean was quite necessary for consistent results. Small quantities of dust were especially troublesome, particularly at high humidities and with electrode separations of less than a millimeter. Fortunately, by the use of polished or semipolished electrode surfaces it was quite easy to detect the presence of dust. Next to dust, oil and grease films were found most likely to give abnormally high power factors. It was found, for example, that cleaning the electrodes with commercial grade carbon tetrachloride or benzene sometimes left an invisible oil film which considerably increased the power factor of the capacitor. Cleansing with soap and water with adequate rinsing was found to give the cleanest surfaces from the point of view of low power factor.

V. CONTRIBUTION OF A SURFACE LAYER TO POWER FACTOR

Inasmuch as the losses in a guard-ring air capacitor appear to occur in surface layers on the electrodes, it is desirable to determine analytically the effect of such layers on the power factors. In figure 13 are shown (a) a section of the electrodes of a capacitor separated by a distance, d, and with a film on each electrode of thickness, t, (b) a circuit diagram of the arrangement showing a perfect capacitor, C_1, in series with a partially conducting capacitor of capacitance and resistance, C_2 and R_2 (the thickness of the dielectric of C_2 will be twice that of the film), and (c) an equivalent circuit of capacitance, C, and resistance, R. The capacitance, C, and power factor, ϕ, of the equivalent circuit are, when $t<<d$ or $C_1<<C_2$ and second-order terms are neglected,

$$C=C_1\left(1-\frac{\omega^2R_2^2C_1C_2}{1+\omega^2R_2^2C_2^2}\right) \tag{1}$$

$$\phi=\frac{\omega R_2C_1}{1+\omega^2R_2^2C_2^2}, \tag{2}$$

where ω is 2π times the frequency, f. If the dielectric constant in esu and conductivity in $\text{ohm}^{-1}\text{cm}^{-1}$, of the film are ϵ and σ, respectively, the above equations may be written

$$C=C_1\left[1-\frac{t}{d}\times\frac{2\epsilon\left(5.5\times10^{-13}\frac{f}{\sigma}\right)^2}{1+\left(5.5\times10^{-13}\frac{f\epsilon}{\sigma}\right)^2}\right]\equiv C_1\left[1-\frac{t}{d}\times N\right] \tag{3}$$

and

$$\phi=\frac{t}{d}\times\frac{1.11\times10^{-12}\frac{f}{\sigma}}{1+\left(5.5\times10^{-13}\frac{f\epsilon}{\sigma}\right)^2}\equiv\frac{t}{d}\times M \tag{4}$$

The numerical factors arise from expressing the capacitance in practical units. In these equations the capacitance change and power factor are linear functions of the t/d ratio and of factors N and M, respectively, which are in turn functions of f/σ and ϵ. The inversely proportional relation of eq 4 between power factor and electrode separation is in accordance with the experimental data for guard-ring capacitors. The manner in which the factors N and M vary with f/σ is shown in figure 14 *with ϵ as a parameter*. Here N and $\log_{10} M$ are plotted against $\log_{10} f/\sigma$ for values of $\epsilon=1$, 10, and 100. The M curves show that a film on an electrode surface produces a maximum power-factor effect for critical values of f/σ. The ratio f/σ is chosen as a variable rather than f, because in general σ will vary appreciably with f, thus making it impossible to consider f as a variable with σ constant. The value of this ratio which produces the greatest power factor is

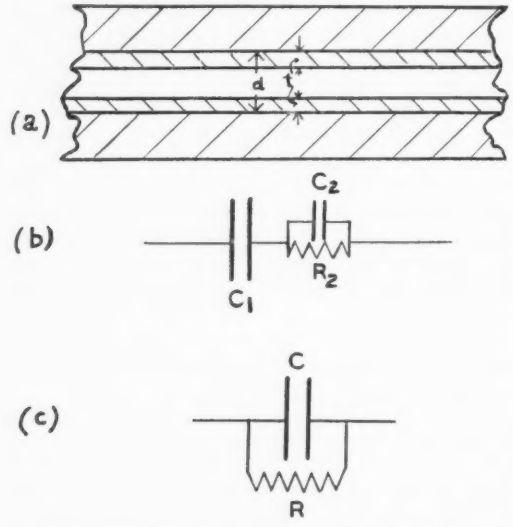

FIGURE 13.—*Electrical representation of an electrode surface layer.*

In (*a*) is shown a section of the electrodes of a capacitor separated by a distance, *d*, with films on each electrode surface of thickness, *t*. In (*b*) is shown the circuit including the electrode film which can be reduced to the equivalent circuit (*c*).

$$\frac{f}{\sigma}=\frac{1.8\times10^{12}}{\epsilon} \tag{5}$$

and the corresponding power factor is

$$\phi_{(\max)}=\frac{t}{d\epsilon}. \tag{6}$$

Since ϵ will always be greater than unity, the maximum possible power-factor effect of a thin film on an electrode surface will always be less than the ratio of the film thickness to the electrode separation. Attention should be called to the fact that the maximum is independent of either the conductivity of the film or the frequency.[3]

[3] Equations 5 and 6 are based on the assumption that ϵ is independent of f/σ. Although this may not be strictly true, it is not likely that the variation of ϵ will be sufficiently great to appreciably affect the value of f/σ at which the maximum of ϕ occurs.

As the power factor passes through its maximum value with varying conductivity and frequency, the capacitance, C, changes from C_1 to

$$C=C_1\left[1-\frac{2t}{\epsilon d}\right], \tag{7}$$

as shown by the N curves of figure 14. These types of simultaneous variations of capacitance and power factor with frequency are well-known dielectric phenomena occurring with polar molecules in a viscous medium [8] and in a heterogeneous dielectric [9] such as was

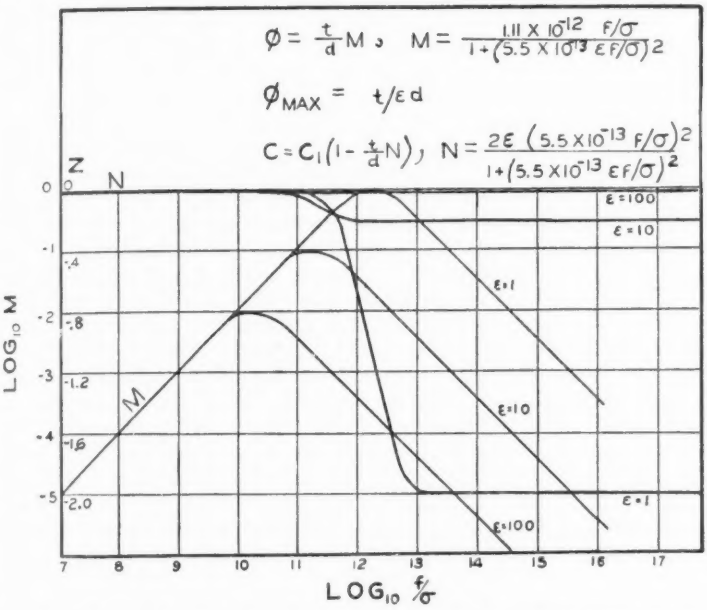

FIGURE 14.—*Curves showing the effect of an electrode film of thickness, t, conductivity, σ, and dielectric constant, ϵ, on the power factor, ϕ, and capacitance, C, of a guard-ring air capacitor of electrode spacing, d; frequency is denoted by f.*

proposed by Maxwell to explain certain types of dielectric absorption. Actually the electrode-film idea may be considered as a special case of the latter reference.

If the power-factor maxima and the over-all change of capacitance with frequency were determined for a guard-ring capacitor with an electrode surface layer, the thickness, dielectric constant, and conductivity of the layer could be determined by applications of eq 5, 6, and 7. Unfortunately, the data obtained in this investigation are inadequate for these computations. The frequency range is not sufficient to obtain the power-factor maxima and the mechanical stability of the capacitors was not sufficient to determine the capacitance changes with the required accuracy. However, the power-factor maxima obtained with varying humidities are subject to explanation by the above equations, and an examination of the data with respect to

these equations yields some information concerning the nature of the electrode films.

According to gravimetric observations [10], the amount of moisture taken up by a metal surface increases continuously with relative humidity, and above 85 percent the increase is very rapid. If the moisture formed a layer on the electrode of regularly increasing thickness, and if the conductivity of the layer were independent of thickness the observed power factors would increase with relative humidity in the same manner as does the amount of moisture deposited. Such a continuous increase is not in accordance with the power-factor maxima shown in figure 12. For the case of aluminum electrodes, these maxima can be readily accounted for by assuming that the conductivity of the oxide layer is a function of the relative humidity. According to eq 6, the value of the maximum-power factor due to variable conductivity is independent of either the conductivity or the frequency. The maxima at 200 c/s and 60 c/s are of approximately the same height, and since they occur at different relative humidities, it seems likely that for relative humidities below 80 percent the most important effect of the moisture is to change the conductivity of the surface film rather than its thickness. Assuming this to be the case, eq 6 can be applied to the maximum value for power factor to deduce a value of $14\times10^{-7}\epsilon$ cm as the thickness of the oxide layer. The somewhat lower maximum value at 1,000 c/s may be due to a higher dielectric constant at this frequency.

The power-factor minima at about 85-percent relative humidity are probably due to the increased importance of the moisture film at very high humidities. Since gravimetric observations show a very rapid increase in the amount of moisture deposited at high relative humidities, it is possible that at humidities higher than 85 percent the moisture layer becomes sufficiently thick to produce a power factor greater than that due to the aluminum oxide layer.

In the case of the silver-plated electrode surfaces and the others of similar nature there is probably no significant oxide layer, as indicated both by well-known properties of these metals and by the power-factor data for a dry atmosphere. Hence, the observed increase in power factor with relative humidity must be due entirely to the moisture on the electrode surfaces. An explanation of the maxima requires that the conductivity of the layer be a function of its thickness, probably increasing as the thickness is increased.

If the moisture layer is alone responsible for the observed power factors it is necessary to assume conductivities considerably below those obtained for water in conductivity cells. These latter values range upward from approximately 1×10^{-6} ohm^{-1} cm^{-1}. Referring to figure 14, it may be seen that such conductivities would give, at commercial and audio frequencies, extremely small power-factor effects unless the film were very thick. For example, with a conductivity of 1×10^{-6} ohm^{-1} cm^{-1} and at a frequency of 60 c/s, a film thickness of 30 microns would be required to produce the maximum power factor shown in figure 12. This is about ten thousand times the thickness of water layers observed on such metals by gravimetric methods [10]. On the other hand, the conductivity necessary to produce the maximum power factor can be computed by eq 5 if the dielectric constant and frequency are known. Assuming a dielectric constant of 80, the power-factor maximum at 60 c/s is produced by a conduc-

tivity of 2.6×10^{-9} ohm^{-1} cm^{-1}, which is considerably less than the normal conductivity of water. Equation 5 also shows that the conductivity of an electrode film necessary to produce a power-factor maximum increases with increasing frequency. Since the maxima at higher frequencies occur at higher humidities, the data and theory are consistent in assuming the conductivity of the moisture layer to increase with increasing thickness of the layer. Further evidence that the observed power factors for all electrode metals except aluminum are due primarily to the moisture layer is found in the fact that in general the magnitude of the maximum power factor is greater at the higher frequencies. This is essential because these maxima occur at higher humidities at the higher frequencies.

Assuming the dielectric constant of the moisture film to be 80, and applying eq 6 to the maximum power factors for silver electrodes, as shown in figure 12, values of 13×10^{-6} cm and 19×10^{-6} cm are obtained as the thicknesses of the film at relative humidities of 52 and 75 percent, respectively. These thicknesses are about 10 times the values obtained gravimetrically but this discrepancy may be due to the assumed value for the dielectric constant of the layer. A dielectric constant of 8 for the moisture layer would make the data consistent with gravimetric observations. More complete data would, as pointed out above, give both the dielectric constant and conductivity of the layer making it unnecessary to assume these values from other types of measurements. Additional data would also furnish more complete evidence as to whether the power factors observed with silver-surfaced and other similar electrodes are due to the moisture film alone or to moisture in combination with a layer of some foreign material. The present data are quite definite in indicating that the conductivity of the electrode film is appreciably less than the normal values for water, but can give only a ratio of film thickness to its dielectric constant. If upon separating these latter two quantities by further measurements it is found that the thicknesses are greater than those observed gravimetrically for water, then it would definitely appear that the electrode film had important constituents other than water. The conductivities necessary to produce a maximum power factor could then be attributed to a mixture of water and the other material of the film.

The data for anodized aluminum (table 1) show no definite power-factor maxima with relative humidity. This would seem to indicate that the moisture does not penetrate the oxide layer sufficiently to cause a large enough average conductivity to produce a maximum.

VI. EFFECT OF A NONHOMOGENEOUS FIELD ON POWER FACTOR

In order to determine the effect, if any, of a nonhomogeneous electric field on the power factor of an air capacitor, sharp-edged, annular grooves were cut in one of the electrodes of a brass guard-ring capacitor, as shown in figure 15. With such a capacitor there is an appreciably nonuniform field between the electrodes. The power factor of this capacitor was then measured at various electrode spacings and relative humidities. The results at 60 c/s are shown in figure 16 with power factor plotted against capacitance with relative humidity as a parameter. The dashed line, which represents the results at 43-percent

relative humidity for smooth brass electrodes (shown previously in fig. 9), is shown for comparison. The increase in power factor due to the nonhomogeneous field is quite pronounced. It is also evident that the power factor increases appreciably with relative humidity in

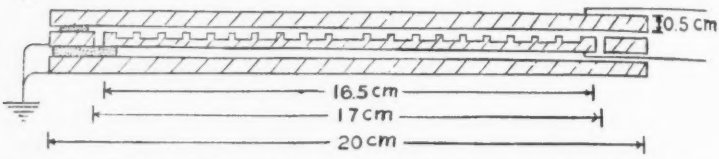

FIGURE 15.—*Section of a guard-ring capacitor showing grooves cut in one of the brass electrodes to produce a nonhomogeneous field.*

the low-humidity range and then drops to low values at high humidities. This latter behavior is qualitatively similar to that observed when the field of the guard-ring capacitor was uniform. On the other hand, there is to be noted in figure 16 a departure of the power-factor-capacitance curve from proportionality at 18-percent relative humidity and from linearity at 85-percent relative humidity. These curves

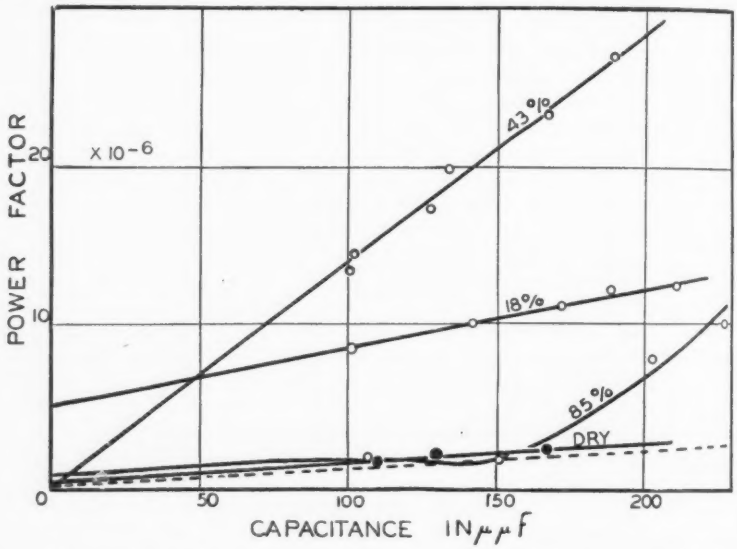

FIGURE 16.—*Power factors of a guard-ring capacitor with nonhomogeneous field at various humidities.*

The dashed line represents the equivalent values for a guard-ring capacitor with a uniform field at 43-percent relative humidity. Measurements were at 60 c/s.

may be due to one or both of the following factors: (1) the capacitance of the grooved-electrode capacitor is not inversely proportional to its electrode separation, and (2) the degree of nonuniformity of the field varies with the capacitance or electrode separation.

It is probable that the power factors represented in figure 16 are also due to energy losses in a layer on the electrode surface because of the fact that power-factor maxima with variable relative humidity

are observed. If corona were a cause of the increase in power factor produced by field distortion, there would very likely be no maximum with relative humidity. Further evidence that measurable corona losses were not present was found in the independence of the power factor upon the voltage applied to the capacitor. Although it was difficult to estimate the maximum potential gradient in the capacitor, the average field was about 500 v/cm. Upon increasing this value to 1,200 v/cm, no change in power factor was observed. The increase in power factor caused by the nonuniform field may be attributable to the fact that in such a field, dipoles as well as ions would undergo a translatory motion.

The question which now aptly arises is, how much of the loss observed in the ordinary guard-ring capacitors was due to the slight nonhomogeneity of field at the gap between the measuring electrode and the guard ring. Tests have been made on guard-ring capacitors with brass electrodes in which the width of the guard-ring gap varied from 0.2 to 2 mm, with a resulting variation in the degree of nonhomogeneity. No appreciable differences in power factors were observed, indicating that the effect of nonhomogeneity in the guard-ring capacitors used for obtaining the data of table 1 was quite negligible.

It is probable that the observed power factor of the three-electrode rotating-plate capacitor, previously discussed, is due to the nonhomogeneous field at the edges of its electrodes. Referring back to figure 1, it is seen that the power factor of this capacitor, C_2, decreases with increasing capacitance. The ratio of nonuniform field to uniform field in a rotating-electrode capacitor decreases as the capacitance increases, hence the part of the power factor originating in the nonuniform field at the edges of the electrodes of such a capacitor would decrease with increasing capacitance. Although qualitatively similar relations between power factor and capacitance were obtained for two-electrode capacitors when there was conductance between the measuring electrodes, such cannot be the cause of the power factor of the three-electrode capacitor, because the guard electrode makes possible the complete elimination of such an effect. Nor is it likely that the power factors represented by the C_2 curves of figure 1 are due to an electrode surface layer of variable thickness or conductivity, because (1) the power-factor variation with capacitance is too uniform to be due to an irregular surface layer, and (2) the same type of variation has been obtained with both aluminum electrodes and nickel-plated brass electrodes in the capacitor. The three-electrode rotating-plate capacitor was originally built with aluminum electrodes and its power-factor characteristic was believed to be due to an irregular surface layer. When it was found that aluminum electrodes gave the largest power factor of the common electrode metals the capacitor was rebuilt with nickel-plated brass electrodes. Although the power factor of the rebuilt capacitor was reduced, the same type of variation with capacitance was obtained, indicating that some source other than surface irregularities must be the cause of its power-factor characteristic. The C_2 curves of figure 1 represent nickel-plated electrodes, approximately 3 mm apart when interleaved. Referring to table 1, it is noted that the power factor due to such electrodes at 3-mm spacing should always be less than 10^{-6} when in a uniform field. It is therefore concluded that the power-factor values shown in figure 1

for the three-electrode rotating-plate capacitor are on account of the nonhomogeneous field at the edges of the electrodes.

As should be expected, it was found that the power factor of the rotating-plate capacitor varied considerably with humidity. It was possible to maintain reasonably constant power-factor values from day to day by directing a gentle stream of dry air through the capacitor. The curves of figure 1 were taken under such conditions.

VII. CONCLUSION

1. The power factors of most variable two-electrode air capacitors may be represented in the form $A+B/C$, where C is the capacitance, A depends upon the electrode material, frequency, and humidity, and B depends upon the insulation material, frequency, and humidity.

2. The losses in two-electrode capacitors are appreciably dependent on the relative humidity and frequency. Specifications of power factor for such capacitors are quite meaningless unless the capacitor is in equilibrium with its surrounding atmosphere and the conditions of measurement are clearly defined.

3. The power factor of a guard-ring capacitor is proportional to its capacitance (inverse electrode separation). The losses are also an important function of relative humidity, showing maximum values in the low-frequency range for relative humidities of about 50 percent.

4. Guard-ring capacitors with aluminum electrodes have appreciably greater power factors than those of other materials. Other materials tested were stainless steel, monel metal, nickel, and brass in addition to brass plated with silver, nickel, chromium, gold, and rhodium. No noteworthy differences between the power factors of capacitors of these materials were observed, although the silver-plated electrodes appeared to be superior by a slight margin.

5. The losses observed in guard-ring capacitors may be explained by a layer of oxide or water or both on the electrode surface. The contribution of such a layer to the power factor of the capacitor will be a maximum when the conductivity, σ, and dielectric constant, ϵ, of the layer are related to the frequency, f, as

$$\frac{f}{\sigma}=\frac{1.8\times10^{12}}{\epsilon}$$

The maximum possible power factor from such a layer for variable f and/or σ is

$$\phi_{(\max)}=\frac{t}{d\epsilon},$$

where t is thickness of the layer and d the electrode separation.

6. The data indicate that (1) the conductivity of moisture films on metals increases as the film thickness is increased and, (2) both the conductivity and dielectric constant of the moisture films are appreciably less than those of water as ordinarily measured.

7. The contribution of a surface layer to power factor is appreciably increased when the electric field is nonuniform. This may give rise to a power factor in a three-electrode rotating-plate capacitor which decreases with increasing capacitance.

VIII. REFERENCES

[1] R. F. Field and D. B. Sinclair, Proc. Inst. Radio Engrs. **24** 255 (1936). This paper contains a good bibliography on previous work on losses in air capacitors.
[2] A. V. Astin, J. Research NBS **21,** 425 (1938) RP1138.
[3] J. C. Balsbaugh and Alfred Herzenberg, J. Franklin Inst. **218,** 49 (1934).
[4] W. B. Kouwenhoven and E. L. Lotz, Am. Inst. Elec. Engrs. Trans. **57,** 766 (1938).
[5] General Radio Experimenter (October 1935).
[6] J. G. Chaffe, Proc. Inst. Radio Engrs. **22,** 1009 (1934).
[7] Cir. BS C74 (1918).
[8] P. Debye, Polar Molecules (The Chemical Catalog Co., New York, N. Y., 1929).
[9] L. Hartshorn, J. Int. Elec. Eng. **64,** 1152 (1926).
[10] Stromberg, Kgl. Svenska Vetenskapsakad Handl. **6,** 113.

WASHINGTON, March 2, 1939.

U. S. Department of Commerce National Bureau of Standards

RESEARCH PAPER RP1213

Part of Journal of Research of the National Bureau of Standards, Volume 22, June 1939

ELECTROANALYTICAL DETERMINATION OF COPPER AND LEAD IN NITRIC ACID SOLUTION CONTAINING SMALL AMOUNTS OF HYDROCHLORIC ACID

By John A. Scherrer, Rosemond K. Bell, and William D. Mogerman

ABSTRACT

In the analysis of copper-base alloys, chiefly brasses and bronze, difficulties have been encountered in consistently obtaining quantitative depositions of copper in nitric acid solutions, unless the nitric acid solution of copper is either fumed with sulfuric acid or evaporated to dryness and baked moderately. As a result of experiments made to remedy this trouble, it has been found that complete deposition of copper is obtained if a trace of chloride ion (1 drop of 0.1 *N* hydrochloric acid) is added to the nitric acid solution either during the solution of the alloy or at the beginning of the electrolysis.

CONTENTS

	Page
I. Introduction	697
II. Procedure	698
III. Discussion	699

I. INTRODUCTION

Electroanalytical determinations of copper in copper-base alloys, such as brass and bronze, are usually made by depositing the metal from an electrolyte containing sulfuric and nitric acids. For example, in analyses of alloys containing moderate amounts of lead, (less than 10 percent), the alloy may be dissolved in diluted nitric acid, the solution evaporated to dryness, and baked moderately. The residue is digested with nitric acid, diluted, and the solution filtered if metastannic acid is present. The solution is then electrolyzed and, after 1.5 to 2.5 hours, when all or most of the lead has been deposited as the peroxide on the anode, 3 to 4 ml of sulfuric acid is added, and the electrolysis continued to complete the deposition of copper on the cathode.

If larger amounts of lead are present, after tin is removed as metastannic acid, sulfuric acid is added to the nitric acid solution and the lead removed by evaporating the solution to fumes of sulfuric acid, diluting, and filtering. Three to four ml of nitric acid is added to the filtrate, which is then electrolyzed for copper and residual lead.

In one of the procedures used at the National Bureau of Standards for the routine analysis of brasses and bronzes, the alloy is dissolved in diluted nitric acid and the solution boiled for about 5 minutes after oxides of nitrogen are no longer visible. The solution is then diluted, neutralized with ammonium hydroxide, made about 3-percent acid with nitric acid, and electrolyzed. If tin is present, the solution is filtered before neutralizing with ammonium hydroxide. This method is shorter than those calling for dehydration, or fuming with

sulfuric acid, and is applicable for the simultaneous determination of copper and lead in many of the alloys which are received for analysis. This procedure had been used at the Bureau for a number of years and yielded satisfactory results for copper and lead. Recently, however, increasing difficulties were experienced in obtaining quantitative deposition of copper. For example, in a series of 10 electrolyses, run at the same time, satisfactory deposition of copper would be obtained in possibly 6 to 8 cases, and only 50- to 80-percent deposition in the other determinations.

Experiments were made from time to time in an attempt to find and eliminate the trouble. A number of so-called addition-agents, such as sulfur dioxide, hydrogen peroxide, urea, and a number of other organic materials, were added to the electrolyte both prior to, and during electrolysis, but none of these were satisfactory. It was observed, however, that if the nitric acid solution was evaporated to dryness and the residue baked moderately, or if the solution was fumed with sulfuric acid and nitric acid added, satisfactory deposition of copper was obtained in the subsequent electrolysis.[1] Prolonged boiling of the nitric acid solution of copper, or evaporation of the solution to dryness on a steam bath, lessened the number of faulty determinations, but did not completely eliminate the difficulty of obtaining quantitative depositions.

With the thought that traces of certain elements possibly in the nitric acid of earlier date might have had a critical effect, experiments were made in which small amounts of halides were added to the nitric acid. Surprisingly, it was found that quantitative deposition of copper is obtained if a trace of chloride ion (1 drop of 0.1 *N* hydrochloric acid) is added to the nitric acid solution, either during solution of the alloy or at the beginning of the electrolysis. Deposits of copper so obtained are of normal appearance, and the attack on the electrodes is no greater than is encountered in the absence of hydrochloric acid.[2]

II. PROCEDURE

The following procedure is recommended for the routine determination of lead and copper in brasses and bronzes.

Cylindrical electrodes 1.5 and 2 inches in diameter, and 1.75 inches in height, made from approximately 50-mesh platinum gauze are the most satisfactory type. Before using the electrodes they must be thoroughly cleaned and ignited to remove any previous deposit or grease. To do this, immerse the electrodes in diluted nitric acid (1+1)[3] until copper, lead or other metals are dissolved.[4] Remove the electrodes, rinse with distilled water, and place them in a fresh solution of diluted nitric acid (1+1). Add a few drops of ethyl alcohol and boil for about 10 minutes. Remove, and rinse the electrodes with distilled water. Ignite in the flame of a large burner, or several burners, so that the entire gauze area is uniformly heated (to bright redness) for 5 minutes or more. Cool in a desiccator, and weigh.

[1] It should be mentioned that very small amounts of copper, usually less than 0.2 mg, may remain in the electrolyte.

[2] In an internal electrolysis method for copper and bismuth, Clark, Wooten, and Luke add a little chloride to open clogged diaphragms (Ind. Eng. Chem. Anal. Ed., 8, 411 (1936).

[3] This denotes, throughout the paper, 1 volume of concentrated nitric acid (sp gr 1.42) diluted with 1 volume of water. If no dilution is specified, the concentrated reagent is meant.

[4] With a heavy deposit of lead peroxide, add a few drops of ethyl alcohol and heat until solution ensues.

Place 1 g of the well-mixed sample in a 250-ml beaker, cover, add 25 ml of diluted nitric acid (1+1) and 1 drop of 0.1 *N* hydrochloric acid. When the action has ceased, heat to boiling, and continue the boiling for about 5 minutes after the red oxides of nitrogen have disappeared. Dilute to about 150 ml with distilled water. If the alloy contains tin, use hot distilled water, digest the solution for an hour or more, filter through a paper of close texture, and wash the precipitate with hot diluted nitric acid (1+99).[5]

Neutralize [6] the filtrate with ammonium hydroxide,[7] add an excess of 6 ml of nitric acid,[8] and dilute to 200 ml. Insert the electrodes so that the surface of the cathode clears the anode by at least 5 mm, and both electrodes almost touch the bottom of the beaker. Cover the beaker with split watch glasses, and electrolyze with a current of 0.2 to 0.4 ampere until deposition is complete, usually overnight. Without interrupting the current, slowly lower the beaker, and, at the same time, wash the electrodes with a stream of distilled water. Immediately immerse the electrodes in another beaker containing distilled water, lower the beaker, discontinue the current, and disconnect the electrodes. Rinse the cathode with ethyl alcohol, shake off the excess alcohol, and dry for a few minutes in an oven at 110° C. Cool in a desiccator and weigh. If a deposit of lead peroxide is indicated on the anode, rinse the latter with water and dry for about an hour at 180° C. Cool in a desiccator, weigh as PbO_2, and use the factor 0.866 to calculate the percentage of lead.[9]

III. DISCUSSION

Results obtained when the recommended procedure was applied to samples of copper and lead of high purity are shown in tables 1 and 2. In addition, the procedure has now been in daily use for the past year in the analysis of various brasses and bronzes in the Bureau's laboratories, without a single instance of unsatisfactory deposition of copper.

The addition of the very small amount of chloride ion does not cause any significant attack on the electrodes. The loss in weight of the anodes in 75 electrolyses averaged less than 0.1 mg, which is of the same order of magnitude as in the absence of hydrochloric acid.

As regards the minimum amount of chloride ion, 5 drops of 0.01 *N* hydrochloric acid generally yielded quantitative deposition of copper, but less than this amount was not satisfactory.

Despite a considerable amount of experimental work, no suitable explanation can be offered at this time as to why the addition of a small amount of chloride ion eliminates the difficulties encountered in obtaining quantitative deposition of copper from a nitric acid solution. Hydrochloric acid had the same effect whether added during solution of the sample, or at the beginning of the electrolysis. It was also

[5] Slight amounts of copper and lead are retained by the metastannic acid and should be recovered in very accurate work, but they are generally disregarded in routine analyses. The recovery can be made by treating the precipitate and paper with sulfuric and nitric acids until the paper is destroyed and then making an alkaline sulfide separation. The presence of the very small amount of hydrochloric acid does not vitiate the complete separation of tin as metastannic acid.

[6] Litmus paper is a suitable indicator, though, with a little experience, the neutral point can be located by the formation of the blue-colored copper complex in ammoniacal solution.

[7] See page 700, for procedure with 5 g of copper.

[8] Tests have shown that when, in the absence of lead, an excess of 5 ml of sulfuric acid is added instead of nitric acid, complete deposition of copper is obtained without the addition of hydrochloric acid.

[9] If manganese is present in the electrolyte some of it will be deposited with the lead. In this case dissolve the deposit in about 10 ml of diluted nitric acid (1+1) containing a few drops of ethyl alcohol. Dilute, and treat with hydrogen sulfide. Filter the lead sulfide, dissolve it in nitric acid, and deposit the lead electrolytically as the peroxide.

found that if the deposition of copper in nitric acid solution was not complete in 18 hours in the old method, continued electrolysis did not help, but if 1 drop of 0.1 *N* hydrochloric acid was then added, quantitative deposition of copper was obtained within the time indicated in the recommended procedure.

TABLE 1.—*Results obtained by applying the recommended procedure in analyses of high-purity copper*

COPPER			
Added	Recovered [1]	Added	Recovered [1]
g	*g*	*g*	*g*
0.0580	0.0580	1.0075	1.0073
.0570	.0571	1.0052	1.0051
.1568	.1568	1.0006	1.0007
.1505	.1506	1.0005	1.0006
1.0056	1.0055	2.0007	2.0008
1.0056	1.0054	2.0001	2.0001

[1] A little copper was usually left in the electrolyte—less than 0.1 mg in electrolyses of 50 to 150 mg of copper and from 0.05 to 0.2 mg in those involving 1 to 2 g of copper.

TABLE 2.—*Results obtained by applying the recommended procedure to mixtures of copper and lead of high purity*

Copper		Lead	
Added	Recovered [1]	Added	Recovered
g	*g*	*g*	*g*
1.0072	1.0072	0.0562	0.0561
1.0026	1.0026	.0543	.0539
1.0073	1.0072	.0636	.0636
1.0066	1.0065	.0635	.0636
1.0002	1.0002	.0559	.0559
1.0007	1.0005	.0559	.0555

[1] A little copper, ranging from 0.05 to 0.2 mg, was usually left in the electrolyte.

Although the recommended procedure is not intended to replace the Battery Assay Method for Copper specified by the American Society for Testing Materials,[10] the procedure is useful, in cases where sulfates are objectionable, for separating copper in large samples. However, with 5 g of copper, neutralization with ammonium hydroxide is not satisfactory, and the procedure is modified as follows: Dissolve 5 g of sample in exactly 30 ml of diluted nitric acid (1+1). Add 1 to 2 drops of 0.1 *N* hydrochloric acid, and boil gently for about 5 minutes after the red oxides of nitrogen have disappeared. Dilute to 225 ml, electrolyze with a current of 0.4 ampere until deposition is complete, usually 17 to 19 hours. Quantitative deposition is obtained. For example, in a series of eight determinations on 5-g samples, the undeposited copper in the electrolyte ranged from 0.1 to 0.3 mg.

Sodium chlorate, potassium bromide or bromate, and potassium iodide or iodate function like hydrochloric acid or sodium chloride, but the weight of the deposited copper was generally a few tenths of a milligram too high. The addition of 1 to 2 drops of 0.1 *N* hydrofluoric acid does not cause complete deposition in the absence of chloride; on the other hand, it does not vitiate the beneficial action of the chloride ion in the recommended method.

WASHINGTON, March 20, 1939.

[10] Methods of Chemical Analysis of Metals, ASTM, p. 111, Designation: B34-36T. (1936). If lead- and tin-free brasses are dissolved in the sulfuric-nitric acid mixture specified in the Battery Assay Method, quantitative deposition of copper will be obtained when the solution is electrolyzed.

U. S. Department of Commerce National Bureau of Standards

RESEARCH PAPER RP1214

Part of Journal of Research of the National Bureau of Standards, Volume 22, June 1939

BUBBLER TIP OF PYREX GLASS FOR DIFFICULT ABSORPTIONS

By Joseph R. Branham and Edward O. Sperling

ABSTRACT

This paper describes a tip made of Pyrex glass to be used in a gas-absorption pipette to divide the stream of gas into small bubbles in order to obtain a large surface of contact with liquid reagents. The tip is made by sealing a number of fine copper wires, radiating from a center in a definite pattern, between a cone formed on the end of a glass tube and a circular glass disk. After the glass parts are sealed together and ground to expose the ends of the wires, the wires are dissolved in warm nitric acid. Drawings which illustrate the method of making the tips are included. The tips are very sturdy and at moderate pressures furnish small bubbles of uniform size and distribution.

This paper describes a tip used for dividing a gas stream into bubbles for the washing of gases or for their absorption in liquid reagents. The tip was developed primarily for the absorption of oxygen in an alkaline solution of potassium pyrogallate in an Orsat apparatus. It is, of course, adaptable to other reagents and to other forms of apparatus. Each unit of the Orsat apparatus for which the tip was designed was made of Pyrex glass and sealed directly together to avoid rubber connections.[1] The extent to which absorption is accelerated by dividing the gas stream passing through the reagent into small bubbles which offer a large surface of contact has been discussed in connection with two gas-absorption pipettes previously described. The gas entering the inlet tube of these pipettes is divided into small bubbles by passage through either a platinum disk drilled with several hundred orifices, 0.06 mm in diameter,[2] or through a porous Jena glass thimble.[3] Other types of porous or perforated disks have also been used to some extent, particularly in wash bottles.

The absorption pipette described in this paper is shown in figure 1. The dimensions of all drawings are given in millimeters. The front and top views of the assembled distributor tip are shown in figure 2, *A* and *B*, respectively. At the left, in figure 2, are shown cross-sectional views of the parts *C*, *D*, and *E*, from which the tip is made and the top view of the copper spider, *F*, which is sealed between *C* and *E* at *D*. A thin copper disk, *G*, may be substituted for *F*, if desired. The spider, *F*, constructed of small copper wires, as is described later, or the thin copper disk, *G*, serve as temporary spacers which are later dissolved in nitric acid to leave channels of like shape in the glass. After *E* is sealed to *C* the outer ends of the wires forming

[1] For a discussion of errors caused by such connections, see, J. R. Branham, *Errors in gas analysis arising from loss of gas by solution in rubber connections and stopcock lubricant*, BS J. Research **12**, 353 (1934) RP661.
[2] Martin Shepherd, *A gas analysis pipette for difficult absorptions.* BS J. Research **4**, 747 (1930) RP177.
[3] Martin Shepherd, Fish-Schurman Catalogue, p. 18.

the spider are fully exposed to the original diameter of the wire by grinding the sides of the assembled tip, *A*.

The cross section of the graphite molds [4] used to make *C* and *E* of figure 2 are shown in figure 3, *A* and *B*, respectively. The part of *A* shown blackened in figure 3 is made of steel which has been heated and dipped into beeswax. When this mold is used, the upper section of *A* is removed and slipped on a glass tube. The glass tube is then heated and thickened into a heavy-walled cone at its lower end. The hot softened glass is then inserted and pressed into the lower section of the mold, which is kept sufficiently hot to prevent the glass from cooling too rapidly. The glass disk, *E* of figure 2, is formed at D, figure 3, in a similar manner, except that glass rod is used and a solid ball of glass is collected instead of the hollow cone. After the glass has cooled, it is file-scratched at *F* and broken from the stem, *E*. The broken edge which results is ground nearly flat before the spider is sealed between the glass parts.

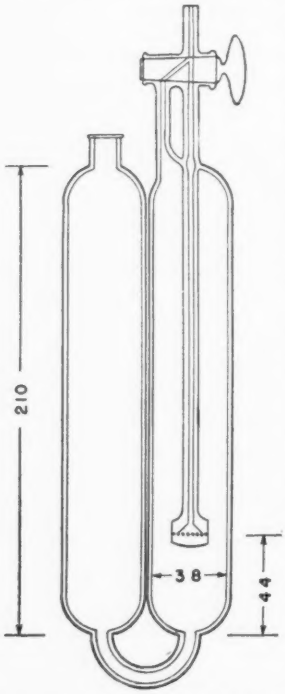

FIGURE 1.—*A Pyrex absorption pipette and bubbler tip.*

The copper spiders are made by winding a single length of copper wire on the hardened steel form, *A*, shown in figure 4. This operation produces one spider at each end of the cylinder. The pegs on the side of the cylinder are used to secure one end of this wire at the start of the winding operation and the other end when the winding is finished. The windings pass nearly vertically up and down the sides of the cylinder and are guided across the top and bottom of the cylinder by the slots shown in *B* of figure 4, so that each turn of wire crosses the axis of the cylinder. After winding is complete, that is, when 10 turns have been made and the ends of wire secured, two brass guides, each with a sliding steel plunger, are slipped over the ends of *A*. One of these guides is shown at *C*, figure 4. Sufficient pressure is then applied to the two plungers, by means of a vise, to mash the wires against a steel rod, the faces of which are flush with the bottom of the guiding slots. As a result of this operation the wires at the center of the spider become matted together sufficiently to permit handling the spider with forceps without its falling apart. Spiders have been made, as described, of copper wires of 0.20-, 0.16-, 0.13-, and 0.10-mm diameter. The spiders become increasingly fragile as the diameter of the wire decreases, and about one-half of the spiders made with 0.10-mm wire fell apart when being handled. This fragility may have resulted from insufficient wire in the center of the spider to mat securely, or from a difference in the quality of the more finely drawn wire. The wires forming the spider are next cut with a sharp tool, for instance,

[4] The authors are indebted to Harry Bailey of this Bureau for advice on design and for making the graphite and steel molds and forms used in this study.

a safety-razor blade,[5] at the outer edge of each slot (fig. 4, *B*) and are then ready to be sealed into glass parts of the tip.

The sealing of the copper spider[6] between *C* and *E* of figure 2 is done in two steps. (1) The spider is first placed between *C* and *E*

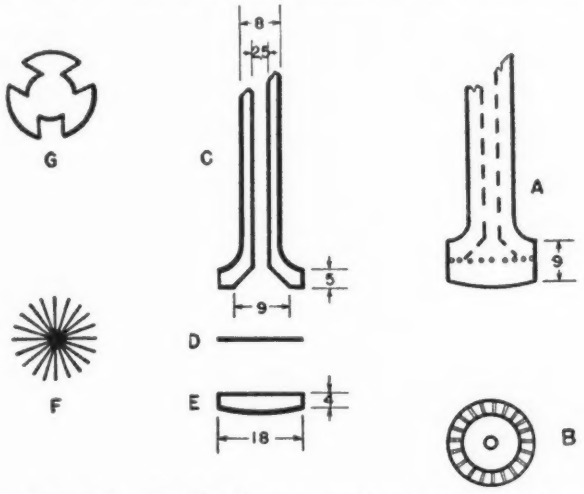

FIGURE 2.—*Details of separate parts and assembled tip.*

in the position shown in figure 5, *C* being supported in a hole bored in a transite block, *A*. The parts are then heated by a hand torch until the glass around the spider softens sufficiently to permit the spider to become partially imbedded in the glass so that its position will not change during the subsequent operations. (2) The tip is then removed from the block and heated to a higher temperature in a blast lamp until the glass is soft enough to flow and completely fill the spaces between the wires when marvered.[7]

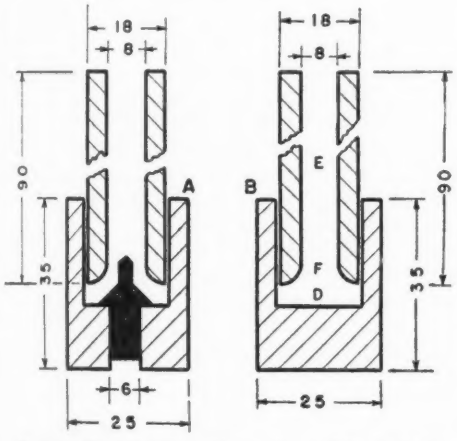

FIGURE 3.—*Cross sections of graphite molds.*

During these operations a thin layer of glass flows and covers the ends of the wires of the spider.[8] This layer of glass is removed by inserting the tip into the chuck of a lathe and grinding it until the ends of the wires are exposed as uniform circles. The final

[5] This blade will cut the copper better if the angle between the sides of the cutting edge is increased to about 60 degrees by grinding it on a whetstone.

[6] Dipping the spider into a dilute solution of borax before this seal is made appears to be of no advantage but may help when *G*, figure 2, is substituted for *F*.

[7] A glass-blowing term which denotes the application of pressure to a thoroughly heated piece of glass by rotating the glass while pressing it against a form of suitable material.

[8] The diameter of the spider should be very slightly less than that of the glass parts, to prevent the wires from oxidizing or fusing. Extreme temperatures which might melt the wire and deform the circular channels should be avoided.

operation is to dissolve the wires by immersing the tip in warm concentrated nitric acid, which leaves channels from which gases will issue as small bubbles.

During the earlier period of this study, several pipette tips similar to those described, except for the orifices, were made by using thin copper disks instead of the copper spiders which were developed later. One of these disks is shown at *G* in figure 2. The disks are about 0.075 mm thick and slotted, as shown, to permit the glass parts to be sealed together over the slotted areas. The bubble-making characteristics of these tips were about the same as those of the tips made with wire spiders. They were, however, somewhat more difficult to make, because excessive strains developed between the glass junctions and frequently caused the glass disk to separate from the cone when the tip was being ground to expose the edge of the disk. It was found in most cases that this breakage could be avoided by making several crisscross incisions at the center of the disk to relieve part of the shrinkage of the copper and by thoroughly annealing the tip after the copper disk had been sealed in place.

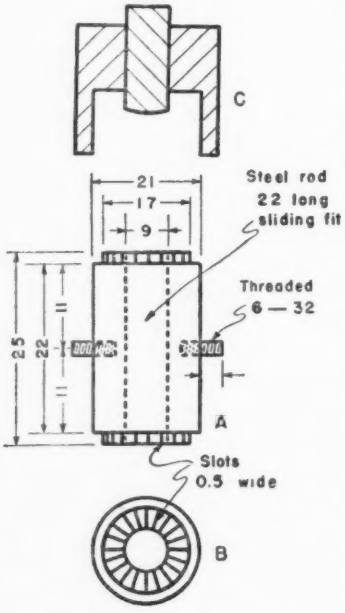

FIGURE 4.—*Form used in making copper spiders.*

The size of the orifices in the pipette tip that should be selected for use for a given absorption will depend primarily on the pressure which can be used without danger of causing leakage of gas in the apparatus, and the rate at which it is desired to pass the gas through the reagent. These two factors determine the size of orifices which may be used and, therefore, the size of bubbles that will result in a given reagent. There are, of course, other variables, such as the rate of reaction between the gas and reagent, the physical solubility of "inert" gases in the reagent, and the dead space of the apparatus, which should be considered so as to obtain the best results under a given set of conditions. The relation between rate of flow, pressure, and the four sizes of orifices used in the Pyrex tips are given in figure 6. These measurements were made with the tips immersed in water while air was bubbled through them. The depths of immersion of the tips below the surface of the water were subtracted from the observed total pressures. It was found advisable to increase the pressure of the gas slowly, until the liquid within the tip was discharged. This prevented the building up of excessive pressures which would cause a surge of relatively large bubbles of gas when the first portion of gas entered the liquid.

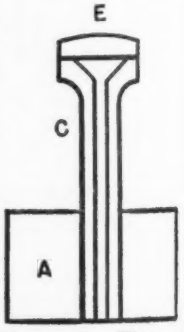

FIGURE 5.—*Tip support used during initial sealing of copper spacers.*

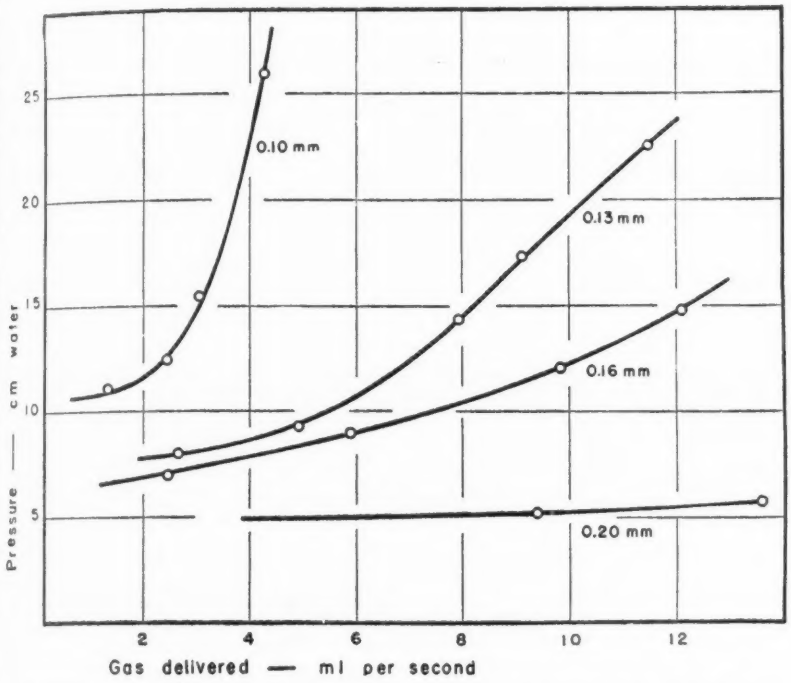

FIGURE 6.—*Pressure-rate relations, air into water, for several sizes of orifices.*

Gas-absorption pipettes equipped with tips of the kind described have been used successfully in this laboratory for the determination of oxygen by absorption in alkaline solutions of potassium pyrogallate. The tips are exceedingly sturdy and will withstand high pressures and rough treatment. The gas stream is divided by the tips into small bubbles of uniform size without subjecting the gas to excessive pressures.

WASHINGTON, March 1, 1939.

146065—39——6

U. S. DEPARTMENT OF COMMERCE NATIONAL BUREAU OF STANDARDS

RESEARCH PAPER RP1215

Part of Journal of Research of the National Bureau of Standards, Volume 22, June 1939

EFFECTS OF ALUMINUM AND OF ANTIMONY ON CERTAIN PROPERTIES OF CAST RED BRASS

By Harold B. Gardner [1] and Charles M. Saeger, Jr.

ABSTRACT

Additions of aluminum in amounts from 0.005 to 0.10 percent were made to red brass, made of remelted metal, of the nominal composition of 85 percent of copper and 5 percent each of tin, zinc, and lead. Determinations of tensile properties, density, hardness, the running property, and the ability to withstand hydraulic pressure, made on various types of test bars and test specimens, showed that all additions of aluminum had a deleterious effect on the properties and the structure. The effect was more pronounced with the higher concentrations of aluminum and was particularly evident on the ductility and the resistance to hydraulic pressure.

Additions of antimony to this alloy in the amounts ranging from 0.10 to 0.25 percent had only a nominal effect on all of the properties studied except the running property, which was increased.

These results indicated that the presence of 0.25 percent of antimony is permissible, but that even 0.005 percent of aluminum has a deleterious effect on the alloy.

CONTENTS

	Page
I. Introduction	707
II. Materials and methods of casting	708
1. Molding, melting, and pouring	708
III. Results and discussion	709
1. Tensile strength	709
2. Yield strength	711
3. Ductility	712
4. Brinell hardness	712
5. Electrical resistivity	712
6. Density	712
7. Running qualities	719
8. Pressure testing	719
9. Metallographic examination	726
IV. Summary	726
V. References	727

I. INTRODUCTION

Upon the recommendation of the American Society for Testing Materials, the Non-Ferrous Ingot Metal Institute has sponsored at the National Bureau of Standards, since 1930, a study of the physical properties of copper-base alloys. A typical alloy of the red-brass group, widely used in industry, having the nominal composition of 85 percent of copper and 5 percent each of tin, zinc, and lead, has been under investigation.

[1] Research Associate at the National Bureau of Standards, representing the Non-Ferrous Ingot Metal Institute.

In 1932 [1] [2] a paper was presented before the American Society for Testing Materials containing the results obtained on the study of the effect of type of test bar and of pouring temperature upon the physical properties of this alloy when made from virgin metal and from remelted metal.

The next phase of the investigation was to study the effect of impurities on the physical properties of the alloy, made from remelted metal. A paper [2] was presented before this Society in 1933 containing the results of the study of the effects of sulfur and iron as individual impurities to the alloy. Since that time, studies have been made of other elements added individually, and the influence of these elements on the physical properties of the alloy has been determined. In the present paper, data on the effects of aluminum and antimony on the remelted alloy are presented.

In carrying out this phase of the work, three types of test bars were used. These were the sand-cast ¼-in. web fin-gate bar, the immersed-crucible bar and the no-side-chill bar cut from a chill-mold ingot. Dimensioned drawings of each of these types of test bars were shown in the first paper of this investigation [1]. By using these three types of test bars, it was possible to obtain comparative data on the physical properties of a heat of the alloy from: (a) specimens uninfluenced by pouring or mold conditions, obtained in a suitably covered crucible immersed beneath the surface of the molten metal, (b) specimens cast in green-sand molds, and (c) specimens cast in chill molds. The test bars were representative of heats of the remelted alloy to which additions of aluminum from 0.005 to 0.10 percent had been made, and from heats containing additions of antimony ranging from 0.10 to 0.25 percent. Specimens were cast at three pouring temperatures: 1,065° C (1,950° F), 1,150° C (2,100° F), and 1,230° C (2,250° F).

Determinations of the following physical properties were made on each bar: Tensile properties, density, and Brinell hardness. In addition, electrical resistivity, the ability to withstand hydraulic pressure, and the fluidity or running property when cast in a green-sand mold were determined. Special test specimens were required for measurements of the two latter properties.

II. MATERIALS AND METHODS OF CASTING

Virgin copper, tin, zinc, and lead similar in grade to those reported in 1932 were used. By chemical analysis, the only significant impurities found in the metal of these grades were approximately 0.005 percent of iron in the copper, 0.01 percent of iron in the zinc, 0.015 percent of iron and 0.1 percent of bismuth in the lead, and 0.02 percent of iron in the tin. Small quantities of commercial antimony were used for additions of this element to the alloy. A copper-aluminum "hardener", containing approximately 50 percent of aluminum, was prepared from virgin copper and notched-bar aluminum and was used for small additions of aluminum.

1. MOLDING, MELTING, AND POURING

Early in this investigation a "standard practice" of molding, melting, and pouring was adopted. This consisted in the preparation of a stock material made from virgin metals melted in a high-frequency

[2] Figures in brackets indicate the literature references at the end of this paper.

induction furnace of the "lift-coil" type and cast into ingots. A portion of the stock (approximately 100 lb) was melted, as needed, under a "Purite" (sodium carbonate) slag in a double-wall clay-graphite crucible. A double-wall crucible, with the interstices filled with chrome ore, was used to avoid an excessive temperature drop during the casting of the test bars. Even when this special crucible was used, it was found that there was a temperature drop of the molten metal of 25° C during the pouring of the 12 molds at 1,230° C (2,250° F). The drop in temperature of the molten metal was less for lower pouring temperatures, being only 15° C at 1,065° C (1,950° F). Because of this cooling of the molten metal during the pouring of each set of specimens, the first bar in each group was poured at a temperature of 10° C above the nominal pouring temperature. The mean pouring temperature for each group of bars, therefore, is a close approximation to the desired pouring temperature.

The green-sand molds used were prepared from grade 00 Albany sand. A permeability number of 12 to 16 (AFA units), a compressive strength of 5 to 7 lb/in.^{2}, and a moisture content of 6 to 7 percent were maintained throughout the preparation of all of the green-sand molds.

Antimony additions were made without difficulty directly to the molten alloy through the Purite slag. However, considerable difficulty was encountered at first in retaining the desired amount of aluminum in the alloy. A method found satisfactory for retaining the desired amount of aluminum was as follows: The metal was melted under a Purite slag which was later removed and replaced by a cover of hot charcoal. The necessary amount of the copper-aluminum hardener was thrust through the charcoal into the molten metal, and the stirring action of the furnace insured a thoroughly uniform distribution throughout the molten metal in the crucible. The melt was then brought to the desired maximum temperature (56° C (100° F) above the pouring temperature), removed from the furnace, allowed to cool to the first pouring temperature, and poured into the molds.

III. RESULTS AND DISCUSSION

The tensile properties were determined with an Amsler universal testing machine of 50,000-lb. capacity, adjusted to give a rate of travel of the free crosshead of 0.1 in./in./min. The test specimen used was 0.505 in. in diameter, with threaded ends and a 2-in. gage length. In most cases, the determinations of tensile strength of the duplicate bars agreed within 1,000 lb/in.^{2} (about ± 3 percent), although there were a few larger variations. In such cases, the higher values were accepted as being more characteristic of the sound metal.

1. TENSILE STRENGTH

In figure 1 are shown the results obtained on the remelted alloy containing additions of aluminum in progressively increasing amounts. A definite but somewhat irregular decrease in tensile strength may be observed. A comparison of the data with the "minimum tensile strength expected for this alloy" (27,000 lb./in.^{2}), indicated by the broken line [3], shows that the addition of even 0.005 percent of aluminum (the amount now permitted in ASTM Specification B 30–36) adversely affected the alloy. The results in figure 2, however, indicate

that antimony did not have a very pronounced influence on the tensile properties of this alloy. A comparison of the values obtained

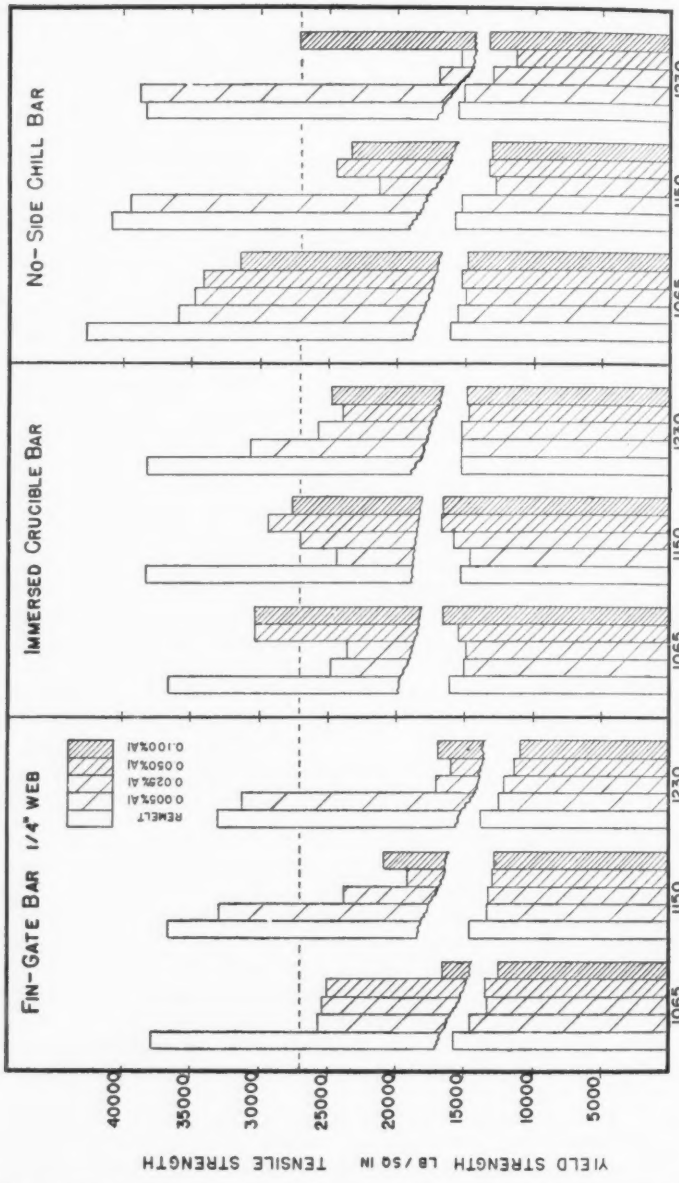

FIGURE 1.—*Effect of additions of aluminum on the yield strength and tensile strength of cast red brass (85–5–5–5) test bars.*
Minimum tensile strength for this alloy (ASTM Spec. B 30-36) is shown by the broken line.

with the three types of test bars with the "minimum tensile strength expected", indicated by the broken line, shows that most of the bars had a tensile strength well above this "minimum."

2. YIELD STRENGTH

Figures 1 and 2 show also the data obtained for yield strength of the alloy containing progressively increasing small additions of aluminum or of antimony. The method used was that outlined in the ASTM Standards (1933) [4] for a permanent set of 0.1 percent.

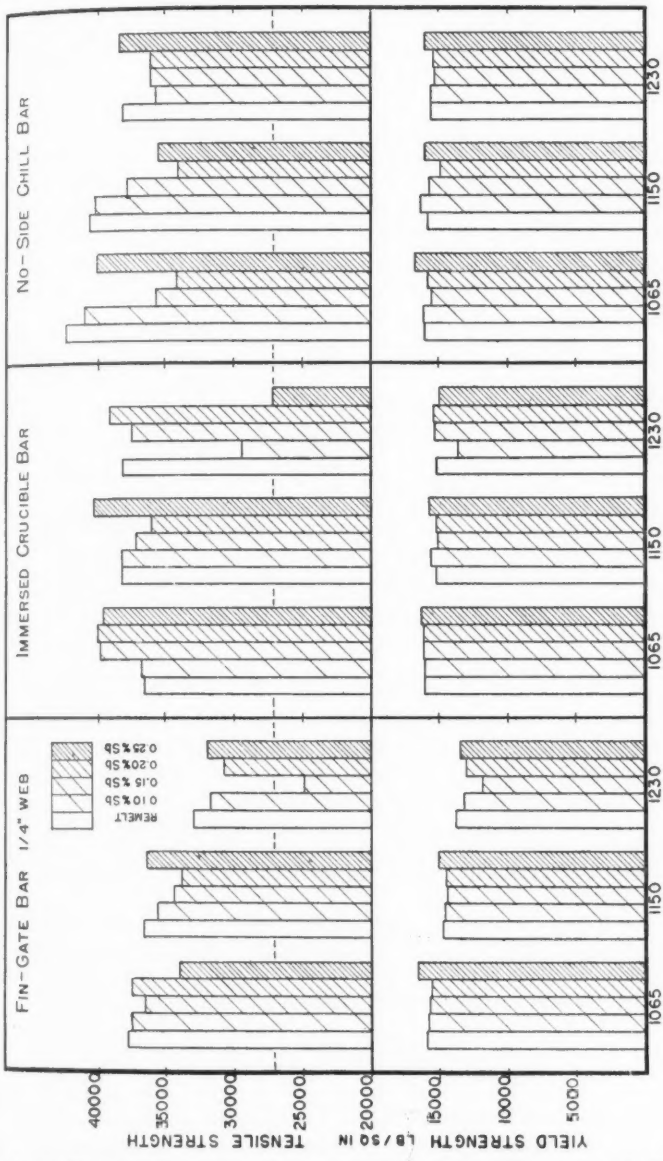

FIGURE 2.—*Effect of additions of antimony on the yield strength and tensile strength of cast red brass (85–5–5–5) test bars.*
Minimum tensile strength for this alloy (ASTM Spec. B 30-36) is shown by the broken line.

According to figure 1, the influence of aluminum in the sand-cast test bars was to produce a gradual reduction in yield strength, which became more pronounced as the pouring temperature was increased.

For the other types of test bars, however, the apparent effect on the yield strength was by no means uniform. As shown in figure 2, antimony, in the small amounts used, did not have a marked influence on the yield strength of the alloy.

3. DUCTILITY

The properties, elongation, and reduction of area, which may be considered as criteria of the ductility of an alloy, will be considered together. In figure 3 are shown the effects of aluminum additions on both elongation and reduction in area. The decrease in both properties was quite large, and, particularly for the sand-cast test bars, was rather uniform as the aluminum content was increased. From the results obtained with the specimens containing antimony (fig. 4), however, it cannot be said that antimony itself adversely affects these properties. The variations noted were inconsistent, and, for several test bars with the higher percentages of antimony, results superior to those of the plain remelted alloy were obtained.

4. BRINELL HARDNESS

Brinell indentations were made on longitudinal parallel flat faces ⅝ in. in width, machined on the threaded portions of the broken tension specimens. As recommended by the American Society for Testing Materials, for testing nonferrous materials, a 500-kg load was applied for 30 seconds on a ball 10 mm in diameter. According to the results, shown in figure 5 for aluminum additions and in figure 6 for antimony, it may be said that the indentation hardness of the alloy was influenced to only a small degree by either added element. The addition of aluminum tended to lower slightly the hardness, but additions of antimony did not result in a significant deviation from the hardness of the untreated alloy.

5. ELECTRICAL RESISTIVITY

Determinations of electrical resistivity were made on the machined specimens used subsequently for tension tests. These determinations were carried out in accordance with the procedure recommended by the American Society for Testing Materials [5].

In figure 5 it is shown that the added aluminum greatly increased the resistivity of the alloy. For both the sand-cast and the no-side-chill test bars the resistivity increased progressively with the increase in aluminum content.

In figure 6 the data show a definite increase in electrical resistivity with the corresponding addition of antimony. With the exception of the immersed-crucible bars cast at 1,230° C, maximum values were obtained with the addition of 0.15 percent of antimony.

6. DENSITY

Density was determined on the ends of the broken tensile test specimens by the conventional method of displacement of water, and the values are corrected to 20° C. The data on the influence of added aluminum are summarized in figure 7 and for antimony in figure 8. In figure 7 it is shown that the general trend is for a lowering in density, which can be attributed to the aluminum present. The

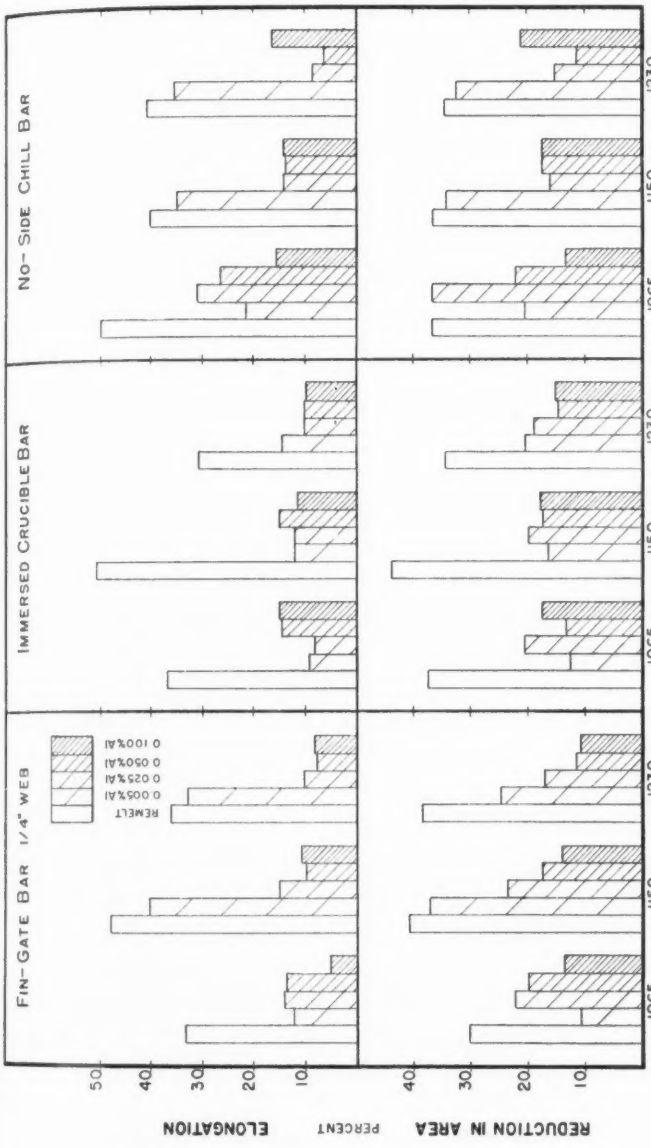

FIGURE 3.—*Effect of additions of aluminum on the elongation and reduction in area of cast red brass (85–5–5–5) test bars.*

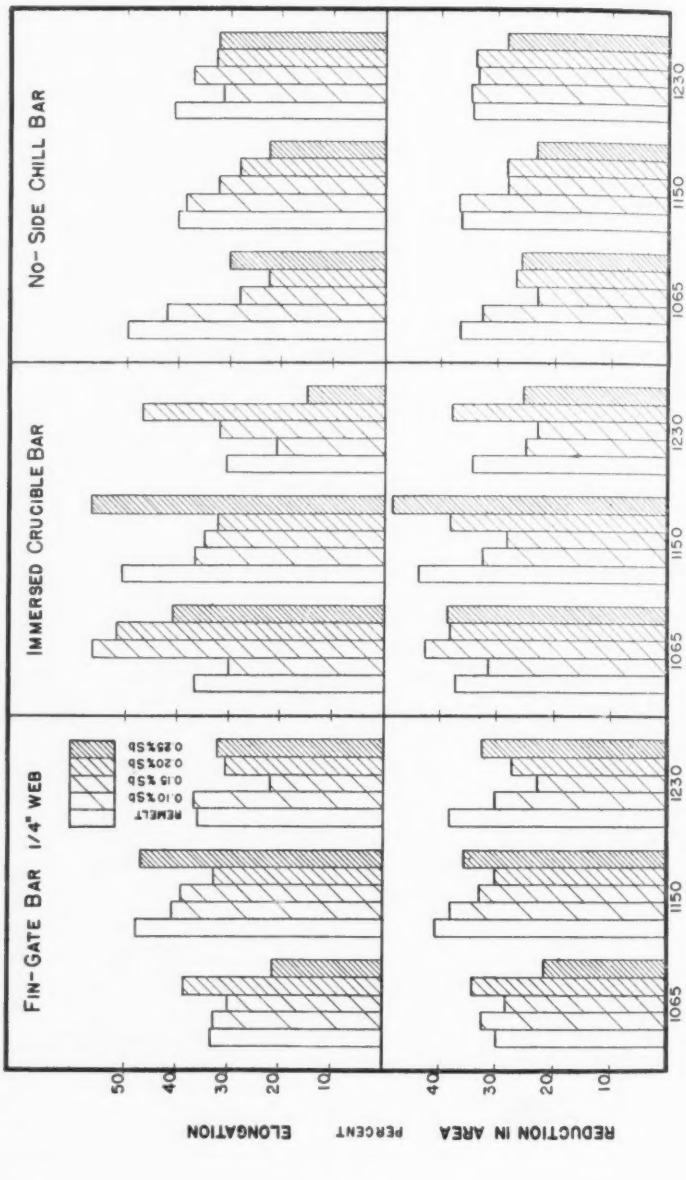

FIGURE 4.—*Effect of additions of antimony on the elongation and reduction in area of cast red brass (85–5–5–5) test bars.*

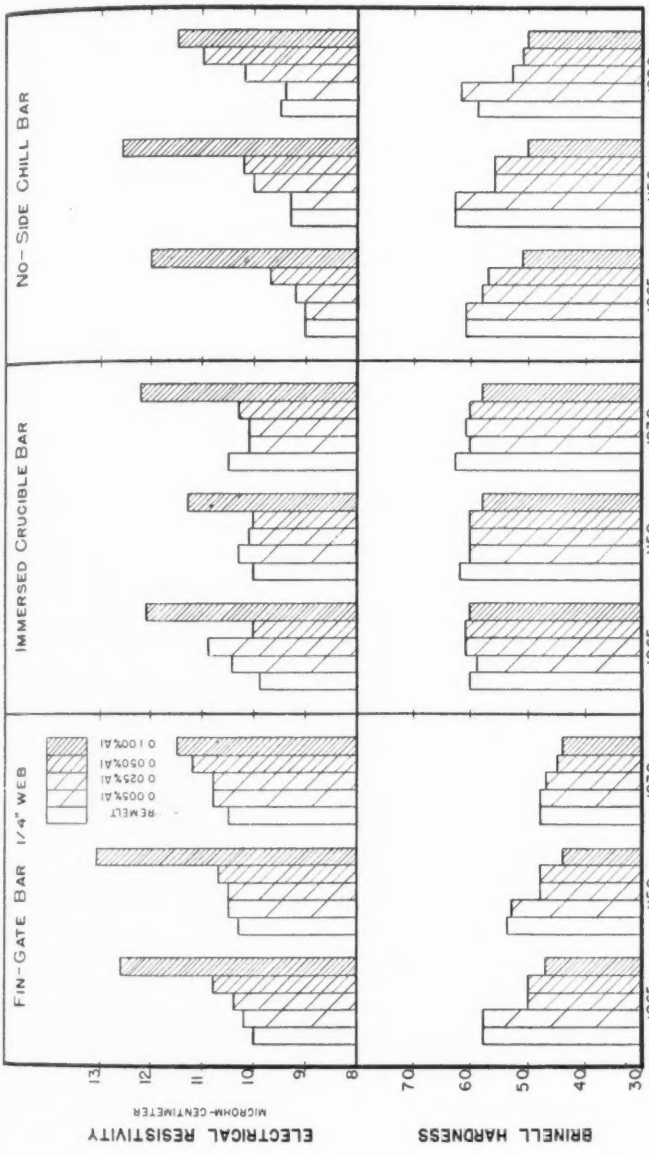

FIGURE 5.—*Effect of additions of aluminum on the electrical resistivity and Brinell hardness of cast red brass (85–5–5–5) test bars.*

FIGURE 4.—*Effect of additions of antimony on the elongation and reduction in area of cast red brass (85–5–5–5) test bars.*

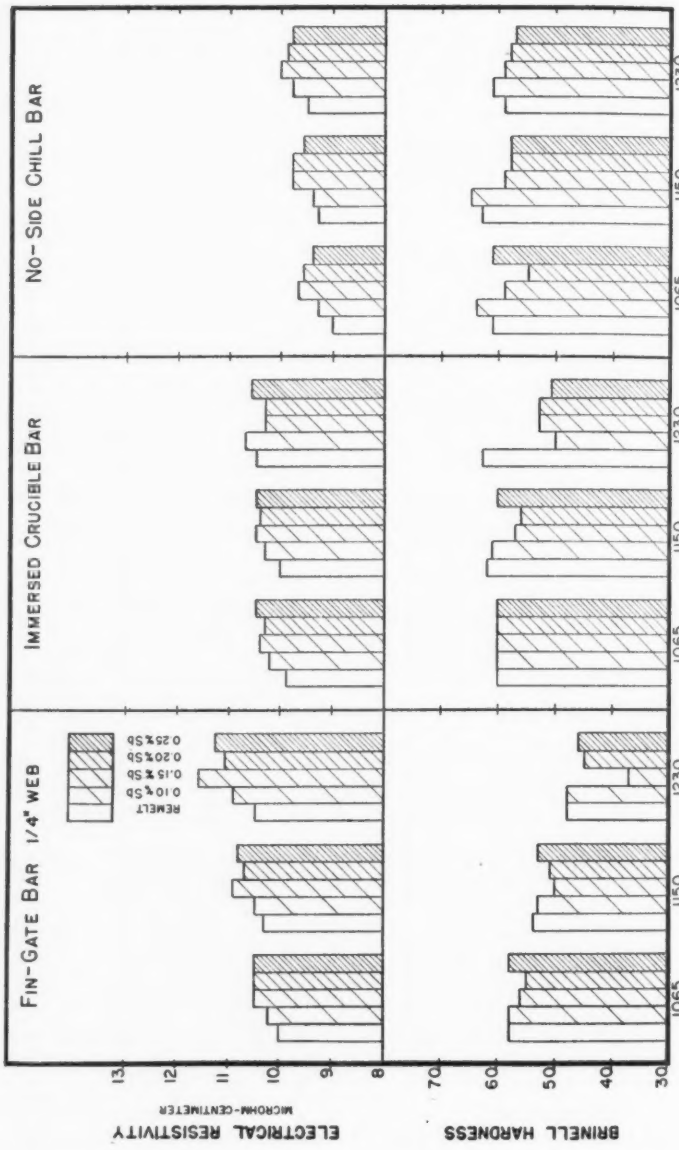

FIGURE 6.—*Effect of additions of antimony on the electrical resistivity and Brinell hardness of cast red brass (85–5–5–5) test bars.*

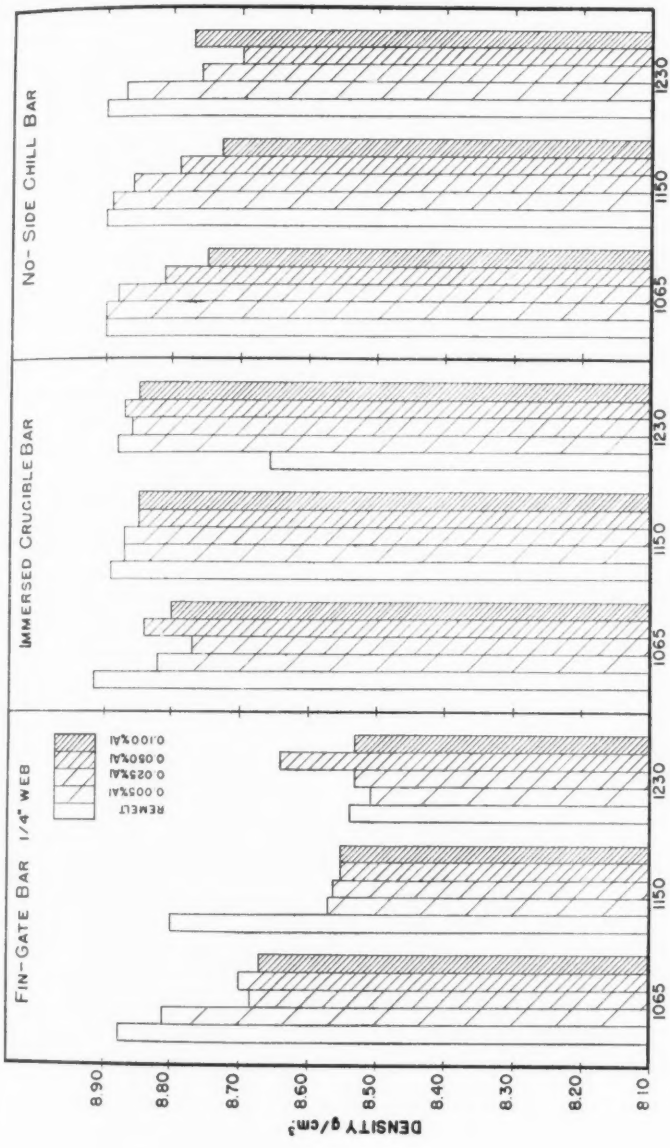

FIGURE 7.—*Effect of additions of aluminum on the density of cast red brass (85–5–5–5) test bars.*

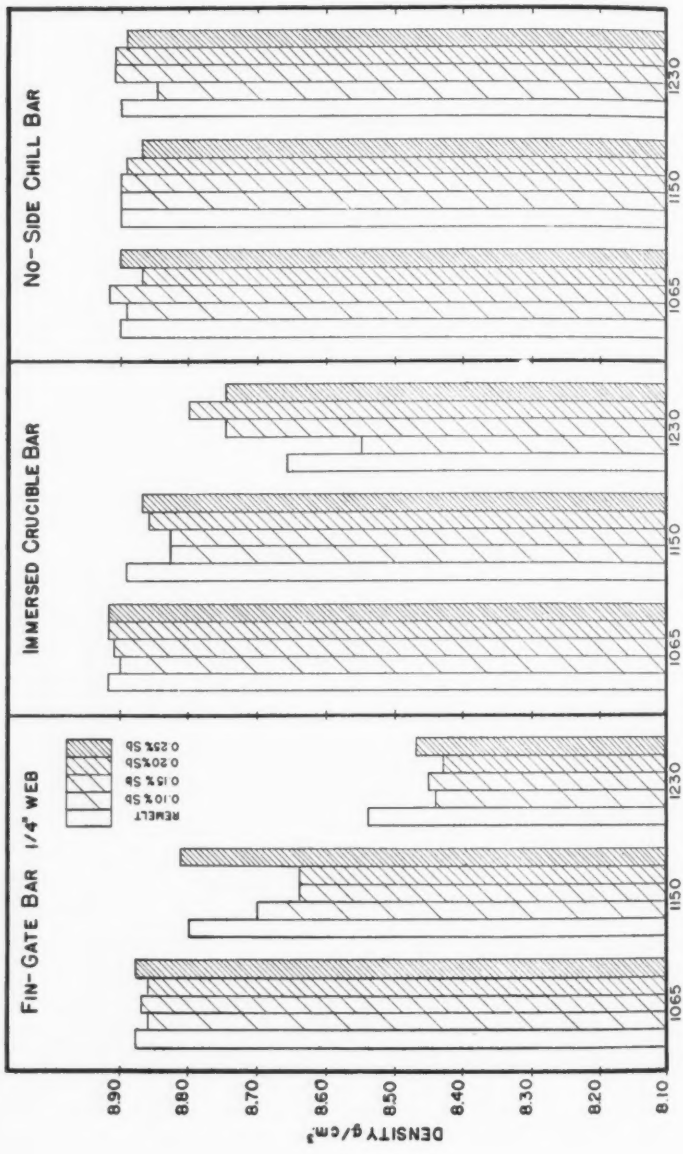

FIGURE 8.—*Effect of additions of antimony on the density of cast red brass (85–5–5–5) test bars.*

no-side-chill bars cast at 1,065° C (1,950° F) and 1,150° C (2,100° F) are the only ones, however, where this decrease was uniform. In figure 8 the deviation from remelted alloy, due to the addition of antimony, was nominal for the bars cut from the chill ingot. The sand-cast bars poured at 1,230° C (2,250° F) showed the most pronounced irregular deviation. Additional determinations of density were made on stepped-bar castings poured from each heat that was cast into tensile bars. Figure 9 shows the dimensions of the stepped-bar castings. In figures 10 and 11 are shown the density data obtained with this type of bar for alloys with added aluminum and antimony, respectively. The general effect of increasing the aluminum content was to decrease the density. The density also tended to decrease with reduction of the thickness of the stepped-bar casting, although this reduction is somewhat irregular. There are some indications, too, of a decrease in density with an increase in pouring temperature, particularly for the specimens with 0.05 and 0.10 percent of aluminum. In general, the addition of antimony had very little effect on the density of the stepped-bar specimens. There were fewer irregularities in the density determinations of the stepped-bars containing antimony than for the corresponding bars containing aluminum. There was a slight tendency for the density to decrease with reduction in thickness of casting of specimens poured at 1,065° C (1,950° F) and 1,150° C (2,100° F), but this was not so evident with specimens cast at 1,230° C (2,250 °F).

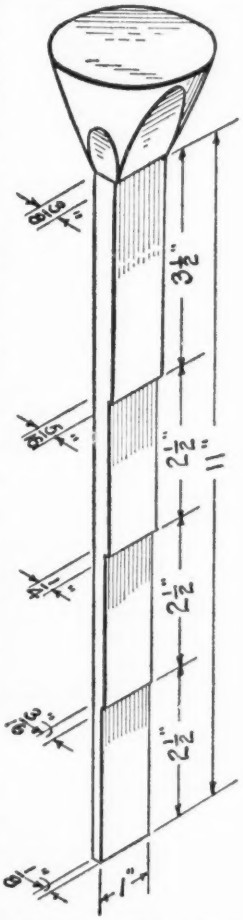

FIGURE 9.—*Dimensions of stepped-bar castings.*

7. RUNNING QUALITIES

The effect of aluminum and of antimony on the running quality of the alloy was studied by the method developed by Saeger and Krynitsky [6], which consists essentially in casting in a green-sand mold a strip of small cross section in the form of a spiral. According to the data summarized in figure 12, aluminum increased the running quality of the alloy. Likewise, the results presented in figure 13 show a marked increase in the running quality of the alloy, which can be attributed to the presence of the antimony. For the specimens poured at temperatures of 1,065° C (1,950° F) and 1,150° C (2,100° F), maximum values were obtained with an antimony content of 0.15 percent, but for the test specimens poured at 1,230° C (2,250° F) the best results corresponded to an antimony content of 0.10 percent.

8. PRESSURE TESTING

Since this alloy is widely used in the manufacture of pressure castings, its tightness is a major factor. This was studied by hydraulic testing. A hydraulic pressure of 300 lb/in.^{2} was applied to the inte-

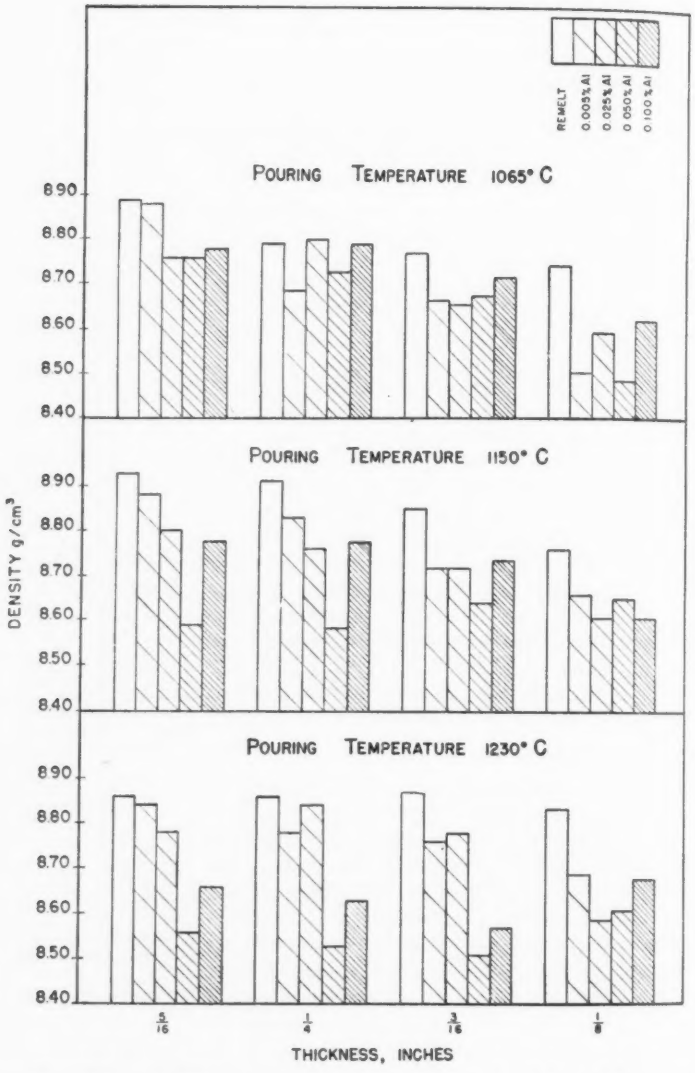

FIGURE 10.—*Effect of additions of aluminum on the density of stepped-bar castings of cast red brass (85–5–5–5).*

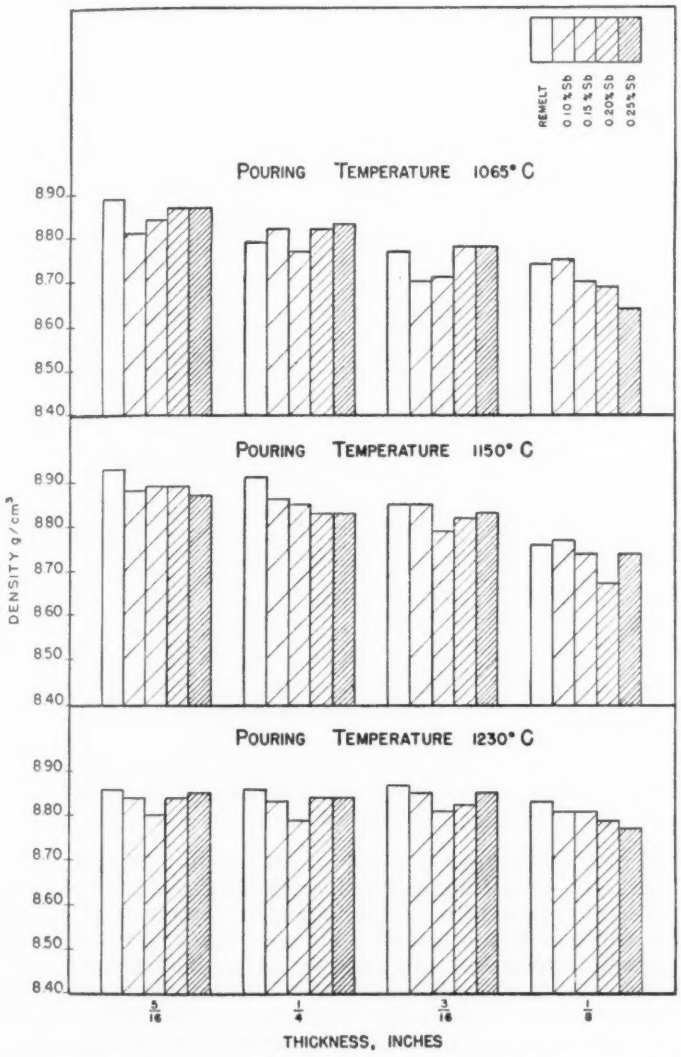

FIGURE 11.—*Effect of additions of antimony on the density of stepped-bar castings of cast red brass (85–5–5–5).*

rior of cylindrical castings. The water within the specimen contained a soluble blue dye, and the appearance of the blue coloration on the outer surface of the specimen under pressure constituted visual evidence of a leak. If no leak was indicated when the pressure had been maintained for 1 minute, the specimen was rated "satisfactory" or "OK".

Cylindrical specimens for these pressure tests were cast in groups of four, as indicated in figure 14. Two of the thin-wall castings in each group were trimmed to a length of 2 in., removing most of the

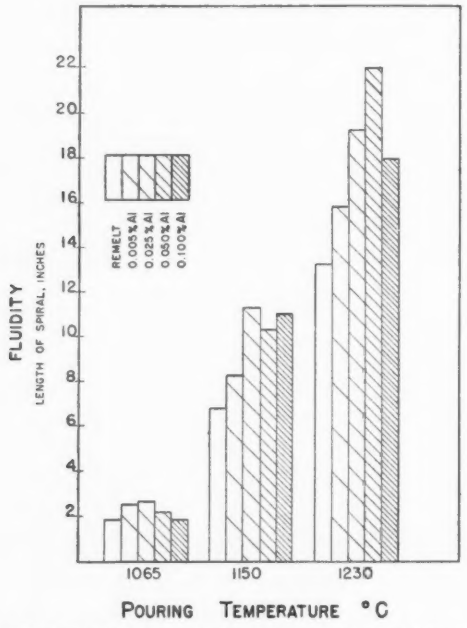

FIGURE 12.—*Effect of additions of aluminum on the fluidity of cast red brass (85–5–5–5).*

material from the gate-end, which might possibly be spongy. These specimens were tested hydraulically with the inner and outer surfaces in the "as cast" condition. The other two cylinders in each group, likewise trimmed to a length of 2 in., were machined both inside and out to a wall-thickness of ⅛ in., and tested in a similar manner. Specimens in both the "cast-to-size" and "machined-to-size" conditions were tested under a hydraulic pressure of 300 lb/in.^{2} Specimens which did not leak under 300 lb/in.^{2} pressure were subsequently tested under a pressure of 600 lb/in.^{2} Results of these pressure tests are listed in tables 1 and 2. The tests at 300 lb/in.^{2} are also shown graphically in figure 15. These data show:

1. The "cast-to-size" specimens were superior to the "machined-to-size" specimens in resistance to hydraulic pressure. This indicates that an important part of the resistance to hydraulic pressure is located in the skin of the casting and that the removal of the surface

skin by machining decreases the capacity of the metal to withstand hydraulic pressure.

2. The best results were obtained with metal cast at the higher pouring temperatures.

3. The presence of aluminum in the alloy increased the tendency for leaks or porosity, particularly when 0.05 percent or more of this element was present.

4. The presence of antimony decreased the porosity of red brass but the effect was practically constant within the range of 0.10 to 0.25 percent of antimony.

5. For the test specimens containing aluminum, all of the "cast-to-size" specimens that withstood 300-lb/in.^{2} pressure were also able to

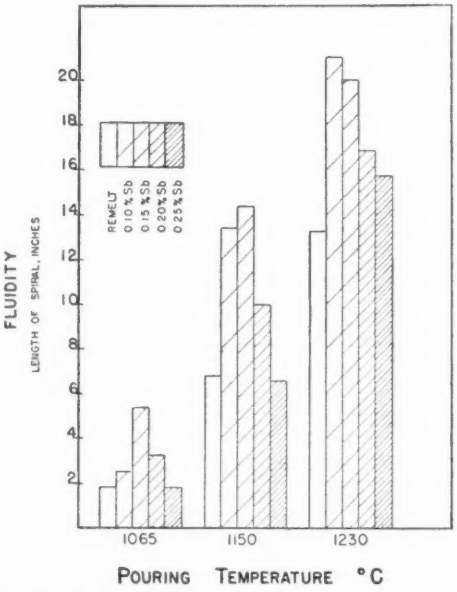

FIGURE 13.—*Effect of additions of antimony on the fluidity of cast red brass (85–5–5–5).*

withstand 600-lb/in.^{2} pressure. Only two of the six "machined-to-size" specimens that withstood 300-lb/in.^{2} pressure passed the 600-lb/in.^{2} test.

6. Most of the "cast-to-size" specimens containing antimony that withstood 300-lb/in.^{2} pressure were satisfactory under 600-lb/in.^{2} pressure, and one-half of the "machined-to-size" specimens tested in like manner were satisfactory.

In general, then, it may be seen that aluminum has a deleterious effect on the pressure tightness of the alloy but that antimony does not deleteriously affect this property. It was interesting to note that the leaks observed in the specimens that failed under test were not localized but were distributed over all portions of the surface of the test specimens.

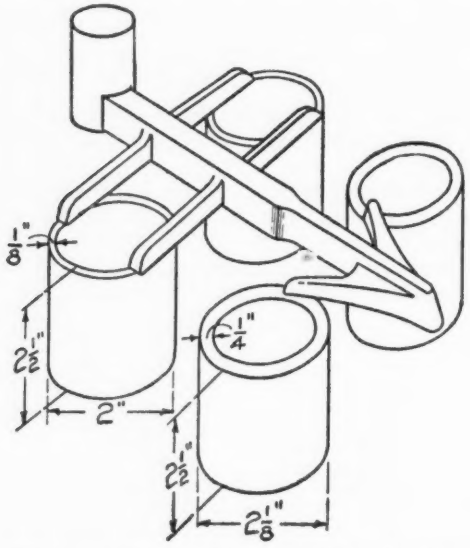

FIGURE 14.—*A casting of specimens for hydraulic tests.*

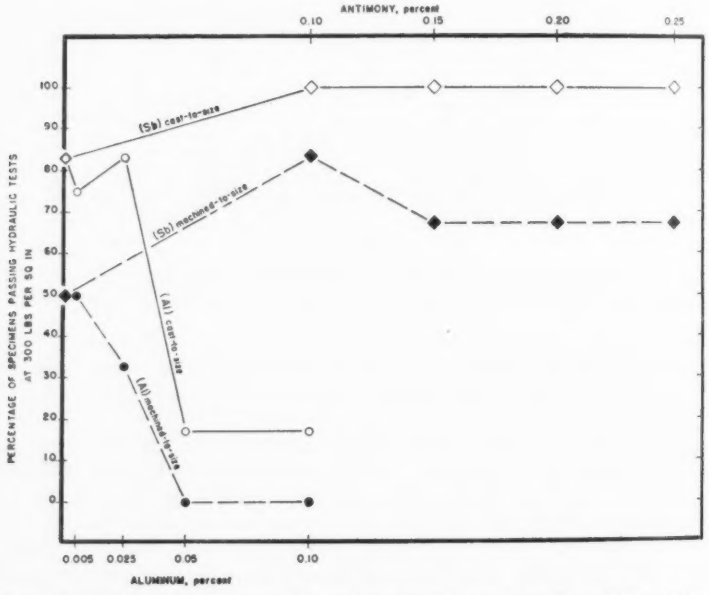

FIGURE 15.—*Effect of additions of aluminum or antimony on the ability of "cast-to-size" and "machined-to-size" specimens of red brass to withstand hydraulic pressure.*

TABLE 1.—*Pressure tests of remelted "85–5–5–5" alloy, with addition of aluminum*

[Only those specimens that withstood a pressure of 300 lb/in.[2] were tested at 600-lb pressure.]

Pouring temperature	Type of metal	Cast-to-size		Machined-to-size	
		300 lb	600 lb	300 lb	600 lb
°C					
1,065	Remelt	NG		NG	
		OK	OK	NG	
1,150	do	OK	OK	OK	NG
		OK	NG	OK	NG
1,230	do	OK	OK	OK	OK
		OK	OK	NG	
1,065	Remelt, plus 0.005% of Al	(1)		NG	
				NG	
1,150	do	OK	OK	OK	NG
		NG		NG	
1,230	do	OK	OK	OK	OK
		OK	OK	OK	OK
1,065	Remelt, plus 0.025% of Al	NG		NG	
		OK	OK	NG	
1,150	do	OK	OK	NG	
		OK	OK	NG	
1,230	do	OK	OK	OK	NG
		OK	OK	OK	NG
1,065	Remelt, plus 0.05% of Al	NG		NG	
		NG		NG	
1,150	do	NG		NG	
		NG		NG	
1,230	do	NG		NG	
		OK	OK	NG	
1,065	Remelt, plus 0.10% of Al	NG		NG	
		NG		NG	
1,150	do	NG		NG	
		OK	OK	NG	
1,230	do	NG		NG	
		NG		NG	

TABLE 2.—*Pressure tests of remelted "85–5–5–5" alloy with additions of antimony*

[Only those specimens that withstood a pressure of 300 lb/in.[2] were tested at 600-lb pressure]

Pouring temperature	Type of metal	Cast-to-size		Machined-to-size	
		300 lb	600 lb	300 lb	600 lb
°C					
1,065	Remelt	NG		NG	
		OK	OK	NG	
1,150	do	OK	OK	OK	NG
		OK	NG	OK	NG
1,230	do	OK	OK	OK	OK
		OK	OK	NG	
1,065	Remelt, plus 0.10% of Sb	OK	OK	OK	NG
		OK	OK	OK	NG
1,150	do	OK	NG	OK	NG
		OK	OK	NG	
1,230	do	OK	OK	OK	OK
		OK	OK	OK	OK
1,065	Remelt, plus 0.15% of Sb	OK	NG	NG	
		OK	OK	NG	
1,150	do	OK	OK	OK	NG
		OK	OK	OK	NG
1,230	do	OK	OK	OK	OK
		OK	NG	OK	OK
1,065	Remelt, plus 0.20% of Sb	OK	NG	NG	
		(1)		OK	NG
1,150	do	OK	OK	NG	
		OK	OK	OK	OK
1,230	do	OK	OK	OK	OK
		OK	OK	OK	OK
1,065	Remelt, plus 0.25% of Sb	OK	NG	NG	
		(1)		NG	
1,150	do	OK	OK	OK	NG
		OK	OK	OK	NG
1,230	do	OK	OK	OK	OK
		OK	OK	OK	OK

[1] Misrun.

9. METALLOGRAPHIC EXAMINATION

Specimens of the remelted alloy (85–5–5–5) with additions of aluminum and of antimony, cast at 1,150° C (2,100° F), were examined to ascertain the effect of the added element on the microstructure of the alloy. Micrographs in figure 16 show the typical appearance of specimens containing 0.0, 0.005, 0.025, 0.05, and 0.10 percent of aluminum, respectively. There may be observed fine networks at the interdendrite boundaries of the specimens containing 0.025 to 0.10 percent of aluminum that were not seen in the untreated alloy or in the specimen containing 0.005 percent of aluminum. These lines were visible on the polished surfaces previous to etching and constitute a characteristic structural feature of the alloys containing the higher aluminum contents. Examination at a magnification of ×500, of both etched and unetched specimens, leads to the conclusion that this structural feature represents solid material, perhaps a film, at some of the dendritic boundaries and does not simply represent shrinkage cracks in the material, although shrinkage may be involved to some extent. It could not be determined whether the film consisted of intermetallic compounds or nonmetallic material. Whatever the nature of these imperfections may be, their presence is associated with the inferior properties, that is, low ductility and high electrical resistivity of the test bars of higher aluminum content, and may be a factor in the increased leakage of these alloys under hydraulic pressure.

In Figure 17 are shown micrographs of companion specimens of the alloy containing 0.0, 0.10, 0.15, 0.20, and 0.25 percent of antimony cast at 1,150° C (2,100° F). No unusual structural condition attributable to the presence of antimony is to observed. Evidently antimony in these amounts exists in solid solution in the copper-rich matrix.

IV. SUMMARY

The influence of pouring temperature, in this phase of the investigation, was subordinate to that of the added elements.

Aluminum had a marked detrimental influence on most of the properties that were studied. The presence of this element lowered the tensile strength, the ductility and the Brinell hardness. It increased the electrical resistivity (i. e., lowered the electrical conductivity) and the porosity of the alloy. The only beneficial effect observed for additions of aluminum was an increase in the fluidity or running property of the alloy.

Antimony, however, had little influence on the properties of the alloy other than a slight increase in the electrical resistivity and, to a somewhat greater degree, an increase of the running quality. Its effect on the other physical properties studied was not significant.

The alloy containing the higher percentages of aluminum shows microstructural imperfections, herein called films, which are not visible in the aluminum-free alloy. It is probable that the low ductility, high electrical resistivity, and possibly the failure of the alloy to withstand hydrostatic pressure are associated with local concentrations of these films at the dendrite interstices.

It was thought that possibly some direct correlations might be observed from the data obtained for the different properties studied. However, no correlation could be established between the electrical

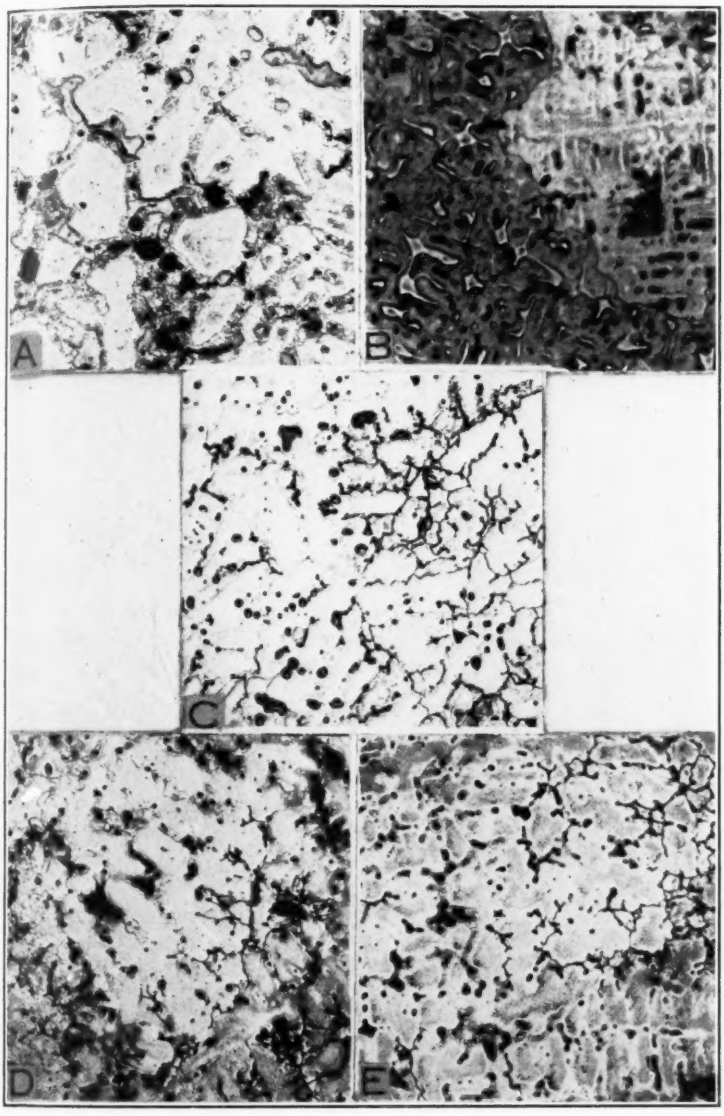

FIGURE 16.—*Microstructure of specimens.*

A, remelted 85–5–5–5; *B*, remelted metal plus 0.005 percent of Al; *C*, remelted metal plus 0.025 percent of Al; *D*, remelted metal plus 0.05 percent of Al; *E*, remelted metal plus 0.10 percent of Al etched electrolytically in 10 percent of ammonium persulphate, ×100.

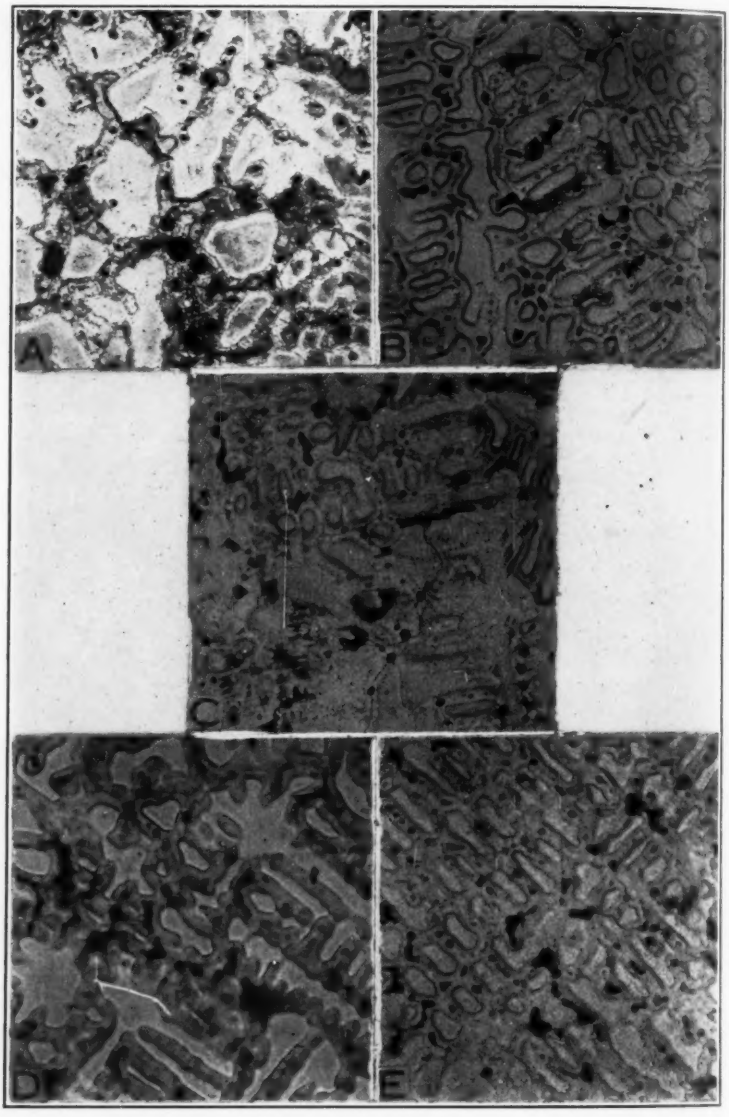

FIGURE 17.—*Microstructure of specimens.*

A, Remelted 85–5–5–5; *B*, remelted metal plus 0.10 percent of Sb; *C*, remelted metal plus 0.15 percent of Sb *D*, remelted metal plus 0.20 percent of Sb; *E*, remelted metal plus 0.25 percent of Sb etched electrolytically in 10 percent of ammonium persulphate, ×100.

resistivity and the physical properties studied, nor between the results of the pressure tests and the density determinations made either on the ends of the tension specimen or on the various sections of the stepped-bar castings. This suggests particularly that density is not a satisfactory indication of the ability of the material to withstand hydraulic pressure. It was found impossible to correlate the data here presented other than as indicative of a general trend. While it has been shown that aluminum has a deleterious effect on the alloy, the diminution of no physical or electrical property studied is proportional to, or regular for the progressively increasing amounts of this element added.

The most important conclusions which the results of this investigation warrant are:

1. The restriction on the presence of aluminum, in the present ASTM Specification B 30–36, is amply justified by the results obtained.
2. The present data indicated that antimony up to 0.25 percent does not have a deleterious effect on this alloy.

V. REFERENCES

[1] H. B. Gardner and C. M. Saeger, Jr., *Factors affecting the physical properties of cast red brass* (*85* Cu, *5* Zn, *5* Sn, *5* Pb), Proc. Am. Soc. Testing Materials **32**, pt. 2, 517 (1932).

[2] H. B. Gardner and C. M. Saeger, Jr., *The effect of sulfur and iron on the physical properties of cast red brass* (*85* Cu, *5* Sn, *5* Zn, *5* Pb), Proc. Am. Soc. Testing Materials **33**, pt. 2, 448 (1933).

[3] *Copper-base alloys in ingot form for sand castings. Appendix, page 541*, Am. Soc. Testing Materials, Standards, pt. 1, Metals, p. 538 (1936).

[4] *Standards methods of tension testing of metallic materials*, Am. Soc. Testing Materials, Standards, pt. 1, Metals, p. 960 (1933).

[5] *Standard method of test for resistivity of metallic materials for resistors*, ASTM Designation B 63–29, Am. Soc. Testing Materials, Standards, pt. 1, p. 860 (1930).

[6] C. M. Saeger, Jr., and A. I. Krynitsky, *A practical method for studying the running quality of a metal cast in foundry molds*, Trans. Am. Foundrymen's Assn. **39**, 513 (1931).

Washington, January 31, 1939.

U. S. Department of Commerce National Bureau of Standards

RESEARCH PAPER RP1216

Part of Journal of Research of the National Bureau of Standards, Volume 22, June 1939

RESOLVING POWER AND DISTORTION OF TYPICAL AIRPLANE-CAMERA LENSES

By Francis E. Washer

ABSTRACT

Tabulations are given of the resolving power and distortion of a number of airplane-camera lenses of the type most commonly used in recent air-mapping projects. Since the image plane of best average definition does not necessarily coincide with the image plane yielding best definition on the axis of the lens, the method of selecting the image plane of best average definition and its use in connection with the determination of the equivalent focal length are described. The manner of the variation of the resolving power across the field is characteristic of the type of lens.

CONTENTS

	Page
I. Introduction	729
II. Method of selection of the image plane of best average definition	730
III. Resolving powers for typical airplane-camera lenses	733
IV. Distortion for typical airplane-camera lenses	744
V. Conclusion	746

I. INTRODUCTION

In 1927 a paper by A. H. Bennett [1] listed the distortion characteristics of some typical photographic objectives. In the intervening 12 years the growth of air-mapping operations has been rapid. This growth, together with the desire to obtain negatives satisfactorily free from distortion and including as great an area of the terrain as possible, has resulted in the construction of wide-angle photographic objectives of short focal length with distortion lower than that of lenses built 15 or 20 years ago. In order to combine the advantages of a convenient negative size and a wide angular field, the focal length of lenses employed in airplane-mapping cameras seldom exceeds 210 mm.

For several years it has been a requirement that all lenses used on Government mapping projects be tested by the National Bureau of Standards. This requirement, and the natural demand of the map makers for greater accuracy in their negatives, has resulted in the submission of a very large number of lenses to the National Bureau of Standards for determination of focal length, distortion, and resolving power. To facilitate these measurements, a precise lens-testing camera has been developed. On the basis of these measurements, this paper presents a survey of the distortion and resolving-power characteristics of a number of airplane-camera lenses. Such a critical comparison and study of the data resulting from so large a

[1] J. Opt. Soc. Am. and Rev. Sci. Instr. **14**, 235 (1927).

number of standardized tests are most useful, because they present definite quantitative data that can be used in the preparation of performance specifications for airplane-camera lenses and for making an estimate of the accuracy possible for a given mapping process.

Only the lenses most commonly used in recent air-mapping projects are studied, thus limiting this survey to lenses of 210-mm focal length and apertures of $f/4$ and $f/6.8$. The lenses are considered in three groups corresponding to the product of three manufacturers, two domestic and one foreign. This study has been limited to the products of three manufacturers, because sufficient recent data on other makes of 210-mm lenses are not available. The three types herein considered comprise more than 80 percent of the total number of 210-mm lenses tested at the National Bureau of Standards in the past 2 years.

II. METHOD OF SELECTION OF THE IMAGE PLANE OF BEST AVERAGE DEFINITION

The lens-testing camera to which reference has been made, the operating technique, and the method of deriving equivalent focal length (E. F. L.) and distortion from the test negative have been described in an article [2] by Gardner and Case. However, to insure clarity in this report, a brief survey of this equipment and procedure is given

The lens-testing camera consists of seven collimators spaced at approximately 5° intervals, a lens holder, and a plateholder. The collimators serve to produce parallel light, so that a lens may be tested under conditions closely approximating those encountered in aerial photography. The angle between each pair of adjacent collimators is measured to five significant figures, with a probable error not in excess of $\pm 0.0010°$, and no systematic error in excess thereof has been found. Each collimator carries a test chart so designed and mounted that the images on the test negative for a distortion-free lens will all be equal in size regardless of their angular separation from the axis of the lens. Each target contains a central vertical line which serves as a fiducial mark for the measurements made, in order to determine the equivalent focal length and distortion of a lens. The lens under test is placed at the intersection point of the seven collimator axes, and is so adjusted that the axis of the first collimator coincides with that of the lens. Hence, the other six collimators make angles with the axis of the lens of approximately 5°, 10°, 15°, 20°, 25°, and 30°, respectively. The plateholder is so constructed that it may be moved along the axis of the bench in equally spaced steps. The plateholder may also be moved in a plane at right angles to the plane of the collimators, so that 19 rows of images may be taken on a single plate where each row shows the imagery in focal planes at successively increasing distances from the lens. The range of movement of the plateholder along the axis is so selected that the middle row of images corresponds to the best visual focus. After the test negative has been produced, a row is selected on the basis of best average photographic definition across the entire field. For this row, measurements are then made of the distances separating the central or fiducial line of each image from that of the axial image. The measured values of these distances are used for the determination

[2] J. Research NBS 18, 449 (1937) RP984.

of equivalent focal length and distortion. Let a be the distance from the 0° to the 5° image and b the distance from the 0° to the 10° image, then $f=(f_1+f_2)\div 2$, where $f_1=a$ cot 5° and $f_2=b$ cot 10°. The measured distances from the axial image to the images at the other 5° intervals are used in computing the distortion of the lens.

A consideration of the resolving power of the lens in different image planes is the basis for the selection on the test negative of the row that is used for the determination of focal length and distortion. To illustrate this and to give an idea of the definiteness with which a given row can be selected as superior to the others, a complete record of the resolving power, as read from a typical test negative, is given in schematic form in table 1. Under the headings "Tangential" and "Radial" is shown the behavior of the resolving power at 5° intervals, expressed in lines per millimeter of the test negative, in image planes spaced 0.15 mm apart. The region studied with this step-by-step process extends from an image plane 1.2 mm nearer the lens to an image plane 1.5 mm farther from the lens than the image plane selected for the determination of the equivalent focal length and which yields best average definition. The two values of the resolving power given for each image arise from two sets of patterns of parallel lines contained by the test chart. One pattern consists of lines perpendicular to a radius drawn from the center of the field, the other consists of lines parallel to the same radius. The tangential and radial resolving powers correspond, respectively, to resolving powers of the rays often referred to as meridional and sagittal, or to the primary and secondary rays, as designated by H. D. Taylor.[3] The lens with which this negative was made had a nominal focal length of 8 1/4 in. and was tested at maximum aperture, which was $f/4$.

TABLE 1.—*Resolving powers as read from a test negative for a typical f/4 lens*

Row [1]	Tangential resolving power in lines per millimeter							Radial resolving power in lines per millimeter						
	Angular distance from axis							Angular distance from axis						
	0°	5°	10°	15°	20°	25°	30°	0°	5°	10°	15°	20°	25°	30°
1	3.5	5	7	28	28	20	14	3.5	3.5	5	10	56	56	10
2	3.5	5	10	28	40	20	14	3.5	3.5	7	14	56	56	10
3	5	7	20	40	40	14	14	5	5	7	28	40	40	14
4	5	10	28	40	28	14	14	5	5	10	40	28	28	20
5	7	14	28	40	20	14	14	7	7	14	56	20	14	40
6	10	20	28	40	20	14	14	7	10	28	40	14	10	56
7	14	20	28	28	10	14	10	10	14	28	40	10	10	56
8	20	20	28	20	7	10	10	14	20	40	14	7	7	56
9	**28**	**28**	**40**	**14**	**7**	**10**	**10**	**20**	**28**	**56**	**14**	**7**	**7**	**40**
10	56	40	40	10	5	7	10	56	40	40	10	5	5	40
11	56	40	28	7	5	7	10	56	56	40	7	5	5	20
12	56	40	14	5	5	5	7	40	40	20	5	5	5	14
13	40	40	10	5	5	5	7	40	40	14	5	3.5	3.5	14
14	40	14	10	5	3.5	5	7	40	40	10	5	3.5	3.5	10
15	40	10	7	3.5	3.5	5	5	28	20	10	3.5	3.5	3.5	7
16	28	10	7	3.5	3.5	5	5	20	14	5	3.5	3.5	3.5	7
17	20	7	5	3.5	------	5	5	14	7	5	3.5	------	3.5	5
18	10	7	5	3.5	------	3.5	5	10	5	3.5	------	------	------	5
19	3.5	5	3.5	------	------	------	5	5	3.5	3.5	------	------	------	5

[1] 19 rows of images are taken on a single negative in the test of a single lens. Row 1 is nearest to the lens. Readings are taken in image planes spaced 0.15 mm apart for a range of 2.70 mm through the region of best focus. Tangential and radial resolving powers are tabulated separately for greater clarity. Row 9 shows the resolving power in that image plane adjudged to yield best average definition.

[3] A System of Applied Optics, p. 115 (Macmillan and Co., Ltd., 1906).

Examination of table 1 shows that the resolving power starts low, rises to a maximum, and drops again as one moves into and out of focus. This behavior is found for both tangential and radial patterns for each angle. The regions of maximum resolving power for the various angles do not all lie in the same image plane because of curvature of field. For this lens, curvature of field produces an axial difference of approximately 1 mm in the positions of best focus at 0° and 15°. Moreover, the regions of maximum resolving power for tangential and radial patterns do not necessarily lie in the same plane for any given angle because of astigmatism. In this instance, astigmatism produces an axial difference of approximately 0.1 mm in the positions of best tangential and radial resolving power at 0° and 15°.

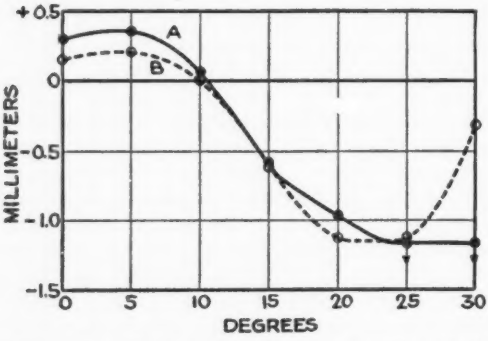

FIGURE 1.—*These curves show the variation of the position of best imagery as measured along the axis of the lens.*

The data are derived from the test negative shown in table 1. Curve *A* represents the position of best tangential imagery at every 5° interval from 0° to 30°. Curve *B* shows the position of best radial imagery at every 5° interval from 0° to 30°. Row 9 in table 1 is taken as the zero of ordinates. The arrows that qualify two points on the tangential curve signify that at these angular separations from the axis the position of best tangential imagery may lie outside the region traversed by the plate.

Figure 1 is a graph which shows the position of maximum resolving power for tangential and radial imagery every 5° from 0° to 30°. The data for the graph were obtained from table 1. The zero ordinate is arbitrarily chosen as corresponding to row 9, which was the row used in determining the reported E. F. L. The ordinates in the graph are the number of millimeters which the photographic plate must be moved toward or from the lens, as measured from the image plane of the reported E. F. L., to get best resolution at any specified angle. The points on the tangential curve for 25° and 30° are qualified by arrows which signify that for these angles the image plane of best tangential definition may be outside the region traversed by the photographic plate during the test. It may be noted that these curves, as might be expected, closely resemble typical curves of primary and secondary curvature. The difference in the ordinates at each angle gives a measure of the astigmatism.

These considerations show that a compromise setting of the lens is necessary to obtain fair usable imagery across the entire negative. To attain this end, one must have some criterion to facilitate the selection of the best row on the test negative, and one must be sure that on repetition of the test one would arrive at sensibly the same value of E. F. L. each time. This goal has been attained by the adoption of two criteria. First, rows are selected for which the resolving power, for both tangential and radial imagery and for all images in the rows selected, is, if possible, not less than 7 lines per millimeter.[4] Second, from all rows which satisfy the first condition, a row is selected for which the resolving power on the axis is as high as possi-

[4] The value, 7 lines per millimeter, herein used as the lower limit of acceptable resolving power was suggested from tentative values for minimum resolving power given on p. 19 and 20 of Standard Specifications (2d ed.) published by the American Society of Photogrammetry on July 22, 1936.

ble, and preferably not less than 15 lines per millimeter. Selection in this manner generally gives the best average definition across the entire field. In some cases, where the tests have shown that the resolving power of a given lens was very low, it has been necessary to drop the first condition below 7 lines per millimeter at 20° and 25° in order to maintain the resolving power in the center of the field at 15 lines per millimeter. However, when this is necessary, there can be little doubt that such a lens is poor indeed and ought not to be used in aerial mapping.

Using these two criteria in studying the test negative whose resolving powers are tabulated in table 1, row 9 is selected. It may be noted that rows 5, 6, 7, 8, and 9 all satisfy the first condition; however, application of the second condition eliminates all except row 9. Row 10 shows much better definition on the axis than row 9, but selection of row 10 would violate the first condition and would result in poor imagery at 20° and 25°. If row 8 had been selected, the second condition would be violated and the central imagery would be inferior to the central imagery of row 9.

The marked differences that exist between the regions of best focus as measured along the axis of the lens can easily give rise to differences in the measured values of E. F. L. of a lens, depending upon the manner in which the lens is focused in a camera. It is clear that if one depends on axial definition only in setting the lens in a camera, then poor definition will result at the wider angles. Conversely, if too much emphasis is placed upon securing best imagery at the edge of the field or at some point midway between the edge and center of the field, then either the central portion or some intermediate zone will probably be poor; possibly poor definition will be present in both places at once (for example, in row 2 of table 1, good imagery at 20° is accompanied by very poor imagery at 0° and 5°, and by only fair imagery at 10° and 30°). However, if care is taken in adjusting the lens in an aerial camera so that useful imagery is present across the entire field, then it is probable that different workers using this same criterion would set the lens to within 0.10 mm of the same position each time, and for that position the corresponding E. F. L. would be that which is found by this best resolving-power method. This method of setting the lens can be used where it is not readily practicable to use the back focal length in mechanically setting the lens in the camera. The back focal length which is customarily given in the reports of the National Bureau of Standards is the distance from the back surface of the lens to the image plane of best average definition.

III. RESOLVING POWERS FOR TYPICAL AIRPLANE-CAMERA LENSES

When selection is made of the image plane that yields the best average resolving power and when the manner in which the resolution varies with angular separation from the axis is studied, it is found that the pattern of variation for a particular lens shows striking similarity to the patterns exhibited by other lenses of the same type, despite the differences in workmanship which are unavoidably present and which do introduce considerable differences in the quality of lenses made according to the same specification. This pattern is a definite property of the lens and is best shown by the accompanying tables of tangential

and radial resolving powers. These tables are compiled from a study of many lenses, and the resolving powers therein are reported for image planes both nearer to and farther from the lens than the image plane considered to have the best average resolving power. In one set of tables, the behavior of 30 $f/4$ lenses of foreign manufacture is shown. In the other sets is shown the behavior of 10 $f/4$ and 20 $f/6.8$ lenses of domestic manufacture.

When these tables are considered, several factors are to be borne in mind. First, the test charts used are so designed that the number of lines to the millimeter as recorded on the test negative form the approximately geometrical series 3.5, 5, 7, 10, 14, 20, 28, 40, and 56. Hence, these are the only values of resolving power which can appear on these test negatives. Second, the upper limit of 56 lines to the millimeter was selected as being certainly equal to if not greater than the limit of resolution of the emulsions commonly used in airplane-camera films; the theoretical resolving power of these lenses is much greater than 56 lines per millimeter. Third, the value reported for any image means that not only is that particular pattern clearly resolved but that all coarser patterns are also clearly resolved; this precaution is necessary to rule out false values of the resolving power. It frequently happens that a fine pattern may appear resolved when coarser patterns in the same image are unresolved. Careful inspection of the fine patterns resolved in these cases reveals that the number of lines present in the pattern on the negative do not agree with the number appearing in the original on the test chart. No thorough analysis of the causes of this phenomenon has yet been made, but preliminary work along these lines indicates that this false resolving power may arise from diffraction effects or the character of the chromatic aberration. Finally, these tests are made with a yellow filter (*K–3*) over the test charts, so that the test conditions are comparable with the conditions that the lens encounters in practice, and the resolving powers obtained under these conditions are not as great as would be obtained with monochromatic light.

Table 2 lists the resolving powers for tangential and radial imagery at 5° intervals from 0° to 30° for 10 $f/4$ lenses of domestic manufacture. This is a three-part table and shows the resolving power in three image planes lying at different distances from the lens. Table 2 (*a*) shows the resolving power in an image plane 0.5 mm farther from the lens than the image plane of best average definition. Table 2 (*b*) shows the resolving power in the image plane that is adjudged to give best average definition and which is used in determining the reported equivalent focal length. Table 2 (*c*) shows the resolving power in an image plane 0.5 mm nearer to the lens than the image plane of best average definition. Cursory examination of this table shows a striking consistency, from lens to lens, of the manner in which the resolving power for a particular image plane varies across the field.

To make this consistency quantitatively discernible, a series of occurrence tables have been prepared. These occurrence tables list for each angular separation from the axis the number of occurrences of each of the series of definite values of the resolving power in lines per millimeter and give a complete, concise picture of the behavior of the 10 lenses as a group. Occurrence tables for these 10 lenses have been formed for each of the three image planes studied and are

assembled in table 3. This table makes possible comparison of the manner in which resolving power varies across the entire image plane for tangential and radial imagery. The table also permits ready comparison of resolving powers in the three image planes of images lying at equal angular separations from the axis of the lens but at different distances from the lens. In table 4 are tabulated the average resolving power for each image plane for each angular separation from the axis for both tangential and radial imagery. These averages are derived from table 3 and cover the 10 lenses. These average resolving powers are those which one might reasonably expect to get from any lens of this type.

TABLE 2.—*Resolving powers of 10 f/4 lenses of domestic manufacture*

Lens number	Tangential resolving power in lines per millimeter, Angular distance from axis							Radial resolving power in lines per millimeter, Angular distance from axis						
	0°	5°	10°	15°	20°	25°	30°	0°	5°	10°	15°	20°	25°	30°
(*a*) Image plane 0.5 mm farther from the lens than the image plane of best average resolving power														
1	20	28	28	14	7	14	7	20	20	14	10	7	10	28
2	20	14	14	14	10	5	10	14	14	14	14	10	7	40
3	40	40	28	14	5	5	5	40	40	40	7	5	5	56
4	56	40	14	7	5	3.5	5	56	40	20	5	5	5	40
5	56	40	10	7	5	7	10	40	40	14	7	5	5	56
6	56	40	20	10	5	7	10	40	40	20	5	5	5	56
7	56	56	28	7	5	5	7	40	56	40	7	5	7	56
8	28	28	28	10	5	5	7	28	40	40	14	5	5	56
9	40	40	20	7	5	5	7	40	40	20	5	5	5	56
10	40	40	14	7	5	7	10	40	40	20	5	5	5	56
(*b*) Image plane of best average resolving power														
1	56	40	28	10	7	14	14	56	40	40	28	10	10	40
2	56	56	40	28	14	14	14	56	56	40	28	14	28	20
3	28	56	40	20	10	7	10	20	56	40	40	20	10	28
4	28	40	40	14	7	5	7	28	40	56	20	7	7	56
5	40	40	56	14	14	14	14	40	40	56	10	10	10	28
6	28	40	56	14	14	10	14	40	56	40	10	7	10	40
7	20	56	40	14	7	7	10	20	56	56	28	10	10	28
8	40	40	28	14	10	10	10	40	28	28	28	10	10	20
9	40	28	40	20	10	7	14	40	28	40	20	10	10	28
10	40	56	40	14	7	10	14	40	56	40	20	7	10	28
(*c*) Image plane 0.5 mm nearer to the lens than the image plane of best average resolving power														
1	28	20	14	10	10	10	14	28	28	28	28	14	14	40
2	20	20	28	20	14	20	20	20	28	40	28	28	28	10
3	7	7	28	40	20	10	14	7	7	14	40	40	40	10
4	7	10	40	40	14	10	14	7	10	20	56	20	10	14
5	10	10	28	56	20	20	20	10	10	28	56	20	28	10
6	7	10	20	40	14	14	20	7	10	28	56	20	20	10
7	7	7	28	40	20	10	14	7	7	28	56	28	28	10
8	10	14	28	20	20	14	14	7	7	14	28	40	20	10
9	10	10	28	40	28	14	20	10	10	28	56	28	40	10
10	14	20	40	28	10	14	14	14	20	56	40	14	10	14

In figure 2, the data from table 4 are graphed to give a clear picture of these characteristics. Although curve *B*, which is the curve of best definition for both tangential and radial imagery, does not always lie above curves *A* and *C*, which show the definition at the other two

image distances, there can be little doubt that this image plane is to be preferred. When tangential definition is considered, curve B lies above curve A at all points save on the axis, where A has a negligible advantage. Curve B lies below curve C from 15° to 30°, inclusive, but the advantage which C has over B for this region is nullified by virtue of the large differences in favor of B for the region 0° to 10°, inclusive. For radial imagery, curve B is above curve A at all points save at 30°, and here one finds good imagery for both image planes, so that the advantage which B holds for this separation from the axis is nullified by its inferior definition at all other points. Curve C is superior to A at 15°, 20°, and 25°, but is very inferior at 0°, 5°, and 30° and somewhat so at 10°.

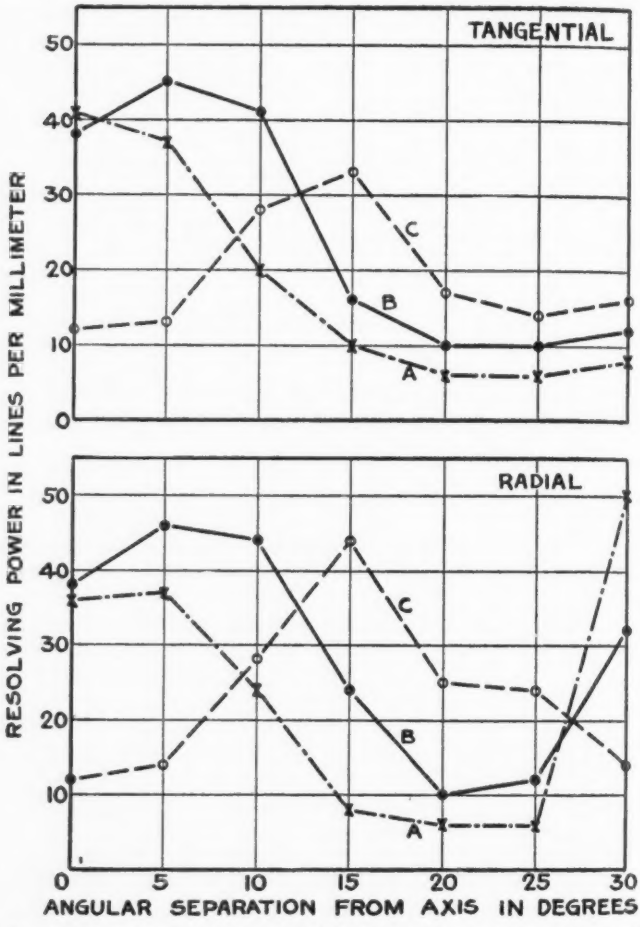

FIGURE 2.—*Graphs showing the tangential and radial resolving powers for 10 f/4 lenses of domestic manufacture.*

A, image plane 0.5 mm farther from the lens than the plane of best average definition; *B*, image plane of best average definition; *C*, image plane 0.5 mm nearer to the lens than the plane of best average definition.

TABLE 3.—*Occurrence tables showing the distribution of maximal values of the resolving power for three image planes*

Resolving power in lines per mm	Distribution of maximal values of the resolving power for the 10 f/4 lenses of domestic manufacture													
	Tangential. Angular distance from axis.							Radial. Angular distance from axis.						
	0°	5°	10°	15°	20°	25°	30°	0°	5°	10°	15°	20°	25°	30°
(a) Image plane 0.5 mm farther from the lens than the image plane of best average definition														
56	4	1						1	1					7
40	3	6						6	7	3				2
28	1	2	4					1						1
20	2	1	2					1	1	4				
14			3	3		1		1	1	3	2			
10			1	2	1		4				1	1	1	
7				5	1	3	4				3	1	2	
5					8	5	2				4	8	7	
3.5						1								
(b) Image plane of best average definition														
56	2	4	2					2	5	3				1
40	4	5	6					5	3	6	1			2
28	3	1	2	1				1	2	1	4		1	5
20	1			2				2			3	1		2
14				6	3	3	6				2	1		
10				1	3	3	3					5	8	
7					4	3	1					3	1	
5						1								
3.5														
(c) Image plane 0.5 mm nearer to the lens than the image plane of best average definition														
56				1						1	5			
40			2	5						1	2	2	2	1
28	1		6	1	1			1	2	5	3	3	3	
20	1	3	1	2	4	2	4	1	1	1		3	2	
14	1	1	1		3	4	6	1		2		2	1	2
10	3	4		1	2	4		2	4				2	7
7	4	2						5	3					
5														
3.5														

TABLE 4.—*Average resolving powers for the 10 f/4 lenses of domestic manufacture*

Image plane	Tangential resolving power in lines per millimeter. Angular distance from axis.							Radial resolving power in lines per millimeter. Angular distance from axis.						
	0°	5°	10°	15°	20°	25°	30°	0°	5°	10°	15°	20°	25°	30°
(a)	41	37	20	10	6	6	8	36	37	24	8	6	6	50
(b)	38	45	41	16	10	10	12	38	46	44	24	10	12	32
(c)	12	13	28	33	17	14	16	12	14	28	44	25	24	14

(a), Image plane 0.5 mm farther from the lens than the image plane of best average definition.
(b), Image plane of best average definition.
(c), Image plane 0.5 mm nearer to the lens than the image plane of best average definition.

Table 5 lists the resolving powers at 5° intervals in the image plane of best average definition for 30 *f*/4 lenses of foreign manufacture. In table 6 are grouped occurrence tables for three image planes that lie at different distances from the lens. Table 7 lists the average

resolving power for each angular separation from the axis for each image plane for both tangential and radial imagery.

In figure 3 the data from table 7 are graphed to present a clear picture of these characteristics. In these graphs of both tangential and radial resolving power, it is evident that with one exception the

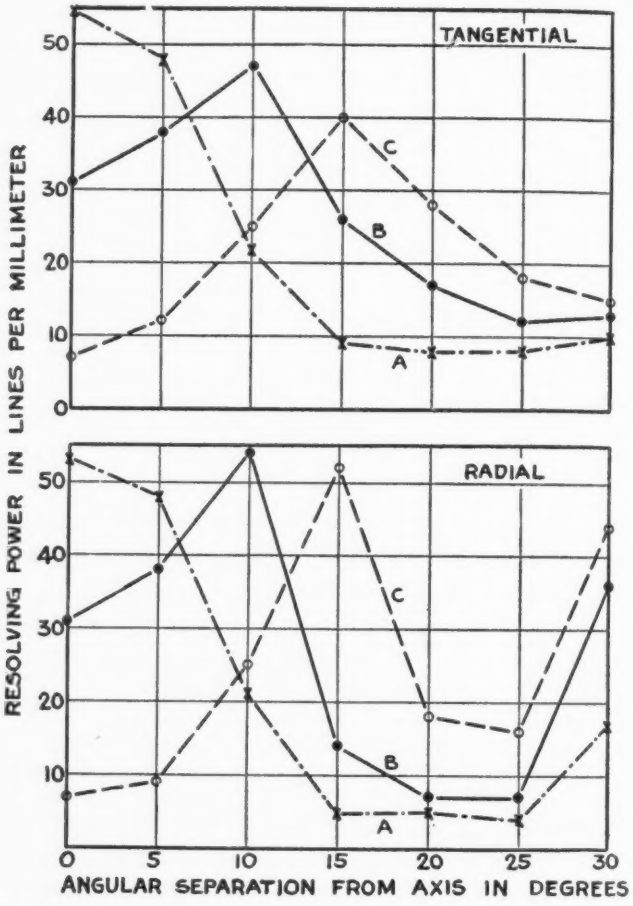

FIGURE 3.—*Graphs showing the tangential and radial resolving powers for 30 f/4 lenses of foreign manufacture.*

A, image plane 0.5 mm farther from the lens than the plane of best average definition. *B*, image plane of best average definition. *C*, image plane 0.5 mm nearer to the lens than the plane of best average definition.

curve *B*, which corresponds to the image plane of best average resolving power, lies between the curves for the other two image planes. This exception is at 10°, where the value of the resolving power of curve *B* is by a considerable margin the highest of the three. The graph shows that if the image plane nearest to the lens were selected the resolving power beyond 15° would greatly improve. However, the values from 0° to 10° would drop so rapidly as to render the advantage very doubtful. In a similar manner, if the image plane

farthest from the lens were selected, the resolving power at 0° and 5° would improve, while from 15° to 30° there would be a definite reduction. In particular, the radial values at 20° and 25° would fall below seven lines to the millimeter.

TABLE 5.—*Resolving power of 30 f/4 lenses of foreign manufacture in the image plane of best average resolving power*

Lens number	Tangential resolving power in lines per millimeter. Angular distance from axis.							Radial resolving power in lines per millimeter. Angular distance from axis.						
	0°	5°	10°	15°	20°	25°	30°	0°	5°	10°	15°	20°	25°	30°
1	40	40	56	40	20	14	14	40	56	56	10	7	7	20
2	20	40	40	28	20	14	20	20	28	40	20	7	7	40
3	28	28	56	28	14	10	10	28	28	56	28	7	7	40
4	40	40	56	40	28	20	20	28	56	56	10	7	7	40
5	40	56	56	40	28	14	20	40	56	56	10	7	7	40
6	28	40	56	40	28	20	14	20	40	56	10	7	7	40
7	40	40	56	28	14	5	5	40	56	56	7	5	5	7
8	28	40	56	40	28	20	10	28	40	56	10	7	7	20
9	20	40	56	28	14	7	7	20	28	56	14	5	5	40
10	20	40	56	28	20	14	14	20	40	56	10	7	7	40
11	28	40	40	20	14	10	10	40	40	56	10	7	7	40
12	40	40	56	28	20	14	10	40	40	56	10	7	7	40
13	40	40	56	20	14	14	10	40	28	56	10	7	7	40
14	14	20	40	40	20	14	10	14	20	56	40	10	10	40
15	40	40	40	10	7	10	10	40	40	56	10	7	7	40
16	28	28	40	28	10	14	14	28	40	56	14	10	10	40
17	28	28	56	14	7	10	10	20	28	56	10	7	7	28
18	40	56	40	28	20	14	14	40	40	56	10	7	7	40
19	28	40	40	14	10	10	10	28	40	40	10	5	5	28
20	28	28	56	20	14	10	10	20	28	56	10	5	5	40
21	28	40	40	28	20	14	14	28	40	56	14	7	7	56
22	40	40	40	10	7	10	10	40	40	56	10	7	7	28
23	40	56	40	14	14	10	10	40	40	56	10	7	7	40
24	40	40	40	10	14	10	10	40	40	56	10	7	7	40
25	56	56	40	40	28	14	14	56	56	56	10	10	7	56
26	14	28	28	20	7	7	14	14	28	40	14	7	7	10
27	20	28	40	28	10	14	28	20	28	56	28	7	7	40
28	20	28	40	20	7	5	14	40	28	56	20	5	5	28
29	20	28	56	40	28	20	14	20	40	56	10	7	7	28
30	40	40	40	14	14	10	10	40	40	56	28	7	7	40

TABLE 6.—*Occurrence tables showing the distribution of maximal values of the resolving power for three image planes*

Resolving power in lines per mm	Distribution of maximal values of the resolving power for the 30 f/4 lenses of foreign manufacture. Tangential. Angular distance from axis.							Radial. Angular distance from axis.						
	0°	5°	10°	15°	20°	25°	30°	0°	5°	10°	15°	20°	25°	30°
(a) Image plane 0.5 mm farther from lens than image plane of best average definition														
56	26	15						24	15					
40	4	15	2					6	15	1				
28			9							10				4
20			11	1	1		1			10				2
14			6	7	2	1	8			3				3
10			2	6	10	11	8			6				7
7				11	2	4	10				4	1		11
5				5	15	12	3				26	20	18	1
3.5						2						9	12	2

TABLE 6.—*Occurrence tables showing the distribution of maximal values of the resolving power for three image planes*—Continued

Resolving power in lines per mm	Distribution of maximal values of the resolving power for the 30 *f*/4 lenses of foreign manufacture													
	Tangential. Angular distance from axis.							Radial. Angular distance from axis.						
	0°	5°	10°	15°	20°	25°	30°	0°	5°	10°	15°	20°	25°	30°
(*b*) Image plane of best average definition														
56	1	4	14					1	5	27				2
40	12	17	15	8				13	15	3	1			16
28	9	8	1	10	6		1	6	9		3			5
20	6	1		5	7	4	3	8	1		2			2
14	2			4	9	12	10	2			4			
10				3	3	10	14				19	3	2	1
7					5	2	1				1	22	23	1
5						2	1					5	5	
3.5														
(*c*) Image plane 0.5 mm nearer to the lens than the image plane of best average definition														
56				6						1	23			10
40			3	15	8	1				1	6	2	1	17
28		1	15	9	9	4	1		1	14	1	6	4	2
20		5	7		12	6	7			11		3	6	1
14	1	6	2		1	16	16			2		14	3	
10	5	10	3			3	5	2	14	1		5	13	
7	18	7					1	25	15				3	
5	6	1						3						
3.5														

TABLE 7.—*Average resolving powers for the 30 f/4 lenses of foreign manufacture*

Image plane	Tangential resolving power in lines per millimeter. Angular distance from axis.							Radial resolving power in lines per millimeter. Angular distance from axis.						
	0°	5°	10°	15°	20°	25°	30°	0°	5°	10°	15°	20°	25°	30°
(*a*)	54	48	22	9	8	8	10	53	48	21	5	5	4	17
(*b*)	31	38	47	26	17	12	13	31	38	54	14	7	7	36
(*c*)	7	12	25	40	28	18	15	7	9	25	52	18	16	44

(*a*) Image plane 0.5 mm farther from the lens than image plane of best average definition.
(*b*) Image plane of best average definition.
(*c*) Image plane 0.5 mm nearer to the lens than the image plane of best average definition.

Table 8 lists the resolving power at 5° intervals in the image plane of best average definition for 20 *f*/6.8 lenses of domestic manufacture. Occurrence tables that give studies of the values of the resolving powers in image planes at different distances from the lens are shown in table 9. Values for an image plane 1.0 mm farther from the lens than the plane of best average definition have been considered admissible for the *f*/6.8 lenses, because their depth of focus is greater than that of the *f*/4 lenses. The limited range covered by the test negatives that were used in this study precluded the showing of analogous data for an image plane 1.0 mm nearer to the lens than

the plane of best average definition. It is evident, however, that most of the values for this condition would be lower than the values reported at 0.5 mm nearer to the lens than the plane of best average definition. This has been corroborated to some extent by inspection of negatives for two similar lenses where the range traversed by the

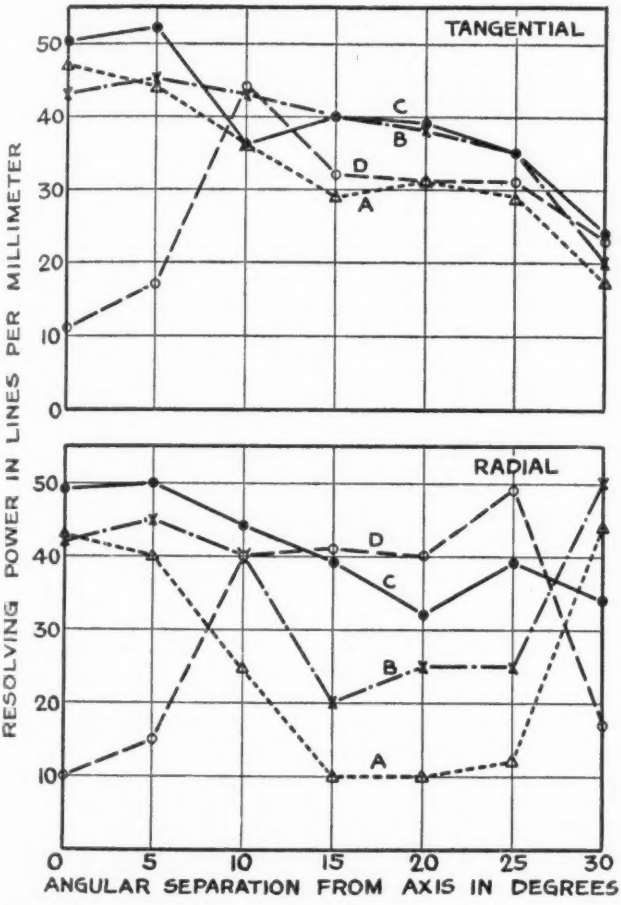

FIGURE 4.—*Graphs showing the tangential and radial resolving powers for 20 f/6.8 lenses of domestic manufacture.*

A, image plane 1.0 mm farther from the lens than the plane of best average definition. *B*, image plane 0.5 mm farther from the lens than the plane of best average definition. *C*, image plane of best average definition. *D*, image plane 0.5 mm nearer to the lens than the plane of best average definition.

test plate permitted a study at 1.0 mm nearer to the lens. A compilation of the average resolving power for each angular separation from the axis of the lens and for each image plane is given in table 10. Curves giving a graphical picture of the resolving powers in the four image planes are shown in figure 4.

TABLE 8.—*Resolving power of 20 f/6.8 lenses of domestic manufacture in the image plane of best average resolving power*

Lens number	Tangential resolving power in lines per millimeter. Angular distance from axis.							Radial resolving power in lines per millimeter. Angular distance from axis.						
	0°	5°	10°	15°	20°	25°	30°	0°	5°	10°	15°	20°	25°	30°
1	56	56	28	28	40	28	20	56	56	28	56	40	56	14
2	56	56	28	40	40	40	20	40	56	40	40	40	40	28
3	56	56	28	40	40	28	20	40	56	28	40	28	40	40
4	56	56	28	40	40	40	28	56	56	40	40	40	40	20
5	40	56	28	40	40	28	14	56	40	40	40	28	40	56
6	56	40	40	40	40	40	28	56	40	40	40	40	40	28
7	56	40	28	40	40	40	28	56	40	40	40	40	40	20
8	56	40	28	40	40	40	20	40	40	40	40	40	40	40
9	56	56	40	40	40	40	28	56	56	40	40	40	40	40
10	56	56	56	28	28	28	28	40	56	28	40	40	56	28
11	40	40	40	40	40	28	28	40	40	56	28	28	28	28
12	56	56	28	40	40	40	28	56	56	56	40	28	28	56
13	56	56	56	56	40	40	20	56	56	56	40	28	40	20
14	56	56	40	40	40	40	28	56	56	56	40	28	40	28
15	56	40	40	40	40	28	28	56	56	56	40	28	40	40
16	56	56	40	40	40	40	28	56	56	56	28	28	40	56
17	40	56	40	40	40	40	14	40	40	56	40	28	28	56
18	40	56	40	40	40	28	28	40	40	40	40	28	40	20
19	20	56	40	40	40	28	28	20	56	40	40	40	40	14
20	40	56	28	40	40	28	10	56	56	40	28	10	20	40

TABLE 9.—*Occurrence tables showing the distribution of maximal values of the resolving power for four image planes*

Resolving power in lines per mm	Distribution of maximal values of the resolving powers for the 20 f/6.8 lenses of domestic manufacture. Tangential. Angular distance from axis.							Radial. Angular distance from axis.						
	0°	5°	10°	15°	20°	25°	30°	0°	5°	10°	15°	20°	25°	30°
(a) Image plane 1.0 mm farther from the lens than image plane of best average definition														
56	10	6						5	2					6
40	9	13	14	4	7	6		14	15	4				13
28	1	1	4	13	11	9	5	1	3	8			1	1
20			2	2	2	4	4			1	1	3	3	
14				1		1	4			5	2	5		
10							5				13	1	16	
7							2			2		8		
5											1	2		
3.5											3	1		
(b) Image plane 0.5 mm farther from the lens than image plane of best average definition														
56	8	8	5					8	8	2				14
40	6	10	14	20	17	11		4	10	16	1		3	5
28	6	2	1		3	9	8	8	2	1	6	3	7	
20							5			1	4	5	8	1
14							4				7	6		
10							2				2	6	2	
7							1							
5														
3.5														

TABLE 9.—*Occurrence tables showing the distribution of maximal values of the resolving power for four image planes*—Continued

Resolving power in lines per mm	Distribution of maximal values of the resolving powers for the 20 *f*/6.8 lenses of domestic manufacture													
	Tangential. Angular distance from axis.							Radial. Angular distance from axis.						
	0°	5°	10°	15°	20°	25°	30°	0°	5°	10°	15°	20°	25°	30°
(c) Image plane of best average definition														
56	14	15	2	1				12	13	7	1		2	4
40	5	5	9	17	19	11		7	7	10	16	9	14	5
28			9	2	1	9	12			3	3	10	3	5
20	1						5	1					1	4
14							2							2
10							1					1		
7														
5														
3.5														
(d) Image plane 0.5 mm nearer to the lens than the image plane of best average definition														
56			9							2	5		11	
40		2	7	8	5	7				16	10	20	9	1
28		1	3	11	15	10	10		1	2	5			1
20		2		1		3	8		5					7
14	5	9	1				2	3	10					7
10	14	6						16	4					4
7	1							1						
5														
3.5														

TABLE 10.—*Average resolving power for the 20 f/6.8 lenses of domestic manufacture*

Image plane	Tangential resolving power in lines per millimeter. Angular distance from axis							Radial resolving power in lines per millimeter. Angular distance from axis						
	0°	5°	10°	15°	20°	25°	30°	0°	5°	10°	15°	20°	25°	30°
(a)	47	44	36	29	31	29	17	43	40	24	10	10	12	44
(b)	43	45	43	40	38	35	20	42	45	40	20	25	25	50
(c)	50	52	36	40	39	35	24	49	50	44	39	32	39	34
(d)	11	17	44	32	31	31	23	10	15	40	41	40	49	17

(a) Image plane 1.0 mm farther from the lens than the image plane of best average definition.
(b) Image plane 0.5 mm farther from the lens than the image plane of best average definition.
(c) Image plane of best average definition.
(d) Image plane 0.5 mm nearer to the lens than the image plane of best average definition.

Inspection of the values of the resolving powers, shown in table 10, indicates that they are generally higher than the corresponding values for the *f*/4 lenses. As a result, it is possible to secure good imagery over a fairly wide range. The selection of the image plane of best definition is here done with the aid of contours drawn on the test negative. Each image on the test negative is labeled with the lower of the two maximum values of the resolving power present therein, that is, tangential and radial. Lines are then drawn on the negative to enclose the regions of equal resolving power across the test negative in a manner closely analogous to the contour lines drawn on a map to show the regions of equal elevation. A row is

then selected which gives the best average definition across the entire negative. Consideration of figure 4 shows that this method has given fairly consistent results. It is clear that the curve showing the resolving power for the image plane adjudged to yield best average definition is more often above than below the curves for the other image planes reported. For tangential definition it is below only at 10°. For radial definition the case is not quite so clear in this respect, but the curve is more uniform than the others. The definition in the selected image plane is definitely superior to the definition in the image planes 1.0 mm and 0.5 mm farther from the lens except at 30°. In four of seven instances, the selected image plane for radial imagery gives better resolution than the image plane 0.5 mm nearer to the lens, and is markedly superior in three of these four instances. For the three instances where the resolving power in the selected image plane is lower than that in the image plane 0.5 mm nearer to the lens, the disparity is small.

IV. DISTORTION FOR TYPICAL AIRPLANE-CAMERA LENSES

A prime requirement of a lens that is to be used in producing negatives suitable for measurement in air-map work is low distortion. Distortion, as herein used, is the linear displacement of an imaged point from the point where it would have been imaged if the lens were perfectly orthoscopic. This displacement is measured in the image plane along a radius drawn from the intersection point of lens axis and image plane. To obtain the value of the distortion at a given angular separation from the axis, it is necessary to measure the distance from the point where the axis cuts the image plane to the image of a point which, in the object space, is at the given angular separation from the axis. Let this distance be L. Then, $L-f \tan \theta = D$, yields the distortion, D, where f is the equivalent focal length corresponding to the image plane in which the measurements are made, and θ is the given angular separation from the axis. If D is positive, the displacement is away from the center of the field.

This section is devoted to a review of the values of the distortion of some of the lenses whose resolving powers are surveyed in section III. Comparison of the values herein reported with those contained in a publication [5] by A. H. Bennett shows that marked reduction of distortion has been made in the past 10 years by the lens manufacturers. In these tabulations of distortion, no attempt is made to strike an average. To do so would tend to confuse matters and to imply that lower values of the distortion than those herein reported are readily possible. If comparisons of the distortions of different lenses are made, the differences in distortion are likely to be as great between two lenses of the same make as would be the case between two lenses of different makes.

No tabulations are given to show the variation of distortion in image planes at differing distances from the lens. The range through which the test plate travels in recording usable imagery is so small in comparison to the focal length that changes in distortion with distance from the lens for the region studied are negligible.

[5] J. Opt. Soc. Am. and Rev. Sci. Instr. **14**, 235 (1927).

The present goal is that distortion should not exceed ±0.10 mm at any point in the field. This value is to be regarded as the upper limit of distortion when the computations of distortion are based upon the paraxial or equivalent focal length. When the lens, mounted in an airplane camera in the position where it is to be used in practice, is tested, it is possible to obtain lower values of the distortion by referring it to the calibrated focal length. This calibrated focal length is obtained by modifying the equivalent focal length in such a manner that the errors arising from distortion are minimized and distributed approximately uniformly over the entire field. Hence, in precision cameras, the requirement is that the distortion must not exceed ±0.025 mm.[6] In the tables that follow, the values of the distortion are based upon the equivalent focal length, and the performance of the lens is to be judged with reference to the ±0.10 mm requirement.

Table 11 gives the distortion at 5° intervals from 5° to 30° for the 10 *f*/4 domestic lenses whose resolving powers are shown in table 2. Inspection of this table shows that none of these 10 lenses has distortion in excess of ±0.10 mm at 30°, and all are well within this limit for the lesser angles. The second column gives the values of the equivalent focal lengths which were used in determining the distortion.

Table 12 surveys the distortion at 5° intervals from 5° to 30° for 25 *f*/4 lenses of foreign manufacture; these are some of the same lenses whose resolving powers are reported in table 5. The equivalent focal length for each lens is given in column 2. Examination of this table shows that all 25 lenses have distortion within the limit of ±0.10 mm for all angular separations from the axis out to and including 20°. At 25°, lens 11 is outside the requirement with a distortion of −0.14 mm, and at 30°, 14 of the 25 lenses show distortion in excess of ±0.10 mm.

Table 13 shows the distortion at 5° intervals from 5° to 30° for 15 of the 20 *f*/6.8 lenses of domestic manufacture whose resolving powers are reported in table 8. The second column gives the equivalent focal length for each lens. All of the values of the distortion for each angle are well within the requirements of ±0.10 mm.

TABLE 11.—*Distortion of 10 f/4 lenses of domestic manufacture*

Lens number	E. F. L.	Angular distance from the axis					
		5°	10°	15°	20°	25°	30°
	mm	*mm*	*mm*	*mm*	*mm*	*mm*	*mm*
1	210.02	0.00	−0.01	−0.01	−0.02	−0.01	0.00
2	211.06	.00	.00	.00	.00	+.02	+.07
3	210.52	.00	−.01	−.02	−.02	−.02	+.01
4	211.33	.00	.00	.00	+.02	+.03	+.02
5	210.09	.00	.00	+.01	+.02	+.04	+.08
6	210.13	.00	.00	+.01	+.02	+.05	+.10
7	210.77	.00	.00	.00	.00	+.01	+.02
8	210.29	.00	.00	−.01	−.02	−.01	+.02
9	210.29	.00	.00	.00	.00	+.01	+.02
10	211.15	.00	.00	+.01	+.02	+.03	+.06

[6] J. Research NBS **22**, 209 (1939) RP1177.

TABLE 12.—*Distortion of 25 f/4 lenses of foreign manufacture*

Lens number	E. F. L.	Angular distance from the axis					
		5°	10°	15°	20°	25°	30°
	mm	*mm*	*mm*	*mm*	*mm*	*mm*	*mm*
1	209.35	0.00	0.00	−0.02	−0.03	−0.06	−0.12
2	208.87	.00	.00	.00	.00	−.01	−.03
3	208.44	.00	.00	.00	+.02	+.04	+.06
4	209.18	.00	.00	+.01	+.02	+.01	+.04
5	210.92	.00	.00	.00	+.01	+.02	+.04
6	211.56	.00	.00	.00	−.01	−.02	−.04
7	211.26	.00	.00	.00	+.01	+.01	.00
8	209.18	.00	.00	+.01	+.02	+.02	+.06
9	209.46	.00	.00	.00	−.01	−.02	−.01
10	210.58	.00	.00	−.02	−.02	−.02	−.02
11	211.07	.00	−.01	−.02	−.06	−.14	−.22
12	210.51	.00	.00	−.01	−.02	−.06	−.11
13	210.61	.00	.00	−.02	−.05	−.08	−.16
14	210.22	.00	.00	−.02	−.06	−.10	−.15
15	210.61	.00	.00	−.02	−.03	−.05	−.08
16	210.56	.00	−.01	−.02	−.05	−.08	−.13
17	210.77	.00	−.01	−.02	−.04	−.06	−.11
18	210.94	.00	.00	−.01	−.03	−.08	−.14
19	210.21	.00	−.01	−.02	−.04	−.07	−.12
20	210.48	.00	−.01	−.02	−.04	−.07	−.12
21	210.77	.00	.00	−.01	−.02	−.04	−.08
22	210.61	.00	−.01	−.02	−.05	−.09	−.14
23	208.73	.00	.00	−.02	−.04	−.07	−.14
24	207.96	.00	−.01	−.03	−.05	−.08	−.12
25	208.56	.00	−.01	−.03	−.05	−.07	−.11

TABLE 13.—*Distortion of 15 f/6.8 lenses of domestic manufacture*

Lens number	E. F. L.	Angular distance from the axis					
		5°	10°	15°	20°	25°	30°
	mm	*mm*	*mm*	*mm*	*mm*	*mm*	*mm*
1	208.70	0.00	0.00	−0.01	−0.02	−0.03	−0.04
2	209.33	.00	.00	.00	+.01	+.02	+.06
3	210.00	.00	.00	.00	−.01	−.01	.00
4	210.05	.00	.00	.00	.00	+.02	+.06
5	209.98	.00	.00	.00	−.01	−.02	.00
6	209.73	.00	.00	.00	−.01	−.01	+.01
7	209.69	.00	.00	.00	−.01	−.02	.00
8	209.73	.00	.00	.00	.00	.00	+.04
9	209.77	.00	.00	.00	−.01	−.01	+.02
10	209.76	.00	.00	−.01	−.01	+.01	+.03
11	209.77	.00	.00	−.01	−.02	−.03	−.02
12	209.56	.00	.00	−.01	−.01	.00	+.05
13	209.66	.00	.00	−.01	−.01	−.01	+.01
14	209.75	.00	.00	.00	.00	+.01	+.03
15	210.01	.00	.00	.00	.00	+.02	+.05

V. CONCLUSION

Only lenses tested since January 1937 have been considered in this study. Each group represents a random sample of the lenses of a given make that were submitted for test. The present requirements for an airplane-camera objective having a focal length of 210 mm and covering a 7- by 9-inch film are that the distortion referred to the paraxial or equivalent focal length shall not exceed ±0.10 mm at 30° from the axis, and that the resolving power in any orientation shall not fall below seven lines to the millimeter throughout the region from 0° to 30° as measured from the axis of the lens. On the basis of the tables contained in this paper, it is clear that the domestic lenses whose test records here appear satisfactorily meet the requirements for use on air-mapping projects.

WASHINGTON, November 18, 1938.

U. S. Department of Commerce National Bureau of Standards

RESEARCH PAPER RP1217

Part of Journal of Research of the National Bureau of Standards, Volume 22, June 1939

EDGE CORRECTION IN THE DETERMINATION OF DIELECTRIC CONSTANT

By Arnold H. Scott and Harvey L. Curtis

ABSTRACT

An edge correction is often required in determining the dielectric constant of an insulating material by the capacitance method. Theoretical formulas by which the edge correction may be computed have been considered for a number of electrode arrangements. Some of these apply to circular electrodes and some to rectangular electrodes. The error in the dielectric constant which may arise from the use of these formulas is discussed for each of the different arrangements.

The accuracies of the methods were experimentally determined by making measurements on the same specimens with the various arrangements of electrodes. The guard-ring arrangement was assumed to give the correct value of the dielectric constant, and the values obtained with the other arrangements were compared with it to determine their errors. Only two methods gave values which were in error by less than 1 percent. Both methods were for arrangements of electrodes in which one electrode was smaller than the other, one being for circular electrodes, the other for rectangular electrodes.

Empirical equations were set up which gave values of the dielectric constant which were in error by less than 1 percent for all electrode arrangements, both for circular and rectangular electrodes. These equations are much simpler than the theoretical equations.

CONTENTS

Part 1. Theoretical Determination of Edge Correction

	Page
I. Introduction	748
II. Theory of edge correction with a single sheet of dielectric	749
1. Edge correction for circular electrodes	750
(a) Theoretical formula when a circular sheet of dielectric has electrodes of the same diameter as the sheet	751
(b) Theoretical formula when a sheet of dielectric has one large electrode and one small circular electrode	752
(c) Theoretical formula when a sheet of dielectric extends beyond the circumferences of the electrodes	753
(d) Elimination of the edge correction for circular electrodes by using a guard electrode	754
2. Edge correction for rectangular electrodes	754
(a) Theoretical formula when a rectangular sheet of dielectric has electrodes covering both faces	755
(b) Theoretical formula when a sheet of dielectric has one large electrode and one small rectangular electrode	755
(c) Theoretical formula when a sheet of dielectric extends beyond the edges of rectangular electrodes	756
(d) Elimination of the edge correction for rectangular electrodes by using a guard electrode	756

III. Theory of edge correction with two sheets of dielectric ..... Page 756
1. Edge correction for circular electrodes 757
(a) Theoretical formula when the two sheets of dielectric and the electrodes have the same diameter 757
(b) Theoretical formula when the outer electrodes and the two sheets of dielectric extend beyond the circumference of the center electrode 758
(c) Theoretical formula when the two sheets of dielectric extend beyond the circumferences of the electrodes 759
2. Edge correction for rectangular electrodes 759
(a) Theoretical formula when the outer electrodes and the two sheets of dielectric extend beyond the perimeter of the center electrode 760

Part 2. Experimental Determination of the Edge Correction

I. Introduction 760
II. Arrangement of electrodes 761
III. Electrical measurements 762
IV. Results 763
1. Test of Kirchhoff's equation 763
2. Dielectric constants when theoretical equations were used 764
(a) Circular electrodes 764
(b) Rectangular electrodes 766
3. Determination of empirical equations 766
4. Dielectric constants when empirical equations were used 773
V. Summary 775

PART 1. THEORETICAL DETERMINATION OF EDGE CORRECTION

I. INTRODUCTION

An edge correction is usually required in those capacitance methods of determining dielectric constant that employ only two electrodes. This necessity arises from the difficulty of making the experimental conditions of a method conform to the requirements implied in the definition of dielectric constant. The dielectric constant of a material is defined as the ratio of the capacitance of a capacitor having the material as a dielectric to the capacitance of another capacitor which has an identical arrangement of electrodes, but has a vacuum as the dielectric. This may conveniently be represented by the equation

$$K=\frac{C_k}{C_v} \tag{1}$$

where

K = the dielectric constant of the material,

C_k = the capacitance of a capacitor, with the material as its dielectric, and

C_v = the capacitance of a capacitor having an identical arrangement of electrodes as for C_k, but having a vacuum [1] as its dielectric.

This definition assumes that, for each capacitor, the dielectric completely fills the electric field surrounding the electrodes. When the dielectric does not completely fill the electric field, there must be applied to C_k a correction which is commonly called the edge correction.

[1] Except for measurements of high precision, air, having a dielectric constant of 1.00059 under normal conditions, may be used instead of a vacuum.

The principal application of the edge correction is in determining the dielectric constant of solids in the form of sheets. A capacitor is constructed from a sheet of the material by placing an electrode on each side. The capacitance of this capacitor is measured, and the capacitance of a capacitor which is identical, except that it has vacuum as a dielectric, is computed. The edge correction is introduced to correct the measured capacitance for the reason that the dielectric under investigation does not completely fill the electric field surrounding the electrodes, and to give an accurate formula for determining the computed capacitance. To avoid the necessity of applying an edge correction, a capacitor having a guard electrode is often employed. In many cases, however, the use of a guard electrode is not feasible, so that a method involving an edge correction is necessary.

Six different arrangements of circular electrodes, besides the one using a guard electrode, are considered. Three of these and the guard-electrode arrangement apply to a single sheet of material with electrodes on opposite sides. Three other arrangements apply to a pair of sheets with one electrode between them and with their outer electrodes joined to form a single electrode. Five arrangements of rectangular electrodes are discussed. Three of these and the guard-electrode arrangement apply to a single sheet of material. Only one arrangement, using two sheets of material, has been investigated for rectangular electrodes.

II. THEORY OF EDGE CORRECTION WITH A SINGLE SHEET OF DIELECTRIC

A sheet of dielectric material is prepared for the determination of its dielectric constant by placing electrodes on its two opposite faces. The electrode may completely cover the two faces of the sheet, or one or both electrodes may be smaller than the sheet. Each such arrangement constitutes a capacitor, the capacitance of which can be measured by comparison with a standard capacitor or by some other suitable method. However, the measured capacitance may include the capacitance between one or both electrodes and the earth. The contribution of this earth capacitance depends on the connection to earth of the measuring circuit. Even with one electrode at earth potential, a change in the connection to earth may change the measured capacitance. This is illustrated by the diagram of figure 1, in which it is indicated that an ungrounded alternating potential is impressed on the plates of a capacitor, and the current in the circuit is measured by the ammeter, A. If the alternating potential has a definite value and frequency, the capacitance is proportional to the reading of the ammeter, A. If the ammeter has a negligible impedance relative to that of the capacitor, the lower plate of the capacitor will be at earth potential when the earth connection is made on either side of the ammeter. If the connection is below the ammeter (x connected to z), the measured current is that through C only, while if the connection is above the ammeter (x connected to y), the measured current is that through both

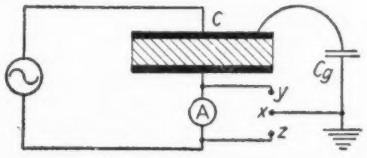

FIGURE 1.—*Diagram showing the effect on the measured capacitance of changing the point at which the ground connection is made.*

C and C_g (capacitance to earth). The following discussion refers to those cases in which C only is measured. If the measuring circuit is so arranged that C_g is included in the measurement, then the following equations will have to be modified to include C_g, the value of which will depend on the proximity of surrounding objects and will have to be determined for each setup.

Although the experimental arrangement is assumed to be such that only the capacitance between the electrodes is measured, yet the theoretical discussion will be simplified by considering the system as two conducting plates situated near the center of a conducting sphere of infinite radius. If the plates are circular disks that are coaxial, and if the sphere is evacuated, all the coefficients of capacitance can be computed from the dimensions of the disks and the distance between them. If the plates are rectangles, no formula is available for computing the capacitance to earth.

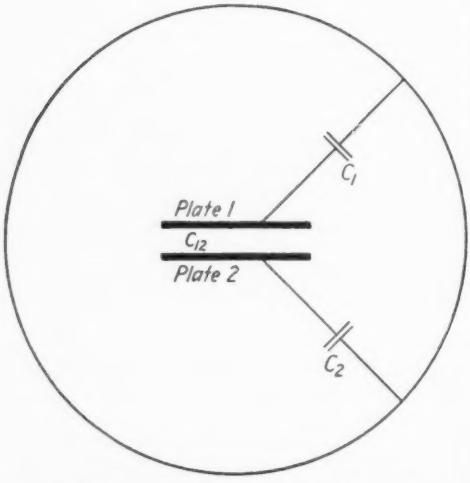

FIGURE 2.—*Diagram illustrating the coefficient of capacitance of two parallel plates surrounded by an infinite sphere.*

The arrangement of electrodes inside of a sphere is shown diagrammatically in figure 2. The mutual capacitance between plates 1 and 2 is designated as C_{12}, whereas the capacitances between the plates and the infinite sphere are designated as C_1 and C_2. It is convenient to consider C_{12} as made up of two parts, C_n and C_e. The normal capacitance, C_n, is the value that C_{12} would have if the electricity were uniformly distributed over the inner surfaces of the electrodes, and if the lines of electrostatic intensity were all straight lines extending directly from one electrode to the other. The edge capacitance, C_e, is the correction that must be added to C_n to give C_{12}. Values of C_n and C_e can be computed for circular electrodes and C_n and (C_e+C_1) for rectangular electrodes. In practical measurements one electrode (plate 2) is usually at earth potential, so that C_2 becomes zero and C_1 becomes the earth capacitance, C_g.

1. EDGE CORRECTION FOR CIRCULAR ELECTRODES

The formulas for computing the capacitances for C_n and C_e for circular electrodes [2] of the same size are

$$C_n=\frac{1.113\ D^2}{16b}\ \mu\mu\text{f}, \tag{2}$$

$$C_e=\frac{1.113\ D}{8\pi}\left[\ln\frac{8\pi D}{b}-3+z\right]\mu\mu\text{f}, \tag{3}$$

[2] G. Kirchhoff, On the Theory of Condensers, Monatsber. Akad. Wiss. Berlin (March 1877), p. 144; also Collected Works, p. 101 (Barth, Leipzig, 1882). A more recent paper is by J. W. Nicholson, Phil. Trans. 224A, 303 (1924), but his formula contains unsolved integrals.

where

D=diameter of each electrode in centimeters,
b=distance between the inner faces of the electrodes in centimeters,
t=thickness of each electrode in centimeters, and
$z=f(x)=(1+x)\ln(1+x)-x\ln x$ (4)
$x=t/b$, and
ln=a natural logarithm (2.303 times the common logarithm).

Values of z for any given value of x can be obtained from the curve of figure 3.

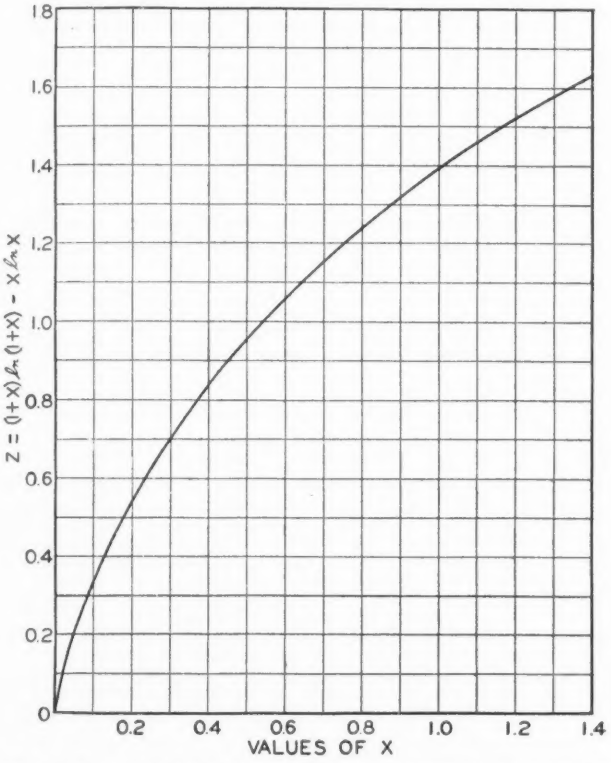

FIGURE 3.—*Values of a function used in computing the edge capacitance.*

Equation 3 was tested experimentally, as described in part 2, and was found to be correct within experimental error. This equation was used with four arrangements of electrodes.

(a) THEORETICAL FORMULA WHEN A CIRCULAR SHEET OF DIELECTRIC HAS ELECTRODES OF THE SAME DIAMETER AS THE SHEET

A capacitor consisting of a circular sheet of dielectric with electrodes completely covering both surfaces, as shown in cross section in figure 4(*a*), has a capacitance, $\boldsymbol{C}$, when measured,[3] as previously described,

[3] Bold-faced symbols will be used to indicate measured capacitance.

with one electrode at earth potential, which is related to the computed capacitance by the equation

$$C=KC_n+C_e, \text{ approximately.} \tag{5}$$

Hence

$$K=\frac{C-C_e}{C_n}, \text{ approximately,} \tag{6}$$

where C_n and C_e are obtained from eq 2 and 3, respectively.

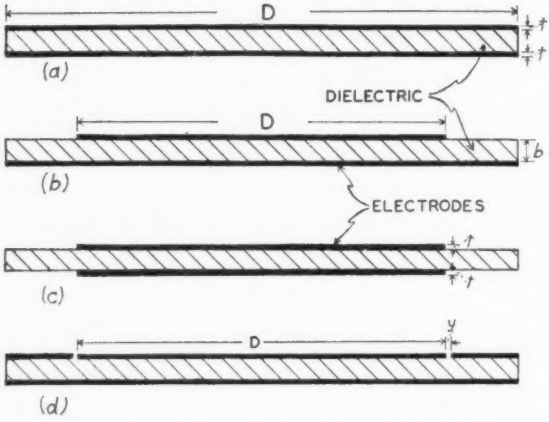

FIGURE 4.—*Arrangement of circular electrodes on a single sheet of dielectric.*

In this arrangement of electrodes, the edge capacitance is probably not exactly equal to C_e, because the configuration of the electric field at the edge is slightly different when the dielectric is between the electrodes from that when a single dielectric fills the field. The experimental determinations of part 2 (table 2) show that this method may yield values in error by as much as 1.1 percent.

(b) THEORETICAL FORMULA WHEN A SHEET OF DIELECTRIC HAS ONE LARGE ELECTRODE AND ONE SMALL CIRCULAR ELECTRODE

A capacitor consisting of a sheet of dielectric between a large electrode which nearly or completely covers one face, and a small circular electrode near the center of the opposite face, as shown in cross section in figure 4(*b*), has a capacitance, C, when measured in the manner already described with the large electrode at earth potential, which is related to the computed capacitances by the equation

$$C=K(C_n+C_e'), \text{ approximately.} \tag{7}$$

In deriving this equation, it was assumed that the large electrode was of infinite extent. In practice it was found sufficient if the large electrode extended beyond the small one by a distance equal to three times the thickness of the dielectric. From eq 7

$$K=\frac{C}{C_n+C_e'}, \text{ approximately,} \tag{8}$$

where C_n is obtained from eq 2, and C_e' is twice the value of the edge capacitance in air of an equal electrode capacitor in which the electrodes have the same diameter as the smaller electrode, and the distance between the electrodes is twice the thickness of the dielectric in the actual capacitor or

$$C_e' = 1.113 \frac{D}{4\pi}\left[\ln \frac{4\pi D}{b} - 3 + z'\right] \mu\mu f, \tag{9}$$

where

D=diameter of the smaller electrode in centimeters,
b=thickness of the dielectric in centimeters, and
$z'=f(x')$, (see eq 4 or fig. 3)
$x'=t/2b$,
t=thickness of smaller electrode in centimeters.

In the above arrangement of electrodes, KC_e' is too large, because some of the lines of electric intensity at the edge pass partly through air. Hence, the value of K obtained by this method will be smaller than the true value. The experimental results of part 2 (table 2) show that this method may be in error by as much as 6 percent.

This method can be made to give more accurate values if thin electrodes are used, by placing on the outside of the small electrode a sheet of dielectric of the same material as is between the electrodes. Although no experimental measurements have been made to prove it, the error of this method can, in this way, probably be made less than 1 percent.

(c) THEORETICAL FORMULA WHEN A SHEET OF DIELECTRIC EXTENDS BEYOND THE CIRCUMFERENCES OF THE ELECTRODES

A capacitor which consists of a relatively large sheet of dielectric between two equal circular electrodes that have their centers directly opposite each other, as shown in cross section in figure 4 (*c*), has a measured capacitance, $\boldsymbol{C}$, which is related to the computed capacitances by the equation

$$\boldsymbol{C} = K(C_n + C_e), \text{ approximately.} \tag{10}$$

Hence

$$K = \frac{\boldsymbol{C}}{C_n + C_e}, \text{ approximately,} \tag{11}$$

where C_n and C_e are obtained from eq 2 and 3, respectively.

This method gives a value of K that is too small, because the electric field beyond the edges of the electrodes was not all in the solid dielectric. The experimental determinations of part 2 (table 2) show that this method may be in error by as much as 7 percent.

It is possible to make this method more accurate by placing the dielectric material in more of the electric field. If thin electrodes such as tinfoil electrodes, are used, this can be done by placing sheets of the dielectric material on the outside of the electrodes as well as between them. The experimental results of part 2 (table 1) show that if sheets of the same dielectric material are placed on the outside of the electrodes as is between them, this method will give results in error by less than 1 percent.

(d) ELIMINATION OF EDGE CORRECTION FOR CIRCULAR ELECTRODES BY USING A GUARD ELECTRODE

When a capacitor consists of a sheet of dielectric between a large electrode and a small circular electrode with a guard electrode surrounding it, as shown in cross section in figure 4 (*d*), the edge correction is eliminated except for a slight effect due to the finite width of the gap between the small electrode and the guard electrode. The measured capacitance, C, between the small or guarded electrode and the large electrode is related to the computed capacitance by the equation

$$C=KC_n'. \tag{12}$$

Hence

$$K=C/C_n'. \tag{13}$$

The value of C_n' is obtained from eq 2 when D is replaced by $D+y$, where D is the diameter of the guarded electrode in centimeters and y is the width of the gap between the guarded electrode and the guard electrode.

The addition of the width of the gap to the diameter of the guarded electrode serves as an approximate correction to take care of the error due to the finite width of the gap. This is equivalent to assuming that the guarded electrode extends to the center of the gap. In the extreme case where the width of the gap is equal to the thickness of the specimen and the thickness of the specimen is one-tenth the diameter of the guarded electrode, the error introduced by this approximation is less than 1 percent. The dimensions used in the experimental part of this paper were such that errors less than 0.1 percent were introduced. The width of the guard ring should be at least twice the thickness of the specimen.

This is the most accurate of the methods discussed in this paper. The dielectric fills the entire field between the electrodes, and this field is uniform except for the slight variation at the edge of the guarded electrode due to the finite width of the gap. If the gap is made small, the correction given above is sufficiently accurate, so that the error by this method is negligible.

It should be observed that the measuring circuit must be such that only the capacitance between the guarded electrode and the opposite electrode is measured.

2. EDGE CORRECTION FOR RECTANGULAR ELECTRODES

The normal capacitance, C_n, and the sum of the edge capacitance, C_e, and the earth capacitance, C_g, when the electrodes are rectangular plates which form the opposite faces of a rectangular parallelopiped, and when they are in an evacuated infinite sphere, are given by the following formulas:

$$C_n=\frac{1.113lw}{4\pi b}\mu\mu f, \tag{14}$$

$$C_e+C_g=1.113\frac{l}{4\pi^2}\left\{1+\ln\left[1+\frac{\pi w}{b}+\ln\left(1+\frac{\pi w}{b}\right)\right]\right\}$$

$$+\frac{1.113w}{4\pi^2}\left\{1+\ln\left[1+\frac{\pi l}{b}+\ln\left(1+\frac{\pi l}{b}\right)\right]\right\}\mu\mu f, \tag{15}$$

where

b=thickness of the dielectric in centimeters,
w=width of the electrodes in centimeters, and
l=length of the electrode in centimeters.

No formula is available for separating C_e and C_g as was the case for circular electrodes. One of the limits to the accuracy of this equation is the uncertainty of the value of C_g.

The formulas were deduced from the equation given by Thomson [4] for the distribution of electricity along the edges of two semi-infinite, parallel electrodes which have their edges in a plane perpendicular to the electrodes. Coursey [5] gives a formula for the capacitance of rectangular plates which is the sum of eq 14 and 15, except that the correction at the ends was neglected. Equation 15 assumes that the electrodes are so wide that the effect of one edge does not extend as far as the opposite edge. Furthermore, the derivation does not consider the thickness of the electrodes. Hence, eq 15 should be used only when the electrodes are thin and wide relative to the thickness of the dielectric. Even with these restrictions, the formula for C_e is less accurate than the similar formula with circular electrodes, especially since C_g is included. Four different arrangements of electrodes for single sheets of material will be considered that are analogous to the four cases for circular electrodes.

(a) THEORETICAL FORMULA WHEN A RECTANGULAR SHEET OF DIELECTRIC HAS ELECTRODES COVERING BOTH FACES

A rectangular sheet of dielectric with electrodes that cover both faces is analogous to the case of circular electrodes that cover both faces of the dielectric. Hence

$$K=\frac{C-C_e}{C_n}, \text{ approximately,} \tag{16}$$

where the values of C_n and C_e must be computed by eq 14 and 15.

The dielectric constant, when determined by this method, is less accurate than when circular electrodes are employed, since the experimental results of part 2 (table 3) show that this method may give values in error by as much as 2.3 percent.

(b) THEORETICAL FORMULA WHEN A SHEET OF DIELECTRIC HAS ONE LARGE ELECTRODE AND ONE SMALL RECTANGULAR ELECTRODE

A sheet of dielectric with a small rectangular electrode on one face and a larger electrode on the opposite face, so placed that it extends beyond the edges of the smaller electrode, is analogous to the case of a large electrode with a small circular electrode opposite it. Hence

$$K=\frac{C}{C_n+C'_e}. \tag{17}$$

The value of C_n is given by eq 14, and the value of C'_e can be obtained from C_e (eq 15) in the same manner as was done for the analogous

[4] J. J. Thomson, Recent Researches in Electricity and Magnetism, p. 216 (Clarendon Press, Oxford, England, 1893).
[5] P. R. Coursey, Electrical Condensers, p. 138 (Sir Isaac Pitman and Sons, Ltd., London, 1927).

case with circular electrodes. The value of C'_e (assuming C_e to be negligible) is given by

$$C'_e=\frac{1.113l}{2\pi^2}\left\{1+\ln\left[1+\frac{\pi w}{2b}+\ln\left(1+\frac{\pi w}{2b}\right)\right]\right\} + \frac{1.113w}{2\pi^2}\left\{1+\ln\left[1+\frac{\pi l}{2b}+\ln\left(1+\frac{\pi l}{2b}\right)\right]\right\} \mu\mu f. \quad (18)$$

This method will give values which are too small, because the electric field beyond the edge of the smaller electrode is not all in the solid dielectric. The experimental data of part 2 (table 3) show that the error may be as much as 14 percent.

(c) THEORETICAL FORMULA WHEN A SHEET OF DIELECTRIC EXTENDS BEYOND THE EDGES OF RECTANGULAR ELECTRODES

A sheet of dielectric which extends beyond the edges of equal rectangular electrodes that are opposite each other is analogous to the case of small circular electrodes. Hence

$$K=\frac{C}{C_n+C_e}, \text{ approximately,} \quad (19)$$

where the values of C_n and C_e are obtained from eq 14 and 15, respectively.

The result is less accurate than for the similar case using circular electrodes. This arrangement may give results that are as much as 10 percent too small, as indicated by the experimental determinations of part 2 (table 3).

(d) ELIMINATION OF THE EDGE CORRECTION FOR RECTANGULAR ELECTRODES BY USING A GUARD ELECTRODE

When a capacitor consists of a sheet of dielectric between a large electrode and a small rectangular electrode surrounded by a guard electrode, the edge correction is eliminated except for a slight effect due to the finite width of the gap between the guarded electrode and the guard electrode. This is analogous to the guarded electrode case of circular electrodes. Hence

$$K=\frac{C}{C'_n}. \quad (20)$$

The value of C'_n is obtained from eq 14 by replacing l by $(l+y)$ and w by $(w+y)$, where y is the width in centimeters of the gap between the guarded electrode and the guard electrode, and l and w are the length and width, respectively, of the guarded electrode.

As in the case of circular electrodes, the dielectric fills the entire field, and this field is uniform except for the slight variation at the edge of the guarded electrode due to the finite width of the gap. Considerations as to the width of the gap and the width of the guard electrode are similar to those for circular electrodes.

III. THEORY OF EDGE CORRECTION WITH TWO SHEETS OF DIELECTRIC

When two similar sheets of dielectric have one common electrode between them, and the two outside electrodes are connected together, the edge correction of this capacitor cannot be computed by the formula given for a single sheet of dielectric. Moreover, the same

symmetry does not exist between the different cases as when only a single sheet of dielectric is employed. However, the capacitance to earth does not enter into the problem in any case.

1. EDGE CORRECTION FOR CIRCULAR ELECTRODES

The normal capacitance, C_n, must be computed for each sheet by the formula given in a preceding section, and the total normal capacitance taken as the sum of the values for the two sheets. The formulas for the edge capacitance do not have as satisfactory theoretical basis

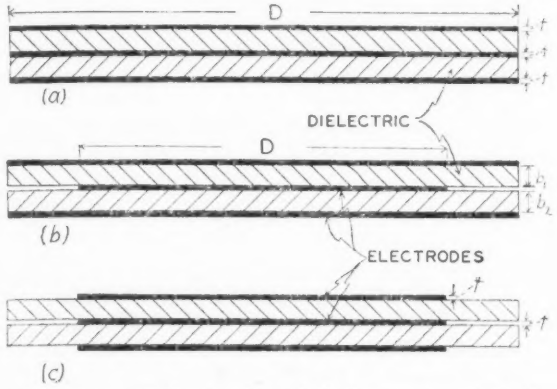

FIGURE 5.—*Arrangement of circular electrodes when two sheets of dielectric are used.*

as the similar formulas for a single sheet. However, experimental determinations with circular electrodes on two sheets give values of the dielectric constant which agree well with accepted values when the center electrode is smaller than the other two.

Formulas are available for three different arrangements of circular electrodes. A diagram, showing a cross section through the center, is given in figure 5 for each of these arrangements.

(a) THEORETICAL FORMULA WHEN THE TWO SHEETS OF DIELECTRIC AND THE ELECTRODES HAVE THE SAME DIAMETER

When two circular sheets of a dielectric material, both having the same diameter, are assembled with three circular electrodes having the same diameter as the sheets of dielectric, as shown in cross section in figure 5 (*a*), the measured capacitance, C, between the center electrode and the two outside ones is related to the computed capacitances by the equation

$$C=K(C_{n1}+C_{n2})+C_e, \text{ approximately,} \tag{21}$$

so that

$$K=\frac{C-C_e}{C_{n1}+C_{n2}}, \text{ approximately,} \tag{22}$$

where

$$C_{n1}=1.113\frac{D^2}{16b_1}\mu\mu f, \tag{23}$$

$$C_{n2}=1.113\frac{D^2}{16b_2}\mu\mu f, \tag{24}$$

$$C_e=\frac{1.113D}{\pi}\left[0.5539+\frac{1}{6}(z_2+z_3)\right]\mu\mu f, \tag{25}$$

where

$z_2=f(x_2)$ (see eq 4 or fig. 3),
$z_3=f(x_3)$ (see eq 4 or fig. 3),
$x_2=2t/b_1$,
$x_3=2t/b_2$,
D=diameter of the electrode in centimeters,
b_1=thickness of one sheet in centimeters,
b_2=thickness of the second sheet in centimeters, and
t=thickness of each conducting disk in centimeters.

The formula for C_e was derived by Grüneisen and Giebe,[6] who have published only the final formula and state that the derivation has not been rigorously carried through.

If the electrodes are thin, as for tinfoil electrodes, both z_2 and z_3 are so small that they can be neglected. Then eq 25 becomes

$$C_e=0.1962D\mu\mu f \tag{26}$$

This equation indicates that the edge capacitance is independent of the thickness of the dielectric. This may be applicable only for a limited range of thicknesses and diameters. However, Grüneisen and Giebe measured and computed the capacitance of 13 air capacitors, in which the diameter of the electrodes varied from 15 to 30 cm, the distance between adjacent electrodes varied from 1 to 3 cm, and the thickness of the electrodes varied from 0.08 to 0.59 cm. The difference between the computed and observed capacitance was, in 1 case, 2 percent of the measured capacitance, but in all the other 12 cases it was less than 1 percent. It appears that the difference was not greater than the error of measurement. Hence, the formula may be considered satisfactory. However, in this arrangement of electrodes with dielectric material between them, the edge capacitance is not exactly equal to C_e because the configuration of the electric field at the edge is slightly different when the dielectric is between the electrodes from that when air is the only dielectric. This error may amount to 1 percent as shown by the experimental data in part 2 (table 2).

(B) THEORETICAL FORMULA WHEN THE OUTER ELECTRODES AND THE TWO SHEETS OF DIELECTRIC EXTEND BEYOND THE CIRCUMFERENCE OF THE CENTER ELECTRODE

When two large sheets of a dielectric are assembled with three electrodes, the center one being circular and smaller than the other electrodes and the sheets, as shown in cross section in figure 5 (b), the measured capacitance C between the center electrode and the two outside ones is related to the computed capacitances by the equation

$$C=K(C_{n1}+C_{n2}+C_e') \text{ approximately,} \tag{27}$$

so that

$$K=\frac{C}{C_{n1}+C_{n2}+C_e'} \quad \text{approximately,} \tag{28}$$

where C_{n1} and C_{n2} are the same as in the two preceding sections, and

$$C_e'=\frac{1.113D}{\pi}[0.6932+z_4+z_5]\ \mu\mu f, \tag{29}$$

[6] E. Grüneisen and E. Giebe, *Use of the three-plate capacitor for the determination of the dielectric constant of solid bodies*, Verhandl. deut. physik. Ges. 14, 921 (1912).

where

$z_4 = f(x_4)$ (see eq 4 or fig. 3)
$z_5 = f(x_5)$ (see eq 4 or fig. 3)
$x_4 = t/4b_1$
$x_5 = t/4b_2$
D = diameter of the small interior electrode in centimeters,
b_1 = thickness of one sheet of dielectric in centimeters,
b_2 = thickness of the second sheet of dielectric in centimenters, and
t = thickness of the inner electrode in centimeters.

The equation for C_e' which was derived by Thomson [7] for the edge of a semi-infinite plate midway between two infinite plates was applied here without alteration to the circular electrodes. If the electrode is so thin, as in the case of tinfoil electrodes, that z_4 and z_5 are negligible,

$$C_e' = 0.2456 D \mu\mu f. \tag{30}$$

This equation has the same form as the one for C_e given by Grüneisen and Giebe for three equal electrodes. However, the relation between the constants of the two equations is not evident. This method gives a value of K that is more nearly correct than any of the other methods described. The experimental data of part 2 (table 2) show that this method will give errors less than 0.6 percent when thin electrodes such as tinfoil are used.

(c) Theoretical formula when the two sheets of dielectric extend beyond the circumferences of the electrodes

When two large sheets of a dielectric are assembled, as shown in cross section in figure 5 (c), with three smaller circular electrodes all of the same diameter and with their centers in a line perpendicular to the faces of the electrodes, the measured capacitance, $\boldsymbol{C}$, between the center electrode and the two outside ones is related to the computed capacitance by the formula

$$\boldsymbol{C} = K(C_{n1} + C_{n2} + C_e) \text{ approximately.} \tag{31}$$

Hence

$$K = \frac{\boldsymbol{C}}{C_{n1} + C_{n2} + C_e} \text{ approximately,} \tag{32}$$

where the values of C_{n1}, C_{n2}, and C_e are the same as given in the preceding section.

The value of K obtained by this method is smaller than the true value, because the field beyond the edges of the electrodes is not all in the solid dielectric. The amount of this error may be as much as 4 percent, as shown by the experimental results given in part 2 (table 2).

2. Edge Correction for Rectangular Electrodes

There is only one arrangement of rectangular electrodes on two sheets of dielectric for which a formula is available. This is analogous to the case just treated of a small circular electrode between two large sheets of dielectric which have large electrodes on their outer faces.

[7] J. J. Thomson, Recent Researches in Electricity and Magnetism, p. 211 (Clarendon Press, Oxford, England, 1893).

(a) THEORETICAL FORMULA WHEN THE OUTER ELECTRODES AND THE TWO SHEETS OF DIELECTRIC EXTEND BEYOND THE PERIMETER OF THE CENTER ELECTRODE

When two sheets of dielectric are assembled with three electrodes, so that both the dielectric sheets and outside electrodes extend some distance beyond the edges of the center electrode which is in the form of a rectangular plate, the dielectric constant is given by the equation

$$K=\frac{C}{C_{n1}+C_{n2}+C'_e}, \tag{33}$$

where

$$C_{n1}=\frac{1.113lw}{4\pi b_1}\mu\mu\text{f}, \tag{34}$$

$$C_{n2}=\frac{1.113lw}{4\pi b_2}\mu\mu\text{f}, \tag{35}$$

$$C'_e=\frac{1.113(2l+2w)}{\pi^2}[0.6932+z_4+z_5]\mu\mu\text{f}, \tag{36}$$

where z_4, z_5, b_1, b_2, and t are the same as the preceding section, which is the analogous case for circular electrodes, and where

w=width of the center electrode in centimeters, and
l=length of the center electrode in centimeters.

The equation for C'_e was obtained from the equation given by Thomson [8] for the distribution of electricity on a semi-infinite plate with one straight edge when midway between two infinite plates. In extending this to the case here considered, the assumption is made that the center strip is so wide that the effect of one edge on the distribution of electricity does not extend to the opposite edge. If the electrodes are so thin that z_4+z_5 can be neglected, then

$$C'_e=0.07818\ (l+w)\mu\mu\text{f}. \tag{37}$$

This method will give results which are in error by less than 0.5 percent as shown by the experimental results in part 2 (table 3).

PART 2. EXPERIMENTAL DETERMINATION OF THE EDGE CORRECTION

I. INTRODUCTION

The assumptions used in the derivations of the theoretical equations given in part 1 for the computation of the dielectric constants of sheet materials were such that appreciable errors in the results might be expected. It was therefore desirable that these equations be experimentally tested to determine their accuracy. This has been done for arrangements where both circular and rectangular electrodes were used. The values of the dielectric constant which were obtained when a guard electrode was used, were taken to be correct, and the values obtained from other arrangements of the electrodes were compared with them.

It was also deemed desirable to test the accuracy of Kirchhoff's equation (eq 3), since it was the basis for the equations used in the

[8] J. J. Thomson, Recent Researches in Electricity and Magnetism, p. 211 (Clarendon Press, Oxford, England, 1893).

methods where a single sheet of dielectric material was equipped with circular electrodes. This was done in two ways. One method was the construction of an air capacitor whose capacitance could be computed as well as measured. The other method was to surround the electrodes, as nearly as possible, by the dielectric. This was accomplished by using small electrodes on a large sheet of dielectric and then placing large sheets of dielectric outside the electrodes.

The specimens on which measurements were made had thicknesses which ranged from 0.07 to 0.70 cm and dielectric constants which ranged from 2.6 to 70.0. The circular specimens were all 15 cm in diameter, except for three samples of titania which were 12 cm in diameter. The rectangular specimens had lengths ranging from 12 to 88 cm and widths from 8 to 12 cm. These specimens are listed in the first columns of tables 2 and 3. All the specimens except the porcelain and titania were cut from uniform sheets of material. The titania, which was a mixture of titanium oxide in a porcelain base, was obtained in disk form. No particular care was taken in the selection of the materials except for the marble specimens, which were cut from slabs carefully selected as to uniformity of appearance. Only two of the materials were measured using rectangular electrodes, namely, methyl methacrylate and glass.

II. ARRANGEMENT OF ELECTRODES

Tinfoil was used as the electrode material. This was applied with a thin coat of petrolatum and carefully rolled down on the surface of the specimen with a narrow roller until no visible imprint could be made on the tinfoil with the roller. Experiments were made which showed that this procedure of rolling was necessary if the formation of bubbles under the electrodes was to be avoided. When the tinfoil was rubbed down in the usual manner, gas bubbles became visible under the tinfoil in less than 24 hours. However, when the tinfoil was rolled down with a narrow roller on which considerable pressure was exerted until no imprint could be made on the tinfoil, no bubbles appeared under the tinfoil within several months.

The electrodes were applied to the specimens only once and served for all the various arrangements. For each material two or more single specimens were used. The electrodes were cut and modified as needed for the different arrangements but were not removed and replaced. This was accomplished by first using the arrangements where the electrodes completely covered the faces of the specimens and removing parts of these electrodes as required for the other arrangements. To provide a guard ring, a strip of electrode 0.05 cm wide was removed from one electrode. The width of the guard ring was 2.0 cm. The removal of the guard ring provided the arrangement having one electrode larger than the other. The arrangement consisting of electrodes of the same size but smaller than the dielectric was obtained by cutting the larger electrode to the size of the smaller one. The double specimens were obtained by facing together two single specimens.

The dielectric constants for these various electrode arrangements were computed by means of the corresponding equations given in part 1. The electrodes used on the solid dielectrics were tinfoil

having a thickness of 0.003 cm. The terms of the equations involving the thickness were so small for this thickness that neglecting them would not alter the result by 0.1 percent; therefore they were omitted from the equations when the dielectric constants were computed.

III. ELECTRICAL MEASUREMENTS

The capacitance measurements were made with a conjugate Schering bridge provided with an earthing arm.[9] The bridge was well shielded and was operated inside an earthed cage. A balance of the bridge was first obtained without the specimen being connected to it. Then the specimen was connected in parallel with the standard capacitor and the bridge rebalanced. The capacitance of the specimen was taken as equal to the change in capacitance of the standard capacitor necessary to again bring the bridge into balance. The

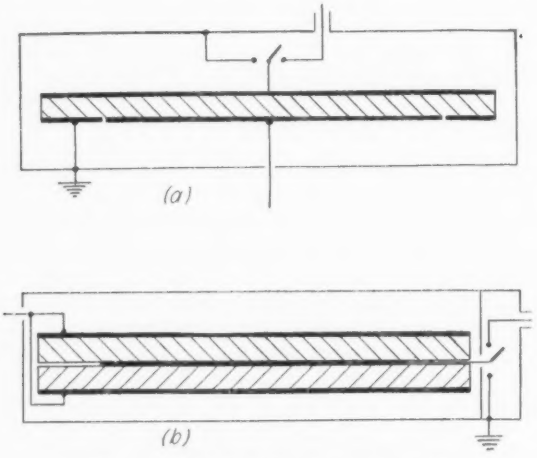

FIGURE 6.—*Shielding arrangements.*

(a) For a single specimen (guard ring may be removed). (b) For a double specimen. These figures are not drawn to scale. The shield should be at least 8 cm from the specimen if serious distortion of the field is to be avoided.

source of 1,000 c/s measuring current for part of the work was a motor-generator energized by storage batteries. For the remainder of the work an amplified 1,000-cycle signal from a crystal clock was filtered and used as a source. In either case a potential of 110 volts was applied across the bridge, which put 55 volts across the specimen.

The specimens were placed in a metal box which served as a shield for the specimens and was part of a constant-temperature chamber. When measured singly, the specimens were mounted as shown diagrammatically in figure 6 (*a*). (The guard and its connection can be removed.) The switch used for disconnecting the high potential lead of the specimen from the bridge and connecting it to earth was mounted in the box. This served effectively to shield the switch. When the double specimens were measured, they were mounted as

[9] This bridge is described in a tentative method of the ASTM entitled, *Tentative methods of testing electrical insulating material for power factor and dielectric constant, D150–36T.* See Proc. Am. Soc. Testing Materials **36**, 955 (1936). A bridge of the same form but with more elaborate shielding than was here used is described by A. V. Astin, *Measurements of relative and true power factors of air capacitors*, J. Research NBS **21**, 425 (1938) RP1138.

shown diagrammatically in figure 6 (*b*). Here it was necessary to mount the switch in a separate compartment. It was found that the shield should be at least 8 cm from any part of the specimen. Closer proximity of the shield to the specimen affected the edge capacitance. The shielding in both cases was designed to eliminate as far as possible direct capacitance between the leads and between each lead and the opposite electrode. This effectively removed from the measurement any capacitance other than the capacitance between the electrodes in all cases except one. When the double specimens were measured and the center electrode was smaller than the outer electrode, it was necessary to make connection to the center electrode with a small wire. This wire could not be shielded along the distance from the edge of the specimens to the center electrode, and the capacitance of this lead to the outer electrode was included in the measured capacitance. This lead capacitance was determined by using a dummy lead as nearly like the real lead as possible and symmetrically placed with respect to it. Assuming that the capacitance of the real lead was the same as that of the dummy, the measured capacitance of the specimen could be corrected for the lead capacitance.

The specimens were maintained at 30° C in a dry atmosphere for at least 48 hours before measurements were made. The capacitance was measured without removing the specimens from the chamber. The marble specimens were dried by placing them in an oven at 115° C for 24 hours before being placed in a measuring chamber.

IV. RESULTS

Measurements were made on both circular and rectangular specimens to determine the accuracy of the theoretical equations which have been given in part 1. The results have also been used to set up empirical equations which give more accurate values of the dielectric constants than the theoretical equations.

Specimens with circular electrodes have been used, not only to measure dielectric constants but also to test the validity of Kirchhoff's formula for edge correction. For the latter purpose, one of the dielectrics used was air.

1. TEST OF KIRCHHOFF'S EQUATION

The validity of Kirchhoff's equation for the capacitance between coaxial circular electrodes when completely surrounded by a uniform dielectric was tested by using both air and methyl methacrylate as the dielectric. When air was used as the dielectric, the field between the electrodes was completely filled with a uniform dielectric as postulated in the theoretical derivation of the equation except for the small volume occupied by the spacers. The electrodes were monel metal disks 20.01 cm in diameter and 0.451 cm thick, whose surfaces were ground flat to within 0.0008 cm. The disks were spaced by three quartz cylinders all of the same length within 2μ and all having a diameter of about 0.3 cm. Three different sets were used having lengths of 0.1874 cm, 0.4027 cm, and 0.5900 cm.

When methyl methacrylate was used as the dielectric, the electrodes were sheets of tinfoil about 30μ thick. In order that the field

should be as nearly as possible all in the solid dielectric, a sheet of the same dielectric 1¼ cm thick and larger than the specimen was placed on each side of the specimen. A hole in each of the outside pieces of dielectric allowed electrical connection to the tinfoil electrodes.

The results of the measurements are given in table 1. The capacitances as measured by the methods described above are given in the fourth column, and the capacitances, as computed by Kirchhoff's equation are given in the fifth column. The percentage differences between the computed and measured values are given in the last column. The differences are all less than 1 percent, which is within experimental error. Hence there is no indication of an error in Kirchhoff's equation.

TABLE 1.—*Test of Kirchhoff's equation for the capacitance between two coaxial circular electrodes of the same diameter*

[Kirchhoff's equation is $C=K(C_a+C_s)$, where C_a and C_s are given by eq 2 and 3, p. 750]

Dielectric	Electrode thickness	Electrode diameter	Spacing	Dielectric constant of surrounding material [1]	Measured capacitance	Computed capacitance	Difference
	cm	*cm*	*cm*		*μμf*	*μμf*	%
Air	0.451	20.01	0.1874	1.000	155.1	154.7	−0.3
Do	.451	20.01	.4027	1.000	74.0	74.0	.0
Do	.451	20.01	.5900	1.000	51.4	51.6	+.4
Methyl methacrylate	.003	11.00	.0887	3.315	323.4	322.8	−.2
Do	.003	10.99	.2591	3.292	113.4	113.1	−.3
Do	.003	10.98	.4680	3.310	65.2	64.7	−.8
Do	.003	11.01	.7020	3.309	44.8	44.5	−.8

[1] Dielectric constant of air was taken from tables; that of methyl methacrylate was measured by a guard-ring capacitor.

2. DIELECTRIC CONSTANTS WHEN THEORETICAL EQUATIONS WERE USED

(a) CIRCULAR ELECTRODES

The percentage errors in a large number of determinations of the dielectric constant for the various arrangements of circular electrodes, using the equations derived in part 1 of this paper, are given in table 2. These errors were computed on the assumption that the dielectric constant as determined by a guard-ring capacitor was correct. The negative sign indicates that the value of the dielectric constant obtained by the theoretical equation is smaller than the correct value.

Each value given in table 2, in most cases, is the average of several determinations. The number of specimens given in the second column is the number of determinations for those electrode arrangements which require a single specimen, namely, arrangements 4a, 4b, and 4c. The number of determinations for the electrode arrangements where two specimens were required is only half the number of specimens. The average values of thickness and dielectric constant are given in the third and fourth columns in order to show the ranges of thickness and dielectric constant which were covered.

The electrode arrangement giving the least error was 5b, which is for a pair of specimens having the center electrode smaller than the other two. It was computed by means of eq 28. The values obtained by this method are correct within experimental error.

TABLE 2.—*Percentage error of dielectric constants computed by means of theoretical equations when circular electrodes were used*

Material	Number of specimens	Thickness in cm	Dielectric constant	4 (*a*) 6	5 (*a*) 22	4 (*b*) 8	5 (*b*) 28	4 (c) 11	5 (c) 32
				Percentage error					
Polystyrene I	2	0.653	2.58			−0.6		−4.1	
Polystyrene II	2	.474	2.57			−1.5		−3.4	
Hard rubber [1]	8	.471	3.12	−0.6	−0.7	−1.8	−0.5	−3.0	−3.1
Methyl methacrylate I	8	.697	3.29	−1.1	−1.1	−1.6	−.2	−4.4	−4.3
Methyl methacrylate II	4	.467	3.31	−0.8	−0.9	−2.1	.0	−3.6	−2.3
Methyl methacrylate III	8	.258	3.28	−.8	−.9	−2.4	+.4	−2.6	−1.3
Methyl methacrylate IV	8	.081	3.32	−.5	−.4	−1.4	+.3	−1.0	−0.2
Aniline formaldehyde	1	.302	3.71			−2.5		−2.9	
Cellulose acetate	4	.312	5.14	−.2	−.2	−3.5	+.2	−3.3	−1.4
Porcelain	1	.597	6.19			−3.2		−4.4	
Glass [1]	8	.467	7.76	+.6	+.5	−4.4	+.1	−4.5	−2.5
White marble [1]	6	.754	8.60	+.1	−.2	−3.8	+.3	−5.7	−3.9
Blue marble [1]	4	.703	8.75	+.1	−.2	−3.9	+.9	−5.5	−3.4
Titania I	2	.608	14.2			−3.4		−5.2	
Titania II	2	.256	15.7			−4.5		−3.5	
Titania III	2	.625	54.0			−5.5		−5.6	
Titania IV	1	.589	57.4			−5.7		−5.6	
Titania V	2	.554	57.0			−6.0		−5.4	
Titania VI	2	.249	57.1			−5.0		−3.7	
Titania VII	3	.609	70.5	−3.8		−5.0		−7.2	
Titania VIII	2	.274	68.5			−5.4		−4.0	
Titania IX	2	.142	70.6			−4.1		−2.6	

[1] The values for glass, hard rubber, and marble, given in this table, differ slightly from the values given in a former paper, *Determination of the edge correction in measurements of dielectric constant*, Proc. Am. Soc. Testing Materials **37**, part II, 655 (1937). The former values were in error, because the shield was placed too close to the specimen (about 3 cm), which distorted the field at the edge and thus gave an erroneous value of edge capacitance.

Arrangements 4a (single specimen, large electrodes) and 5a (double specimen, large electrodes) yielded values which were in error by less than 1.5 percent except for titania VII which was in error by 3.8 percent. The other arrangements gave values of the dielectric constant which were too small by amounts varying from 2 to 7 percent.

Buchner[10] tested arrangement 4a (single specimen, large electrodes), using eq 6, by making measurements on sheets of potassium chloride (dielectric constant 4.68) of varying diameters and thicknesses. His measurements indicate that the error, if any, was small.

Grüneisen and Giebe[11] tested arrangements 4c (single specimen, small electrodes) and 5c (double specimen, small electrodes), using eq 11 and 31, by measuring the dielectric constant of porcelain (dielectric constant 5.60), using sheets of various thicknesses. The conclusions reached in both the above researches are in substantial agreement with those of the present paper.

(b) RECTANGULAR ELECTRODES

Measurements were made on only two materials using rectangular electrodes. Specimens having high dielectric constants were not used because of the difficulty of getting them in the shape desired.

Theoretical equations were available for only four electrode arrangements aside from the guard-ring arrangement as was noted in part 1. The dielectric constants were computed by these equations, and the percentage errors computed, assuming the guard ring value to be correct, as was done for the circular electrodes. The results are given in table 3. As for circular electrodes, the number of specimens is the number of determinations for those arrangements using a single sheet of dielectric. Where two sheets of dielectric were required, the number of determinations was half the number of specimens. The length and width of the specimens are given for comparative purposes.

Arrangement 5b (double specimens, center electrode small) gave values which were in error by less than 1 percent, and arrangement 4a (single specimen, large electrodes) gave values which were in error by less than 2.5 percent. The other arrangements gave errors as high as 14 percent. These errors are higher than for the analogous cases of circular electrodes with the exception of arrangement 5b (double specimen, center electrode small).

3. DETERMINATION OF EMPIRICAL EQUATIONS

A set of empirical equations for the computation of edge capacitances for both circular and rectangular electrodes was determined from the data used in testing the accuracy of the theoretical equations. The values of the edge capacitances, C_E (C_E is here used as distinguished from C_e which is used for the edge capacitance when vacuum is the dielectric), were determined for all the circular specimens listed in table 2 by subtracting the value of the guard-ring capacitance (corrected for the width of the gap between the guarded electrode and the guard electrode) from the value of the capacitance of each of the other arrangements where the electrode was the same diameter as that of the guarded electrode. The values of the edge capacitance per centi-

[10] A. Buchner, *Measurements of dielectric constants*, Z. tech. Physik. **16**, 10 (1935).
[11] E. Grüneisen and E. Giebe, *Use of the three-plate capacitor for the determination of the dielectric constant of solid bodies*, Verhandl. deut. physik. Ges. **14**, 921 (1912).

TABLE 3.—*Percentage error of dielectric constants computed by means of theoretical equations when rectangular electrodes were used*

Material	Thickness	Length	Width	Number of specimens	Dielectric constant	Percentage errors			
Electrode arrangement: Diagram									
Electrode arrangement: Figure						4 (*a*)	4 (*b*)	5 (*b*)	4 (*c*)
Equation number						16	17	33	19
	cm	*cm*	*cm*						
Methyl methacrylate V	0.659	88	9	4	3.25	−2.3	−11.2	+0.3	−10.6
Methyl methacrylate VI	.476	88	9	4	3.26	−2.0	−9.8	.0	−7.7
Methyl methacrylate VII	.252	88	9	4	3.19	−0.8	−6.5	+.4	−4.6
Methyl methacrylate VIII	.070	63	8	2	3.42	−.6	−2.6		−1.6
Methyl methacrylate IX	.671	12	11	2	3.25		−13.2		−10.3
Methyl methacrylate X	.493	12	11	2	3.27		−11.1		−8.4
Glass I	.606	12	12	2	7.65		−14.1		−10.1
Glass II	.396	12	12	2	7.62		−11.5		−7.5

meter of circumference, C_E/P (P is the perimeter in centimeters) are given in table 4.

The edge capacitances per centimeter for rectangular electrodes were determined by first measuring the capacitance with the guard electrode surrounding the small electrode, then measuring the capacitance after the portion of the guard electrode along the side had been removed but the guard electrodes left on the ends. This eliminated the effects of the ends and corners. The edge capacitances per centimeter for rectangular electrodes are given in table 5.

TABLE 4.—*Edge capacitance per centimeter of circumference of circular electrodes*

Electrode arrangement: Diagram						
Electrode arrangement: Figure			4(*b*)	5(*b*)	4(*c*)	5(*c*)
Material	Thickness	Dielectric constant	Edge capacitance per centimeter			
	cm		*μμf*	*μμf*	*μμf*	*μμf*
Polystyrene I	0.653	2.58	0.165		0.067	
Polystyrene II	.474	2.57	.171		.072	
Hard rubber	.471	3.12	.202	0.232	.096	0.088
Methyl methacrylate I	.697	3.29	.194	.266	.084	.119
Methyl methacrylate II	.467	3.31	.204	.258	.090	.127
Methyl methacrylate III	.258	3.28	.223	.290	.107	.148
Methyl methacrylate IV	.081	3.32	.269	.327	.136	.206
Aniline formaldehyde	.302	3.71	.243		.107	
Cellulose acetate	.312	5.14	.289	.428	.133	.222
Porcelain	.597	6.19	.324		.153	
Glass	.467	7.76	.385	.620	.177	.295
White marble	.754	8.60	.408	.698	.182	.316
Blue marble	.733	8.75	.412	.730	.179	.339
Titania I	.608	14.2	.663		.321	
Titania II	.256	15.7	.723		.365	
Titania III	.625	54.0	2.267		1.094	
Titania IV	.589	57.4	2.385		1.115	
Titania V	.554	57.0	2.290		1.094	
Titania VI	.249	57.1	2.304		1.031	
Titania VII	.609	70.5	2.927		1.141	
Titania VIII	.274	68.5	2.863		1.427	
Titania IX	.142	70.6	2.979		1.604	

TABLE 5.—*Edge capacitance per centimeter for rectangular electrodes*

Electrode arrangement: Diagram						
Electrode arrangement: Figure			4(*b*)	5(*b*)	4(*c*)	5(*c*)
Material	Thickness	Dielectric constant	Edge capacitance per centimeter			
	cm		*μμf*	*μμf*	*μμf*	*μμf*
Methyl methacrylate V	0.659	3.25	0.181	0.261	0.078	0.135
Methyl methacrylate VI	.476	3.26	.194	.266	.085	.132
Methyl methacrylate VII	.252	3.19	.211	.273	.099	.156
Methyl methacrylate VIII	.070	3.42	.270		.138	
Methyl methacrylate IX	.671	3.25	.186		.081	
Methyl methacrylate X	.493	3.27	.193		.084	
Glass I	.606	7.65	.376		.167	
Glass II	.396	7.62	.376		.171	

The effect that a corner had on the edge capacitance was determined by measuring the edge capacitance for rectangular electrodes when the guard electrode along the sides was removed and again when the guard electrode at the ends was also removed. The edge capacitance

per centimeter of length was computed from the value of edge capacitance obtained when the guard electrode along the side had been removed. The total capacitance due to the edge was computed by multiplying the capacitance per centimeter by the perimeter. The difference between the total measured edge capacitance and the computed edge capacitance gave the effect of the corners. The capacitances due to the corners are given in table 6. From this it is discovered that within experimental error the corner has a negligible effect for all of the electrode arrangements.

TABLE 6.—*Capacitance of corners of rectangular electrodes*

Electrode arrangement	Diagram				
	Figure	4 (*b*)	5 (*b*)	4 (*c*)	5 (*c*)
Material		Capacitance of corners			
		$\mu\mu f$	$\mu\mu f$	$\mu\mu f$	$\mu\mu f$
Methyl methacrylate V		+0.05	−0.1	−0.05	−0.025
Methyl methacrylate VI		−.1	−.025	−.05	−.025
Methyl methacrylate VII		+.05	+.25	+.05	.0
Methyl methacrylate VIII		+.05		+.2	
Methyl methacrylate IX		−.2			
Methyl methacrylate X		−.05			

The results in tables 4 and 5 show that there is little if any difference between the edge capacitances per centimeter for circular and rectangular electrodes. The fact that the corners have little effect on the edge capacitance should lead one to expect this agreement.

Since the capacitances per centimeter are the same for circular as for rectangular electrodes, it was possible to set up a single set of empirical equations for computing the dielectric constant. The equations apply equally well to both rectangular and circular electrodes.

The results in tables 4 and 5 also show that, for any arrangement of electrodes the edge capacitance depends both on the dielectric constant of the material and on the thickness of the specimen. In order to construct an empirical equation involving both these variables, the effect of each separately was determined. The effect of the dielectric constant of the material on the edge capacitance was determined by selecting a group of samples all of which had about the same thickness. The data for this group (for both circular and rectangular electrodes) are shown in figure 7. The edge capacitances per centimeter of circumference, C_g/P, are plotted against the dielectric constant for arrangements 4b (single specimen, one electrode small) and 4c (single specimen, small electrodes).

It is quite clear that the points lie on a straight line and that this line extended does not pass through the origin. This indicates that the relationship between the edge capacitance, C_g, and the dielectric constant for a given thickness can be expressed as the sum of two terms, one of which, C_m, is directly proportional to the dielectric constant, while the other, C_i, has a value that is given by the intercept on the axis of zero dielectric constant.

In order to develop the empirical equations, it was assumed that the slopes of the lines in figure 7 do not change with thickness of the

specimens, that is, that the part, C_m, of the edge capacitance which is a function of the dielectric constant does not change with thickness of the specimen. From the slopes of the lines it was determined that for arrangement 4b (single specimen, one electrode small)

$$\frac{C_m}{P}=0.0405K, \tag{38}$$

and for arrangement 4c (single specimen, small electrodes)

$$\frac{C_m}{P}=0.185K. \tag{39}$$

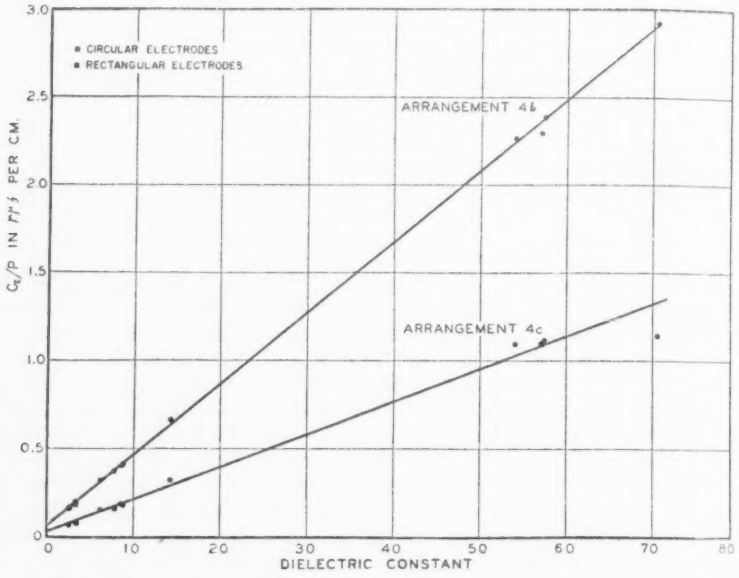

FIGURE 7.—*Relation, for circular electrodes, between the edge capacitane C_E and the dielectric constant.*

Arrangement 4b is a single specimen with one electrode smaller than the other. Arrangement 4c is a single specimen with both electrodes small.

Since the dielectric constants of the specimens listed in tables 4 and 5 were determined with the guard electrode, the values of C_m/P for these specimens could be computed.

The value of the portion, C_i/P, of the edge capacitance per centimeter of circumference, which was independent of the dielectric constant, was obtained for each specimen by subtracting the value of C_m/P from the value of C_E/P, given in tables 4 and 5. These values of C_i/P for the specimens having dielectric constants less than 9 are plotted in figure 8 against the logarithm of the thickness of the specimen. The values of C_i/P for the specimens of higher dielectric constant were not used, because the values of C_i become relatively less important, as compared to the total capacitances of the specimens, as the dielectric constant increases. The points of figure 8 fall along straight lines, showing that C_i/P is a linear function of the logarithm

of the thickness. The relationship for arrangement 4b (single specimen, one electrode small) is

$$\frac{C_t}{P}=\frac{1}{30}\ln\frac{3.8}{b}, \tag{40}$$

and for arrangement 4c (single specimen, small electrodes) is

$$\frac{C_t}{P}=\frac{1}{40}\ln\frac{1.5}{b}. \tag{41}$$

The ability to make the separation of the edge capacitance into two parts, one of which is a function of the dielectric constant of the material and the other independent of it, indicates a superiority of

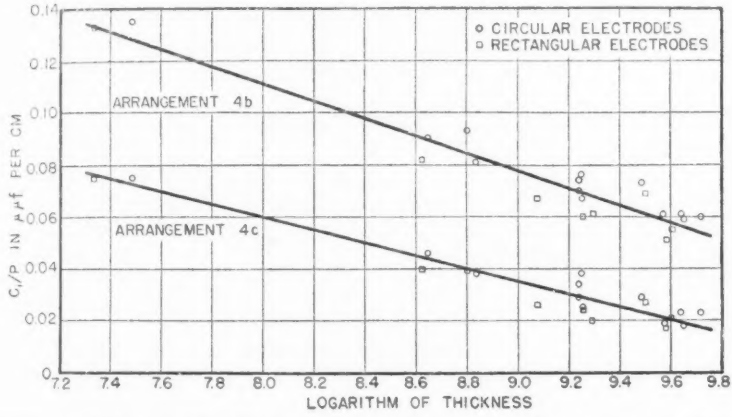

FIGURE 8.—*Relation, for circular electrodes, between the edge capacitance which is not a function of the dielectric constant, C_t, and the thickness of the specimen*

Arrangement 4b is a single specimen with one electrode smaller than the other. Arrangement 4c is a single specimen with both electrodes small.

this method over any of the theoretical methods for determining edge corrections. The theoretical equations cannot make this separation, because they were derived on the assumption that the field at the edge was all in a uniform dielectric. This, as well as the direction of the error due to nonfulfillment of the assumption, was pointed out in part 1.

Equations for the edge capacitances of arrangements 4b and 4c can now be set up. The edge capacitance for arrangement 4b (single specimen, one electrode small) is given by

$$C_g=C_t+C_m=\left(\frac{1}{30}\ln\frac{3.8}{b}+.0405K\right)P, \tag{42}$$

where P is the perimeter of the small electrode in cm, b is the thickness in centimeters, and K is the dielectric constant. The edge capacitance for arrangement 4c (single specimen, small electrodes) is given by

$$C_g=C_t+C_m=\left(\frac{1}{40}\ln\frac{1.5}{b}+.0185K\right)P. \tag{43}$$

It should be pointed out that eq 42 and 43 were developed from data obtained with electrodes having a diameter of 11.0 cm and a thickness of 0.003 cm. However, they will apply in most practical applications because 11 cm is within a few percent of what has practically become a standard diameter, and 0.003 cm is the thickness of the tinfoil which is generally used for electrode material.

It is now possible to set up accurate equations for the computation of the dielectric constant for arrangements 4b (single specimen, one electrode small) and 4c (single specimen, small electrodes). The total capacitance of a specimen having a circular electrode arrangement 4b is given by

$$C=KC_n+\left(\frac{1}{30}\ln\frac{3.8}{b}+.0405K\right)P. \tag{44}$$

Hence,

$$K=\frac{C-\frac{P}{30}\ln\frac{3.8}{b}}{C_n+0.0405P}, \tag{45}$$

where C_n is given by eq 2. The total capitance for arrangement 4c is given by

$$C=KC_n+\left(\frac{1}{40}\ln\frac{1.5}{b}+0.0185K\right)P, \tag{46}$$

from which is obtained the equation

$$K=\frac{C-\frac{P}{40}\ln\frac{1.5}{b}}{C_n+0.0185P}. \tag{47}$$

The evaluation of C_t for arrangement 4b (single specimen one electrode small) makes it possible to determine the equation for the dielectric constant for arrangement 5b (double specimen, center electrode small). If it is assumed that C_t is the part of the edge capacitance arising from the electric field in the air, then facing two specimens of arrangement 4b (single specimen, one electrode small) together to form arrangement 5b eliminates C_t, since the center electrode is practically completely surrounded by dielectric.

The value of C_m for the double specimen should be twice that for a single specimen, and C_n should be the sum of the values for the individual specimens. The equation for arrangement 5b would then be

$$K=\frac{C}{C_{n1}+C_{n2}+0.081P}, \tag{48}$$

where C_{n1} and C_{n2} are the values of C_n for the single specimens making up the double specimen.

As noted in part 1, the theoretical equation (eq 28) for this arrangement gave values that were in error by less than 0.6 percent. This equation has the same form as eq 48 except that the coefficient of P is 0.0782 rather than 0.081.

An equation for the dielectric constant for arrangement 5c (double specimen, small electrodes) can be obtained in the same way as for

arrangement 5b. Facing together two specimens of arrangement 4c (single specimen, small electrodes) eliminated C_t. The value of C_m for the double specimen should be twice that for the single specimen, and the value of C_n for the double specimen should be the sum of those for the single specimens. Thus for arrangement 5c

$$K=\frac{C}{C_{n1}+C_{n2}+0.037P}. \tag{49}$$

This equation has the same form as the theoretically derived equation (eq 32), but the coefficient of P in the theoretical equation is 0.0625 instead of 0.037.

The equation for the dielectric constant for arrangement 4a (single specimen, large electrodes) was obtained from eq 46 for arrangement 4c (single specimen, small electrodes). For arrangement 4a the edge capacitance was all assumed to be in air; therefore the dielectric constant in the term for edge capacitance became unity. Thus for arrangement 4a

$$K=\frac{C-\left(\frac{1}{40}\ln\frac{1.5}{b}+0.0185\right)P}{C_n}. \tag{50}$$

The equation for the dielectric constant for arrangement 5a (double specimen, large electrodes) was obtained from eq 49 for arrangement 5c (double specimen, small electrodes). Assuming the edge capacitance for arrangement 5a all to be in air, the dielectric constant in the edge capacitance term was taken as unity. Thus, for arrangement 5a

$$K=\frac{C-0.037P}{C_{n1}+C_{n2}}. \tag{51}$$

The theoretical equation given for this arrangement (eq 22) has the same form as eq 51, but the coefficient of P was 0.0625 instead of 0.037.

4. DIELECTRIC CONSTANTS WHEN EMPIRICAL EQUATIONS WERE USED

The dielectric constants of all the specimens listed in tables 2 and 3 were recomputed using the empirical equations which are given above. The results for circular electrodes are given in table 7, and for rectangular electrodes in table 8.

In only one case is the error greater than 1.0 percent. For circular electrodes five-sixths of the results have errors 0.5 percent or less, whereas one-sixth of them have errors less than 0.1 percent. For rectangular electrodes three-fourths of the results have errors of 0.5 percent or less, whereas one-fifth of them have errors less than 0.1 percent.

The one case where the error was greater than 1 percent was that for titania VII having a dielectric constant of 70.5 when arrangement 4a (single specimen, large circular electrodes) was used. This large error (3.8 percent) can probably be explained, since the edges of this disk were rather irregular, and therefore the area of the electrodes

was not the same as for the specimen. The great disadvantage of arrangements 4a (single specimen, large electrodes) and 5a (double specimen, large electrodes) is the difficulty of preparing the specimens so that they have good sharp edges, and thus making sure that the electrodes come exactly to the edge of the specimen. For this reason these arrangements are not as easily used as the other arrangements.

These results indicate that rectangular electrodes can be as readily used as circular electrodes and will give as much accuracy. The effect of the corners can be ignored.

TABLE 7.—*Percentage error of dielectric constants computed by means of empirical equations when circular electrodes were used*

Electrode arrangement: Diagram						
Figure	4 (*a*)	5 (*a*)	4 (*b*)	5 (*b*)	4 (*c*)	5 (*c*)
Equation number	50	51	45	48	47	49
Material	Percentage error					
Polystyrene I			+0.2		−0.4	
Polystyrene II			−.2		−.2	
Hard rubber	−0.4	−0.2	+.4	−0.6	+.6	−0.6
Methyl methacrylate I	−.5	−.4	+.1	−.3	+.2	−.2
Methyl methacrylate II	−.7	−.4	+.3	−.2	+.1	+.2
Methyl methacrylate III	−.9	−.5	.0	+.4	−.1	+.2
Methyl methacrylate IV	−.6	−.3	+.1	+.3	+.1	+.4
Aniline formaldehyde			+.3		−.1	
Cellulose acetate	−.2	.0	−.2	.0	.0	+.3
Porcelain			+.6		+.7	
Glass	+.7	+.7	+.1	−.1	.0	.0
White marble	+.4	+.1	+.2	.0	.0	−.1
Blue marble	+.3	+.2	+.3	+.2	.0	+.2
Titania I			+.6		+.9	
Titania II			+.1		+.2	
Titania III			+.1		+.4	
Titania IV			.0		+.1	
Titania V			−.3		+.1	
Titania VI			−.2		−.1	
Titania VII	−3.8				−.8	
Titania VIII					+.3	
Titania IX					+.3	

TABLE 8.—*Percentage error of dielectric constants computed by means of empirical equations when rectangular electrodes were used*

Electrode arrangement: Diagram						
Figure	4 (*a*)	5 (*a*)	4 (*b*)	5 (*b*)	4 (*c*)	5 (*c*)
Equation number	50	51	45	48	47	49
Material	Percentage error					
Methyl methacrylate V	−0.6	0.0	−0.6	−0.1	−0.3	+0.7
Methyl methacrylate VI	−1.0	−.1	−.6	+.1	−.3	+.7
Methyl methacrylate VII	−0.4	−.2	−.3	+.3	−.2	+.7
Methyl methacrylate VIII	−.7	−.4	.0			
Methyl methacrylate IX			−.1		+.1	
Methyl methacrylate X			−.2		.0	
Glass I			−.1		.0	
Glass II			+.1		.0	

The method which is the easiest to use and which will therefore give the most accurate results in general is arrangement 4b (single specimen, one electrode large) using eq 45. Since one electrode is smaller than the other, no great care is needed for centering the

electrodes. On the other hand, great care must be taken with arrangement 4c (single specimen, small electrodes) and 5c (double specimen, small electrodes) to see that the two electrodes on each specimen are opposite each other, and this is sometimes quite difficult. Arrangement 5b (double specimen, center electrode small) is somewhat difficult to use because it is necessary that the two electrodes which are faced together should be exactly opposite each other when the two specimens are placed together to make the double specimen. Also, correction must be made for the capacitance of that part of the lead to the center electrode which is between the larger electrodes, as this cannot be shielded without disturbing the field. However, these difficulties can be overcome with care, and this method has the great advantage that the unit is practically a shielded capacitor. By connecting the outer electrodes to the low potential side of the bridge, the high potential electrode is completely shielded. This allows a number of test units to be stacked on each other without interference between them.

V. SUMMARY

The theoretical equations given in part I all had edge corrections which overcorrected for the edge capacitance except eq 28 for circular electrodes and eq 33 for rectangular electrodes. Both of these equations apply to the electrode arrangement for a pair of specimens where the center electrode is smaller than the other two, and both gave values of the dielectric constant which were in error by less than 1 percent.

Kirchhoff's equation for the capacitance between two circular disks of the same diameter and thickness was found to be correct within experimental error.

Empirical equations were set up which gave values that were in error by less than 1 percent for all electrode arrangements and which were simpler than most of the theoretical equations.

Electrode arrangements which have electrodes extending to the edge of the specimen are very difficult to use because of the difficulty of preparing the specimens with good sharp edges and fixing the electrodes so that they extend exactly to the edges.

The most accurate method for the determination of the dielectric constant, aside from the guard-ring method, is that using one specimen and having one electrode appreciably smaller than the other. Part of the accuracy is due to the fact that the electrodes do not have to be accurately centered on the specimen.

The arrangement consisting of a double specimen with a center electrode smaller than the outer electrodes gives accurate values if the small electrodes of the two single specimens making up the double specimen are exactly opposite each other. This is somewhat difficult, but with care this can be accomplished, and this arrangement has the advantage that the center electrode is completely shielded by the outer electrodes, which may be connected to the low-potential side of the bridge for measurement. Such test units can be stacked without interference between them.

Washington, March 14, 1939.

INDEX TO VOLUME 22

A

Page

Absolute determination of the ampere, RP1200 485
Absorption pipettes, RP1214 701
Acids, organic, solubility of colored glazes in, RP1196 441
Adsorption with silica gel, separation of hydrocarbons of high molecular weight by, RP1185 321
Air capacitors, energy losses, RP1212 673
Air-mapping projects, distortion and resolving power of lenses used, RP1216 729
Airplane camera lenses, resolving power and distortion, RP1216 729
Airplane mapping, camera errors, RP1177 209
Airship fabrics, permeability, RP1166 71
Alloy, gold-chromium, for resistance coils, RP1206 565
Aluminum, effect on properties of cast red brass, RP1215 707
Ampere, absolute determination, RP1200 485
Analysis of ethylene oxide and carbon dioxide, RP1175 171
Antimony, effect on certain properties of cast red brass, RP1215 707
Astatic loads, RP1163 1
Astin, Allen V., L. L. Stockmann, B. W. Brown, L. F. Curtiss and, An improved radio meteorograph on the Olland principle, RP1169 97
——, Nature of energy losses in air capacitors at low frequencies, RP1212 673

B

Balloons, unmanned, radio transmission of ultraviolet intensity measurements from {RP1181 295 / RP1207 573}
Base-combining capacity of wool, RP1203 535
Bell, Rosemond K., William D. Mogerman, John A. Scherrer and, Electroanalytical determination of copper and lead in nitric acid solution containing small amounts of hydrochloric acid, RP1213 697
Benzylcysteine, effect on polarographic determination of cystine, RP1211 669
Book papers, printing tests, RP1180 285
Branham, Joseph R., and Edward O. Sperling, Bubbler tip of Pyrex glass for difficult absorptions, RP1214 701
——, *and Martin Shepherd,* Gasometric method and apparatus for the analysis of mixtures of ethylene oxide and carbon dioxide, RP1175 171
Brass, cast red, effect of aluminum and of antimony on properties, RP1215 707
Brickwedde, Ferdinand G., Harold J. Hoge and, Establishment of a temperature scale for the calibration of thermometers between 14° and 83° K., RP1188 351
Bromides, volatility, RP1198 465
Brown, B. W., A. V. Astin, L. L. Stockmann, L. F. Curtiss and, An improved radio meteorograph on the Olland principle, RP1169 97
Bubbler tips for use in gas-absorption pipette, RP1214 701
Buckling of elastic structures, RP1163 1

C

C_2, or second radiation constant, RP1189 375
Calibrated focal length of airplane cameras, RP1177 209
Calibration of resistance thermometers between 14° and 83° K, RP1188 351
Callingaert, George, Harold Soroos, Frank W. Rose, Jr., Joseph D. White and, 2, 6-Dimethylheptane; Its synthesis, properties, and comparison with an isononane from petroleum, RP1184 315
Camera errors of photogrammetric mapping, RP1177 209

Page

Camera lenses, airplane, resolving power and distortion, RP1216 729
Capacitance, edge correction in determination of dielectric constant, RP1217 747
Capacitors, energy losses, RP1212 673
Carbon dioxide, determination of, in presence of ethylene oxide, RP1175 171
Carbon dioxide, permeability of Neoprene to, RP1166 71
Carbon monoxide, and water, heat of formation, RP1192 407
Cast iron, elastic properties, RP1176 191
Cast red brass, effect of aluminum and of antimony on properties, RP1215 707
Cellulose, fluidity measurement in cuprammonium, RP1179 271
Chlorides, volatility, RP1198 465
Chloroprene, permeability of, to gases, RP1166 71
Chromium-gold resistance coils, RP1206 565
Clamp, toggle, for testing rubber, RP1204 543
Clark, George L., Siegfried T. Gross, and W. Harold Smith, X-ray diffraction patterns of crystalline sol rubber prepared from ethereal solution, RP1170 105
Clay, flow-point pressure, RP1186 329
Coaxial helices, mutual inductance, RP1178 239
Coblentz, W. W., and R. Stair, Distribution of ozone in the stratosphere, RP1207 573
——, ——, Note on the spectral reflectivity of rhodium, RP1168 93
Coils, gold-chromium resistance, RP1206 565
Cold-working of metals, RP1210 651
Color standardization of railroad signal glasses, RP1209 627
Composition and density of glass, RP1197 453
Composition of petroleum distillate, 100° to 130° C., RP1174 153
Concentric solenoids, RP1208 607
Constants, physical, values, RP1189 375
Copper and lead, electrolysis, RP1213 697
Copper, structural changes in working, RP1210 651
Corrections to Southwell's method, RP1163 1
Corrosion of buried pipes, RP1171 109
Craig, D. Norman, and George W. Vinal, Solubility of lead sulfate in solutions of sulfuric acid, determined by dithizone with a photronic cell, RP1165 55
Creamer, A. S., R. F. Geller and, Solubility of colored glazes in organic acids, RP1196 441
Critchfield, Charles L., Roger W. Curtis, Harvey L. Curtis and, An absolute determination of the ampere, using improved coils, RP1200 485
Critical loads, RP1163 1
Critical temperatures of enamel frits, RP1172 127
Crystalline sol rubber from solutions, X-ray diffraction patterns of, RP1170 105
Cuprammonium solution, preparation of standard, RP1179 271
Current balance, absolute determination of the ampere, RP1200 485
Curtis, Harvey L., Arnold H. Scott and, Edge correction in the determination of dielectric constant, RP1217 747
——, *Roger W. Curtis, and Charles L. Critchfield,* An absolute determination of the ampere, using improved coils, RP1200 485
Curtis, Roger W., Charles L. Critchfield, Harvey L. Curtis and, An absolute determination of the ampere, using improved coils, RP1200 485
Curtiss, L. F., A. V. Astin, L. L. Stockmann, and B. W. Brown, An improved radio meteorograph on the Olland principle, RP1169 97
Cysteine, polarographic determination, RP1211 669
Cystine in wool, effect of alkali on, RP1203 535
Cystine, polarographic determination, RP1211 669

D

Page

Deflection of cast iron transverse-test bars, RP1176 ... 191
Deformation of metals, RP1210 ... 651
Deformation of structures, RP1163 ... 1
Density and composition of glass, RP1197 ... 453
β-d-2-Desoxygalactose, preparation and properties, RP1190 ... 397
Dielectric constant, edge correction in determination of, RP1217 ... 747
Diffraction patterns, X-ray, of crystalline sol rubber prepared from solutions, RP1170 ... 105
2,6-Dimethylheptane, preparation, properties, and presence in petroleum, RP1184 ... 315
Distillation column, rotary, RP1201 ... 519
Distortion and resolving power of airplane camera lenses, RP1216 ... 729
Distortion, effects on photogrammetric mapping, RP1177 ... 209
Dithizone method for lead sulfate, RP1165 ... 55
Djenkolic acid, effect on polarographic determination of cystine, RP1211 ... 669

E

Edge corrections in determination of dielectric constant, RP1217 ... 747
Elastic instability, problems of, RP1163 ... 1
Elastic properties of cast iron, RP1176 ... 191
Electric current, absolute determination of the ampere, RP1200 ... 485
Electrode material, effect on power factor, RP1212 ... 673
Electrodes, glass, voltage departures and solubility, RP1187 ... 339
Electrodes, silver-silver bromide, chloride, and iodide, reproducibility, RP1183 ... 307
Electrolytical determination of copper and lead, RP1213 ... 697
Electromotive forces, measurement of small, RP1194 ... 425
RP1195 ... 431
Enamels, thermal-expansion, RP1172 ... 127
Energy losses in air capacitors, RP1212 ... 673
Ethylene oxide, analysis, RP1175 ... 171
Expansivity of enamels, RP1172 ... 127

F

Fabrics, aircraft, permeability, RP1166 ... 71
Faick, Conrad A., Alfred N. Finn, Francis W. Glaze, John C. Young and, Density of some soda-potash-silica glasses as a function of the composition, RP1197 ... 453
Faraday constant, values of, RP1189 ... 375
Fermentation of galactose and talose, RP1191 ... 403
Fibrous structure of metals, RP1210 ... 651
Finn, Alfred N., Edgar H. Hamilton, Donald Hubbard and, Effect of the solubility of glass on the behavior of the glass electrode, RP1187 ... 339
——, *Francis W. Glaze, Conrad A. Faick, John C. Young and,* Density of some soda-potash-silica glasses as a function of the composition, RP1197 ... 453
Flow-point pressure of plastic clay, RP1186 ... 329
Fluidity of cellulose solutions, measurement, RP1179 ... 271
Focal-plane shutter, efficiency and distortion, RP1177 ... 209
Fractionation of petroleum: RP1173 ... 137; RP1174 ... 153; RP1184 ... 315; RP1185 ... 321
Free energy of formation of water and carbon monoxide, RP1192 ... 407
Frequency graphs, maximum usable, application to communication problems, RP1167 ... 81
Frits, enamel, thermal expansion, RP1172 ... 127

G

Galactose yeast, action on *d*-talose, RP1191 ... 403
Gardner, Harold B., and Charles M. Saeger, Jr., Effects of aluminum and of antimony on certain properties of cast red brass, RP1215 ... 707
Gardner, Irvine C., Relation of camera error to photogrammetric mapping, RP1177 ... 209

Page

Gas-analysis apparatus, RP1214 ... 701
Gases, permeability of Neoprene to, RP1166 ... 71
Gasometric method for analysis of mixtures of ethylene oxide and carbon dioxide, RP1175 ... 171
Gas thermometer, used in establishing temperature scale between 14° and 83° K, RP1188 ... 351
Geller, R. F., and A. S. Creamer, Solubility of colored glazes in organic acids, RP1196 ... 441
Gibson, Kasson S., and Geraldine Walker Haupt, Standardization of the luminous-transmission scale used in the specification of railroad signal glasses, RP1209 ... 627
Gilliland, Theodore R., Samuel S. Kirby, Newbern Smith and, Application of graphs of maximum usable frequency to communication problems, RP1167 ... 81
Glasgow, Augustus R., Jr., Joseph D. White and, Separation of 1,2,4-trimethylcyclohexane and an isononane from a mid-continent petroleum, RP1173 ... 197
Glass, density and composition, RP1197 ... 453
Glass electrodes, voltage departures and solubility, RP1187 ... 339
Glasses, railroad signal, standardization RP1209 ... 627
Glaze, Francis W., Conrad A. Faick, Alfred N. Finn, John C. Young and, Density of some soda-potash-silica glasses as a function of the composition, RP1197 ... 453
Glazes, solubility of colored, RP1196 ... 441
Godfrey, Theodore B., Further data on gold-chromium resistance wire, RP1206 ... 565
Gold-chromium resistance coils, RP1206 ... 565
Gross, Siegfried T., W. Harold Smith, George L. Clark and, X-ray diffraction patterns of crystalline sol rubber prepared from ethereal solution, RP1170 ... 105
Ground-coat enamel frits, thermal expansion, RP1172 ... 127

H

Hamilton, Edgar H., Alfred N. Finn, Donald Hubbard and, Effect of the solubility of glass on the behavior of the glass electrode, RP1187 ... 339
Harris, Milton, and Henry A. Rutherford, Base-combining capacity of wool, RP1203 ... 535
Harrison, William N., Benjamin J. Sweo, and Stephen M. Shelton, Thermal-expansion characteristics of some ground-coat enamel frits, RP1172 ... 127
Haupt, Geraldine Walker, Kasson S. Gibson and, Standardization of the luminous-transmission scale used in the specification of railroad signal glasses, RP1209 ... 627
Heat of formation of water and carbon monoxide, RP1192 ... 407
Helices, mutual inductance, RP1178 ... 209
Helium, permeability of Neoprene to, RP1166 ... 71
Heterostatic loading, RP1163 ... 1
Hoffman, James I., and G. E. F. Lundell, Volatilization of metallic compounds from solutions in perchloric or sulfuric acid, RP1198 ... 465
Hoge, Harold J., and Ferdinand G. Brickwedde, Establishment of a temperature scale for the calibration of thermometers between 14° and 83° K, RP1188 ... 351
Holt, William L., and Archibald T. McPherson, Toggle clamp for rubber tensile specimens, RP1204 ... 543
Hubbard, Donald, Egdar H. Hamilton, and Alfred N. Finn, Effect of the solubility of glass on the behavior of the glass electrode, RP1187 ... 339
Humphreys, Curtis J., Second spectrum of xenon, RP1164 ... 19
Hydrocarbon, rubber, behavior of in a molecular still, RP1202 ... 529
Hydrocarbons in petroleum: RP1173 ... 137; RP1174 ... 153; RP1184 ... 315; RP1185 ... 321
Hydrocarbons of high molecular weight, separation of by adsorption with silica gel, RP1185 ... 321
Hydrochloric acid, use of in electrolysis of copper and lead, RP1213 ... 697
Hydrogen, permeability of Neoprene to RP1166 ... 71

I

Page

Inductance, mutual, of coaxial helices, RP1178.. 239
Inductance, mutual, of concentric solenoids, RP1208.. 607
Instability of structures, RP1163.. 1
Interferometer, method for measuring expansion of enamels, RP1172.. 127
Interferometric measurements of solubility of glass, RP1187.. 339
International Temperature Scale above the gold point, RP1189.. 375
Ionosphere, application to communication, RP1167.. 81
Iron, cast, elastic properties, RP1176.. 191
Isbell, Horace S., Action of baker's yeast on *d*-talose, RP1191.. 403
——, *and William W. Pigman*, Preparation and properties of β-*d*-2-desoxygalactose, RP1190.. 397
Isononane in petroleum {RP1173.. 137 / RP1184.. 315
Isopentane, heat of combustion, RP1193.. 415

J

Johnson, Paul V., Ray T. Stull and, Relation between moisture content and flow-point pressure of plastic clay, RP1186.. 329

K

Kirby, Samuel S., Theodore R. Gilliland, Newbern Smith and, Application of graphs of maximum usable frequency to communication problems, RP1167.. 81
Krouskop, John W., and Frederick D. Rossini, Heats of combustion of tetramethylmethane and 2-methylbutane, RP1193.. 415
Krynitsky, Alexander I., and Charles M. Steger, Jr., Elastic properties of cast iron, RP1176.. 191

L

Launer, Herbert F., and William K. Wilson, Determination of pentosans in pulps and papers, RP1199.. 471
——, Determination of the pH value of papers, RP1205.. 553
Lead and copper, electrolysis, RP1213.. 697
Lead, dissolved from colored glazes, RP1196.. 441
Lead sulfate, solubility, RP1165.. 55
Leaks in pipe lines, RP1171.. 109
Lenses, airplane camera, resolving power and distortion, RP1216.. 729
Leslie, Robert T., Summary of an investigation of the composition of a midcontinent petroleum distillate, boiling between 100° and 130° C., RP1174.. 153
Loads, critical, RP1163.. 1
Logan, Kirk H., Engineering significance of National Bureau of Standards soil-corrosion data, RP1171.. 109
Luminous transmission of railroad signal glasses, RP1209.. 627
Lundell, G. E. F., James I. Hoffman and, Volatilization of metallic compounds from solutions in perchloric or sulfuric acid, RP1198.. 465

M

Mair, Beveridge J., and Charles B. Willingham, Efficiency of a rotary distillation column, RP1201.. 519
Maximum usable frequency, radio application, RP1167.. 81
McPherson, Archibald T., William L. Holt and, Toggle clamp for rubber tensile specimens, RP1204.. 543
Mease, Ralph T., Measurement of the apparent fluidity of dispersions of cellulose in cuprammonium solution, RP1179.. 271
Mechanical equivalent of light, RP1189.. 375
Metallographic examination of cast iron, RP1176.. 191
Metals, cold-working, RP1210.. 651
Meteorograph, improved, for upper-air measurements, RP1169.. 97

Page

Meter, radio, for transmitting stratosphere ultraviolet intensity measurements from unmanned balloons {RP1181.. 295 / RP1207.. 573
Methionine, effect on polarographic determination of cystine, RP1211.. 669
2-Methylbutane, heat of combustion, RP1193.. 415
Microstructure of cast iron, RP1176.. 191
Modulus of rupture of transverse-test bars of cast iron, RP1176.. 191
Mogerman, William D., Rosemond K. Bell, John A. Scherrer and, Electroanalytical determination of copper and lead in nitric acid solutions containing small amounts of hydrochloric acid, RP1213.. 697
Moisture, effect of, on flow-point pressure of clay, RP1186.. 329
Molding of cast iron, RP1176.. 191
Molecular still, behavior of rubber in, RP1202.. 529
Mutarotation of β-*d*-2-desoxygalactose, RP1190.. 397

N

Neopentane, heat of combustion, RP1193.. 415
Neoprene, permeability to gases, RP1166.. 71
Noble gases, RP1164.. 19

O

Olland-type radio telemeter, RP1169.. 97
Optical method for measuring deflection of transverse-test bars of cast iron, RP1176.. 191
Optical pyrometry, laws of, RP1189.. 375
Optical rotation of β-*d*-2-desoxygalactose, RP1190 397
Oxygen of high purity, preparation, RP1182.. 301
Ozone, distribution in stratosphere, RP1207.. 573

P

Papers and pulps, pentosans in, RP1199.. 471
Papers, book, printing tests, RP1180.. 285
Papers, pH values, RP1205.. 553
Pentosans in pulps and papers, RP1199.. 471
Perchloric acid, volatilization by, RP1198.. 465
Permeability of Neoprene to gases, RP1166.. 71
Petroleum, fractionation {RP1173.. 137 / RP1174.. 153 / RP1184.. 315 / RP1185.. 321
Photogrammetric mapping, camera errors, RP1177.. 209
Photronic cell, use in lead determinations, RP1165.. 55
pH values of papers, RP1205.. 553
Physical constants, RP1189.. 375
Pickering, S. F., E. R. Weaver, Martin Shepherd and, Preparation of oxygen of high purity, RP1182.. 301
Pigman, William W., Horace S. Isbell and, Preparation and properties of β-*d*-2-desoxygalactose, RP1190.. 397
Pipe-line corrosion, RP1171.. 109
Pipettes, absorption, bubbler tips for, RP1214.. 701
Planck's law, constants entering, RP1189.. 375
Plastic clay, flow-point pressure, RP1186.. 329
Plastic deformation of metals, RP1210.. 651
Polarographic determination of cystine, RP1211.. 669
Porcelain enamels, thermal expansion, RP1172.. 127
Potentiometer circuit, method of reducing effect of disturbances in galvanometer branch: RP1194.. 425 / RP1195.. 431
Potentiometer for measurement of 10 microvolts to an accuracy of 0.01 microvolt, RP1195.. 431
Power factors of air capacitors, RP1212.. 673
Pressure coefficient of resistance of gold-chromium alloy, RP1206.. 565
Pressure, flow-point of clay, RP1186.. 329
Printing tests of book papers, RP1180.. 285
Producer-gas reaction, heat and free energy, RP1192.. 407
Pulps and papers, pentosans in, RP1199.. 471

R

Page

Radiation constants values, RP1189 375
Radio, application of maximum usable frequency, RP1167 81
Radio meteorograph, improved, for upper-air measurements, RP1169 97
Radio transmission of stratosphere ultraviolet intensity measurements {RP1181 295 / RP1207 573
Railroad signal glasses, standardization and specification, RP1209 627
Red brass, effect of aluminum and of antimony on properties, RP1215 707
Reflecting power of rhodium, RP1168 93
Relative modulus of elasticity of transverse test bars of cast iron, RP1176 191
Resilience of cast iron, RP1176 191
Resistance bridge, gold-chromium coils for, RP1206 565
Resistance coils, gold-chromium, RP1206 565
Resistance thermometers, calibration between 14° and 83° K, RP1188 351
Resolving power and distortion of airplane-camera lenses, RP1216 729
Rhodium, spectral reflectivity, RP1168 93
Rodden, Clement James, Edgar Reynolds Smith and, Effects of methionine, djenkolic acid, and benzylcysteine on the estimation of cystine by the dropping mercury cathode, RP1211 669
Rose, Frank W., Jr., George Calingaert, Harold Soroos, Joseph D. White and, 2,6-Dimethylheptane: Its synthesis, properties, and comparison with an isononane from petroleum, RP1184 315
Rossini, Frederick D., Heat and free energy of formation of water and of carbon monoxide, RP1192 407
——, *John W. Knowlton and,* Heats of combustion of tetramethyimethane and 2-methylbutane, RP1193 415
Rotary distillation column, RP1201 519
Rubber, behavior of, in a molecular still, RP1202 529
Rubber, crystalline sol, X-ray diffraction patterns of, RP1170 105
Rubber, permeability to gases, RP1166 71
Rubber, toggle clamp for tensile testing specimens of, RP1204 543
Rutherford, Henry A., Milton Harris and, Base-combining capacity of wool, RP1203 535

S

Saeger, Charles M., Jr., Alexander I. Krynitsky and, Elastic properties of cast iron, RP1176 191
——, *Harold B. Gardner and,* Effects of aluminum and of antimony on certain properties of cast red brass, RP1215 707
Sager, Theron P., and Max Sucher, Permeability of Neoprene to gases, RP1166 71
Scherrer, John A., Rosemond K. Bell, and William D. Mogerman, Electroanalytical determination of copper and lead in nitric acid solution containing small amounts of hydrochloric acid, RP1213 697
Schuhmann, Shuford, Ray P. Teele and, A potentiometer for measuring voltages of 10 microvolts to an accuracy of 0.01 microvolt, RP1195 431
Scott, Arnold H., and Harvey L. Curtis, Edge correction in the determination of dielectric constant, RP1217 747
Second critical Euler column load RP1163 1
Shaw, Merle B., and Robert H. Simmons, Printing tests of experimental book papers, RP1180 285
Sheet-iron ground frits, thermal expansion, RP1172 127
Shelton, Stephen M., Benjamin J. Sweo, William N. Harrison and, Thermal-expansion characteristics of some ground-coat enamel frits, RP1172 127
Shepherd, Martin, E. R. Weaver, and S. F. Pickering, Preparation of oxygen of high purity, RP1182 301
——, *Joseph R. Branham and,* Gasometric method and apparatus for the analysis of mixtures of ethylene oxide and carbon dioxide, RP1175 171
Signal glasses, railroad, standardization and specification, RP1209 627
Silica gel, separation of hydrocarbons of high molecular weight by adsorption with, RP1185 321
Silver-silver bromide, chloride, and iodide electrodes, reproducibility, RP1183 307
Simmons, Robert H., Merle B. Shaw and, Printing test of experimental book papers, RP1180 285
Single-layer coils, coaxial, inductance of, RP1178 239
Single-layer coils, torque between, RP1208 607
Smith, Edgar Reynolds, and Clement James Rodden, Effects of methionine, djenkolic acid, and benzylcysteine on the estimation of cystine by the dropping mercury cathode, RP1211 669
——, *John Keenan Taylor and,* Reproducibility of silver-silver halide electrodes, RP1183 307
Smith, Newbern, Samuel S. Kirby, and Theodore R. Gilliland, Application of graphs of maximum usable frequency to communication problems, RP1167 81
Smith, W. Harold, and Henry J. Wing, Behavior of rubber hydrocarbon in a molecular still, RP1202 529
——, *Siegfried T. Gross, George L. Clark and,* X-ray diffraction patterns of crystalline sol rubber prepared from ethereal solution, RP1170 105
Snow, Chester, Mutual inductance and force between two coaxial helical wires, RP1178 239
——, Torque between concentric single-layer coils, RP1208 607
Soil corrosion of pipe lines, RP1171 109
Solenoids, coaxial, mutual inductance, RP1178 239
Sol rubber, crystalline, from solutions, X-ray diffraction patterns of, RP1170 105
Solubility of colored glazes in organic acids, RP1196 441
Solubility of glass, measurement by interferometry, RP1187 339
Solubility of lead sulfate, RP1165 55
Soroos, Harold, Frank W. Rose, Jr., George Calingaert, Joseph D. White and, 2, 6-Dimethylheptane: Its synthesis, properties, and comparison with an isononane from petroleum, RP1184 315
Southwell's method of analysis, RP1163 1
Specification of railroad signal glasses, RP1209 627
Spectral reflectivity of rhodium, RP1168 93
Spectral transmission of railroad signal glasses, RP1209 627
Spectra of ionized xenon, RP1164 19
Spectra of noble gases, RP1164 19
Sperling, Edward O., Joseph R. Branham and, Bubbler tip of Pyrex glass for difficult absorptions, RP1214 701
Stability of structures, RP1163 1
Stair, R., A precision radio instrument for transmitting measurements of ultraviolet intensities from unmanned balloons to a ground station, RP1181 295
——, *W. W. Coblentz and,* Distribution of ozone in the stratosphere, RP1207 573
——, ——, Note on the spectral reflectivity of rhodium, RP1168 93
Standards, gold-chromium resistance, RP1206 565
Stefan-Boltzmann constant, σ, RP1189 375
Still, molecular, behavior of rubber in, RP1202 529
Stockmann, L. L., B. W. Brown, A. V. Astin, L. F. Curtiss and, An improved radio meteorograph on the Olland principle, RP1169 97
Stratosphere measurements, using radio telemeter, RP1169 97
Stratosphere, ozone distribution, RP1207 573
Stratosphere ultraviolet intensity measurements, radio meter for transmitting {RP1181 295 / RP1207 573
Structures, stability, RP1163 1
Stull, Ray T., and Paul V. Johnson, Relation between moisture content and flow-point pressure of plastic clay, RP1186 329
Sucher, Max, Theron P. Sager and, Permeability of Neoprene to gases, RP1166 71
Surface layers on metals, effect on power factor, RP1212 673
Sweo, Benjamin J., Stephen M. Shelton, William N. Harrison and, Thermal-expansion characteristics of some ground-coat enamel frits, RP1172 127

T

d-Talose, action of baker's yeast on, RP1191 — 403
Taylor, John Keenan, and Edgar Reynolds Smith, Reproducibility of silver-silver halide electrodes, RP1183 — 307
Teele, Ray P., and Shuford Schuhmann, A potentiometer for measuring voltages of 10 microvolts to an accuracy of 0.01 microvolt, RP1195 — 431
Telemeter, radio, for upper-air measurements, RP1169 — 97
Temperature coefficient of resistance of gold-chromium alloy, RP1206 — 565
Temperature scale, basis of, RP1189 — 375
Temperature scale, establishment between 14° and 83° K, RP1188 — 351
Temperatures, critical, of enamels, RP1172 — 127
Temperatures of heating and pouring of cast iron, RP1176 — 191
Tensile testing of rubber, RP1204 — 543
Tetramethylmethane, heat of combustion, RP1193 — 415
Thermal expansivity of enamels, RP1172 — 127
Thermal shield and neutral galvanometer key, RP1195 — 431
Thermodynamic temperature scale, high temperatures, RP1189 — 375
Thermoelectromotive force in galvanometer branch of a potentiometer circuit, RP1194 — 425; RP1195 — 431
Thermometers, resistance, calibration between 14° and 83° K, RP1188 — 351
Third critical Euler column load, RP1163 — 1
Toggle clamp for testing rubber specimens, RP1204 — 543
Torque between concentric solenoids, RP1208 — 607
Transmission, luminous, of railroad glasses (Association of American Railroads scale), RP1209 — 627
Transverse properties of cast iron, RP1176 — 191
1, 2, 4-Trimethylcyclohexane in petroleum, RP1173 — 137
Tuckerman, L. B., Heterostatic loading and critical astatic loads, RP1163 — 1

U

Ultraviolet intensities, stratosphere, radio instrument for transmitting measurements from unmanned balloons, RP1181 — 295; RP1207 — 573
Ultraviolet solar radiation, measurements of spectral quality and total intensity, RP 1181 — 295; RP 1207 — 573
Units, electrical, the ampere, RP1200 — 485
Upper-air measurements, using radio telemeter, RP1169 — 97

V

Vacher, Herbert C., Development of a fibrous texture in cold-worked rods of copper, RP1210 — 651
Vinal, George W., D. Norman Craig and, Solubility of lead sulfate in solutions of sulfuric acid, determined by dithizone with a photronic cell, RP1165 — 55
Viscometer, calibration of pipette, RP1179 — 271
Viscosity measurement of cuprammonium solutions of cellulose, RP1179 — 271
Vitreous enamels, thermal expansion, RP1172 — 127
Volatilization by distillation with perchloric acid, RP1198 — 465
Voltage departures and solubility of glass electrodes, RP1187 — 339

W

Washer, Francis E., Resolving power and distortion of typical airplane-camera lenses, RP1216 — 729
Water-gas reaction, heat and free energy, RP1192 — 407
Weaver, E. R., S. F. Pickering, Martin Shepherd and, Preparation of oxygen of high purity, RP1182 — 301
Wenner, Frank, A method of reducing the effect of disturbances in the galvanometer branch of a potentiometer circuit, RP1194 — 425
Wensel, H. T., International Temperature Scale and some related physical constants, RP1189 — 375
Westergaard's theory of buckling, RP1163 — 1
White, Joseph D., and Augustus R. Glasgow, Jr., Separation of 1, 2, 4-trimethylcyclohexane and an isononane from a midcontinent petroleum, RP1173 — 137
——, *Frank W. Rose, Jr., George Calingaert, and Harold Soroos,* 2, 6-Dimethylheptane: Its synthesis, properties, and comparison with an isononane from petroleum, RP1184 — 315
Willingham, Charles B., Beveridge J. Mair and, Efficiency of a rotary distillation column, RP1201 — 519
——, Separation of hydrocarbons of high molecular weight by adsorption on silica gel, RP1185 — 321
Wilson, William K., Herbert F. Launer and, Determination of pentosans in pulps and papers, RP1199 — 471
Wing, Henry J., W. Harold Smith and, Behavior of rubber hydrocarbon in a molecular still, RP1202 — 529
Wool, alkaline degradation, RP1203 — 535

X

Xenon spectra, RP1164 — 19
X-ray diffraction applied to metal structure, RP1210 — 651
X-ray diffraction patterns of crystalline sol rubber prepared from solutions, RP1170 — 105

Y

Young, John C., Francis W. Glaze, Conrad A. Faick, and Alfred N. Finn, Density of some soda-potash-silica glasses as a function of the composition, RP1197 — 453